Explorations of four and five dimensional black hole spacetimes

Hoskisson, James

Explorations of Four and Five Dimensional Black Hole Spacetimes

James Hoskisson

A Thesis presented for the degree of
Doctor of Philosophy

Centre for Particle Theory
Department of Mathematical Sciences
University of Durham
England

May 2009

Explorations of Four and Five Dimensional Black Hole Spacetimes

James Hoskisson

Submitted for the degree of Doctor of Philosophy
May 2009

Abstract

This thesis concentrates on four and five dimensional black holes and their associated geodesics. Some coordinate charts are presented, which are useful in the analysis of both static and rotating black holes, and their mathematical properties investigated before some methods of solving Einstein's vacuum field equations are examined. The Myers-Perry black hole metric is derived before going on to describe the Inverse Scattering Method of generating new vacuum solutions. The Inverse Scattering Method is used to generate the single and doubly spinning black ring metrics and then the physical properties of these solutions is explored in detail.

The latter part of this thesis looks at different ways of visualising geodesics in various spacetimes and examines the pros and cons of each particular method, as well as looking at several examples of geodesics with different parameters. The geodesics of the singly spinning black ring are calculated and it is shown that they cannot in general be analytically integrated. In light of this, some restricted analytic scenarios are investigated with the intention of gaining some insight into how the geodesics behave in the spacetime as a whole.

Finally, a method is presented which allows string charges to be added to any vacuum solution to Einstein's equations. The properties of this new charged solution are then compared with the neutral starting solution. The doubly spinning black ring is used as a model to demonstrate how the method can be used to charge up a specific black hole solution and the resulting thermodynamic properties of this charged doubly spinning black ring are then examined.

Declaration

The work in this thesis is based on research carried out at the Department of Mathematical Sciences, the Centre for Particle Theory, Durham University, England. No part of this thesis has been submitted elsewhere for any other degree or qualification.

The first four chapters of this work review and re-derive various results which are already in the literature. Chapter 5 is composed of some original work as well as some re-derivations of well known results and the work in chapters 6 and 7 is all my own, except where referenced to the contrary in the text.

Acknowledgements

Thanks to Mukund Rangamani for a great deal of help in the preparation of this thesis and the work contained within.

Contents

List of Figures

Chapter 1

Introduction

Traditionally, black holes have been studied exclusively in only four dimensions, for the obvious reason that our everyday experience is of only three spatial dimensions and one time dimension. The first black hole solution was discovered by Schwarzschild [2] in 1916 and it was soon realised that this solution exhibited an interesting feature whereby test particles were restricted to only move toward the centre of the black hole after crossing a particular spacetime boundary. This spacetime boundary become known as the event horizon and, in the Schwarzschild case, its location is directly determined by the point-like mass at the centre of the space.

The idea of a black hole was originally postulated by John Michell [1] (although not referred to as a black hole) in a letter he sent to Henry Cavendish, where he hypothesised that a very massive star would not emit any light because the escape velocity of any body would be greater than that of the speed of light. This was based on Newton's theory of gravity and was later promoted by Pierre-Simon Laplace in the first two editions of his book "Exposition du systme du Monde" (Paris, 1796). These so called "dark stars" were largely ignored since it was then thought that light was exempt from the influence of gravity.

Even after it was observed that the Schwarzschild solution could exhibit a black hole, the notion of an event horizon was initially thought to be of purely academic interest, since it was generally accepted that no physical system could be small enough to fit within its event horizon [3]. However, further research into gravitational collapse indicated that this view was mistaken and research into what later came to

be called black holes, progressed very quickly. The modern notion of a black hole, where light can't escape to infinity from inside the event horizon, doesn't occur in the Newtonian theory of gravity, so the idea that they might be physically realisable caused a flurry of activity at the end of the 1950's [4–8] that led to a comprehensive understanding of the Schwarzschild black hole topology.

Although the Schwarzschild metric was well understood by the beginning of the 1960's, it was expected that a more general solution to Einstein's equations existed, whereby the black hole also rotated. This is because it was well known that most large stars have at least some angular momentum and if the inevitable consequence of their collapse was to form a black hole, the black hole would also have to rotate. Thus, it was timely that Kerr [9] discovered a solution to Einstein's equation where the black hole rotated about the origin of the space.

The addition of angular momentum to the black hole made the metric significantly more complicated and thus made gaining an understanding of its properties significantly more difficult. Throughout the 1960's work that gave a much greater insight into the behaviour of the Kerr solution was carried out, such as [3, 10–13], but the key insight was provided by Boyer and Lindquist [14] where they devised new coordinates which cast the Kerr metric in a form where the symmetry between the axial and stationary Killing vectors is explicit. These Boyer Lindquist coordinates then allowed Carter [15] to show that the metric in this form has an extra conserved quantity related to the angular momentum about an ellipse [16], rather than a point.

Having devised a black hole with angular momentum it was shown that, disregarding the possibility of adding charge to the black hole, the Kerr metric is the only possible black hole in four dimensions[1]. This statement is known as black hole uniqueness and was proved for non-rotating black holes by Israel [17] in 1967 and was extended to include rotating black holes in a series of papers throughout the 1970's. The observation that made the extension of the uniqueness theorem to Kerr black holes possible, came in a paper by Carter [18] where he showed that the Einstein

[1]The Kerr metric includes the Schwarzschild solution, since it will reduce to the static Schwarzschild metric in the limit as the angular momentum is reduced to zero.

equations reduce to a two dimensional boundary value problem when considering stationary and axisymmetric solutions. This ultimately culminated in an identity by Robinson [19], which he used to prove that the Kerr metric is the unique vacuum solution to the Einstein equations. This meant that all the solutions to the vacuum Einstein equations, for pure gravity, are contained within the Kerr metric and thus can be described using only two parameters: the mass and the angular momentum.

Over the last two decades, the study of black holes in higher dimensions has gained much greater prominence, due primarily to the growing interest in string theory [20, 21] and other higher dimensional models, such as Brane worlds [22]. In these models, more than three spatial dimensions are a necessity, but higher dimensional black hole solutions are also useful in the study of theories such as the AdS/CFT correspondence [23], where the properties of an n dimensional black hole are related to a quantum field theory in $n-1$ dimensions. There is also speculation that higher dimensional black holes may be produced in future particle collider experiments, in scenarios where the extra dimensions are accessible at the TeV scale [24].

Increasing the number of dimensions that are considered to more than the usual three spatial and one time dimension, instantly increases the sophistication of any desired solutions because the extra spatial dimensions increase the number of degrees of freedom that the solution can have and thus increases the complexity. In 5D, for example, it is possible to have simultaneous rotation in two perpendicular planes, leading to black hole solutions that have more than one angular momentum parameter. The first higher dimensional solution was that of Myers and Perry [25], where they generalised the 4D Kerr solution to $N+1$ dimensions, to give a spherical black hole with $N/2$ angular momentum parameters (or $(N-1)/2$ parameters if N is odd.) This instantly increases the number of parameters that are required to specify the black hole, once n is increased above 4.

The other factor, that allows for much greater variety in the behaviour of black holes in higher dimensions, is the competition between the centrifugal and gravitational potentials. To get an idea of how this occurs, consider the Newtonian limit of a particular spacetime in n dimensions: the potential will vary as r^{3-n} but the cen-

trifugal barrier in a particular direction only depends on the rotation in the plane, so will vary as r^{-2} in each of the planes of rotation. It is easy to see from this argument that the balance between the gravitational and centrifugal potentials will be significantly different as n is increased.

It wasn't generally thought that there should exist any black holes with non-spherical topology because of the uniqueness theorems of 4D black holes. Although some people suspected that a non-spherical black hole might exist, it wasn't until Emparan and Reall discovered a black hole with $S^2 \times S^1$ topology [26] that attention was actively focussed on searching for more exotic black hole solutions to Einstein's equations. Since then, various higher dimensional black holes have been discovered with the most notable solution being the more general doubly spinning black ring [27] which rotates in both of its mutually perpendicular planes. These black ring solutions also demonstrated black hole non-uniqueness and thus disproved the assumption that the 4D uniqueness theorems would automatically hold in higher dimensions. Further properties of the black ring solutions will be investigated in later chapters, along with those of other higher dimensional black hole solutions.

In the following chapters both rotating and non-rotating black hole spacetimes are examined and some of their pertinent properties are discussed, along with the mathematical problems associated with some of these properties. Having gained an understanding of the different black holes' properties, the geodesics in these four and five dimensional black hole spacetimes are investigated and various methods of visualising their geodesics are considered. Some methods of solving the vacuum Einstein equations are also presented, with the 5D black ring solutions being introduced and their properties explored. Finally, a generic method of adding string charges to black hole solutions is investigated, with the doubly spinning black ring used as an example of a charged black hole solution. The properties of this new solution are then explored.

Chapter 2 introduces some useful coordinates charts that will be used in later chapters, as well as showing why it is not always possible to derive all the properties of a particular solution in a single coordinate system. The proceeding chapter then looks at some different techniques for solving Einstein's field equations and discusses

the applicability of the techniques in question, before going on to show how they are used to derive some black hole solutions. The solutions that are generated by the various techniques are not necessarily free of singularities, so there is also some discussion of the necessary constraints to ensure that the generated metric is free from unphysical conical and coordinate singularities where possible.

Having derived the black ring solutions, chapter 4 investigates the physical properties of these metrics and contrasts them with the corresponding 5D Myers-Perry solution, as well as showing how they share many of the properties of the more familiar solutions in certain limits. In general, the addition of an extra angular momentum parameter to the black ring makes quite a marked difference to its physical properties, so the singly and doubly spinning rings are described separately with the similarities as well as the differences being highlighted.

The geodesics of various different spacetimes, when considered in 5D, are examined in section 5 with the geodesics in these spaces plotted on a Penrose diagram. This gives a greater insight into the behaviour of test particles undergoing geodesic motion because it is possible to relate the path that the particle takes with the global structure of the spacetime, which is usually only approximated by sketching possible causal paths. The geodesics in flat space, Schwarzschild space, and Kerr space are all examined with an alternate means of mapping Kerr space also investigated. The geodesics in the Kerr spacetime are generally more complicated than those in the static spacetimes by virtue of the Kerr black hole having angular momentum and thus causing a frame dragging effect.

After investigating the motion of geodesics in some familiar spacetimes, the geodesics of the black ring solution are discussed in detail in chapter 6. Unfortunately, the geodesic equations of the black ring solution aren't separable so various different sub-spaces of the black ring are examined, where the geodesic equations can be quantitatively analysed. Based on these results, some scenarios where the geodesics are unrestricted are also investigated by numerically integrating the equations of motion.

The final chapter looks at black hole solutions more generally and adapts a pre-existing method of adding string charges to a vacuum black hole solution to

construct an algorithm for charging up a black hole solution without having to know the exact form of the metric. This then allows the physical properties of any black hole solution with string charges to be investigated and the effect of adding charge to a vacuum solution quantified. To give an example of how the method can be applied, fundamental string and momentum charges are added to the doubly spinning black hole solution and its new properties then examined.

Overall, it is shown that the behaviour of the four and five dimensional versions of the black holes with spherical topology are qualitatively similar but once the topology is varied both the black holes, and the test particles moving in the exterior of the black hole, behave in a markedly different manner. This can be thought of as a consequence of the non-uniqueness of 5D black holes, since the addition of an extra spatial dimension allows for the possibility of several different types of black hole to exist, even if the parameters of the different black holes are exactly the same. It is the aim of the following chapters to go some way toward classifying the behaviour of the various black hole spacetimes in order to better understand the physics behind the mathematical solutions.

Chapter 2

Coordinate Charts in the Schwarzschild and Kerr Metrics

This chapter examines the Schwarzschild and Kerr metrics as examples of static and rotating spacetimes and the various coordinate systems that have been developed to investigate these spacetimes. These coordinate transformations will prove to be useful in the analysis of the black holes later on as they can be used to circumvent coordinate singularities that occur in some coordinate charts. Often, a coordinate system that is useful in finding a particular solution isn't particularly well adapted to the overall geometry of the solution. In light of this, it is often helpful to find a coordinate chart where the nature or existence of the singularities is much more obvious.

Solutions to Einstein's equations often exhibit singularities of one type or another, but just because a particular metric becomes singular at some point in spacetime does not necessarily mean that the solution breaks down at that point. Often a singularity is caused because the coordinate system of the metric is inappropriate to describe the space at that particular point. A simple example of this is the apparent singularity in the Schwarzschild metric, given by

$$\mathrm{d}s^2 = -\left(1 - \frac{2GM}{r}\right)\mathrm{d}t^2 + \left(1 - \frac{2GM}{r}\right)^{-1}\mathrm{d}r^2 + r^2\mathrm{d}\Omega^2\,, \tag{2.1}$$

where it appears that the g_{rr} coefficient blows up when $r = 2GM$. This has the consequence that, in these coordinates, it appears that an in-falling particle would

take an infinite time to cross the event horizon. In fact, this is simply a property of the t and r coordinates that the metric is usually expressed in. As shown in the following section, a change of coordinates shows that this point in spacetime is actually well behaved and any in-falling particle would continue across the event horizon without incident.

The apparent singularity in the Schwarzschild case is caused by the coordinate system breaking down at the horizon. This behaviour occurs at event horizons in many metrics, so the problem has been thoroughly investigated and many different techniques have been developed to generate coordinates which can be used to investigate regions of space where these coordinate singularities occur. In theory it is possible to investigate these coordinate singularities in a generic manner but this would be a very cumbersome way to go about it. The approach of this chapter is to look at some specific examples of coordinate systems for the Schwarzschild and Kerr metrics, since they are the most familiar static and rotating black holes and prove to be useful models of the problems encountered in more complicated metrics.

2.1 Coordinate Charts in the Schwarzschild Metric

In general it is difficult to exhaustively identify all of the possible singularities in a metric just by looking at it. In light of this, only singularities that are caused by one of the metric coefficients blowing up at a particular point will be considered. In the case of the Schwarzschild metric, in the r and t coordinates

$$\mathrm{d}s^2 = -\left(1 - \frac{2GM}{r}\right)\mathrm{d}t^2 + \left(1 - \frac{2GM}{r}\right)^{-1}\mathrm{d}r^2 + r^2\mathrm{d}\Omega^2 \,, \tag{2.2}$$

there are two possible points where there might be a problem with the metric coefficients becoming infinite. These are when $r = 0$ and when $r = 2GM$. Other than at these two points the metric appears to be well behaved.

One way of checking whether a singularity is a consequence of the actual spacetime, or just a problem with the coordinate chart, is to calculate the curvature of the metric at that particular point. The curvature of the space is measured by

the Riemann tensor but, as a tensor, it is difficult to decide when exactly this is infinite. Fortunately, it is possible to construct various different scalars using the Riemann tensor, which are easy to check whether they are infinite or not at the point in question. The simplest scalar that can be constructed from the Riemann tensor is the Ricci scalar, which is formed by contracting the Ricci tensor, giving $R = g^{\mu\nu}R_{\mu\nu}$, but it is also possible to produce higher order scalars by constructing various other contractions. For example, it is possible to multiply the Ricci scalar with itself, giving $R^{\mu\nu}R_{\mu\nu}$, or contracting over three occurrences of the Riemann tensor $R_{\mu\nu\rho\sigma}R^{\rho\sigma\lambda\tau}R_{\lambda\tau}{}^{\mu\nu}$ and so on. This condition is sufficient to identify a physical singularity in the metric, rather than a singularity in the coordinate system, but it is not a necessary condition.

To check whether the singularity at $r = 0$ is a physical singularity, form the scalar $R^{\mu\nu\rho\sigma}R_{\mu\nu\rho\sigma}$, giving

$$R^{\mu\nu\rho\sigma}R_{\mu\nu\rho\sigma} = \frac{48G^2M^2}{r^6} \,. \tag{2.3}$$

Substituting $r = 0$ into this expression shows immediately that the curvature scalar blows up and thus that the singularity at this point is a physical singularity. Since this singularity is a consequence of the actual spacetime, rather than the coordinate system, it will appear no matter what coordinates are used to span the spacetime.

The other possible singularity is when $r = 2GM$. After calculating all the other curvature scalars it is possible to show that they are all finite at $r = 2GM$, which indicates that this particular singularity is not an inherent property of the spacetime, so may well be a coordinate singularity. Indeed, as will be seen, it is possible to find some new coordinates where this point is completely well behaved.

2.1.1 Eddington-Finkelstein Coordinates

To get an idea of what is happening when approaching $r = 2GM$, consider radial null curves for which

$$\frac{\mathrm{d}t}{\mathrm{d}r} = \pm\left(1 - \frac{2GM}{r}\right)^{-1} \,. \tag{2.4}$$

It is obvious that there is a problem with these coordinates because as $r \to 2GM$, $\mathrm{d}t/\mathrm{d}r \to \infty$, which means that it would take an infinite time for a light ray to get

to this point but, from the calculations of the curvature, there doesn't appear to be anything special about $r = 2GM$. One way around this particular problem is to define a tortoise coordinate r^* [30], so that

$$r^* = r + 2GM \ln\left(\frac{r}{2GM} - 1\right) . \tag{2.5}$$

In terms of this new coordinate the Schwarzschild metric becomes

$$\mathrm{d}s^2 = \left(1 - \frac{2GM}{r}\right)\left(-\mathrm{d}t^2 + \mathrm{d}r^{*2}\right) + r^2\mathrm{d}\Omega^2 , \tag{2.6}$$

where r is now a function of r^*. The metric is now completely well behaved at $r = 2GM$ but both g_{tt} and $g_{r^*r^*}$ go to zero. Furthermore, the surface at $r = 2GM$ is now given by $r^* = -\infty$, which defeats the object of changing the coordinates in the first place. Clearly a slightly different coordinate transformation is required.

In terms of the r^* coordinate, the null radial geodesics are given by

$$t = \pm r^* + \text{constant} \tag{2.7}$$

so, to follow these geodesics, it is a good idea to define a new coordinate

$$v = t + r^* . \tag{2.8}$$

Now, the infalling radial null geodesics are defined by constant values of v. If this coordinate is then used in place of t in (2.2) the metric becomes

$$\mathrm{d}s^2 = -\left(1 - \frac{2GM}{r}\right)\mathrm{d}v^2 + 2\mathrm{d}v\mathrm{d}r + r^2\mathrm{d}\Omega^2 . \tag{2.9}$$

This is exactly what is required as none of the metric coefficients blow up at $r = 2GM$ and although $g_{vv} \to 0$, the determinant of the metric is non-zero, meaning that the inverse metric is also perfectly well defined. These (v, r) coordinates are known as the Eddington-Finkelstein coordinates.

2.1.2 Kruskal Coordinates

In the derivation of the Eddington-Finkelstein coordinates, it was assumed that only ingoing geodesics were being considered. For outgoing geodesics, where $t = r^* + \text{constant}$, the analogue of equation (2.4) in the (v, r) coordinates is

$$\frac{\mathrm{d}v}{\mathrm{d}r} = 2\left(1 - \frac{2GM}{r}\right)^{-1} , \tag{2.10}$$

which again blows up at $r = 2GM$. It is possible to define a version of the Eddington-Finkelstein coordinates in terms of an outgoing null coordinate $u = t - r^*$ using the same method as above, but this will then breakdown when considering ingoing null geodesics. It is clearly desirable to have a coordinate system where both ingoing and outgoing geodesics can be considered simultaneously. This is where the Kruskal coordinates come in.

To construct the Kruskal coordinates, start by defining two new null coordinates

$$v' = e^{v/4GM}, \qquad u' = -e^{-u/4GM}, \tag{2.11}$$

where u and v are defined as before. In terms of these coordinates, the Schwarzschild metric becomes

$$\mathrm{d}s^2 = -\frac{32G^3M^3}{r}e^{-r/2GM}\mathrm{d}v'\mathrm{d}u' + r^2\mathrm{d}\Omega^2 , \tag{2.12}$$

where r is now defined implicitly in terms of u and v by

$$\frac{1}{2}(v-u) = r + 2GM\ln\left(\frac{r}{2GM} - 1\right) . \tag{2.13}$$

A quick examination of this metric shows that all of the coefficients are well behaved at $r = 2GM$ and, because both the null coordinates have been used, it is possible to follow both the infalling and outgoing geodesics across the surface at $r = 2GM$. There is a slight problem with this metric, however, in that it no longer has a timelike coordinate - just two null coordinates. There is no reason why it should have a timelike coordinate but, from a conceptual point of view, it is easier to work with a metric that has the usual one timelike and three spacelike directions.

Fortunately, it is possible to combine the null coordinates to produce a timelike coordinate and a radial coordinate, without compromising any of the desirable properties of the metric. To do this form

$$T = \frac{1}{2}(v' + u') , \qquad R = \frac{1}{2}(v' - u') . \tag{2.14}$$

In terms of these coordinates the metric becomes

$$\mathrm{d}s^2 = \frac{32G^3M^3}{r}e^{-r/2GM}\left(-\mathrm{d}T^2 + \mathrm{d}R^2\right) + r^2\mathrm{d}\Omega^2 . \tag{2.15}$$

These (T, R) coordinates are the Kruskal coordinates and define r implicitly as

$$T^2 - R^2 = \left(1 - \frac{r}{2GM}\right)e^{r/2GM} . \tag{2.16}$$

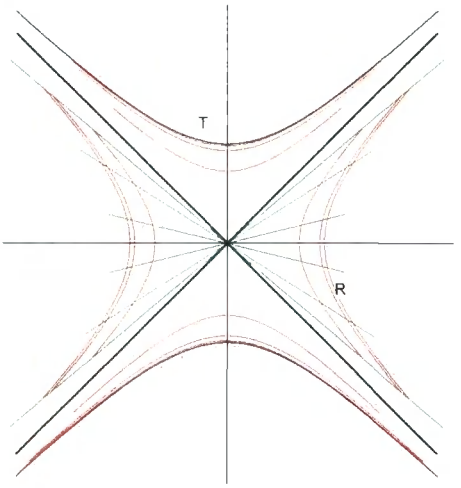

Figure 2.1: Kruskal diagram with the curves of constant t plotted in green and the curves of constant r plotted in red. The past and future event horizons are given by the thick black lines, with the thin black lines indicating $r = 0$.

Figure 2.1 plots the Kruskal coordinates for a range of different values of r and t. In the Kruskal coordinates, the null curves are given by

$$T = \pm R + \text{constant} \,, \tag{2.17}$$

where the past and future event horizons are defined by $T = \pm R$. It is obvious from the Kruskal diagram in figure 2.1 that these event horizons separate the space up into four distinct sections: the right hand sector represents the starting space outside the horizon, the bottom and top sectors represent the white hole and the black hole respectively, and the left hand sector represents the parallel asymptotically flat space outside the horizon. The left hand sector can only be accessed by following spacelike geodesics through the event horizon, so is inaccessible to physical particles.

The hyperbolas of constant r are plotted at constant intervals in r, so it can be seen that the space has been warped. It is stretched as it approaches the horizons with the hyperbolas asymptoting to the horizon with increasing t. Indeed, the surfaces of constant t are given by straight lines through the origin with equation

$$\frac{T}{R} = \tanh\left(\frac{t}{4GM}\right) \,, \tag{2.18}$$

so it can be seen that as $t \to \infty$, the above equation becomes $T = R$, which is the same as the equation for the future event horizon.

The equation of the hyperbolas can be determined from (2.16), where r is constant, so

$$T^2 - R^2 = \text{constant} \, . \tag{2.19}$$

This can be used to calculate the limits on R and T, since R and T can take every value outside of the curvature singularity at $r = 0$. This gives the limits on R and T as

$$-\infty \leq R \leq \infty, \qquad T^2 < R^2 + 1 \, . \tag{2.20}$$

2.2 Coordinate Charts in the Kerr Metric

The addition of angular momentum to the black hole makes the structure of the spacetime significantly more complex. The Kerr metric has two event horizons where there are coordinate singularities as well as having a curvature singularity that is no longer a point but a ring. These qualitative differences from the Schwarzschild solution mean that more coordinate systems have been developed in order to examine the different properties. Some of these coordinate systems are explored in the following sections.

2.2.1 Kerr-Schild Form of the Metric

This coordinate system was described in [28] to aid in the analysis of the Kerr metric, although the basic principle can be generalised to describe any spinning black holes. The idea of the Kerr-Schild coordinate transformations is to express the metric in the form

$$g_{\mu\nu} = \eta_{\mu\nu} + S(x^a) k_\mu k_\nu \, , \tag{2.21}$$

where k_μ is defined as a null vector with respect to the Minkowski metric $\eta_{\mu\nu}$ and $S(x^a)$ is a function that is to be determined.

The Kerr-Schild form of the metric is particularly useful because the covector k_μ is also null with respect to the full metric $g_{\mu\nu}$. To show that $g_{\mu\nu} k^\mu k^\nu = 0$ it is useful to invert (2.21) as follows

$$g^{\lambda\mu} g_{\mu\nu} = g^{\lambda\mu} \eta_{\mu\nu} + S(x^a) g^{\lambda\mu} k_\mu k_\nu \equiv \delta^\lambda_\nu$$

$$\begin{aligned} \eta^{\sigma\nu}g^{\lambda\mu}\eta_{\mu\nu} + S(x^a)k^\lambda\eta^{\sigma\nu}k_\nu &= \eta^{\sigma\nu}\delta^\lambda_\nu \\ g^{\lambda\mu}\delta^\sigma_\mu + S(x^a)k^\lambda\eta^{\sigma\nu}k_\nu &= \eta^{\sigma\lambda} \\ g^{\lambda\sigma} + S(x^a)k^\lambda\eta^{\sigma\nu}k_\nu &= \eta^{\sigma\lambda} \\ g^{\lambda\sigma} &= \eta^{\lambda\sigma} - S(x^a)k^\lambda\eta^{\sigma\nu}k_\nu \,. \end{aligned} \tag{2.22}$$

This can now be used to raise an index on the null vector k_μ giving

$$k^\mu = g^{\mu\nu}k_\nu = \eta^{\mu\nu}k_\nu - Sk^\mu\eta^{\nu\sigma}k_\sigma k_\nu \,. \tag{2.23}$$

Since k_μ is null with respect to the Minkowski metric, the second term must go to zero, leaving

$$k^\mu = \eta^{\mu\nu}k_\nu \,. \tag{2.24}$$

It is now possible to show that k_μ is null with respect to the full metric $g_{\mu\nu}$, as follows

$$\begin{aligned} g_{\mu\nu}k^\mu k^\nu &= k^\mu k_\mu \\ &= \eta^{\mu\nu}k_\nu k_\mu \\ &= 0 \,, \end{aligned} \tag{2.25}$$

where the fact that k_μ is null with respect to $\eta_{\mu\nu}$ is again used in the last line.

To show that the Kerr-Schild coordinate transformations give the metric in the form given in (2.21), consider the Kerr metric in Boyer-Lindquist coordinates

$$\mathrm{d}s^2 = -\mathrm{d}t^2 + (r^2+a^2)\sin^2\theta\mathrm{d}\phi^2 + \frac{\Sigma}{\Delta}\mathrm{d}r^2 + \Sigma\mathrm{d}\theta^2 + \frac{2Mr}{\Sigma}\left[\mathrm{d}t - a\sin^2\theta\mathrm{d}\phi\right]^2 \,, \tag{2.26}$$

where

$$\Delta(r) = r^2 - 2Mr + a^2 \tag{2.27}$$

$$\Sigma(r,\theta) = r^2 + a^2\cos^2\theta \,. \tag{2.28}$$

The event horizons, which only exist for $a < M$, are given by calculating when $\Delta = 0$ and thus are given by

$$r_\pm = M \pm \sqrt{M^2 - a^2} \,. \tag{2.29}$$

Now, the Kerr-Schild transformations can be given by

$$(x+iy) = (r+ia)\sin\theta\exp\left[i\int\left(\mathrm{d}\phi+\frac{a}{\Delta}\mathrm{d}r\right)\right] \tag{2.30}$$

$$z = r\cos\theta \tag{2.31}$$

$$\tilde{t} = \int\left(\mathrm{d}t+\frac{r^2+a^2}{\Delta}\mathrm{d}r\right)-r\ . \tag{2.32}$$

To get to the Kerr-Schild metric, form

$$rx+ay = (r^2+a^2)\sin\theta\cos\left(\phi+\int\frac{a}{\Delta}\mathrm{d}r\right) \tag{2.33}$$

$$ry-ax = (r^2+a^2)\sin\theta\sin\left(\phi+\int\frac{a}{\Delta}\mathrm{d}r\right) \tag{2.34}$$

These equations can then be used to solve for $\sin^2\theta$, giving

$$\sin^2\theta = \frac{x^2+y^2}{r^2+a^2}\ . \tag{2.35}$$

Also, from (2.32), $\mathrm{d}\tilde{t}$ is given by

$$\mathrm{d}\tilde{t} = dt+\frac{2Mr}{\Delta}\,\mathrm{d}r\ . \tag{2.36}$$

The transformations given in (2.30) and (2.31) allow $\mathrm{d}r$ to be given by

$$\mathrm{d}r = \frac{r\mathrm{d}x+r\mathrm{d}y}{\Sigma}+(r^2+a^2)\frac{z}{r\Sigma}\,\mathrm{d}z\ . \tag{2.37}$$

It is possible to define $\mathrm{d}\phi$ in a similar manner as

$$\mathrm{d}\phi = -\frac{2Mar}{(r^2+a^2)\Delta}\mathrm{d}r+\frac{x\mathrm{d}y-y\mathrm{d}x}{(r^2+a^2)\sin^2\theta}\ . \tag{2.38}$$

Equation (2.31) is now used to give the other required transformation

$$\mathrm{d}z = \cos\theta\mathrm{d}r-r\sin\theta\mathrm{d}\theta\ . \tag{2.39}$$

Combining these expressions gives

$$\begin{aligned}\frac{\Sigma}{r^2+a^2}\,\mathrm{d}r &+ \frac{2Ma^2r\sin^2\theta}{\Delta(r^2+a^2)}\mathrm{d}r+\frac{2Mr}{\Delta}\mathrm{d}r+\mathrm{d}t-a\sin^2\theta\mathrm{d}\phi \\ &= \left[\frac{r(x\mathrm{d}x+y\mathrm{d}y)-a(x\mathrm{d}y-y\mathrm{d}x)}{r^2+a^2}+\frac{z\mathrm{d}z}{r}+\mathrm{d}\tilde{t}\right]\end{aligned} \tag{2.40}$$

The left hand side now gives the two terms in the square bracket in (2.26), along with some additional terms, but these will cancel out later.

Equations (2.37) and (2.38) can be used to get expressions for $\mathrm{d}x^2$ and $\mathrm{d}y^2$, which can then be summed with the expressions for $\mathrm{d}z^2$ and $-\mathrm{d}\tilde{t}^2$, giving

$$\begin{aligned}\mathrm{d}x^2+\mathrm{d}y^2+\mathrm{d}z^2-\mathrm{d}\tilde{t}^2 &= -\mathrm{d}t^2+\left(1-\frac{4M^2r^2}{\Delta^2}\right)\frac{\Sigma}{r^2+a^2}\,\mathrm{d}r^2+(r^2+a^2)\sin^2\theta\mathrm{d}\phi^2 \\ &\quad +\Sigma\mathrm{d}\theta^2+\left(a\sin^2\theta\mathrm{d}\phi-\mathrm{d}t\right)\frac{4Mr}{\Delta}\,\mathrm{d}r\,. \end{aligned} \tag{2.41}$$

Squaring (2.40) and then combining with (2.41), allows the metric given in (2.26) to be expressed in the Kerr-Schild form, given by

$$\mathrm{d}s^2=-\mathrm{d}\tilde{t}^2+\mathrm{d}x^2+\mathrm{d}y^2+\mathrm{d}z^2+\frac{2Mr^3}{r^4+a^2z^2}\left[\frac{r(x\mathrm{d}x+y\mathrm{d}y)-a(x\mathrm{d}y-y\mathrm{d}x)}{r^2+a^2}+\frac{z\mathrm{d}z}{r}+\mathrm{d}\tilde{t}\right]^2 \tag{2.42}$$

and it is now obvious that the metric is in the form

$$g_{\mu\nu}=\eta_{\mu\nu}+S(x^a)k_\mu k_\nu \tag{2.43}$$

where

$$S(x^a)=\frac{2Mr^3}{r^4+a^2z^2} \tag{2.44}$$

and

$$k_\mu=\left(1,\frac{(rx+ay)}{(r^2+a^2)},\frac{(ry-ax)}{(r^2+a^2)},\frac{z}{r}\mathrm{d}z\right)\,. \tag{2.45}$$

Given the metric in the Kerr-Schild form, it is simple to see that the spacetime approaches Minkowski space as $M\to 0$. This is because the mass acts as a scale parameter for all the terms inside the square brackets so setting $M=0$ makes the solution identical to the Minkowski metric, as expected.

To check that k_μ is null, form

$$\eta^{\mu\lambda}k_\lambda=\left[-1,\frac{(rx+ay)}{(r^2+a^2)},\frac{(ry-ax)}{(r^2+a^2)},\frac{z}{r}\mathrm{d}z\right]\,. \tag{2.46}$$

Multiplying by k_μ and contracting the indices then gives

$$\eta^{\mu\nu}k_\mu k_\nu=\eta_{\mu\nu}k^\mu k^\nu=\frac{(rx+ay)^2}{(r^2+a^2)^2}+\frac{(ry-ax)^2}{(r^2+a^2)^2}+\frac{z^2}{r^2}-1 \tag{2.47}$$

Using (2.35) and (2.31) gives

$$\eta_{\mu\nu}k^\mu k^\nu=\frac{(r^2+a^2)^2\sin^2\theta}{(r^2+a^2)^2}+\cos^2\theta-1=0 \tag{2.48}$$

Thus confirming that k^μ is a null vector with respect to the Minkowski metric.

The Kerr-Schild form of the metric uses Cartesian coordinates which don't have a coordinate singularity when $\theta = 0$ i.e. on the axis of symmetry, like the polar coordinates do. They also allow easy analysis of the curvature singularity when $\Sigma = 0$. This is because Σ is defined to be the sum of two manifestly positive terms, r^2 and $a^2\cos^2\theta$, so it can only be zero if r and $\theta = 0$. This corresponds to a ring, which is given by $x^2 + y^2 = a^2$ and $z = 0$ in the Cartesian coordinates.

2.2.2 Kerr Coordinates

As previously mentioned, the Kerr metric when $M^2 > a^2$ has two coordinate singularities at the two event horizons $r_\pm$, where $r_\pm$ are the points where $\Delta = 0$. To be able to analyse the Kerr black hole without having to worry about these coordinate singularities it is useful to introduce another set of coordinate transformations, so that none of the metric coefficients become infinite on either of the horizons. To find these transformations, consider two new coordinates, v and χ, given by

$$t = v - g(r) \qquad\qquad \phi = \chi + h(r)\ . \tag{2.49}$$

Using these to transform the Kerr metric gives

$$\begin{aligned} \mathrm{d}s^2 \;=\; & -\left(1 - \frac{2Mr}{\Sigma}\right)\left(\mathrm{d}v^2 + g'^2\mathrm{d}r^2 - 2g'\mathrm{d}v\mathrm{d}r\right) + \frac{\Sigma}{\Delta}\mathrm{d}r^2 + \Sigma\mathrm{d}\theta^2 \\ & + \left[\frac{(r^2+a^2)\Sigma + 2Mra^2\sin^2\theta}{\Sigma}\right]\sin^2\theta\left(\mathrm{d}\chi^2 + h'^2\mathrm{d}r^2 + 2h'\mathrm{d}\chi\mathrm{d}r\right) \\ & - \frac{4Mra\sin^2\theta\left(\mathrm{d}v\mathrm{d}\chi - g'\mathrm{d}\chi\mathrm{d}r + h'\mathrm{d}v\mathrm{d}r - g'h'\mathrm{d}r^2\right)}{\Sigma} \end{aligned} \tag{2.50}$$

The idea of this coordinate transformation is to adapt the coordinates so that they are naturally suited to null geodesics and thus don't exhibit any coordinate singularities at the event horizon. In order to achieve this, choose (2.50) so that it satisfies $g_{rr} = 0$ and $g_{vr} = 1$, which corresponds to ingoing null geodesics. Applying these constraints then allows the functions $g(r)$ and $h(r)$ to be determined so that

$$t = v + \sigma\int\frac{r^2+a^2}{\Delta}\,\mathrm{d}r \qquad\qquad \phi = \chi - \int\frac{a}{\Delta}\,\mathrm{d}r \tag{2.51}$$

where the signs have been chosen to coincide with ingoing geodesics and σ is determined so that Δ remains positive in the different regions of the space. This means

that σ is given by

$$\sigma = \begin{cases} -1 & (r > r_+) \\ +1 & (r_- < r < r_+) \\ -1 & (r < r_-) \end{cases} .$$

The metric in terms of the new coordinates is then given by

$$\begin{aligned} \mathrm{d}s^2 &= -\frac{(\Delta - a^2 \sin^2\theta)}{\Sigma}\mathrm{d}v^2 + 2\mathrm{d}v\mathrm{d}r - \frac{4Mra\sin^2\theta}{\Sigma}\mathrm{d}v\mathrm{d}\chi + \Sigma\mathrm{d}\theta^2 \\ &\quad -2a\sin^2\theta\mathrm{d}\chi\mathrm{d}r + \frac{\left[(r^2+a^2)^2 - \Delta a^2\sin^2\theta\right]}{\Sigma}\sin^2\theta\mathrm{d}\chi^2 . \end{aligned} \tag{2.52}$$

This new coordinate system is analogous to the Eddington-Finkelstein coordinate system for the Schwarzschild metric and behaves in the same way at the two horizons. It is easy to see, from this form of the metric, that none of the metric coefficients are singular when $\Delta = 0$.

2.2.3 Hayward Coordinates

Although the Kerr coordinates described in the previous section are very useful for following geodesics falling into the Kerr black hole, since the coordinate singularity at the event horizon has been removed, they aren't particularly useful for constructing Penrose diagrams (discussed later). This is because the coordinates only describe future directed paths and have to be adapted in order to follow past directed paths. This is simple to achieve but having to use two different coordinate systems on the same diagram causes more problems than it solves. What is needed is a generalisation of the Kruskal coordinates, which are used to maximally extend the Schwarzschild spacetime, so that the different varieties of geodesics can be followed to all of the permissible connected spacetime regions.

Fortunately, suitable coordinates that generalise Kruskal's coordinates for the Kerr metric are given in [29]. The transformations are detailed in two steps: the first step is to transform the (t, r, θ, ϕ) coordinates such that

$$t^* = t - a\sin\theta , \tag{2.53}$$

$$r^* = \int \frac{R^2}{\Delta}\mathrm{d}r , \tag{2.54}$$

$$\varphi = \phi - \Omega_+(t - a\sin\theta) , \tag{2.55}$$

and θ remains unchanged. The constant $\Omega_+ = a/2Mr_+$ is the angular velocity of the outer event horizon and

$$R(r) = \left[(r^2+a^2)^2 - a^2\Delta\right]^{1/4} = (r^4 + a^2r^2 + 2Ma^2r)^{1/4} . \tag{2.56}$$

These coordinate transformations ensure that the combination $r^* \pm t^*$ is null and thus generates two null coordinates analogous to those used to define the Kruskal coordinates.

The major difference between the generation of these coordinates and those of Kruskal is the introduction of the t^* coordinate. This coordinate transformation removes the dependence of $\mathrm{d}r^*$ on the θ terms, leaving r^* as a function of r alone. The r^* function can then be integrated to give an explicit expression (although not a particularly succinct one) in terms of r. The new coordinate r^* can then be thought of as the Kerr analogue of the well known Regge-Wheeler tortoise coordinate [30], which behaves so that $r^* \to -\infty$ as $r \to r_+$.

The transformation in the ϕ direction is necessary so that φ is normal to the horizon generating Killing vector $\chi = \partial_t + \Omega_+\partial_\phi$ for all radii. This contrasts with the coordinate transformation

$$\varphi = \phi - \Omega_+ t , \tag{2.57}$$

which is also normal to χ near r_+ but is no longer spatial when r becomes large [29]. The original coordinate transformation, given in (2.55), can be thought of as the natural normal vector to χ after allowing for the transformation in the t coordinate.

The second step toward finding generalised Kruskal coordinates for Kerr, is simply to exponentiate the newly found normal vectors, giving

$$x^\pm = \pm e^{\kappa(r^* \pm t^*)} , \tag{2.58}$$

where κ is the surface gravity on the event horizon. These two null coordinates now vary between 0 and $\pm\infty$ for $x^\pm$ respectively, with the event horizon given when $x^\pm = 0$. To generate well behaved timelike and spacelike "Kruskalesque" coordinates it is now simply a matter of combining the two null coordinates so that

$$T = \frac{1}{2}(x^+ + x^-) , \qquad R = \frac{1}{2}(x^+ - x^-) . \tag{2.59}$$

These coordinates will now cover the spacetime region outside of the inner event horizon. In order to consider the regions of space inside the inner event horizon it is necessary to use a different coordinate patch.

So far, it has been assumed that the region outside of the inner event horizon is being considered. To cover the region within the inner event horizon (up to the asymptotically flat region for $r < 0$) it isn't necessary to re-derive the coordinate transformations because the only differences are that the angular velocity of the outer horizon Ω_+ becomes that of the inner horizon given by $\Omega_- = a/2Mr_-$, and the surface gravity κ becomes that of the inner horizon $\kappa = -\sqrt{M^2 - a^2}/2Mr_-$. This new coordinate patch will now cover the region inside the outer event horizon, right through the ring singularity at $r = 0$ to an asymptotically flat space parameterised by negative r.

Having constructed some coordinates that replicate the Kruskal coordinates of the Schwarzschild metric, it is now possible to follow the causal paths of ingoing and outgoing test particles using the same coordinate system. This is a significant improvement on the original (t, r) coordinate system because it is now possible to easily investigate the causal behaviour of particles as they cross the event horizon - provided the correct coordinate transformations are used for the inner and outer horizons. The fact that the coordinate transformations differ slightly when considering the two different event horizons is a slight drawback, but if only causal paths in the vicinity of one of the horizons are being considered then this doesn't cause a problem.

If it is necessary to follow geodesics through both the inner and outer horizons then the Kerr coordinates are significantly simpler to use since the coordinate transformations only change sign upon crossing a horizon. This means that it is a lot easier to match up the different coordinate patches than for the Hayward coordinates, where the coordinates are dependent upon the angular velocity and surface gravity of the event horizon under consideration. The fact that the Kerr coordinate charts don't overlap at any point means that they are also a lot more straightforward to use than the Hayward coordinates, although they are limited in only being applicable to geodesics going in one direction.

Chapter 3

Generating Five Dimensional Black Hole Solutions

In this chapter, some methods for generating higher dimensional black hole solutions are looked at, with the Myers Perry black hole, and the singly and doubly spinning black rings used as examples to show how the vacuum Einstein equations can be solved. A wide range of different methods to solve the Einstein equations exist, due mainly to the non-linear nature of the equations and the fact that many of the methods that have already been developed have a very limited range of applicability. In practice this means that the equations have to be simplified by making a number of assumptions. For example, just to derive the Schwarzschild metric, it is necessary to demand that the solution be Lorentzian, spherically symmetric, static, and that it reproduces Newtonian gravity in the weak-field limit. The Kerr solution [9] which uses similar assumptions, but only requires the solution to be stationary rather than static, took a further 47 years to discover after Schwarzschild [2] found the static solution to Einstein's equations.

Many algorithms for solving the Einstein equations also rely on having a known solution as a starting point, so their applicability is often heavily dependent on the starting solution. In practice this means that the new solutions will share many of the properties of the seed solution. This statement is particularly true for the Inverse Scattering Method, but it has recently been successfully used to gain a great deal of insight into five dimensional black hole solutions, so it is examined in some

detail in section 3.3.

This chapter also includes a section on Generalised Weyl solutions. This work has been carried out over the last few years by a few different authors and is so called because it builds upon an early result in General Relativity showing that in 4D all of the possible axisymmetric solutions to Einstein's vacuum equations can be expressed in a particular form that reduces the non-linear equations to a matter of considering infinitely thin rods acting like Newtonian potentials [33]. This result has been generalised to higher dimensions by Emparan and Reall originally [34] and further extended by Harmark [35], so their results are examined in section 3.2 as a precursor to the Inverse Scattering Method. The Inverse Scattering Method is useful for solving a wide range of differential problems, but it has been greatly refined over the last three decades as a method for solving axisymmetric solutions to the Einstein equations. In light of this, much of the formalism that is used for the Inverse Scattering algorithm comes from studying Weyl solutions.

3.1 Myers Perry Black Hole Solution

This section shows how the 4D Kerr black hole [9] was generalised to higher dimensions by Myers and Perry in [25]. Before Myers and Perry, the static Schwarzschild solution had been generalised to higher dimensions by Tangherlini in [32] but the higher dimensional analogues of the Kerr solution were considered of little physical interest and thus weren't investigated until the late eighties when the resurgence of String Theory prompted renewed interest in higher dimensional solutions.

The Kerr solution to the Einstein vacuum equations can be written

$$ds^2 = -dt^2+\sin^2\theta(\rho^2+a^2)d\phi^2+\Psi(dt+a\sin^2\theta d\phi)^2+\frac{\Delta(\rho,\theta)d\rho^2}{(\rho^2+a^2)-2GM\rho}+\Delta(\rho,\theta)d\theta^2 \tag{3.1}$$

where $\Delta(\rho,\theta)$ and Ψ are defined as

$$\Delta(\rho,\theta) = \rho^2+a^2\cos^2\theta \tag{3.2}$$

$$\Psi = \frac{2GM\rho}{\Delta(\rho,\theta)}, \tag{3.3}$$

and a is a constant which determines the angular momentum of the black hole. This

solution has only one plane of rotation, characterised by the cross terms involving the t and ϕ coordinates, but in higher dimensions it is possible to have more than one orthogonal plane and thus more than one plane of rotation. This is the major departure of the Myers Perry solution from the Kerr metric.

The Myers Perry solution is particularly useful in the study of black holes in higher dimensions by virtue of the fact that no matter what the topology of the solution, it should look like the Myers Perry solution at a large enough distance. This is because for a particular observer, any variations in the spacetime due to the geometry of the black hole will become more and more insignificant the further away from the black hole the observer is. If this is the case, then it is possible to ascertain many of the physical properties of non-spherical black holes by examining the properties of the Myers Perry metric at asymptotic infinity.

Most of the time it is suitable to use a system where the basis vectors are defined by the coordinates in use for a particular metric. However, especially when finding a metric solution, it is often more expeditious to work in a general orthonormal basis. The derivation of the Myers Perry solution is a good example of this, as it relies heavily on non-coordinate bases. In view of this, Appendix A gives some details and notation used with general orthonormal bases.

3.1.1 The N dimensional Myers Perry Solution

The most general metric for an $N+1$ spherical black hole is where the black hole is rotating in $\lfloor N/2 \rfloor$ planes. This means that the most general Myers Perry black hole will have $\lfloor N/2 \rfloor + 1$ parameters characterising the mass and various angular momenta parameters corresponding to rotation in the respective planes.

To derive the Myers Perry solution it is best to use Kerr-Schild coordinates so that the metric is written in the form

$$g_{\mu\nu} = \eta_{\mu\nu} + h k_\mu k_\nu \tag{3.4}$$

where k_μ is a null vector with respect to the Minkowski metric $\eta_{\mu\nu}$ (and also $g_{\mu\nu}$) and h is a function of r, x^i, and y^i.

The fact that the number of rotation planes is dependent on the integer part of

$N/2$ means that the odd N and even N cases have to be considered separately. For even N

$$k_\mu \mathrm{d}x^\mu = \mathrm{d}t + \sum_i^{N/2} \frac{r(x^i \mathrm{d}x^i + y^i \mathrm{d}y^i) + a_i(x^i \mathrm{d}y^i - y^i \mathrm{d}x^i)}{r^2 + {a_i}^2} \tag{3.5}$$

and

$$h = \frac{\mu r^2}{\Pi F} , \tag{3.6}$$

where

$$F = 1 - \sum_i^{N/2} \frac{{a_i}^2({x^i}^2 + {y^i}^2)}{(r^2 + {a_i}^2)^2} \tag{3.7}$$

$$\Pi = \prod_{i=1}^{(N-1)/2} \left(r^2 + {a_i}^2\right) , \tag{3.8}$$

and μ is a constant given by

$$\mu = \frac{16\pi GM}{(N-1)A_{N-1}} , \tag{3.9}$$

where G is Newton's gravitational constant, M is the black hole mass, and A_N is the surface area of a unit N-sphere.

The coordinate r that appears in the above equations can be defined in terms of x^i and y^i by the fact that k_μ is a null covector, i.e.

$$\sum_i^{N/2} \frac{({x^i}^2 + {y^i}^2)}{(r^2 + {a_i}^2)} = 1 . \tag{3.10}$$

The x^i and y^i coordinates in (3.5)-(3.10) can be paired up because N is even, so the sets of coordinates can be given by $x^k = \{x^i, y^i\}$.

In the case where N is odd, k_μ is defined by

$$k_\mu \mathrm{d}x^\mu = \mathrm{d}t + \sum_i^{(N-1)/2} \frac{r(x^i \mathrm{d}x^i + y^i \mathrm{d}y^i) + a_i(x^i \mathrm{d}y^i - y^i \mathrm{d}x^i)}{r^2 + {a_i}^2} + \frac{z\mathrm{d}z}{r} \tag{3.11}$$

and

$$h = \frac{\mu r}{\Pi F} \tag{3.12}$$

where Π and F are the same as in (3.8) and (3.7), but the index i has to now take the values $i = 1, ..., (N-1)/2$ in (3.7). The definition of the radial coordinate r also changes, it is now defined by

$$\sum_i^{(N-1)/2} \frac{({x^i}^2 + {y^i}^2)}{(r^2 + {a_i}^2)} + \frac{z^2}{r^2} = 1 . \tag{3.13}$$

The definitions for the odd N case are similar to the even case but have to be altered to take account of an extra unpaired coordinate which is denoted z.

Having defined the associated expressions for suitable Kerr-Schild coordinates it is necessary to lay out some further formalism in order to solve the Einstein equations. This is mainly taken from [25] which was in turn generalised from [28]. For the case where N is odd, consider the metric

$$\mathrm{d}s^2 = -\mathrm{d}t^2 + \mathrm{d}x^{i2} + \mathrm{d}y^{i2} + \mathrm{d}z^2 + 2H\left(\tilde{k}_\mu \mathrm{d}x^\mu\right)^2 \tag{3.14}$$

where H is a function to be determined and $\tilde{k}_\mu$ is related to the null vector given in (3.11) by

$$\tilde{k}_\mu \mathrm{d}x^\mu = n k_\mu \mathrm{d}x^\mu \tag{3.15}$$

where n is a normalisation factor given by

$$n = \frac{\sqrt{2}r}{r+z} \tag{3.16}$$

and the condition that $\tilde{k}_\mu$ is null is given by (3.13). The normalisation of the null vector allows the introduction of two light-like coordinates in a simple form, given by

$$\sqrt{2}u = t + z \qquad\qquad \sqrt{2}v = t - z\,. \tag{3.17}$$

Using these light-like coordinates it is now possible to choose some simple basis forms

$$E^u = \tilde{k}_\mu \mathrm{d}x^\mu = \mathrm{d}u + A^k \mathrm{d}x^k + \frac{1}{2}(A^k)^2 \mathrm{d}v \tag{3.18}$$

$$E^v = \mathrm{d}v - HE^u \tag{3.19}$$

$$E^k = \mathrm{d}x^k + A^k \mathrm{d}v \tag{3.20}$$

where k takes the values so that $x^k = \{x^i, y^i\}$ with $i = 1, ..., (N-1)/2$. The coefficients A^k are defined as

$$A^k = \begin{cases} n\tilde{A}^i = \frac{\sqrt{2}r\left(rx^i - a_i y^i\right)}{(r+z)(r^2+a_i{}^2)} & \text{when } x^k = x^i \\ n\tilde{B}^i = \frac{\sqrt{2}r\left(ry^i + a_i x^i\right)}{(r+z)(r^2+a_i{}^2)} & \text{when } x^k = y^i \end{cases} . \tag{3.21}$$

The benefit of this choice of basis forms is that the metric takes a simple null form given by

$$\eta_{ab} = \begin{pmatrix} 0 & -1 & & \\ -1 & 0 & & \\ & & & \\ & & & \delta_{kl} \end{pmatrix} \tag{3.22}$$

Having defined a set of basis forms $E^a = e^a_\mu dx^\mu$, it is now possible to calculate the dual basis vectors given by

$$D \equiv D_v = \frac{\partial}{\partial v} - A^k \frac{\partial}{\partial x^k} + \frac{1}{2}(A^k)^2 \frac{\partial}{\partial u} \tag{3.23}$$

$$\Delta \equiv D_u = \frac{\partial}{\partial u} + H D_v \tag{3.24}$$

$$\delta^k \equiv D_k = \frac{\partial}{\partial x^k} - A^k \frac{\partial}{\partial u} \,. \tag{3.25}$$

Note that with these basis vectors, $DA^k = 0$, which implies that the null vector field is geodesic. It is now possible to calculate the non-zero components of the Ricci tensor in the new basis

$$R^v{}_v = R^u{}_u = DDH + \delta^l A^k \delta^l A^k H - \delta^l A^k A^l H - \delta^l A^l DH \tag{3.26}$$

$$R^v{}_u = \delta^l \delta^l H + 2H\Delta A^l \Delta A^l - 2\delta^l (H \Delta A^l) - \delta^l A^l (\Delta - HD) H \tag{3.27}$$

$$\begin{aligned} R^v{}_k = {} & \delta^k DH - DH\Delta A^k - 2H\Delta A^l \delta^l A^k \\ & + 2\delta^l H \delta^l A^k - \delta^k H \delta^l A^l + H(\delta^l \delta^l A^k - \delta^k \delta^l A^l) \end{aligned} \tag{3.28}$$

$$R^l{}_k = -(DH - H\delta^m A^m)(\delta^l A^k + \delta^k A^l) - 2H\delta^m A^l \delta^m A^k \,. \tag{3.29}$$

At this point H can be determined by considering any of the Ricci equations because $R_{\mu\nu} = 0$ for the vacuum Einstein equations. In practice it is simplest to consider (3.29) because it only involves first order derivatives in H. Re-writing this equation and setting it equal to zero gives

$$\frac{DH}{H} - \delta^m A^m + \frac{\delta^m A^l \delta^m A^k}{\delta^{(l} A^{k)}} = 0 \,, \tag{3.30}$$

where neither l or k are summed. For this equation to have a solution for H the third term on the left hand side must be the same for all l and k. Checking this shows that

$$\frac{\delta^m A^l \delta^m A^k}{\delta^{(l} A^{k)}} = \frac{\sqrt{2}}{r+z} \equiv \frac{n}{r} \tag{3.31}$$

which verifies that a solution for H exists. In order to find a solution for H, the second term also has to be calculated giving

$$\delta^m A^m = 2nr \left(\sum_{i=1}^{(N-1)/2} \frac{1}{r^2 + {a_i}^2} + \frac{N_3}{F} \right) , \tag{3.32}$$

where F is given in (3.7) and N_3 is given by

$$N_3 = \sum_{i}^{(N-1)/2} \frac{{a_i}^2(x^{i2} + y^{i2})}{(r^2 + {a_i}^2)^3} \equiv \sum_{i}^{(N-1)/2} \frac{{a_i}^2 {\mu_i}^2}{(r^2 + {a_i}^2)^2} . \tag{3.33}$$

Now, to calculate H it is simply a matter of substituting (3.32) and (3.31) into (3.30). Doing this shows that H is

$$H = \frac{1}{2} \left(\frac{r+z}{r\sqrt{2}} \right)^2 \frac{\mu r}{\Pi F} \equiv \frac{h}{2n^2} . \tag{3.34}$$

Having found H it is now necessary to make sure that it also satisfies the other Einstein equations.

Proving that $R^v{}_v$ and $R^u{}_u$ are satisfied for the function of H given in (3.34) is quite straightforward. Using the Ricci equations it is possible to show that

$$DH = H \left(\delta^m A^m - \frac{\sqrt{2}}{r+z} \right) \tag{3.35}$$

$$D\delta^m A^m = [D, \delta^m] A^m = \delta^m A^l \delta^l A^m \tag{3.36}$$

$$D\frac{\sqrt{2}}{r+z} = \frac{2}{(r+z)^2} . \tag{3.37}$$

Using these equations it is possible to show that

$$DDH = DH \left(\delta^m A^m - \frac{\sqrt{2}}{r+z} \right) + H \left(\delta^m A^l \delta^l A^m - \frac{2}{(r+z)^2} \right) \tag{3.38}$$

and thus

$$R^v{}_v = -\frac{\sqrt{2}}{r+z} \left(DH - \delta^m A^m H + \frac{\sqrt{2}}{r+z} H \right) = 0 , \tag{3.39}$$

which verifies that the $R^u{}_u$ and $R^v{}_v$ Ricci equations are satisfied when $R^l{}_k = 0$.

Checking that the $R^v{}_k$ and $R^v{}_u$ components also goes to zero is a slightly lengthier process, but they can be shown to be zero by considering the Bianchi identities $\nabla_\mu (R^\mu_\nu - \frac{1}{2}\delta^\mu_\nu R) = 0$. Using the previous results, the Bianchi identity for the $R^v{}_k$ component can be reduced to

$$\tilde{D} R^v{}_k = \left(-\frac{z}{r}\frac{\partial}{\partial z} - \tilde{A}^i \frac{\partial}{\partial x_i} - \tilde{B}^i \frac{\partial}{\partial y^i} \right) R^v{}_k = 0 . \tag{3.40}$$

It is then possible to show that $R^v{}_k = 0$ by considering the possible solutions to this differential equation.

The final remaining Ricci component $R^v{}_u$ can be shown to go to zero by considering the relevant Bianchi identity $DR^v{}_u = \delta^m A^m R^v{}_u$. The most general solution to this differential equation for $R^v{}_u$ is then given by

$$R^v{}_u = \frac{H}{r}\frac{\tilde{f}_j(\tilde{A}^i, \tilde{B}^i)}{a_j}\,, \tag{3.41}$$

where dimensional analysis has been used to determine the appearance of the spin coefficients a_j. It is now possible to show that in order for this equation to remain well behaved, in the limit as all the a_j spin coefficients go to zero (i.e. as the spinning black hole becomes static), $\tilde{f}_j = 0$ otherwise a singularity would occur when any of $a_j \longrightarrow 0$.

The process for calculating the solution when N is even parallels that of the odd N case but a few modifications are required to allow for the fact there there isn't an extra "odd" coordinate to use for forming light-like coordinates. In this case the last pair of x^i-y^i coordinates is chosen to stand in for the z coordinate.

Firstly form two new coordinates $z = x^{N/2}$ and $q = y^{N/2}$, along with the spin parameter $a_{N/2} = b$. Now form a Kerr-Schild metric in the same manner as for equation (3.14)

$$\mathrm{d}s^2 = -\mathrm{d}t^2 + \mathrm{d}x^{i\,2} + \mathrm{d}y^{i\,2} + 2H(\tilde{k}_\mu \mathrm{d}x^\mu)^2 \tag{3.42}$$

where the various functions are the same as before but $\tilde{k}_\mu$ is multiplied by a new normalising factor $\tilde{k}_\mu \mathrm{d}x^\mu = n k_\mu \mathrm{d}x^\mu$, where now

$$n = \frac{\sqrt{2}(r^2 + b^2)}{r(r+z) + b(b+q)}\,. \tag{3.43}$$

This then allows the light-like coordinates u and v to be defined in the same manner as before. The basis forms are also the same as those previously used but now the coordinate pairs x^k are chosen so that $x^k = \{x^i, y^i\}$ with $i = 1, ..., (N-2)/2$ and $y^{N/2} = q$. From then on, the process of solving Einstein's equations is very much the same as for odd N.

Although, the metrics given in (3.14) and (3.42) solve the vacuum Einstein equations they are often used in a different form because the nature of the metric at

asymptotic infinity isn't easily manageable. However, this problem is easily solved by transforming to Boyer-Lindquist coordinates. Firstly, however, it is necessary to introduce some angular coordinates via the transformations

$$x^i = \sqrt{r^2 + {a_i}^2}\mu_i \cos\left(\phi_i - \tan^{-1}\frac{a_i}{r}\right) \tag{3.44}$$

$$y^i = \sqrt{r^2 + {a_i}^2}\mu_i \sin\left(\phi_i - \tan^{-1}\frac{a_i}{r}\right), \tag{3.45}$$

when N is even. In these transformations r is a radial coordinate and the μ_i functions are direction cosines which specify the direction of r. The ϕ_i coordinates are angles in each x^i-y^i plane and so, along with the r and μ_i coordinates, specify any point in the N dimensional space.

Now, the transformations to Boyer-Lindquist coordinates can be made using

$$\mathrm{d}\bar{t} = \mathrm{d}t - \frac{\mu r^2}{\Pi - \mu r^2}\mathrm{d}r \tag{3.46}$$

$$\mathrm{d}\bar{\phi} = \mathrm{d}\phi + \frac{\Pi a_i \mathrm{d}r}{(\Pi - \mu r^2)(r^2 + {a_i}^2)} \tag{3.47}$$

which, when combined with the previous set of coordinate transformations, gives the Myers Perry metric as

$$\begin{aligned}\mathrm{d}s^2 = &-\mathrm{d}\bar{t}^2 + \sum_i^{N/2}(r^2 + {a_i}^2)(\mathrm{d}\mu_i^2 + \mu_i^2\mathrm{d}\bar{\phi}_i^2) \\ &+ \sum_i^{N/2}\frac{\mu r^2}{\Pi F}(\mathrm{d}\bar{t} + a_i\mu_i^2\mathrm{d}\bar{\phi}_i)^2 + \frac{\Pi F}{\Pi - \mu r^2}\mathrm{d}r^2 .\end{aligned} \tag{3.48}$$

If N is odd, then the transformation of the metric into the Boyer-Lindquist coordinates is slightly different because the odd z coordinate has to be taken into account. This requires the additional transformation $z = r\alpha$, where $-1 \leq \alpha \leq 1$, but other than that the angular transformations of (3.44) and (3.45) remain the same.

The Boyer-Lindquist transformations for odd N are

$$\mathrm{d}\bar{t} = \mathrm{d}t - \frac{\mu r}{\Pi - \mu r}\mathrm{d}r \tag{3.49}$$

$$\mathrm{d}\bar{\phi}_i = \mathrm{d}\phi_i + \frac{\Pi a \mathrm{d}r}{(\Pi - \mu r)(r^2 + {a_i}^2)} \tag{3.50}$$

which yield the final metric for odd N as

$$\begin{aligned} ds^2 &= -d\bar{t}^2 + r^2 d\alpha^2 + \sum_i^{(N-1)/2} (r^2 + a_i{}^2)(d\mu_i^2 + \mu_i^2 d\bar{\phi}_i^2) \\ &\quad + \sum_i^{(N-1)/2} \frac{\mu r}{\Pi F}(d\bar{t} + a_i \mu_i^2 d\bar{\phi}_i)^2 + \frac{\Pi F}{\Pi - \mu r} dr^2 \,. \end{aligned} \tag{3.51}$$

Note that the range of i has now become $i = 1, ..., (N-1)/2$. This metric for odd N bears a striking resemblance to that of the Kerr solution, given in (3.1), which is no coincidence since it reduces to the Kerr metric when $N = 3$.

The solution that Myers and Perry managed to construct, which is applicable in any dimension, is quite remarkable. The fact that the Kerr solution can be generalised to arbitrary dimension is an indication that, in any dimension, stationary black holes can be constructed whose horizons share the property of spherical symmetry. This doesn't necessarily mean that the Myers-Perry solution is exhaustive for non-charged black holes because the uniqueness theorems that hold in 4D can't be extended to higher dimensions, indeed the black ring solution [26] is proof that spherical black holes are not the only black hole solution in 5D.

3.2 Generalised Weyl Solutions

At this point it is useful to stop and consider a special metric that is axisymmetric and gives a general solution to the vacuum Einstein equations. As previously mentioned, it is very difficult to solve Einstein's equations without making some simplifying assumptions. If it is assumed that the desired metric is static and axisymmetric then it is possible to show that all the possible solutions can be written in the form

$$ds^2 = -e^{2U} dt^2 + e^{-2U} \left(e^{2\xi} \left(d\rho^2 + dz^2 \right) + \rho^2 d\phi^2 \right) \tag{3.52}$$

where $U(\rho, z)$ is an arbitrary axisymmetric solution of Laplace's equation in three-dimensional flat space with the metric given by[1]

$$ds^2 = d\rho^2 + \rho^2 d\gamma^2 + dz^2 \tag{3.53}$$

[1]The angular coordinate γ is an unphysical coordinate used to describe the solution $U(\rho, z)$ and has period 2π.

and ξ satisfies

$$\partial_\rho \xi = \rho\left[(\partial_\rho U)^2 - (\partial_z U)^2\right] \tag{3.54}$$

$$\partial_z \xi = 2\rho\,(\partial_\rho U)\,(\partial_z U)\ . \tag{3.55}$$

This solution was originally found by Weyl [33] for four dimensional black holes.

The form of this solution is particularly enticing because the non-linear Einstein equations have now been reduced to finding solutions to Laplace's equation in flat space, which has been studied in great detail. The function $U(\rho, z)$ will be harmonic, so it is possible to consider it as a Newtonian potential sourcing an infinitesimally thin rod along the z axis with mass per unit length of $1/2$ [34]. This "rod structure" approach for visualising axisymmetric solutions to Einstein's equations proves to be particularly useful as it is possible to ascertain many of the properties of a particular solution by examining it's rod structure [35].

All of the black hole solutions that are investigated in the remainder of the chapter share the property of axisymmetry, so it would be useful to generalise Weyl's solution to higher dimensions. Fortunately, this has already been done in [34] and [35], with the latter paper further generalising to axisymmetric solutions of the vacuum Einstein equations with non-orthogonal Killing fields. The following analysis follows the derivation of [35] but concentrates on solutions with orthogonal Killing vectors, since this case is the most pertinent for the black hole solutions considered later on.

3.2.1 The Canonical form of the metric

The aim of this section is to determine a version of the Weyl solution when it is generalised to D dimensions. Doing this will give the metric in the form

$$\mathrm{d}s^2 = \sum_{i,j=1}^{D-2} G_{ij}\mathrm{d}x^i\mathrm{d}x^j + e^{2\nu}\left(\mathrm{d}\rho^2 + \mathrm{d}z^2\right)\ . \tag{3.56}$$

Re-expressing an axisymmetric solution in the form given in (3.56) is known as giving the solution in "canonical form". This then allows the solution to be analysed by examining its rod structure.

The first step in deriving the canonical form of the metric is to consider a D-dimensional space-time with $D-2$ orthogonal (and thus commuting) Killing vectors $V_{(i)} = \partial_i$, where $i = 1, ..., D-2$. This clearly implies that the metric components describing this space-time will only depend upon two coordinates y^1 and y^2.

Having done this it is now possible to apply the following theorem

Theorem 3.2.1 Let $V_{(i)}$, $i = 1, ..., D-2$, be $D-2$ commuting Killing vector fields such that

1. The tensor $V_{(1)}^{[\mu_1} V_{(2)}^{\mu_2} ... V_{(D-2)}^{\mu_{D-2}} \nabla^\nu V_{(i)}^{\lambda]}$ vanishes at at least one point of the space-time for a given $i = 1, ..., D-2$.

2. The tensor $V_{(i)}^\nu R_\nu^{[\lambda} V_{(1)}^{\mu_1} V_{(2)}^{\mu_2} ... V_{(D-2)}^{\mu_{D-2}]} = 0$ for all $i = 1, ..., D-2$.

Then the two-planes orthogonal to the Killing vector fields, $V_{(i)}$ for $i = 1, ..., D-2$, are integrable. □

This theorem is proved for four dimensions in [37] and generalised to five dimensions by Emparan and Reall in [34]. This theorem is particularly useful for the present purposes because the two conditions for it to hold are trivially satisfied. If the solutions under consideration are restricted to the vacuum Einstein equations, then $R_{\mu\nu} = 0$ at all points, so the second condition will be satisfied automatically. Furthermore, for solutions where one of the Killing vectors represents an angle, it is easy to see that the tensor in condition 1 will go to zero on the axis of rotation. Asymptotically flat solutions in four and five dimensions are a good example of this as they necessarily have angular Killing vectors.

Since only solutions to Einstein's equations which satisfy theorem 3.2.1 will be considered, the two-planes orthogonal to the Killing vectors, given by $V_{(i)}$, will all be integrable. This property of the two-planes means that a two dimensional submanifold that is always orthogonal to all of the Killing vectors can be constructed. It is then possible to generate coordinates, given by (y^1, y^2), on this two dimensional manifold by demanding that the coordinates follow the integral curves of the Killing vector fields. These new coordinates will be orthogonal to the coordinates of the space spanned by the Killing vectors at all points i.e. ∂_{x^i} is orthogonal to ∂_{y^a} every-

where, where x^i are the coordinates spanning the Killing vector space, $i = 1, ..., D-2$ and $a = 1, 2$. Given this, it is now possible to express the metric in the form

$$ds^2 = \sum_{i,j=1}^{D-2} G_{ij} dx^i dx^j + \sum_{a,b=1}^{2} \hat{g}_{ab} dy^a dy^b \tag{3.57}$$

where G_{ij} and $\hat{g}_{ab}$ only depend upon y^1 and y^2.

To proceed further define $\rho(y^1, y^2)$ as

$$\rho = \sqrt{|\det(G_{ij})|} \tag{3.58}$$

For the purposes of this analysis it is assumed that $\det(G_{ij})$ is non-constant, since this is applicable for all the solutions examined later.

At this point it is helpful to examine the behaviour of $\det G_{ij}$ for a general G_{ij}. To do this note that the metric given by (3.57) can be expressed as

$$ds^2 = \sum_{i,j=1}^{D-2} G_{ij} dx^i dx^j + C(u, v)(du^2 + dv^2) \tag{3.59}$$

where G_{ij} is a function of u and v. This is possible since any two dimensional metric is automatically conformally flat, so a conformal transformation can always be found to transform the metric into the form given above.

Now, consider an arbitrary function

$$f = \sqrt{|\det(G_{ij})|} \tag{3.60}$$

where f is obviously a function of u and v. This allows the Ricci tensor to be computed for (3.59) as

$$\sum_{i,j=1}^{D-2} G^{ij} R_{ij} = -\frac{1}{Cf} \left(\frac{\partial^2}{\partial u^2} + \frac{\partial^2}{\partial v^2} \right) f \,. \tag{3.61}$$

This sum has to be equal to zero because only Ricci flat solutions are being considered, meaning that

$$\left(\frac{\partial^2}{\partial u^2} + \frac{\partial^2}{\partial v^2} \right) f = 0 \,. \tag{3.62}$$

If a new complex variable $\omega = u + iv$ is defined, along with the complex derivatives $\partial = \partial_u + i\partial_v$ and $\bar{\partial} = \partial_u - i\partial_v$, equation (3.62) implies that $\partial\bar{\partial} f = 0$. Therefore ∂f is a holomorphic function and thus is identically zero or has isolated zeros (assuming that the set that f is defined on is simply connected).

Given that $\partial f = \partial_u f + i\partial_v f$, the implication is either

- $f(u,v)$ is a constant function, or
- $(\partial_u f, \partial_v f) \neq (0,0)$ except at isolated points.

If only non-constant values of $\det(G_{ij})$ are to be considered, then the latter condition must be assumed. Bearing this in mind, and identifying (u,v) with (y^1,y^2), means that $\left(\frac{\partial\rho}{\partial y^1}, \frac{\partial\rho}{\partial y^2}\right) \neq (0,0)$. Armed with this knowledge it is now possible to diagonalise the 2D metric in the second term of (3.57), to give

$$\sum_{a,b=1}^{2} \hat{g}_{ab} \mathrm{d}y^a \mathrm{d}y^b = e^{2\nu}\left(\mathrm{d}\rho^2 + \Lambda \mathrm{d}z^2\right) \tag{3.63}$$

where $\Lambda(y^1,y^2)$ and $\nu(y^1,y^2)$ are two new functions. The full metric is thus given by

$$\mathrm{d}s^2 = \sum_{i,j=1}^{D-2} G_{ij}\mathrm{d}x^i\mathrm{d}x^j + e^{2\nu}\left(\mathrm{d}\rho^2 + \Lambda \mathrm{d}z^2\right) \tag{3.64}$$

To get to the canonical form of the metric it is necessary to use the result of Appendix B

$$\sum_{i,j=1}^{D-2} G^{ij}R_{ij} = -\frac{\partial_\rho \Lambda}{2e^{2\nu}\Lambda\rho} \,. \tag{3.65}$$

This expression is identically equal to zero since $R_{\mu\nu} = 0$ for the vacuum Einstein equations, which from (3.65) implies that $\partial_\rho \Lambda = 0$. This means that $\Lambda = \Lambda(z)$ and thus allows $\Lambda(z)$ to be set to 1, since (3.64) is invariant under the coordinate transformation $z \to z' = f(z)$. This method of setting $\Lambda = 1$ has the consequence of determining z up to transformations $z \to z +$ constant. Having done this, the final form for the canonical metric can now be written as

$$\mathrm{d}s^2 = \sum_{i,j=1}^{D-2} G_{ij}\mathrm{d}x^i\mathrm{d}x^j + e^{2\nu}\left(\mathrm{d}\rho^2 + \mathrm{d}z^2\right) \,. \tag{3.66}$$

Having obtained the Weyl solution in a generalised form, the analogous results to equations (3.52)-(3.55) can be written as follows

$$\mathrm{d}s^2 = -e^{2U_1}\mathrm{d}t^2 + \sum_{i=2}^{D-2} e^{2U_i}(\mathrm{d}x^i)^2 + e^{2\nu}(\mathrm{d}\rho^2 + \mathrm{d}z^2) \,, \tag{3.67}$$

$$\sum_{i=1}^{D-2} U_i = \log\rho \,, \tag{3.68}$$

where now ρ is the radial coordinate in the D dimensional space, and $t \equiv x^1$. Furthermore, the functions $U_i(\rho, z)$ solve the equations

$$\left(\partial_\rho^2 + \frac{1}{\rho}\partial_\rho + \partial_z^2\right) U_i = 0 \tag{3.69}$$

for $i = 1, ..., D-2$. These equations are just Laplace's equations in flat space as before but now there are $D-2$ of them. The function $\nu(\rho, z)$ satisfies

$$\partial_\rho \nu = -\frac{1}{2\rho} + \frac{\rho}{2}\sum_{i=1}^{D-2}\left[(\partial_\rho U_i)^2 - (\partial_z U_i)^2\right], \qquad \partial_z \nu = \rho\sum_{i=1}^{D-2}(\partial_\rho U_i)(\partial_z U_i), \tag{3.70}$$

where the two equations are integrable, meaning that given any solution for U_i, it is always possible to find ν from (3.70). When this fact is combined with the constraint (3.68), it allows all the U_i to be found by only solving $D-3$ of the free Laplace equations given in (3.69).

3.2.2 The Einstein Equations for the Canonical Form of the Metric

Having computed the form of the canonical metric in D dimensions, it is now possible to check that the vacuum Einstein equations are fulfilled, given the constraint (3.58). To do this, the Ricci tensor has to be calculated for (3.66). Using techniques similar to those in Appendix B, gives the non-zero components of the Ricci tensor as

$$\begin{aligned}
2e^{2\nu}R_{ij} &= -\left(\partial_\rho^2 + \frac{1}{\rho}\partial_\rho + \partial_z^2\right)G_{ij} + \sum_{k,l=1}^{D-2} G^{kl}\partial_\rho G_{ki}\partial_\rho G_{lj} + \sum_{k,l=1}^{D-2} G^{kl}\partial_z G_{ki}\partial_z G_{lj}\,, \\
R_{\rho\rho} &= -\partial_\rho^2\nu - \partial_z^2\nu + \frac{1}{\rho^2} + \frac{1}{\rho}\partial_\rho\nu - \frac{1}{4}\sum_{i,j,k,l=1}^{D-2} G^{ij}G^{kl}\partial_\rho G_{ik}\partial_\rho G_{jl}\,, \\
R_{zz} &= -\partial_\rho^2\nu - \partial_z^2\nu - \frac{1}{\rho}\partial_\rho\nu - \frac{1}{4}\sum_{i,j,k,l=1}^{D-2} G^{ij}G^{kl}\partial_z G_{ik}\partial_z G_{jl}\,, \\
R_{\rho z} &= \frac{1}{\rho}\partial_z\nu - \frac{1}{4}\sum_{i,j,k,l=1}^{D-2} G^{ij}G^{kl}\partial_\rho G_{ik}\partial_z G_{jl}\,.
\end{aligned} \tag{3.71}$$

Considering the $R_{ij} = 0$ equations, gives the equations of motion for G_{ij}

$$\left(\partial_\rho^2 + \frac{1}{\rho}\partial_\rho + \partial_z^2\right)G_{ij} = \sum_{k,l=1}^{D-2} G^{kl}\partial_\rho G_{ki}\partial_\rho G_{lj} + \sum_{k,l=1}^{D-2} G^{kl}\partial_z G_{ki}\partial_z G_{lj} = 0\,. \tag{3.72}$$

The equations for ν can be obtained by considering $R_{\rho\rho} - R_{zz} = 0$ and $R_{\rho z} = 0$ to give

$$\begin{aligned} \partial_\rho \nu &= -\frac{1}{2\rho} + \frac{\rho}{8} \sum_{i,j,k,l=1}^{D-2} G^{ij} G^{kl} \partial_\rho G_{ik} \partial_\rho G_{jl} - \frac{\rho}{8} \sum_{i,j,k,l=1}^{D-2} G^{ij} G^{kl} \partial_z G_{ik} \partial_z G_{jl} \,, \\ \partial_z \nu &= \frac{\rho}{4} \sum_{i,j,k,l=1}^{D-2} G^{ij} G^{kl} \partial_\rho G_{ik} \partial_z G_{jl} \,. \end{aligned} \tag{3.73}$$

These equations are sufficient to be able to calculate ν and G_{ij} but it is necessary to check that these equations are consistent.

If the equations given in (3.73) are to be integrable, they have to satisfy the condition $\partial_z \partial_\rho \nu = \partial_\rho \partial_z \nu$. This can be shown to be true by using (3.72) and differentiating (3.73) with respect to z and ρ. Thus, having found a solution for $G_{ij}(\rho, z)$ from (3.72), it is possible to calculate $\nu(\rho, z)$ by integrating (3.73).

The other necessary check on equations (3.72) and (3.73), is that the equation formed by adding $R_{\rho\rho}$ and R_{zz} goes to zero for all ρ and z. This equation is calculated from (3.71) and is given by

$$\partial_\rho^2 \nu + \partial_z^2 \nu = \frac{1}{\rho^2} - \frac{1}{4} \sum_{i,j,k,l=1}^{D-2} G^{ij} G^{kl} \partial_\rho G_{ik} \partial_\rho G_{jl} - \frac{1}{4} \sum_{i,j,k,l=1}^{D-2} G^{ij} G^{kl} \partial_z G_{ik} \partial_z G_{jl} \,. \tag{3.74}$$

This equation can be seen to hold for the $\nu(\rho, z)$ and $G_{ij}(\rho, z)$, calculated from (3.72) and (3.73), by differentiating the expressions given in (3.73) and then using (3.72). Having shown that all of the Einstein equations are satisfied it now only necessary to consider (3.72) and (3.73) to obtain expressions for $G_{ij}(\rho, z)$ and $\nu(\rho, z)$. These functions can then be substituted into (3.66) to give an axisymmetric solution of the vacuum Einstein equations.

If the $D-2$ Killing vectors that span the space described by G_{ij} are all orthogonal then it is possible to set $G_{11} = -e^{2U_1}$ and $G_{ii} = e^{2U_i}$ for $i = 2, ..., D-2$. Identifying x^1 with t transforms the canonical form of the metric given in (3.66) to the Generalised Weyl Form given in (3.67). The equation given in (3.68) is then just a consequence of the constraint that $\det G_{ij} = -\rho^2$ and the Einstein equations given in (3.72) and (3.73) reduce to the equations given by (3.69) and (3.70).

Having shown that equations (3.72) and (3.73) solve the vacuum Einstein equations, it is helpful to rephrase them in a form that is more conducive to algebraic

manipulation. The essential insight is to view G_{ij} as a $D-2 \times D-2$ real symmetric matrix, with G^{ij} being its inverse. This immediately allows (3.72) to be re-written in a much more compact form as

$$G^{-1}\left(\partial_\rho^2 + \frac{1}{\rho}\partial_\rho + \partial_z^2\right) G = \left(G^{-1}\partial_\rho G\right)^2 + \left(G^{-1}\partial_z G\right)^2 , \tag{3.75}$$

with the constraint that $\det G_{ij} = -\rho^2$ coming from (3.68) when Lorentzian metrics are being considered. In fact, this equation can be written even more succinctly once it is noticed that the differential operators are equivalent to those of a 3D Euclidean space with metric

$$\mathrm{d}s^2 = \mathrm{d}\rho^2 + \rho^2\mathrm{d}\gamma^2 + \mathrm{d}z^2 . \tag{3.76}$$

In this metric, γ is an unphysical coordinate with period 2π that is introduced for notational convenience.

Having made this observation it is now a simple matter to re-write (3.75) in terms of the gradient operator ∇ on the space described by (3.76), giving

$$G^{-1}\nabla^2 G = \left(G^{-1}\nabla G\right)^2 . \tag{3.77}$$

This form of the equation of motion for G_{ij} is extremely useful because now the problem of finding axisymmetric solutions has been reduced to just finding solutions to a differential matrix equation in 3D flat Euclidean space, which obey the constraint $\det G = -\rho^2$.

3.2.3 The Rod Structure of the Generalised Weyl Solutions

As has already been noted, it is possible to consider the axisymmetric solutions, given in the Generalised Weyl form, as being a series of Newtonian potentials sourcing infinitesimally thin rods that lie along the z axis. For this approach to be valid it is necessary for the solution $G(\rho, z)$ to be continuous, which is satisfied by most physical solutions and certainly by all of the solutions considered here. The first step is to examine $\det G$ at $\rho = 0$.

From equation (3.68), $\det G = -\rho^2$ for a Lorentzian metric, so the product of the eigenvalues of G must be zero when $\rho = 0$. This implies that at least one of the eigenvalues is zero for all points along the z axis. In fact, it is argued in [35] that

for $G(\rho, z)$ to be a regular solution, only one of the eigenvalues for $G(0, z)$ is zero, except at isolated points.

Harmark [35] argues that in order for the solution $G(\rho, z)$ to be free from curvature singularities it is necessary for $G(0, z)$ to only have one eigenvalue going to zero over a closed interval in z. To illustrate this, consider a metric of the form (3.66) with the non-zero components of the matrix G given by

$$G_{11} = \rho^{2a}, \qquad G_{22} = \rho^{2-2a} \tag{3.78}$$

and the function ν defined by

$$e^{2\nu} = \rho^{-2a(1-a)}\ , \tag{3.79}$$

where $0 \leq a \leq 1$. These expressions solve (3.72) and (3.73), so they form a valid solution of the vacuum Einstein equations. Calculating the curvature invariant in this case, gives

$$R_{\mu\nu\lambda\sigma}R^{\mu\nu\lambda\sigma} = 16a^2(1-a)^2(1-a+a^2)\rho^{-4(1-a+a^2)}\ . \tag{3.80}$$

Examining this expression shows that there is generally a curvature singularity when $\rho = 0$, since $(1-a+a^2)$ is positive definite for all permissible a. The only values of a where there is no curvature singularity are when $a = 0$ or $a = 1$, which corresponds to the solution only having one eigenvalue. This implies that having two eigenvalues going to zero will lead to a curvature singularity.

The more general case, where any possible solution to Einstein's vacuum equations has two eigenvalues going to zero is considered in detail by Harmark [35]. The basic outline of the argument is that for any $z \in [z_1, z_2]$ it is possible to make a constant orthogonal transformation of $G(r, z)$ so that $G_{1i}(0, z) = G_{2i}(0, z) = 0$ for $i = 1, 2, ..., D-2$ and thus reduce the equations of motion (3.72) and (3.73) to the example given above. Thus, it is shown that it is impossible to have two eigenvalues going to zero for a given value of z, except possibly at the endpoints of the interval. The more general argument, where more than two eigenvalues go to zero, can then be derived along the same lines.

Given that there can only be isolated points where two eigenvalues go to zero, it is now possible to split the z-axis up into a number of different intervals with

the endpoints demarcated by the points where two eigenvalues go to zero. If these points are labelled as $a_1, a_2, ..., a_N$ where $a_1 < a_2 < ... < a_N$ then the z-axis has been divided up into $N+1$ intervals $[-\infty, a_1]$, $[a_1, a_2]$,..., $[a_{N-1}, a_N]$, and $[a_N, \infty]$, with the number of intervals being potentially infinite. These intervals are the "rods" of the solution.

In order to deduce anything about the solution by examining its rod structure, it is necessary to invoke a theorem proved in [35]

Theorem 3.2.2 Consider a rod $[z_1, z_2]$ for a solution $G(\rho, z)$. Then we can find an orthogonal matrix Λ_* such that the solution $\tilde{G}(\rho, z) = \Lambda_*^T G(\rho, z)\Lambda_*$ has the property that $\tilde{G}_{1i}(0, z) = 0$ for $i = 1, ..., D-2$ and $z \in [z_1, z_2]$. □

Using this theorem it is possible to make a constant coordinate transformation of the x^i coordinates so that $G(\rho, z)$ can be put into a form where $G_{1i}(0, z) = 0$ for $i = 1, ..., D-2$ when $z \in [z_1, z_2]$. Given $G(\rho, z)$ in this form, it is now possible to express $G(\rho, z)$ as

$$G(\rho, z) = \begin{pmatrix} \pm a(z)\rho^2 & & \\ & & \\ & & A(z) \end{pmatrix} \tag{3.81}$$

to leading order for $r \to 0$, where $z_1 < z < z_2$ [35]. In this approximation, $a(z)$ is a strictly positive function for $z \in]z_1, z_2[$ and $A(z)$ is a 3×3 matrix, which is solely a function of z.

Examining this expression for the metric in the vicinity of $\rho = 0$, $G_{11} \sim \pm a(z)\rho^2$. This can then be used to check that the equations of motion from (3.72) and (3.73) are still satisfied. From (3.72), the left hand side gives $\nabla^2 G_{11} = \pm 4a(z) + \mathcal{O}(\rho)$ and the right hand side becomes $G^{11}(\partial_\rho G_{11})^2 = \pm 4a(z) + \mathcal{O}(\rho)$, thus showing that the first equation is consistent.

From (3.73), the first of the equations gives $\partial_\rho \nu \to 0$ for $\rho \to 0$ because $\partial_\rho G_{11} = \pm 2a(z)\rho$. Thus, in order to get an expression for ν, the second equation for $\partial_z \nu$ has to be considered. This gives

$$\partial_z \nu = \frac{a'}{2a} + \mathcal{O}(\rho)\,. \tag{3.82}$$

Solving for ν gives $e^{2\nu} = c^2 a(z)$, where c is a positive constant.

It is now possible to give an expression for the canonical metric (3.66) in the limit as $\rho \to 0$ when $z_1 < z < z_2$

$$ds^2 = \sum_{i,j=2}^{D-2} A_{ij}(z)dx^i dx^j + a(z)\left[\pm r^2(dx^1)^2 + c^2(d\rho^2 + dz^2)\right] . \tag{3.83}$$

This metric can then be used to deduce the behaviour of a canonical metric near a particular rod. For example, if G_{11}/ρ^2 is positive as $r \to 0$ then the x^1 coordinate is spacelike and thus the rod is said to be spacelike. Similarly, if G_{11}/ρ^2 is negative then the x^1 coordinate is timelike and the rod is said to be timelike.

In order to agree with the Generalised Weyl solution given in (3.67), the x^1 coordinate will henceforth be chosen to be timelike and denoted by t. Therefore, in this case, the metric in the vicinity of the z axis will look like

$$ds^2 = \sum_{i,j=2}^{D-2} A_{ij}(z)dx^i dx^j + a(z)\left[-\rho^2 dt^2 + c^2(d\rho^2 + dz^2)\right] . \tag{3.84}$$

In this case the t coordinate is always timelike, so it is only necessary to determine the direction of the other rods x^i, where $i = 2, ..., D-2$.

A more rigorous way to define the direction of a rod is given by defining $N+1$ vectors $v_{(k)}$ in R^{D-2}, with $k = 1, ..., N+1$,

$$G(0,z)v_{(k)} = 0 \text{ for } z \in [a_{k-1}, a_k] , \tag{3.85}$$

where $v_{(k)} \neq 0$ for all k. In this case, the solution $G_{ij}(0,z)$ is split up into $N+1$ rods $[a_{k-1}, a_k]$ with the rods starting/ending at z values $a_1 < a_2 < ... < a_N$, where the values $a_0 = -\infty$ and $a_{N+1} = \infty$ are defined for notational convenience. Under this definition $v_{(k)}$ gives the direction of the respective rod $[a_{k-1}, a_k]$.

Using this definition for the direction of the rods it is possible to find a vector for a specific rod such that

$$\sum_{j=1}^{D-2} G_{ij}(0,z)v^j = 0 , \tag{3.86}$$

which follows from Theorem 3.2.2. It is now possible to define the direction of the rod by considering $G_{ij}v^i v^j/\rho^2$ in the limit as $\rho \to 0$. The direction of the rod $[z_1, z_2]$ is then said to be timelike or spacelike depending on whether $G_{ij}v^i v^j/\rho^2$ is respectively negative or positive in the limit as $\rho \to 0$.

One further consideration is to ensure that the solution has no conical singularities. This can be seen by examining the expression for the metric near the rods (3.83). Consider a spacelike rod, if a new coordinate η is introduced as a linear combination of x^i where $i = 1, ..., D-2$, so that

$$\frac{\partial}{\partial \eta} = v = v^i \frac{\partial}{\partial x^i} , \tag{3.87}$$

then the conical singularity at the rod can be removed by demanding that η have period

$$\Delta\eta = 2\pi \lim_{\rho \to 0} \sqrt{\frac{\rho^2 e^{2\nu}}{G_{ij} v^i v^j}} . \tag{3.88}$$

This implies that a spacelike rod necessarily corresponds to a compact direction. If the rod is timelike, then via a similar analysis to the spacelike case, it is possible to do a Wick rotation and then find an associated temperature for the Wick rotated coordinate by eliminating the conical singularity. This then implies that there is an event horizon at this rod.

The fixed points at the end of the rods, and the periodic identification of the respective coordinates, allows certain assumptions to be made about the solution. The space is asymptotically flat so, for spacelike coordinates, a rod that stretches to infinity will indicate a fixed point in the asymptotically flat space. This then indicates that the coordinate under consideration is part of a rotational isometry and thus that there is an axis of rotation parameterised by that coordinate.

For a finite spacelike rod, the fixed points at the end of the rod indicate that the coordinate is a periodically identified circle direction. If there are no other rods which stretch out to infinity, then this rod has to correspond to a Kaluza Klein direction because it is impossible to have an asymptotically flat spacetime with one of the coordinates identified as a circle. If there is an additional semi-infinite rod, then the direction corresponds to a rotation axis for reasons given above, but the finite rod introduces a singularity with a conical defect.

Other than the direction of the rod, the length of the rod has to be considered. In general, if the interval $[z_1, z_2]$ for a particular rod is finite, then it is known as a finite rod. If either z_1 or z_2, but not both, are infinite, then the rod is known as a semi-infinite rod and if $z_1 = -\infty$ and $z_2 = \infty$ then the rod is known as an infinite

rod.

Putting these definitions together, along with the direction of the rods, allows a number of conclusions about the properties of G_{ij} to be made. These can be summarised as follows: [34, 36]

- A finite timelike rod corresponds to an event horizon.
- A finite spacelike rod corresponds to a Kaluza-Klein direction, provided there are no semi-infinite spacelike rods in the same direction.
- Any semi-infinite or infinite spacelike rod corresponds to an axis of rotation with the associated coordinate giving the rotation angle.
- A semi-infinite timelike rod corresponds to an acceleration horizon because of the fixed point at infinity.

The formalism of the Weyl solution gives a way to build up an intuitive picture of the way different axisymmetric solutions are composed, but knowing the general form of an axisymmetric solution isn't enough to find a new solution. This is because the Weyl form can be used to generate the rod structure of a known solution but having a collection of rods and directions isn't enough to guarantee that the associated Weyl metric will solve Einstein's equations i.e. the Weyl form can be used to restrict the possible number of solutions, but it doesn't provide a method of generating solutions. To produce a new solution, the Weyl form must be used with a solution generating algorithm. An example of such an algorithm is explored in the next section.

3.3 The Inverse Scattering Method

The closest thing that we presently have to a systematic method of producing five dimensional solutions to Einstein's equations is the inverse scattering method (ISM). This was first proposed in the 1960s [38] as a method of solving the Korteweg-de-Vries shallow water wave equations. These equations were of interest because certain solutions exhibited the first known examples of soliton waves. Solitons are special

because they behave in many respects like an extended particle: they have a finite and localised energy, a characteristic propagation velocity, and a structure that is resistant to dissipation [39]. It wasn't long before solitonic solutions were found to other non-linear equations, such as the sine-Gordon and the non-linear Schrödinger equations.

At the end of the 1970s, it was shown that the ISM could be extended to solve the vacuum Einstein equations, provided the spacetimes allowed an orthogonally transitive two-parameter group of isometries [40–42]. In practice this usually means that the metric only depends on two coordinates. Metrics of this form encompass a wide variety of physical situations but the most pertinent solutions, for the purposes of this work, are the stationary axisymmetric solutions. These solutions have cylindrical symmetry and $D-2$ commuting Killing vectors, so are ideal for use with the ISM.

The basic idea behind the ISM when applied to gravitational situations, is to generate new solutions given a previously calculated one. The starting metric is known as the seed solution and is derived from a solution that has already been calculated using a different method. The new solutions, generated after applying the ISM, are known as soliton solutions of the gravitational field (often abbreviated to "gravitational solitons"). This name may be a little disingenuous because the gravitational solitons only share some, if any, of the properties of conventional solitons.

Although the ISM gives an explicit algorithm for generating new solutions it isn't a panacea for generating all possible solutions to Einstein's equations. This is because the newly generated solutions depend heavily upon the starting seed metric, so new solutions tend to share many of the properties of the seed metric. Even given this limitation, the ISM has been successfully used to generate many new solutions to Einstein's equations including the Black Saturn [43], the Bicycling Black Ring solution [44], and the doubly spinning black ring [27, 45]. The ISM has also been used to re-derive solutions that were previously calculated using different methods, such as the singly spinning black ring [26, 46], the di-ring [48], and the Kerr-NUT solution.

3.3.1 The ISM Algorithm

The ISM can be roughly broken down into two main steps. In the first step a group of linear differential equations (known as spectral equations) are found, which are related to the non-linear differential equation by means of the integrability conditions for the linear equations. The second step consists of integrating these spectral equations to find the class of soliton solutions. These gravitational solitons have the remarkable property that they can be expressed in analytic form and thus allow new solutions to be generated by adding and subtracting them from a seed solution.

The first step toward generating new 5D solutions, is to express the seed solution in the form

$$ds^2 = G_{ab}\mathrm{d}x^a\mathrm{d}x^b + e^{2\nu}(\mathrm{d}\rho^2 + \mathrm{d}z^2) \tag{3.89}$$

where $1 \leq (a, b) \leq 3$ and all the metric components are solely functions of ρ and z. As previously discussed, it is shown in [34] that this is always possible provided that there are $D-2$ orthogonal Killing vectors, which is always the case for axially symmetric solutions.

Utilising the diffeomorphism invariance of the seed metric (3.89), it is possible to choose

$$\det G = -\rho^2 \tag{3.90}$$

without any loss of generality. This is possible for axisymmetric solutions because $\det G < 0$, whereas in the more general case $\det G$ could be positive or negative.

Having chosen this form of the metric, it is now possible to divide Einstein's equations into two separate groups. The equations corresponding to the 3×3 matrix G are given by

$$\partial_\rho U + \partial_z V = 0 \tag{3.91}$$

where

$$U = \rho(\partial_\rho G)G^{-1} \qquad\qquad V = \rho(\partial_z G)G^{-1} \tag{3.92}$$

and the equation for $e^{2\nu}$ is given by

$$\partial_\rho \nu = \frac{1}{2}\left[-\frac{1}{\rho} + \frac{1}{4\rho}\mathrm{Tr}(U^2 - V^2)\right] \tag{3.93}$$

$$\partial_z \nu = \frac{1}{4\rho}\mathrm{Tr}(UV) \tag{3.94}$$

The integrability condition for these two equations is

$$\partial_\rho \partial_z \nu = \partial_z \partial_\rho \nu \tag{3.95}$$

and is automatically satisfied if G satisfies (3.91). This can be seen by taking ∂_ρ of (3.94) and ∂_z of (3.93) to give

$$\partial_\rho \partial_z \nu = \frac{1}{4\rho} \mathrm{Tr} \left(-V \partial_z V + U \partial_\rho V - U \frac{V}{\rho} \right)$$
$$\partial_z \partial_\rho \nu = \frac{1}{4\rho} \mathrm{Tr} \left(U \partial_z U - V \partial_z V \right)$$

where (3.91) has been used to give $(\partial_\rho U) = -(\partial_z V)$. A little further manipulation shows

$$\partial_z U = \partial_\rho V - \frac{V}{\rho} \tag{3.96}$$

which proves that equations (3.91)-(3.94) satisfy the integrability condition. This means that once a solution for $G(\rho, z)$ is found from (3.91), $\nu(\rho, z)$ can be found by direct integration.

Since the idea behind the ISM is that the integrability condition of equations (3.90) and (3.91) is the non-linear equation that is to be solved, in this case Einstein's equations, these two equations have to form a completely integrable system. Fortunately, it was shown (see for example [49]) that this can be dealt with via a generalisation of the Zakharov-Shabat [50] form of the ISM. The procedure for doing this is to find some compatibility conditions, for a more general system of eigenfunction equations, that are the same as (3.91) and the integrability condition for U and V from (3.92). This integrability condition is given by

$$\partial_z U - \partial_\rho V + \frac{UV}{\rho} - \frac{VU}{\rho} + \frac{V}{\rho} = 0 \tag{3.97}$$

Having done this it is now theoretically possible to find a system of overdetermined eigenfunction matrix equations which depend upon U, V, and λ, where λ is a complex spectral parameter that parameterises the different eigenfunction equations. However, there is currently no systematic method for doing this in general, but it was shown in [40] that there is a way to do this for the specific equations given by (3.90) and (3.91).

These spectral equations, known as an L-A pair, are given by

$$D_1\Psi = \frac{\rho V - \lambda U}{\lambda^2 + \rho^2}\Psi, \qquad D_2\Psi = \frac{\rho U + \lambda V}{\lambda^2 + \rho^2}\Psi \tag{3.98}$$

where λ is a complex parameter independent of ρ and z and $\Psi(\lambda, \rho, z)$ is a 3×3 matrix known as the generating matrix. The commuting differential operators D_1 and D_2 are given by

$$D_1 = \partial_z - \frac{2\lambda^2}{\lambda^2 + \rho^2}\partial_\lambda, \qquad D_2 = \partial_\rho + \frac{2\lambda\rho}{\lambda^2 + \rho^2}\partial_\lambda \tag{3.99}$$

To show that these equations are compatible, form $[D_1, D_2]\Psi \equiv D_1 D_2\Psi - D_2 D_1\Psi$ where the left hand side goes to zero because D_1 and D_2 commute and the right hand side is evaluated using (3.98) and (3.99). Evaluating the right hand side shows that it will only go to zero if equations (3.91) and (3.97) are satisfied. This result implies that these L-A equations will also give a solution to (3.92), when $\lambda = 0$ because equation (3.97) is derived from (3.92) i.e.

$$G(\rho, z) = \Psi(0, \rho, z) \tag{3.100}$$

Having found two linear equations (3.98) that yield solutions to (3.92), it is possible to generate new solutions given a known seed solution G_0 via the "dressing method". This simply involves multiplying the known generating matrix Ψ_0 by a dressing matrix χ to obtain a new solution

$$\Psi = \chi\Psi_0 \tag{3.101}$$

In this case χ is found by generating U_0 and V_0 from (3.92) and then substituting (3.101) into (3.98). This gives

$$D_1\chi = \frac{\rho V - \lambda U}{\lambda^2 + \rho^2}\chi - \chi\frac{\rho V_0 - \lambda U_0}{\lambda^2 + \rho^2} \qquad D_2\chi = \frac{\rho U + \lambda V}{\lambda^2 + \rho^2}\chi - \chi\frac{\rho U_0 + \lambda V_0}{\lambda^2 + \rho^2} \tag{3.102}$$

In principle, these equations can now be integrated to find χ but there are some constraints on χ.

In order for G to be real, only solutions where Ψ and χ are real can be chosen. Furthermore, G must also be symmetric, which means that

$$G = -\frac{\rho^2}{\lambda}\chi(\lambda, \rho, z)G_0\chi^T \tag{3.103}$$

This introduces a further constraint because $\chi(\infty, \rho, z) = I$ in order for this constraint to be compatible with (3.101).

To find soliton solutions for G it is necessary to consider the pole singularities of the dressing matrix $\chi(\lambda, \rho, z)$, where the poles are only in the λ plane because ρ and z are real by definition. In the general case there are n poles in the λ plane, so the dressing matrix can be represented in the form

$$\chi = I + \sum_{k=1}^{n} \frac{R_k}{\lambda - \tilde{\mu}_k} \tag{3.104}$$

where R_k and $\tilde{\mu}_k$ are solely functions of ρ and z.

The pole trajectories $\tilde{\mu}_k(\rho, z)$ and the matrices $R_k(\rho, z)$ can now be completely determined by substituting (3.104) into (3.102). The functions $\tilde{\mu}_k$ are determined by demanding that the left hand side of the equations in (3.102) have no poles of second order at $\lambda = \tilde{\mu}_k$, otherwise the solution will become singular. This results in two differential equations for $\tilde{\mu}_k$

$$\partial_z \tilde{\mu}_k = -\frac{2\tilde{\mu}_k^2}{\tilde{\mu}_k^2 + \rho^2} \qquad \partial_\rho \tilde{\mu}_k = \frac{2\rho\tilde{\mu}_k}{\tilde{\mu}_k^2 + \rho^2} \tag{3.105}$$

which have solutions

$$\tilde{\mu}_k = \pm\sqrt{\rho^2 + (z - a_k)^2} - (z - a_k) \tag{3.106}$$

where a_k are n arbitrary constants. In general a_k is complex but this introduces the possibility of $\tilde{\mu}_k$ having discontinuities, therefore only poles on the real axis will be considered, meaning a_k will be constrained to be real. The solution with a positive square root is a soliton and will be denoted μ_k whilst the solution with a negative square root is an anti-soliton and will be denoted $\bar{\mu}_k$.

The R_k matrices are degenerate and can be expressed in the form

$$(R_k)_{ab} = n_a^{(k)} m_b^{(k)} \tag{3.107}$$

where $m_a^{(k)}$ are calculated by requiring the above equation to be satisfied at the poles $\lambda = \tilde{\mu}_k$ when it is substituted into (3.102). The vectors $n_a^{(k)}$ can then be determined using the constraint given in (3.103).

It is possible to express the $m_a^{(k)}$ vectors in terms of the generating matrix formed from the seed metric Ψ_0. These vectors take the form

$$m_a^{(k)} = \sum_{b=0}^{2} \frac{m_{0b}^{(k)}}{[\Psi_0(\mu_k, \rho, z)]_{ba}} \tag{3.108}$$

where $m_{0b}^{(k)}$ are the arbitrary components of "BZ vectors". Note that in the above equation, Ψ is evaluated at $\lambda = \mu_k$.

Having determined $\tilde{\mu}$ and R, it is now possible to express the new solution G in terms of the seed metric G_0. The new metric, determined via the n-soliton transformation, gives

$$G_{ab} = (G_0)_{ab} - \sum_{k,l=1}^{n} \frac{(G_0)_{ac} m_c^{(k)} (\Gamma^{-1})_{kl} m_d^{(l)} (G_0)_{db}}{\tilde{\mu}_k \tilde{\mu}_l} \tag{3.109}$$

where the repeated indices $a, b, c, d = 1..3$ are summed over. The symmetric matrix Γ is defined as

$$\Gamma_{kl} = \frac{m_a^{(k)} (G_0)_{ab} m_b^{(l)}}{\rho^2 + \tilde{\mu}_k \tilde{\mu}_l} \tag{3.110}$$

with Γ^{-1} being given by the inverse of this matrix.

Having obtained the expression for the metric of the new solution, it is necessary to ensure that the determinant of the new metric still satisfies (3.90). In general, the determinant of (3.109) is given by

$$\det G = (-1)^n \rho^{2n} \left(\prod_{k=1}^{n} \tilde{\mu}_k^{-2} \right) \det G_0 \tag{3.111}$$

which is clearly not always equal to $-\rho^2$. The traditional way of rectifying this is to multiply G by a suitable factor of ρ and $\tilde{\mu}^{-2}$ to reduce (3.111) to $\det G = -\rho^2$. In practice this means that the renormalized solution $G^{(phys)}$ is given by

$$G^{(phys)} = (-1)^{n/3} \rho^{-2n/3} \left(\prod_{k=1}^{n} \tilde{\mu}_k^{2/3} \right) G \tag{3.112}$$

This approach works well for 4D solutions, such as the Kerr-Nut solution, but causes problems when applied to 5D metrics because it typically leads to naked-singularities. One way around this, as will be seen for the singly spinning black ring solution, is to restrict the soliton transformations to a 2×2 block of the seed metric, and then perform the renormalization process on this sub-section of the new metric.

The obvious drawback of this procedure is that the newly generated solution can only have rotation in at most one plane.

A more general procedure, for ensuring that the metric given in (3.109) has the desired determinant, was mooted in [51]. In this paper, Pomeransky notes that the factor multiplying $\det G_0$ is independent of any of the BZ vectors $m_0^{(k)}$ and thus allows $\det G$ to be altered by varying the BZ parameters in the seed solution. The basic idea is to remove any solitons with trivial BZ parameters, being careful not to introduce any off-diagonal terms in G, and then add the same solitons back but this time with more generanl BZ parameters. These extra degrees of freedom can then be chosen to fine-tune (3.109) in such a way that $\det G = -\rho^2$, even if the seed solution no longer has $\det G_0 = -\rho^2$. Another by-product of this construction is that the metric factor $e^{2\nu}$ can now be succinctly given as

$$e^{2\nu} = e^{2\nu_0} \frac{\det \Gamma_{kl}}{\det \Gamma^{(0)}_{kl}} \tag{3.113}$$

where $\Gamma^{(0)}$ and Γ can be calculated from (3.110) by substituting G_0 and G respectively, where G_0 appears.

3.4 Generating Black Ring Solutions

In this section, the power of the Inverse Scattering Method to produce new solutions is demonstrated by reproducing the singly spinning and doubly spinning black ring metrics. As shown in the previous section, new solutions can be simply generated through a series of algebraic manipulations but there is an art in choosing the correct seed metric to give the desired solution. As an example of this, the Minkowski metric has been used to generate the Myers-Perry metric in [52] and [53] but as will be seen, it is necessary to use a different seed solution to generate the singly spinning black ring. Seeing as the Myers-Perry metric is well known, the remainder of this section will concentrate on the black ring solutions.

3.4.1 The Singly Spinning Black Ring

To generate the singly spinning black ring it is first necessary to come up with a suitable seed solution. An appropriate choice for this starting metric is given in [54], although this can be considered as a specific case of a seed solution used in [55]. Seeing as it is only necessary to determine the 3×3 matrix G in order to generate the whole metric, the seed solution for the singly spinning black ring is given by

$$\mathrm{d}s^2 = -\mathrm{d}t^2 + g_2 \mathrm{d}\phi^2 + g_3 \mathrm{d}\psi^2 \tag{3.114}$$

where

$$g_2 = \frac{(R_{-\eta_1} - z - \eta_1\sigma)(R_\kappa - z + \kappa\sigma)}{R_{\eta_2} - z + \eta_2\sigma}, \qquad g_3 = \frac{(R_{-\eta_1} + z + \eta_1\sigma)(R_{\eta_2} - z + \eta_2\sigma)}{R_\kappa - z + \kappa\sigma} \tag{3.115}$$

and $(\sigma, \kappa, \eta_1, \eta_2)$ are constants. Also

$$R_b = \sqrt{\rho^2 + (z - b\sigma)^2}\,. \tag{3.116}$$

This metric already satisfies $\det G = -\rho^2$ and reduces to the Minkowski metric when $\kappa = \eta_2$.

It is worth noting that the metric given in (3.114) is a diagonal metric, thus simplifying the ISM transformations, because it is possible to obtain diagonal solutions by setting some of the parameters to zero, e.g. $m_{01}^{(k)} = m_{02}^{(k)} = 0$. This then allows the generating matrix Ψ_0 to be expressed as a diagonal matrix $\Psi_0 = \mathrm{diag}(\psi_1, \psi_2, \psi_3)$, where ψ_i are functions depending on λ, ρ, and z. Having expressed Ψ_0 in this form, the partial differential equations given by (3.98) can be decoupled and allow the equations to be solved for each ψ_i independently.

In the case of the singly spinning black ring, there is only angular momentum in one plane, so there will only be off-diagonal terms involving the t and ψ coordinates, assuming that the rotation is in the ψ direction. This allows the $m_{03}^{(k)}$ parameter to be set to zero and thus separates the metric into block diagonal form

$$G = \left(\begin{array}{c|c} G_{AB} & 0 \\ \hline 0 & (G_0)_{33} \end{array}\right) \tag{3.117}$$

where G_{AB} is a 2×2 matrix, with $A, B = 1..2$, dependent only on $m_{01}^{(k)}$ and $m_{02}^{(k)}$. If the coordinates are chosen such that $x^i \in (t, \psi, \phi)$, then this can be interpreted as only adding solitons to the metric components involving t and ψ.

Having expressed the matrix in block diagonal form, it is now possible to choose a normalisation that multiplies the components of the 2×2 matrix in such a way as to ensure that the overall determinant of the metric satisfies $\det G = -\rho^2$. In practice, this means that the G_{33} component remains unchanged and the other components are scaled as

$$G^{(phys)} = \left(\begin{array}{c|c} \left(\prod_{k=1}^{n} \frac{\mu_k}{\rho}\right) G_{AB} & 0 \\ \hline 0 & (G_0)_{33} \end{array} \right) \tag{3.118}$$

Now, if the seed metric has $\det G_0 = -\rho^2$, this normalisation will ensure that the resulting metric G also satisfies $\det G = -\rho^2$. Writing the metric components out explicitly gives

$$G_{tt}^{(phys)} = \left(\prod_{k=1}^{n} \frac{\mu_k}{\rho}\right) (G_0)_{tt}, \quad G_{\psi\psi}^{(phys)} = -\frac{\rho^2}{G_{tt}^{(phys)} G_{\phi\phi}^{(phys)}}, \quad G_{\phi\phi}^{(phys)} = (G_0)_{\phi\phi} \tag{3.119}$$

To obtain the singly spinning black ring solution, it is necessary to add two solitons and set $a_1 = -a_2 = -\sigma$. After using the normalisation given in (3.119) the various metric coefficients become

$$\begin{aligned} G_{tt}^{(phys)} &= -\frac{g_{tt}}{\mu_1 \mu_2 \Sigma}, \quad G_{t\psi}^{(phys)} = -\frac{g_2(\rho^2 + \mu_1\mu_2) g_{t\psi}}{\mu_1 \mu_2 \Sigma}, \quad G_{\psi\psi}^{(phys)} = -\frac{g_2 g_{\psi\psi}}{\mu_1 \mu_2 \Sigma}, \\ G_{\phi\phi}^{(phys)} &= g_3, \qquad G_{\psi\phi}^{(phys)} = G_{t\phi}^{(phys)} = 0 \end{aligned} \tag{3.120}$$

where the functions g_{tt}, $g_{t\psi}$, $g_{\psi\psi}$, and Σ are

$$\begin{aligned} g_{tt} &= \left[\left(m_{01}^{(1)} m_{02}^{(2)} \mu_2 \psi_2(\mu_1)\right)^2 + \left(m_{01}^{(2)} m_{02}^{(1)} \mu_1 \psi_2(\mu_2)\right)^2\right] (\rho^2 + \mu_1\mu_2)^2 g_2 \\ &\quad - \left(m_{01}^{(1)} m_{01}^{(2)} \psi_2(\mu_1)\psi_2(\mu_2)(\mu_1 - \mu_2)\rho^2\right)^2 - \left(m_{02}^{(1)} m_{02}^{(2)} g_2 \mu_1 \mu_2 (\mu_1 - \mu_2)\right)^2 \\ &\quad - 2 m_{01}^{(1)} m_{01}^{(2)} m_{02}^{(1)} m_{02}^{(2)} g_2 \psi_2(\mu_1)\psi_2(\mu_2)(\rho^2 + {\mu_1}^2)(\rho^2 + {\mu_2}^2)\mu_1\mu_2 \end{aligned} \tag{3.121}$$

$$\begin{aligned} g_{\psi\psi} &= \left(m_{01}^{(1)} m_{01}^{(2)} \mu_1\mu_2(\mu_1 - \mu_2)\psi_2(\mu_1)\psi_2(\mu_2)\right)^2 + \left(m_{02}^{(1)} m_{02}^{(2)} g_2 (\mu_1 - \mu_2)\rho^2\right)^2 \\ &\quad - \left[\left(m_{01}^{(1)} m_{02}^{(2)} \mu_1 \psi_2(\mu_1)\right)^2 + \left(m_{01}^{(2)} m_{02}^{(1)} \mu_2 (g_2 - \mu_2)\right)^2\right] (\rho^2 + \mu_1\mu_2)^2 g_2 \\ &\quad + 2 m_{01}^{(1)} m_{01}^{(2)} m_{02}^{(1)} m_{02}^{(2)} g_2 \mu_1\mu_2 \psi_2(\mu_2)\psi_2(\mu_1)(\rho^2 + {\mu_1}^2)(\rho^2 + {\mu_2}^2) \end{aligned} \tag{3.122}$$

$$
\begin{aligned}
g_{t\psi} &= m_{01}^{(1)} m_{02}^{(1)} \mu_2(\mu_1-\mu_2)\psi_2(\mu_1)(\rho^2+{\mu_1}^2)\left({m_{01}^{(2)}}^2\psi_2(\mu_2)^2-{m_{02}^{(2)}}^2 g_2\right) \\
&\quad -m_{01}^{(2)} m_{02}^{(2)} \mu_1(\mu_1-\mu_2)\psi_2(\mu_2)(\rho^2+{\mu_2}^2)\left({m_{01}^{(1)}}^2\psi_2(\mu_1)^2-{m_{02}^{(1)}}^2 g_2\right) \qquad (3.123)
\end{aligned}
$$

$$
\begin{aligned}
\Sigma &= \left[\psi_2(\mu_1)^2\psi_2(\mu_2)^2+{g_2}^2\right]\left(m_{01}^{(1)} m_{02}^{(2)}(\mu_1-\mu_2)\rho\right)^2 \\
&\quad +\left[\left(m_{01}^{(1)} m_{02}^{(2)}\psi_2(\mu_1)\right)^2+\left(m_{02}^{(1)} m_{01}^{(2)}\psi_2(\mu_2)\right)^2\right](\rho^2+\mu_1\mu_2)^2 g_2 \\
&\quad -2m_{01}^{(1)} m_{01}^{(2)} m_{02}^{(1)} m_{02}^{(2)} g_2\psi_2(\mu_1)\psi_2(\mu_2)(\rho^2+{\mu_1}^2)(\rho^2+{\mu_2}^2) \qquad (3.124)
\end{aligned}
$$

The functions g_2 and g_3 are given in (3.115), and

$$\psi_1(\lambda) = -1 \qquad (3.125)$$

$$\psi_2(\lambda) = \frac{(R_{-\eta_1}-z-\eta_1\sigma-\lambda)(R_\kappa-z+\kappa\sigma-\lambda)}{R_{\eta_2}-z+\eta_2\sigma-\lambda} \qquad (3.126)$$

$$\psi_3(\lambda) = \frac{(R_{-\eta_1}+z+\eta_1\sigma+\lambda)(R_{\eta_2}-z+\eta_2\sigma-\lambda)}{R_\kappa-z+\kappa\sigma-\lambda} \qquad (3.127)$$

Although these functions are denoted $\psi_i(\lambda)$, they are actually functions of λ, ρ, and z. The ρ and z dependence is suppressed to make the equations more compact.

It may be noted that the ψ_i functions defined in (3.125)-(3.127) are similar to the metric coefficients defined in (3.115). In fact, this is no coincidence, since $\Psi = \mathrm{diag}(\psi_1, \psi_2, \psi_3)$ is actually the generating matrix for the seed metric. Thus, the seed metric can be recovered by substituting the ψ_i functions into (3.100).

The metric coefficients given in (3.120) give the raw results from the ISM, so they will be a solution to Einstein's equations but they take no account of the physical niceties that we would expect for the solution to be physically realisable. To ensure that the solution is asymptotically flat, it is necessary to apply the transformations

$$t \to t' = t - C_1\phi, \qquad \psi \to \psi' = \psi \qquad (3.128)$$

This now allows the constant C_1 to be chosen so that the solution is asymptotically flat and also ensures that the solution still satisfies $\det G = -\rho^2$. Applying these transformations to the metric coefficients gives

$$G_{tt}^{(phys)} \to G_{t't'}^{(phys)} = G_{tt}^{(phys)} \qquad (3.129)$$

$$G_{t\psi}^{(phys)} \to G_{t'\psi'}^{(phys)} = G_{t\psi}^{(phys)} + C_1 G_{tt}^{(phys)} \qquad (3.130)$$

$$G_{\psi\psi}^{(phys)} \to G_{\psi'\psi'}^{(phys)} = G_{\psi\psi}^{(phys)} + 2C_1 G_{t\psi}^{(phys)} + C_1^2 G_{tt}^{(phys)} \qquad (3.131)$$

Seeing as the desired black ring solution will only have angular momentum in one direction, it should be possible to parametrise it in terms of its mass and angular momentum. Examination of the functions given in (3.121)-(3.124) shows that there are far too many parameters to describe such a solution. To reduce the number of parameters it is necessary to make a number of identifications

$$m_{01}^{(1)} m_{01}^{(2)} = \beta \tag{3.132}$$

$$m_{01}^{(2)} m_{02}^{(1)} = \sqrt{\sigma}(\kappa_2 - 1) \tag{3.133}$$

$$m_{01}^{(1)} m_{02}^{(2)} = -\sqrt{\sigma}\alpha\beta(\kappa_1 + 1) \tag{3.134}$$

$$m_{02}^{(1)} m_{02}^{(2)} = -\sigma\alpha(\kappa_1 + 1)(\kappa_2 - 1) \tag{3.135}$$

and

$$C_1 = \frac{2\sqrt{\sigma}\alpha}{1 + \alpha\beta} \tag{3.136}$$

where C_1 is chosen to ensure that the metric is asymptotically flat. The functions κ_1 and κ_2 are given by

$$\kappa_1 + 1 = \frac{(1 - \kappa)(\eta_1 + 1)}{1 - \eta_2}, \qquad \kappa_2 - 1 = \frac{(\kappa + 1)(\eta_1 - 1)}{\eta_2 + 1} \tag{3.137}$$

Having applied these identities there remain six parameters which have to be restricted further to produce the balanced black ring solution. To avoid the solution having closed timelike curves α and β have to be restricted as

$$\alpha = \sqrt{\frac{2(1 - \eta_2)}{(\kappa - 1)(1 + \eta_1)}}, \qquad \beta = \sqrt{\frac{(\kappa + 1)(1 - \eta_1)}{2(1 + \eta_2)}} \tag{3.138}$$

These conditions come from demanding that the ∂_ψ orbit closes at $(\rho, z) = (0, \pm\sigma)$. This reduces the number of free parameters to four, so two further restrictions are required to give the solution in terms of two parameters representing the mass and angular momentum.

One further restriction is provided by demanding that the solution should be free from conical singularities. This gives an implicit function relating α and β to κ, η_1, and η_2

$$1 + \alpha\beta = \sqrt{\frac{\kappa + 1}{\kappa - 1}} \left(\frac{\kappa - \eta_2}{\kappa + \eta_1}\right) \left(1 + \alpha\beta \frac{\kappa - 1}{\kappa + 1}\right) \tag{3.139}$$

Applying this restriction leaves the solution specified in terms of three free parameters, which is in-line with the conventional presentation of the black ring metric.

As will be seen later, a further restriction is needed to ensure that the metric is completely free from conical singularities, which then reduces the number of free parameters to two, as anticipated.

It is now theoretically possible to give the metric for the black ring in terms of the remaining free parameters, but it is helpful to introduce some further constants to give the solution in a more compact form. These extra constants are defined in terms of the existing constants as

$$b = \frac{[\kappa+1+(\kappa-1)\alpha\beta]^2-(\kappa^2-1)(1+\alpha\beta)^2}{[\kappa+1+(\kappa-1)\alpha\beta]^2+(\kappa^2-1)(1+\alpha\beta)^2} \tag{3.140}$$

$$c = \frac{\eta_1+\eta_2}{2\kappa+\eta_1-\eta_2} \tag{3.141}$$

$$\tilde{\kappa}^2 = \left(\kappa+\frac{\eta_1-\eta_2}{2}\right)\sigma \tag{3.142}$$

$$\tilde{z} = z+\frac{\eta_1-\eta_2}{2}\sigma \tag{3.143}$$

where b and c are constrained to be in the range

$$0<c\leq b<1 \tag{3.144}$$

In terms of these new parameters, the balanced black ring solution is given by

$$\mathrm{d}s^2 = g_{tt}\mathrm{d}t^2+g_{t\psi}\mathrm{d}t\mathrm{d}\psi+g_{\psi\psi}\mathrm{d}\psi^2+g_{\phi\phi}\mathrm{d}\phi^2+e^{2\nu}(\mathrm{d}\rho^2+\mathrm{d}z^2) \tag{3.145}$$

where

$$g_{tt} = \frac{4b(1-c^2)\tilde{\kappa}^2}{\Phi}-1 \tag{3.146}$$

$$g_{t\psi} = -\frac{2\mathcal{C}\tilde{\kappa}(1-c)\left[\tilde{R}_3-\tilde{R}_1+(1+c)\tilde{\kappa}^2\right]}{\Phi} \tag{3.147}$$

$$g_{\psi\psi} = -\frac{\rho^2}{g_{tt}g_{\phi\phi}}+\frac{g_{t\psi}^2}{g_{tt}} \tag{3.148}$$

$$g_{\phi\phi} = \frac{(\tilde{R}_3+z-\tilde{\kappa}^2)(\tilde{R}_2-z+c\tilde{\kappa}^2)}{\tilde{R}_1-z-c\tilde{\kappa}^2} \tag{3.149}$$

$$e^{2\nu} = \frac{\Phi\left[(1-c)\tilde{R}_1+(1+c)\tilde{R}_2+2c\tilde{R}_3\right]}{8(1-c^2)^2\tilde{R}_1\tilde{R}_2\tilde{R}_3} \tag{3.150}$$

and

$$\Phi = (1+b)(1-c)\tilde{R}_1+(1-b)(1+c)\tilde{R}_2-2(b-c)\tilde{R}_3+2b(1-c^2)\tilde{\kappa}^2 \tag{3.151}$$

The constant C is defined as

$$C = \sqrt{2b(b-c)\frac{1+b}{1-b}} \tag{3.152}$$

and

$$\tilde{R}_1 = \sqrt{\rho^2 + (\tilde{z} + c\tilde{\kappa}^2)^2}, \quad \tilde{R}_2 = \sqrt{\rho^2 + (\tilde{z} - c\tilde{\kappa}^2)^2}, \quad \tilde{R}_3 = \sqrt{\rho^2 + (\tilde{z} - \tilde{\kappa}^2)^2} \tag{3.153}$$

Examination of (3.145) shows that the determinant of the 3×3 block G satisfies (3.90) and the $g_{\phi\phi}$ component is the same as that of the seed metric given in (3.114). This verifies that the normalisation given in (3.119) is valid.

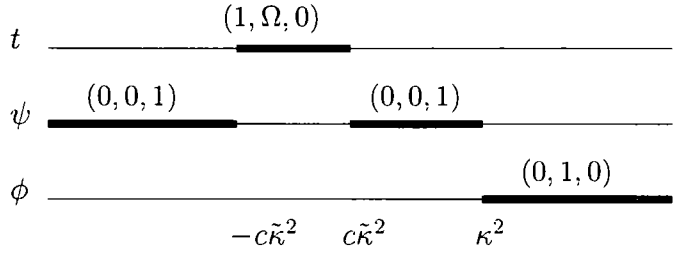

Figure 3.1: This figure shows the rod structure of the singly spinning black ring, with the rod directions and end-points marked. The angular velocity of the black ring is denoted Ω.

Figure 3.1 shows the rod structure of the singly spinning ring. This allows the solution in the Weyl form to be interpreted pictorially. The fact that the t rod is finite means that there is an event horizon between $-c\tilde{\kappa}^2$ and $c\tilde{\kappa}^2$ for $\rho = 0$. Moreover, the fact that the timelike rod is bookended by two rods in the ψ direction indicates that the horizon will have topology $S^2 \times S^1$, with the z and ψ coordinates parameterising the S^2 and the remaining ϕ coordinate parameterising the S^1.

To get from the metric given in (3.145) to the more familiar metric for the singly spinning ring, given in terms of toroidal coordinates, it is necessary to make some further transformations. These transformations are given in [54] and [35] as

$$\rho = \frac{2\tilde{\kappa}^2\sqrt{-G(x)G(y)}}{(x-y)^2}, \qquad \tilde{z} = \frac{\tilde{\kappa}^2(1-xy)(2+cx+cy)}{(x-y)^2} \tag{3.154}$$

where $G(\xi)$ is a structure function given by

$$G(\xi) = (1-\xi^2)(1+c\xi) \tag{3.155}$$

and the coordinates lie in the range

$$-1 \leq x \leq 1, \qquad y \leq -1 \tag{3.156}$$

Applying these transformations gives (3.145) in a considerably more compact form

$$\begin{aligned} \mathrm{d}s^2 &= -\frac{F(y)}{F(x)}\left(\mathrm{d}t - \frac{C\tilde{\kappa}(1+y)}{F(y)}\mathrm{d}\psi\right)^2 \\ &\quad + \frac{2\tilde{\kappa}^2 F(x)}{(x-y)^2}\left[\frac{\mathrm{d}x^2}{G(x)} + \frac{G(x)}{F(x)}\mathrm{d}\phi^2 - \frac{\mathrm{d}y^2}{G(y)} - \frac{G(y)}{F(y)}\mathrm{d}\psi^2\right] \end{aligned} \tag{3.157}$$

where

$$F(\xi) = 1 + b\xi \tag{3.158}$$

and b and c are given by (3.140) and (3.141) respectively.

The solutions given by (3.145) and (3.157) actually have an additional conical singularity at $x = 1$, which can be rectified by setting

$$b = \frac{2c}{1+c^2} \tag{3.159}$$

This then ensures that the ∂_ψ and ∂_ϕ orbits close off smoothly at $x = 1$ and gives a balanced black ring solution in terms of the two parameters κ and c. These variables can then be related to the mass and angular momentum of the ring.

3.4.2 The Doubly Spinning Black Ring

The method for deriving the doubly spinning black ring is similar in many respects to that of the singly spinning ring. The basic outline of the derivation can be split up into three steps. Firstly, the seed metric is generated by taking the singly spinning black ring given in [46] and removing two solitons from it. Then, two more solitons with more general rotation parameters are added to this seed solution using the Inverse Scattering Method. Thirdly, the ranges and values of the parameters are set so as to ensure that the metric remains real and of the correct signature, as well as removing any potential singularities or closed-timelike-curves.

The idea behind finding a seed metric by removing solitons was first suggested by Pomeransky in [51]. He noticed that it was possible to remove solitons from a solution that had been generated via the inverse scattering method by dividing

certain metric coefficients by a simple function $\frac{-\rho^2}{\mu^2}$. This technique works because multiplying a seed metric by a function commutes with adding solitons to a seed solution. In the case of the doubly spinning ring, this involves taking the Emparan-Reall solution and removing two solitons from the t, ψ, ϕ sector.

The next step toward obtaining the solution is to replace the solitons that have been removed with new solitons that have extra rotation parameters. The ISM guarantees that the new metric will still solve the Einstein equation, and so long as the solution isn't re-scaled at any point (or at least without being undone afterwards) it will also satisfy the condition that $\det G = -\rho^2$. The extra parameters allow the ring to have angular momentum in more than one plane, but they also introduce more singular points into the solution which have to be dealt with.

In the case of the doubly spinning black ring, there are four independent parameters that have to satisfy $0 \leq \nu < 1$, $2\sqrt{\nu} \leq \lambda < 1+\nu$, $k > 0$ and $c \leq b < 1$, where c is defined in terms of λ, and ν as

$$c = \frac{\sqrt{\lambda^2 - 4\nu}}{1-\nu} \tag{3.160}$$

Furthermore, if the ring is to be completely free from conical singularities then

$$b = \frac{2c}{1+c^2} \tag{3.161}$$

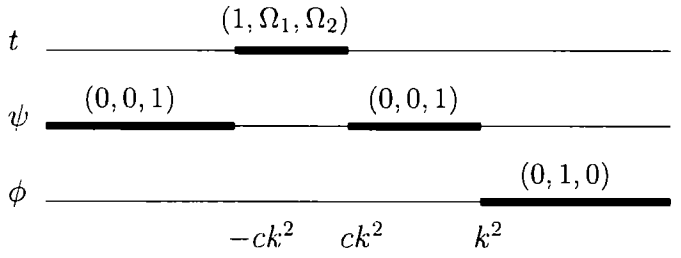

Figure 3.2: This figure shows the rod structure of the doubly spinning black ring, with the rod directions and end-points marked.

Figure 3.2 shows the rod structure of the doubly spinning black ring solution. The rods all lie along the z axis, with the rod endpoints given by $-ck^2$, ck^2, and k^2 along the horizontal axis on the plot. The vertical axis labels each of the directions, and the position of the rod in the vertical direction indicates the direction of the rod. All of the rods except the one between $-ck^2$ and ck^2 lie in only one direction.

The rod on the t line in figure 3.2 has direction vector (t, Ω_1, Ω_2), so actually has components in three directions.

The semi-infinite spacelike rod $[-\infty, -ck^2]$ and $[ck^2, k^2]$ have direction $v = (0, 0, 1)$, which means that when $\rho = 0$, for $-\infty < z < -ck^2$ and $ck^2 < z < k^2$, $g_{\alpha\beta}v^\beta = 0$. These rods indicate that the ψ direction is an axis of rotation and in order to avoid conical singularities at the finite rod $ck^2 < z < k^2$, the period of ψ has to be restricted as

$$\begin{aligned}\Delta\psi &= \lim_{\rho\to 0} 2\pi\sqrt{\frac{\rho^2\tilde{f}}{g_{\alpha\beta}v^\alpha v^\beta}} \\ &= 2\pi\sqrt{\frac{-(-1+b)(-1+c)^2(c\alpha+b(-2(1+c)^2+c\alpha))^2}{(1+b)(1+c)^2(c\alpha-b(2(-1+c)^2+c\alpha))^2}}\,,\end{aligned} \tag{3.162}$$

where α is defined as

$$\alpha = \frac{4(\lambda+q)(\lambda+2-q)(\lambda-2-q)}{(\lambda-q)(\lambda+2+q)(\lambda-2+q)} \tag{3.163}$$

and $q = \sqrt{\lambda^2 - 4\nu}$.

The semi-infinite rod $-\infty < z < -ck^2$ implies that the periodicity of the ψ variable should also be given by $\Delta\psi = 2\pi$, which can only be reconciled with (3.162) if

$$b = \frac{2c}{1+c^2}\,, \tag{3.164}$$

or

$$b = \pm\frac{c\alpha}{\sqrt{4-8c^2+4c^4+c^2\alpha^2}}\,. \tag{3.165}$$

Unfortunately, the choice of (3.165) leads to the metric becoming singular, which is why b has to be restricted as (3.161).

The finite timelike rod $-ck^2 < z < ck^2$ corresponds to an event horizon because it is the only timelike rod. Also, the topology of the horizon has to be $S^1 \times S^2$ because $\partial_\psi = 0$ at both ends of the rod. The direction of the timelike rod is given by $v = (1, \Omega_1, \Omega_2)$, where

$${\Omega_1}^2 = \frac{(1+b)(b-c)\left[2b(1-c)^2-(1-b)c\alpha\right]C}{2(1-b)b(1-c)^2\left[2b(1+c)^2-(1+b)c\alpha\right]Dk^2} \tag{3.166}$$

$${\Omega_2}^2 = \frac{(1+b)C(1+c)^2\left[2b(1-c^2)-c\alpha\right]^2\left[2b(1-c)^2-(1-b)c\alpha\right]^2}{\alpha(1-b)Dc^2\left[4b^2(1-c^2)^2-(1-b^2)c^2\alpha^2\right]^2k^2} \tag{3.167}$$

where $C = 2b(1-c^2) - (1-b)c\alpha$ and $D = 2b(1-c^2) - (1+b)c\alpha$. These variables Ω_1 and Ω_2 represent the angular velocities of the horizon in the ∂_ϕ and ∂_ψ directions respectively.

The semi-infinite spacelike rod $k^2 < z < \infty$ is in the direction of $v = (0,1,0)$ and means that the ϕ coordinate is an angular coordinate with period $\phi = 2\pi$. This comes from calculating the periodicity that is required in ϕ to eliminate any conical singularities i.e.

$$\Delta\phi = \lim_{\rho\to 0} 2\pi \sqrt{\frac{\rho^2 \tilde{f}}{g_{\alpha\beta} v^\alpha v^\beta}} = 2\pi \tag{3.168}$$

The doubly spinning black ring in canonical coordinates is rather unwieldy so, to express it in a more compact form, transform to the C-metric coordinates via

$$\rho^2 = -\frac{4k^4 G(x)G(y)}{(x-y)^2(1-\nu)^2}, \tag{3.169}$$

$$z = \frac{k^2(1-xy)(2+(x+y)\lambda+2xy\nu)}{(x-y)^2(1-\nu)}. \tag{3.170}$$

This then gives the doubly spinning ring metric as

$$\begin{aligned} ds^2 = & -\frac{H(y,x)(\mathrm{d}t+\Omega)^2}{H(x,y)} - \frac{F(x,y)\mathrm{d}\psi^2}{H(y,x)} - \frac{2J(x,y)\mathrm{d}\phi\mathrm{d}\psi}{H(y,x)} \\ & + \frac{F(y,x)\mathrm{d}\phi^2}{H(y,x)} + \frac{k^2 H(x,y)}{(x-y)^2(1-\nu)^2}\left(\frac{\mathrm{d}x^2}{G(x)} - \frac{\mathrm{d}y^2}{G(y)}\right) \end{aligned} \tag{3.171}$$

where

$$\begin{aligned} \Omega = & -\frac{k\lambda\sqrt{2(1+\nu)^2-2\lambda^2}}{H(y,x)}\Big[(1-x^2)y\sqrt{\nu}\mathrm{d}\phi \\ & + \frac{(1+y)\left[1+\lambda-\nu+x^2y\nu(1-\lambda-\nu)+2\nu x(1-y)\right]\mathrm{d}\psi}{(1-\lambda+\nu)}\Big] \end{aligned} \tag{3.172}$$

$$G(x) = (1-x^2)(1+\lambda x+\nu x^2) \tag{3.173}$$

$$\begin{aligned} H(x,y) = & \ 1+\lambda^2-\nu^2+2\lambda\nu(1-x^2)y+2x\lambda(1-y^2\nu^2) \\ & + x^2y^2\nu(1-\lambda^2-\nu^2) \end{aligned} \tag{3.174}$$

$$\begin{aligned} J(x,y) = & \ k^2(1-x^2)(1-y^2)\lambda\sqrt{\nu}\times \\ & \frac{\left[1+\lambda^2-\nu^2+2(x+y)\lambda\nu-xy\nu(1-\lambda^2-\nu^2)\right]}{(x-y)(1-\nu)^2} \end{aligned} \tag{3.175}$$

$$\begin{aligned} F(x,y) = & \ \frac{k^2}{(x-y)^2(1-\nu)^2}\times \\ & \Big[G(x)(1-y^2)\left\{[(1-\nu)^2-\lambda^2](1+\nu)+y\lambda[1-\lambda^2+2\nu-3\nu^2]\right\} \end{aligned}$$

$$+G(y)\left\{2\lambda^2+x\lambda[(1-\nu)^2+\lambda^2]+x^2[(1-\nu)^2-\lambda^2](1+\nu)\right.$$
$$\left.+x^3\lambda(1-\lambda^2-3\nu^2+2\nu^3)-x^4(1-\nu)\nu(\lambda^2+\nu^2-1)\right\}\Big] \qquad (3.176)$$

Note that the constraint given in (3.161) has been applied to this metric, so that it is non-singular.

Chapter 4

Physical Properties of Black Ring Solutions

In this chapter the physical properties of both the singly spinning and doubly spinning black ring solutions to the vacuum Einstein equations will be examined and their thermodynamic properties calculated. The various properties are re-derived from results given in [26, 27, 44, 46, 61]. It is directly shown that the topology of the singly spinning ring solution is $S^2 \times S^1$ and that it asymptotes to the Minkowski solution. The toroidal coordinate systems used in both solutions are also described, along with plots of the contours in the two different sets of coordinates.

Although, the singly spinning ring is just a specific case of the doubly spinning ring when the angular momentum in the S^2 direction is zero, it is worth investigating in its own right. This is because the singly spinning solution provides a simplified model of the more general doubly spinning ring since a lot of the behaviour of the more general doubly spinning ring is duplicated when the ring is only spinning around the axis of the S^1. Having said this, the causal structure of the spacetime is significantly different when angular momentum is added in the ϕ direction because the ring gains an extra horizon. This has a major effect on the spacetime in the vicinity of the curvature singularity.

4.1 Properties of the Singly Spinning Black Ring

The notation for the singly spinning black ring solution has changed slightly since it was first discovered in [26]. The modern most compact notation, as presented in [46], gives the metric as

$$ds^2 = \frac{R^2F(x)}{(x-y)^2}\left[\frac{dx^2}{G(x)} + \frac{G(x)}{F(x)}d\phi^2 - \frac{G(y)}{F(y)}d\psi^2 - \frac{dy^2}{G(y)}\right] - \frac{F(y)}{F(x)}\left(dt - CR\frac{1+y}{F(y)}d\psi\right)^2 \tag{4.1}$$

and

$$F(\xi) = 1 + \lambda\xi \qquad\qquad G(\xi) = (1-\xi^2)(1+\nu\xi)\,. \tag{4.2}$$

Also, C is given by

$$C = \sqrt{\lambda(\lambda-\nu)\frac{1+\lambda}{1-\lambda}}\,. \tag{4.3}$$

The form of $G(\xi)$ given above has three explicit roots, given by

$$\xi_2 = -1, \qquad \xi_3 = +1, \qquad \xi_4 = -\frac{1}{\nu} \tag{4.4}$$

and the single root of $F(\xi)$ can be labelled analogously as

$$\xi_1 = -\frac{1}{\lambda}\,. \tag{4.5}$$

Labelling the roots in this manner allows the metric to be compared with the singly rotating ring solution given in [26], although the form of the structure functions are slightly different.

The black ring metric was originally derived from a Wick rotation of a metric in [47] and was given in the form [26]

$$\begin{aligned} ds^2 \;=\; & -\frac{F(x)}{F(y)}\left(dt - \sqrt{\frac{\nu}{\xi_1}}\frac{\xi_2 - y}{A}d\psi\right)^2 + \frac{1}{A^2(x-y)^2} \\ & \times\left[F(y)^2\left(\frac{dx^2}{G(x)} + \frac{G(x)}{F(x)}d\phi^2\right) - F(x)\left(G(y)d\psi^2 + \frac{F(y)}{G(y)}dy^2\right)\right]\,, \end{aligned} \tag{4.6}$$

where the structure functions were given by

$$F(\xi) = 1 - \xi/\xi_1\,, \qquad\qquad G(\xi) = 1 - \xi^2 + \nu\xi^3\,. \tag{4.7}$$

In order for this metric to be free from singularities, the roots ξ_1-ξ_3 all have to satisfy the conditions given for the derivation of the black ring in the previous section. The

modern labelling of the roots given in (4.4) and (4.5) was devised in [26] after it was realised that the function $G(\xi)$ could be factored into a linear and a quadratic part similar to that given in (4.2). Also, in (4.6), the parameter A represented an acceleration but it was later realised that it was more sensible to relate this to a radius parameter R, which occurs in (4.1).

Going back to (4.1), the remaining parameters λ and ν are dimensionless, and R has dimensions of length. The parameters ν and λ control the shape and rotation of the black ring. As $\nu \to 0$, the solution describes a thinner and slower rotating black ring until it becomes infinitely thin and non-rotating when $\nu = 0$. The other parameter λ controls the nature of the horizon and, as shown later, has to be restricted to avoid the appearance of conical singularities in the solution. Examination of (4.1) shows that in order for the signature of the metric to remain Lorentzian, λ and ν have to be restricted so that $0 < \nu \leq \lambda < 1$.

Examination of (4.1) shows straight away that there are three Killing directions given by ∂_t, ∂_ψ, and ∂_ϕ. This will prove useful when analysing the geodesics of the metric as there will be three conserved quantities associated with these Killing vectors. The metric also has two Killing horizons where ∂_t and $\partial_t + \Omega\partial_\psi$ become null. These Killing horizons correspond to the ergosurface at $y = -1/\lambda$ and the event horizon at $y = -1/\nu$ respectively. Since the hypersurface $y = -1/\nu$ is the event horizon, Ω will give the angular velocity of the event horizon, as calculated later.

The x, y coordinates used in (4.1) are inherited from the original C-metric derivation of the Black Ring and are particularly suited to this solution, since they are toroidal coordinates. To get a better idea of how these toroidal coordinates foliate the space, it is useful to consider the transformations [46]

$$r_1 = R\frac{\sqrt{1-x^2}}{(x-y)}\,, \qquad r_2 = R\frac{\sqrt{y^2-1}}{(x-y)}\,. \tag{4.8}$$

Applying these transformations to a manifestly flat metric given by

$$\mathrm{d}{x_4}^2 = \mathrm{d}{r_1}^2 + {r_1}^2\mathrm{d}\phi^2 + \mathrm{d}{r_2}^2 + {r_2}^2\mathrm{d}\psi^2 \tag{4.9}$$

re-casts the metric in the form

$$\mathrm{d}{x_4}^2 = \frac{R^2}{(x-y)^2}\left[(y^2-1)\mathrm{d}\psi^2 + \frac{\mathrm{d}y^2}{y^2-1} + \frac{\mathrm{d}x^2}{1-x^2} + (1-x^2)\mathrm{d}\phi^2\right]\,. \tag{4.10}$$

which, not coincidentally, bears a marked resemblance to the metric given in (4.1). Indeed, (4.10) is the zero mass limit of (4.1), which is obtained by taking the limit as $\lambda, \nu \to 0$. Furthermore, the transformations given in (4.8) give limits on the (x, y) coordinates, as r_1 and r_2 have to remain real and non-negative. This implies limits on x and y as

$$-1 \leq x \leq 1 \,, \qquad\qquad -\infty < y \leq -1 \,, \tag{4.11}$$

which ensures that the signature of the metric always remains Lorentzian.

To understand how (x, y) span a constant ψ cross-section it is useful to combine the two transformations given in (4.8) to get a set of transformations with a single radial coordinate and two angular coordinates. Doing this gives

$$r = \sqrt{r_1^2 + r_2^2} = \frac{R\sqrt{y^2 - x^2}}{x - y} \tag{4.12}$$

and

$$\tan\theta = \frac{r_2}{r_1} = \sqrt{\frac{y^2 - 1}{1 - x^2}} \,. \tag{4.13}$$

These coordinates can now be used to span a three dimensional cross-section of constant ψ, with rotation in the ϕ direction providing the third degree of freedom.

To check that these coordinates do actually reduce to the spherical polar coordinates on flat space, consider the case where $\lambda = \nu = 0$. Transforming (4.1) using (4.12) and (4.13) and then dispensing of all of the terms involving λ and ν the metric becomes

$$\mathrm{d}s^2 = -\mathrm{d}t^2 + \mathrm{d}r^2 + r^2(\mathrm{d}\theta^2 + \sin^2\theta \mathrm{d}\psi^2 + \cos^2\theta \mathrm{d}\phi^2) \,, \tag{4.14}$$

which is familiar as the 5D metric for flat space, thus confirming that the new set of coordinates are just the familiar spherical polar coordinates in five dimensions.

Figure 4.1 uses these coordinates to show the lines of constant y and x when ϕ and ψ are held constant. The ψ coordinate would define the plane coming out of the page, perpendicular to the vertical axis. As can be seen from the plot, the lines of constant y define circles (or spheres when the ϕ coordinate is included) that foliate the space, with the x coordinate varying around the circle. The circles get bigger as y increases towards -1 with $y = -1$ defining the axis of rotation of the ring, and $x = y = -1$ being equivalent to $r = \infty$ in polar coordinates. It is worth pointing

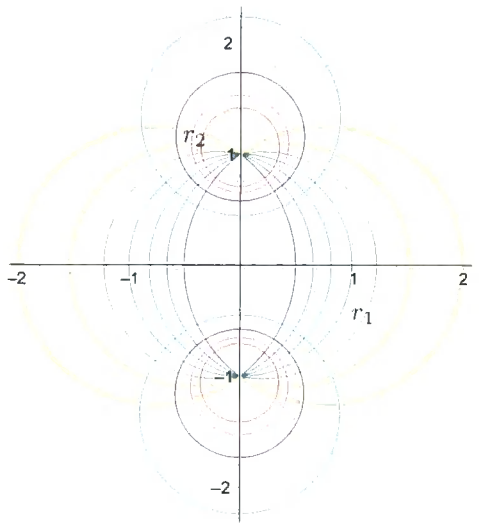

Figure 4.1: A two dimensional cross-section of constant ϕ and ψ (as well as the antipodal points $\phi + \pi$ and $\psi + \pi$) of the (x, y) coordinates. The red-turquoise circles (centred on the horizontal axis) are lines of constant y and the blue-orange circles (centred on the vertical axis) are lines of constant x. The horizontal axis on this plot corresponds to $y = -1$ and the vertical axis corresponds to $x = \pm 1$, where $x = +1$ corresponds to the centre of the ring up to the inner edge, and $x = -1$ corresponds to the region from the outer edge of the ring to infinity.

out that the (x, y) coordinates only cover a semi-circle in one of the quadrants, depending on the values of ϕ and ψ. The contour lines plotted in figure 4.1 cover all four quadrants to emphasise how well adapted the coordinates are to the shape of the black ring.

It is now possible to check that (4.1) is asymptotically flat in the limit as $x = y = -1$. To do this it is necessary to consider slightly different transformations from (4.8), as given in [26]. These are

$$\zeta = \frac{\tilde{R}\sqrt{-1-y}}{(x-y)}\,, \qquad \eta = \frac{\tilde{R}\sqrt{x+1}}{(x-y)} \tag{4.15}$$

where

$$\tilde{R} = \frac{2R(1-\lambda)}{\sqrt{2(1-\nu)}}\,. \tag{4.16}$$

Substituting these coordinate transformations in shows that in the vicinity of $x = y = -1$ the metric takes the form

$$\mathrm{d}s^2 = -\mathrm{d}t^2 + \frac{R^2(1-\lambda)}{(x-y)^2}\left[-\frac{(1-y^2)(1-\nu)}{(1-\lambda)}\,\mathrm{d}\psi^2 - \frac{\mathrm{d}y^2}{(1-\nu)(1-y^2)}\right.$$

$$+\frac{\mathrm{d}x^2}{(1-x^2)(1-\nu)}+\frac{(1-x^2)(1-\nu)}{(1-\lambda)}\mathrm{d}\phi^2\Big] \quad (4.17)$$

To examine the region near $x = y = -1$, consider $x = -1+\epsilon$ and $y = -1+\epsilon$, implying

$$1-x^2 = 2\epsilon-\epsilon^2\,, \qquad 1-y^2 = 2\epsilon-\epsilon^2\,. \quad (4.18)$$

In these expressions, ϵ is defined to be small, so the ϵ^2 terms can be ignored since they will be even smaller. Substituting into (4.17) now gives

$$\mathrm{d}s^2 = -\mathrm{d}t^2+\mathrm{d}\zeta^2+\zeta^2\mathrm{d}\tilde{\psi}+\mathrm{d}\eta^2+\eta^2\mathrm{d}\tilde{\phi}^2\,. \quad (4.19)$$

Here $\tilde{\psi} = \frac{2\pi\psi}{\Delta\psi}$ and $\tilde{\phi} = \frac{2\pi\phi}{\Delta\phi}$ with $\Delta\psi$ and $\Delta\phi$ defined as in (4.27). It is now obvious, using these coordinates, that the metric is asymptotically flat with two pairs of radial and angular coordinates parameterising the space.

To show that the event horizon of (4.1) is ring shaped it is necessary to use a further set of coordinate transformations given by

$$r = -\frac{R}{y}\,, \qquad \cos\theta = x\,, \quad (4.20)$$

which gives the limits on r and θ as

$$0\le r\le R\,, \qquad 0\le\theta\le\pi\,. \quad (4.21)$$

These transformations can then be used to transform the flat metric, given in (4.10), to a form which is easier to analyse

$$\mathrm{d}{x_4}^2 = \frac{1}{\left(1+\frac{r\cos\theta}{R}\right)^2}\left[\left(1-\frac{r^2}{R^2}\right)R^2\mathrm{d}\psi^2+\frac{\mathrm{d}r^2}{1-r^2/R^2}+r^2\left(\mathrm{d}\theta^2+\sin^2\theta\mathrm{d}\phi^2\right)\right]. \quad (4.22)$$

In these coordinates it is easy to see that the surfaces of constant r describe an S^2 parameterised by ϕ and θ, with the S^1 parameterised by ψ. This form of the metric shows that the S^2 is metrically round but when the full black ring metric is considered, the S^2 surfaces are deformed away from a perfectly round sphere.

The full black ring metric, given in terms of the coordinates in (4.20), is

$$\mathrm{d}s^2 \;=\; -\frac{\hat{f}}{\hat{g}}\left(\mathrm{d}t-r_0\sinh\sigma\cosh\sigma\sqrt{\frac{R+r_0\cosh^2\sigma}{R-r_0\cosh^2\sigma}}\frac{r/R-1}{r\hat{f}}R\mathrm{d}\psi\right)^2$$

$$+\frac{\hat{g}}{\left(1+\frac{r\cos\theta}{R}\right)^2}\left[\frac{f}{\hat{f}}\left(1-\frac{r^2}{R^2}\right)R^2\mathrm{d}\psi^2+\frac{\mathrm{d}r^2}{(1-r^2/R^2)\,f}\right.$$
$$\left.+\frac{r^2}{g}\mathrm{d}\theta^2+\frac{g}{\hat{g}}r^2\sin^2\theta\mathrm{d}\phi^2\right], \tag{4.23}$$

where some extra functions have been defined as

$$f=1-\frac{r_0}{r}, \qquad \hat{f}=1-\frac{r_0\cosh^2\sigma}{r},$$
$$g=1+\frac{r_0}{R}\cos\theta, \qquad \hat{g}=1+\frac{r_0\cosh^2\sigma}{R}\cos\theta, \tag{4.24}$$

and the parameters (ν,λ) have been redefined as

$$\nu=\frac{r_0}{R}, \qquad \lambda=\frac{r_0\cosh^2\sigma}{R}. \tag{4.25}$$

This recasting of the metric shows why the S^2 surfaces are no longer perfectly spherical because the $g_{\theta\theta}$ and $g_{\phi\phi}$ terms have now acquired extra factors of g and $\hat{g}$. To see that these surfaces still have S^2 topology consider the limit where

$$r, r_0, r_0\cosh^2\sigma \ll R, \tag{4.26}$$

which implies that $g,\hat{g}\approx 1$ and thus shows that the $g_{\theta\theta}$ and $g_{\phi\phi}$ coefficients parameterise a two-sphere in this limit. As g and $\hat{g}$ are increased from 1, the two spheres become increasingly deformed until they are completely flattened into a disc perpendicular to the axis of rotation.

Making a further redefinition, $\psi = z/R$, puts the metric into the form of a boosted black string in the z direction, with σ parameterising the boost. Also, for the metric to be free from conical singularities, it is necessary for ψ to have period 2π, which means that z has to be compactified into a circle with radius R. This now allows the limit given in (4.26) to be interpreted as taking the radius (R) of the black ring being much larger than the thickness of the ring (r_0), and then looking at the region close to the horizon i.e. $r\approx r_0$.

Having shown that the metric can be thought of as a boosted black string, under certain conditions, it is now possible to interpret the parameters λ and ν physically. The redefinitions given in (4.25) indicate that ν measures the ratio between the radius of the S^2 at the horizon r_0 and the radius of the ring R. This means that smaller values of ν correspond to thin rings where the radius of the ring is larger

than the thickness of the ring. The definitions in (4.25) can also be combined to give an idea of the speed of rotation of the ring in terms of λ and ν, since the local boost velocity is given by $v = \tanh\sigma = \sqrt{1-(\nu/\lambda)}$.

Before going on to calculate the thermodynamical properties of the black ring, it is necessary to consider the conical singularities of the metric. There are two sets of points in (4.1) where conical singularities occur. One set at $(x, y) = (-1, -1)$ and one at $x = +1$. The singularity at $x = -1$ can be avoided by restricting the ϕ and ψ coordinates so that

$$\Delta\psi = \Delta\phi = \frac{4\pi\sqrt{F(-1)}}{|G'(-1)|} = \frac{2\pi\sqrt{1-\lambda}}{1-\nu} \,. \tag{4.27}$$

The other possible conical singularity at $y = -1$ and $x = +1$ then forces ϕ to satisfy

$$\Delta\phi = \frac{4\pi\sqrt{F(+1)}}{|G'(+1)|} = \frac{2\pi\sqrt{1+\lambda}}{1+\nu} \,. \tag{4.28}$$

The only way that this restriction can simultaneously be enforced whilst still satisfying (4.27) is to restrict the value of λ or ν. If λ is fixed in terms of ν, then it is given by

$$\lambda = \frac{2\nu}{1+\nu^2} \,. \tag{4.29}$$

This ensures that $\Delta\phi$ satisfies both (4.27) and (4.28) meaning that the singularities at $x = \pm 1$ are both simultaneously removed. Since λ and ν control the speed of rotation of the ring, this method of restricting λ is equivalent to balancing the centrifugal force on the ring with the tension in the ring. Although the number of parameters has been reduced, the topology of the solution remains a ring with x and ϕ describing an S^2 surface and the surfaces of varying (y, ψ) describing a circle.

The other method of avoiding the singularity at $x = +1$ is to make sure that $g_{xx} \neq \infty$ at $x = -1$. This is easily achieved by setting

$$\lambda = 1 \,, \tag{4.30}$$

which makes $g_{xx} = 0$ at $x = -1$, thus negating the need to impose (4.29). The conical singularity at $x = +1$ still exists, which necessitates ψ and ϕ being restricted like in (4.28). Since λ is now constant for all values of ν the constant t and y cross-sections have an S^3 topology i.e. a three-sphere meaning that ψ and ϕ are now independent angular coordinates of the sphere.

To calculate the thermodynamical properties of the singly spinning black ring it is easiest to use the coordinates described in (4.12) and (4.13). These coordinates have the advantage of asymptotic infinity being at surfaces of constant $r = \infty$, thus simplifying the calculations. As described earlier, as $r \to \infty$ the black ring metric approaches the 5D Myers Perry solution with angular momentum in one direction, so the thermodynamic properties of the black ring can be ascertained by comparing the metric coefficients in the weak field limit with the Myers Perry metric.

To calculate the ADM mass, it is only necessary to compare the asymptotic form of the black ring metric with the 5D Schwarzschild metric, as any terms contributing to the angular momentum of the ring should fall off as $r \to \infty$. Bearing this in mind, the asymptotic black ring metric should be in the form

$$ds^2 = -\left(1 - \frac{8GM}{3\pi r^2}\right) \mathrm{d}t^2 + \left(1 - \frac{8GP}{3\pi r^2}\right)^{-1} \mathrm{d}r^2 + \ldots , \tag{4.31}$$

where M and P are constant functions independent of r and θ. The metric coefficients relating to the angular coordinates have been suppressed as they are redundant when calculating the ADM mass.

To calculate the g_{tt} and g_{rr} coefficients for the black ring metric, transform to spherical polar coordinates and then take the Taylor expansion about $r = \infty$. The first two terms of the Taylor expansion for g_{tt} and g_{rr} are then given by

$$g_{tt} = -1 - \frac{2\lambda R^2}{(\lambda - 1) r^2} \tag{4.32}$$

$$g_{rr} = \frac{\lambda - 1}{\nu - 1} + \frac{2R^2 \left[\lambda \cos^2\theta - \lambda\nu \sin^2\theta - \nu \cos(2\theta)\right]}{(1 - \nu)^2 r^2} . \tag{4.33}$$

Usually, the mass can then be read off straight away by comparing the g_{tt} coefficients between (4.32) and (4.31) but in this case, the g_{rr} coefficient in (4.33) is not in the same form as (4.31). Taking the taylor expansion about $r = \infty$ of (4.31) gives

$$ds^2 = -\left(1 - \frac{8GM}{3\pi r^2}\right) \mathrm{d}t^2 + \left(1 + \frac{8GP}{3\pi r^2}\right) \mathrm{d}r^2 + \ldots , \tag{4.34}$$

showing that the coefficient of g_{rr} has to be in the form $1 + P/r^2$ in order for the expressions in (4.32) and (4.33) to be used to obtain the ADM mass. Fortunately, this problem can be easily remedied by re-scaling the r coordinate so that

$$r \to r' = r\sqrt{\frac{\nu - 1}{\lambda - 1}} , \tag{4.35}$$

which then allows $\frac{\lambda-1}{\nu-1}$ to be factored out of (4.33) giving it in the form of (4.34). Applying this transformation to (4.32) then gives

$$g_{tt} = -1 + \frac{2\lambda R^2}{(1-\nu)r^2} \tag{4.36}$$

which can now be compared with (4.34) to obtain the ADM mass,

$$M = \frac{3\pi R^2 \lambda}{4G(1-\nu)} , \tag{4.37}$$

where G is Newton's gravitational constant.

The angular momentum of the singly spinning black ring can be obtained in a similar manner by comparing the asymptotic expansion of the black ring metric with the singly rotating 5D Myers Perry metric. From [25] the angular momentum is given by the $g_{t\psi}$ coefficient,

$$g_{t\psi} = \frac{4GJ\sin^2\theta}{\pi r^2} . \tag{4.38}$$

This can then be compared with the Taylor expansion of the $g_{t\psi}$ coefficient from the black ring metric to obtain the angular momentum.

Taking the Taylor expansion of $g_{t\psi}$ for the black ring metric gives

$$g_{t\psi} = \frac{2R^3\sin^2\theta}{r^2}\sqrt{\frac{\lambda(\lambda-\nu)(1+\lambda)}{1-\lambda}} . \tag{4.39}$$

Comparing this with (4.38) would usually give the angular momentum straight away, but r has to be re-scaled in accordance with (4.35) and a further re-scaling is required because the period of ψ is assumed to be 2π in (4.38) which isn't the case for the black ring metric, since ψ has to satisfy (4.27). Combining these two transformations means that the $g_{t\psi}$ coefficient of the black ring metric becomes

$$g'_{t\psi} = \frac{2R^3\sin^2\theta\sqrt{\lambda(\lambda-\nu)(1+\lambda)}}{(1-\nu)^2 r^2} . \tag{4.40}$$

The angular momentum can then be read off, giving

$$J = \frac{\pi R^3\sqrt{\lambda(\lambda-\nu)(1+\lambda)}}{2G(1-\nu)^2} . \tag{4.41}$$

The entropy of a black hole is given by the area integral taken over the event horizon. In the case of the black ring, this means that the integral has to be taken

over a spacelike cross-section of constant $y = -1/\nu$. Written mathematically, this gives

$$A = \int \sqrt{|\gamma|} \mathrm{d}\phi \mathrm{d}\psi \mathrm{d}x \tag{4.42}$$

where γ is the induced metric on the horizon. The induced metric is obtained by demanding that t and y remain constant, which is equivalent to removing the $\mathrm{d}t$ and $\mathrm{d}y$ terms from the metric and then substituting $y = -1/\nu$. Doing this and taking the determinant gives

$$|\gamma| = \frac{R^3 \nu(\nu-1)\sqrt{\nu\lambda(1-\lambda^2)}}{(1+\nu x)^2(\lambda-1)} \,. \tag{4.43}$$

Plugging this into (4.42) and integrating over the coordinate space given by (4.27) and $x = -1 \to 1$, gives the area

$$A = 8\pi^2 R^3 \frac{\nu\sqrt{\nu\lambda(1-\lambda^2)}}{(1-\nu)^2(1+\nu)} \tag{4.44}$$

To calculate the angular velocity of the black ring, consider a photon on a null trajectory at the event horizon. The trajectory is chosen such that it has no momentum components in the y, x, or ϕ directions i.e. it is restricted so that it stays in the plane of rotation of the black ring. Plugging all this into the geodesic equation and setting $x = 0$ gives the condition for the null trajectory

$$\mathrm{d}t - CR\frac{(\nu-1)\sqrt{1-\lambda}}{(\nu-\lambda)(1-\nu)}\mathrm{d}\psi = 0 \,, \tag{4.45}$$

where ψ has been rescaled according to (4.27) to account for the conical singularities. This equation can now be solved for $\frac{\mathrm{d}\psi}{\mathrm{d}t}$ to give the angular velocity of the black ring as

$$\Omega = \frac{1}{R}\sqrt{\frac{\lambda-\nu}{\lambda(1+\lambda)}} \tag{4.46}$$

The surface gravity (and hence the temperature) of any black hole is calculated by forming the Killing vector

$$\chi^\mu = \partial_t{}^\mu + \Omega \partial_\psi{}^\mu \,. \tag{4.47}$$

The surface gravity is then given by

$$\kappa = \sqrt{-\frac{1}{2}\left(\nabla_\mu \chi_\nu\right)\left(\nabla^\mu \chi^\nu\right)} \,. \tag{4.48}$$

It is then just a matter of substituting for the various quantities.

Substituting (4.46) into (4.47) and evaluating (4.48) gives the surface gravity of the black ring as

$$\kappa = \frac{(1+\nu)}{2R}\sqrt{\frac{(1-\lambda)}{\lambda\nu(1+\lambda)}} \,. \tag{4.49}$$

The temperature of the black ring is then easily calculated since $T = \kappa/2\pi$.

There is a curvature singularity in the black ring metric at $y = -\infty$ where $R_{\mu\nu\rho\sigma}R^{\mu\nu\rho\sigma}$ blows up. This singularity is expected to be spacelike, since in falling geodesics would only cross one event horizon and thus the singularity must be spacelike for all geodesics to terminate at that point. This conclusion, drawn by considering global phenomena, can also be checked by examining the local properties of the metric near the singularity.

Considering the metric given in (4.1) when y is large and negative gives

$$\begin{aligned} \mathrm{d}s^2 \sim\ & \frac{\lambda y}{(1+\lambda x)}\left(\mathrm{d}t - \frac{CR}{\lambda}\mathrm{d}\psi\right)^2 + \frac{R^2\nu(1+\lambda x)}{\lambda}\mathrm{d}\psi^2 - \frac{R^2(1+\lambda x)}{\nu y^5}\mathrm{d}y^2 \\ & + \frac{R^2(1+\lambda x)}{y^2}\left(\frac{\mathrm{d}x^2}{G(x)} + \frac{(1-x^2)(1+\nu x)}{(1+\lambda x)}\mathrm{d}\phi^2\right) \,. \end{aligned} \tag{4.50}$$

Now, since y is very large it is only necessary to consider the terms of $\mathcal{O}(y)$, which reduces the metric to

$$\mathrm{d}s^2 \sim \frac{\lambda y}{1+\lambda x}\mathrm{d}\xi^2 - \frac{R^2(1+\lambda x)}{\nu}\frac{\mathrm{d}y^2}{y^5} \,, \tag{4.51}$$

where $\mathrm{d}\xi$ combines the $\mathrm{d}t$ and $\mathrm{d}\psi$ terms and is given by

$$\mathrm{d}\xi = \mathrm{d}t - \frac{CR}{\lambda}\mathrm{d}\psi \,. \tag{4.52}$$

Considering the metric for constant values of $x = x_0$ and introducing the coordinate transformation $Y = 1/y$ gives

$$\mathrm{d}s^2 \sim \frac{\lambda}{(1+\lambda x_0)Y}\mathrm{d}\xi^2 - \frac{R^2(1+\lambda x_0)Y}{\nu}\mathrm{d}Y^2 \tag{4.53}$$

as the metric in the vicinity of the singularity.

The metric given in the form of (4.53) is suggestive because it looks very similar to the $\mathrm{d}t$-$\mathrm{d}r$ part of the Schwarzschild metric near the horizon. Indeed, the non-angular parts of the Schwarzschild metric, in the limit where r is small, is given by

$$\mathrm{d}s^2 \sim \frac{2GM}{r}\,\mathrm{d}t^2 - \frac{r}{2GM}\,\mathrm{d}r^2 \,. \tag{4.54}$$

It is now possible to compare it with (4.53). If ξ is identified with t and Y is identified with r then the two metrics can be shown to be the same near the singularity (up to some constant factors), therefore the nature of the two singularities must be the same i.e. the black ring singularity must be spacelike as per the Schwarzschild singularity.

4.2 Properties of the Doubly Spinning Black Ring

The doubly spinning black ring metric was first discovered by Pomeransky and Senkov in [27], where they give the metric for the balanced ring solution. The metric is given by

$$\begin{aligned} ds^2 &= -\frac{H(y,x)(dt+\Omega)^2}{H(x,y)} - \frac{F(x,y)d\psi^2}{H(y,x)} - \frac{2J(x,y)d\phi d\psi}{H(y,x)} \\ &\quad + \frac{F(y,x)d\phi^2}{H(y,x)} + \frac{k^2 H(x,y)}{(x-y)^2(1-\nu)^2}\left(\frac{dx^2}{G(x)} - \frac{dy^2}{G(y)}\right) \end{aligned} \tag{4.55}$$

where

$$\begin{aligned} \Omega &= -\frac{k\lambda\sqrt{2(1+\nu)^2-2\lambda^2}}{H(y,x)}\Big[(1-x^2)y\sqrt{\nu}d\phi \\ &\quad + \frac{(1+y)\left[1+\lambda-\nu+x^2y\nu(1-\lambda-\nu)+2\nu x(1-y)\right]d\psi}{(1-\lambda+\nu)}\Big] \end{aligned} \tag{4.56}$$

$$G(x) = (1-x^2)(1+\lambda x+\nu x^2) \tag{4.57}$$

$$\begin{aligned} H(x,y) &= 1+\lambda^2-\nu^2+2\lambda\nu(1-x^2)y+2x\lambda(1-y^2\nu^2) \\ &\quad + x^2y^2\nu(1-\lambda^2-\nu^2) \end{aligned} \tag{4.58}$$

$$\begin{aligned} J(x,y) &= k^2(1-x^2)(1-y^2)\lambda\sqrt{\nu}\times \\ &\quad \frac{\left[1+\lambda^2-\nu^2+2(x+y)\lambda\nu-xy\nu(1-\lambda^2-\nu^2)\right]}{(x-y)(1-\nu)^2} \end{aligned} \tag{4.59}$$

$$\begin{aligned} F(x,y) &= \frac{k^2}{(x-y)^2(1-\nu)^2}\times \\ &\quad \Big[G(x)(1-y^2)\left\{[(1-\nu)^2-\lambda^2](1+\nu)+y\lambda[1-\lambda^2+2\nu-3\nu^2]\right\} \\ &\quad + G(y)\left\{2\lambda^2+x\lambda[(1-\nu)^2+\lambda^2]+x^2[(1-\nu)^2-\lambda^2](1+\nu)\right. \\ &\quad \left.+x^3\lambda(1-\lambda^2-3\nu^2+2\nu^3)-x^4(1-\nu)\nu(\lambda^2+\nu^2-1)\right\}\Big]. \end{aligned} \tag{4.60}$$

The metric given in (4.55) is for the balanced doubly spinning black ring. A more general solution with a conical singularity, analogous to the singly spinning ring

(4.1), is given in [45]. Furthermore, since (4.55) is expressed in a form free of conical singularities, the coordinates ψ and ϕ have the familiar period of 2π.

The λ and ν parameters in (4.55) are slightly different from those of the singly spinning ring. Since the doubly spinning ring has angular momentum in an extra plane, it isn't surprising that the balanced solution depends on an extra parameter (unlike in the singly spinning ring case where λ is fixed in terms of ν). In this case λ and ν must satisfy $0 \leq \nu < 1$ and $2\sqrt{\nu} \leq \lambda < 1 + \nu$. The x and y coordinates satisfy the same limits as (4.11) and ∂_t, ∂_ψ and ∂_ϕ are all Killing directions.

The limits on λ and ν are determined by demanding that both of the horizons exist for $y < -1$, that the metric should always be real, and that the black ring has positive mass. The condition that the metric remains real is satisfied so long as $\nu \geq 0$ and the positivity of the black ring mass is satisfied for $\lambda > 0$, as can be seen from (4.73). The constraint that λ satisfies $2\sqrt{\nu} \leq \lambda < 1$ is determined by demanding that the event horizons be at real values of y, which is calculated from (4.61).

The doubly spinning ring solution given in (4.55) can be reduced to the singly spinning ring metric, when the condition (4.29) has been applied, by setting $\nu = 0$. Doing this recovers (4.1) with ν replaced by λ and the ψ and ϕ coordinates rescaled so that $\Delta\phi$ and $\Delta\psi$, from (4.27), are equal to 2π. The ring radius parameter R is also replaced by k.

The event horizons of the doubly spinning metric are given by the points where $g^{yy} = 0$ i.e. the non-trivial roots of $G(y)$. Solving $G(y) = 0$ gives the positions of the horizons as

$$y_h = \frac{-\lambda \pm \sqrt{\lambda^2 - 4\nu}}{2\nu}\,, \tag{4.61}$$

where the positive solution gives the outer event horizon and the negative solution the inner Cauchy horizon. The ergosurface is calculated by considering the hypersurface where the vector ∂_t becomes null. This surface is where $H(y, x) = 0$, which isn't a constant value of y as for the singly spinning ring.

Although the limits on the x and y coordinates are the same for the doubly and singly spinning ring, they don't cover the manifold in the same manner. To get an idea of how the dual spinning ring coordinates span the space, obtain the flat space

metric by substituting $\lambda = 0$ into (4.55). Having done this, the ring metric becomes

$$ds^2 = -\mathrm{d}t^2 + \frac{k^2}{(x-y)^2(1-\nu)}\left[\frac{(1+\nu)(1+\nu x^2y^2)}{(1-x^2)(1+\nu x^2)}\mathrm{d}x^2 + (1-x^2)(1+\nu y^2)\mathrm{d}\phi^2 - \frac{(1+\nu)(1+\nu x^2y^2)}{(1-y^2)(1+\nu y^2)}\mathrm{d}y^2 - (1-y^2)(1+\nu x^2)\mathrm{d}\psi^2\right] \quad (4.62)$$

Comparing this with the five dimensional flat space metric in polar coordinates

$$ds^2 = -dt^2 + \mathrm{d}r_1^2 + r_1^2\mathrm{d}\phi^2 + \mathrm{d}r_2^2 + r_2^2\mathrm{d}\psi^2 \quad (4.63)$$

allows the transformations between r_1 and r_2 and x and y to be determined. These are

$$r_1 = \frac{k\sqrt{(1-x^2)(1+\nu y^2)}}{(x-y)\sqrt{1-\nu}} \qquad r_2 = \frac{k\sqrt{(y^2-1)(1+\nu x^2)}}{(x-y)\sqrt{1-\nu}} \quad (4.64)$$

Theoretically these coordinate transformations can be used directly to plot lines of constant x and y. In practice it is more useful to transform coordinates once again to get spherical polar coordinates where r and θ are given in terms of x and y. The r_1, r_2 coordinates are related to the r, θ coordinates by

$$r^2 = r_1^2 + r_2^2 = -\frac{k^2(1+\nu)(x+y)}{(x-y)(1-\nu)} \quad (4.65)$$

$$\tan^2\theta = \frac{r_2}{r_1} = \frac{(y^2-1)(1+\nu x^2)}{(1-x^2)(1+\nu y^2)} \quad (4.66)$$

Having obtained these coordinate transformations it is now possible to plot the contour lines for constant x and y. A sample plot for $\nu = \frac{1}{2}$ is given in figure 4.2.

Unlike for the singly spinning ring, the contour lines of constant y are now elliptical, rather than circular. This is due to the factors of ν that appear in the coordinate transformations. If ν is set to zero then the ellipses become circles, as one would expect since the $\nu \to 0$ limit of (4.55) gives the singly spinning ring metric. As ν is increased from zero, the ellipses become more elongated and the contours of constant y become more widely spaced.

To calculate the thermodynamic properties of the doubly spinning ring, it is once again useful to transform to spherical polar coordinates using [44]

$$x = -1 + \frac{4k^2}{r^2}\alpha^2\cos^2\theta \qquad y = -1 - \frac{4k^2}{r^2}\alpha^2\sin^2\theta \quad (4.67)$$

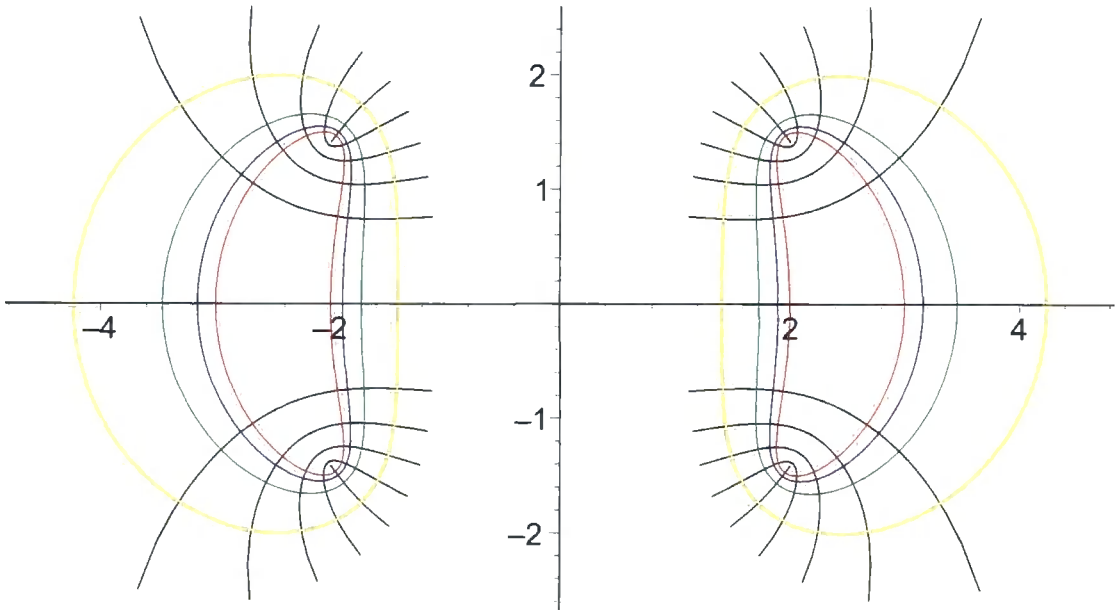

Figure 4.2: A two dimensional cross-section of constant ϕ and ψ (as well as the antipodal points $\phi + \pi$ and $\psi + \pi$) of the (x, y) coordinates. The red through yellow lines show the lines of constant y from -5 through to -2 respectively and the black lines show the x contours. The vertical axis on this plot corresponds to asymptotic infinity at $y = -1$ and the horizontal axis corresponds to $x = \pm 1$.

where

$$\alpha = \sqrt{\frac{1+\nu-\lambda}{1-\lambda}} \tag{4.68}$$

In these coordinates $0 \leq r < \infty$ and $0 \leq \theta \leq 2\pi$ and asymptotic infinity is approached as $r \to \infty$.

The approach used to calculate the ADM mass is similar to that described in section 4.1, with the first order terms for g_{tt} and g_{rr} given by

$$g_{tt} = -1 + \frac{8\lambda(\nu-1)k^2}{(1+\nu-\lambda)(\lambda-1)r^2} \tag{4.69}$$

$$\begin{aligned} g_{rr} = {} & \frac{\lambda-1}{2(\nu-1)} + \frac{3\lambda^2 - 8\lambda\nu + \lambda^2\nu + 1 + (1-\nu)(1+\nu)^2}{(1-\lambda-\nu-\nu^2+2\lambda\nu+\nu^3-\lambda\nu^2)r^2}\, k^2 \cos(2\theta) \\ & -4\lambda k^2 \frac{\nu - \nu^2\cos^2\theta - \sin^2\theta}{(1-\lambda-\nu-\nu^2+2\lambda\nu+\nu^3-\lambda\nu^2)r^2} \end{aligned} \tag{4.70}$$

As before, g_{rr} isn't of the form given in (4.34), so a rescaling is needed

$$r \to r' = r\sqrt{\frac{2(\nu-1)}{\lambda-1}} \tag{4.71}$$

Applying this to (4.69) gives

$$g_{tt} = -1 + \frac{4\lambda k^2}{(1+\nu-\lambda)r^2}\,, \tag{4.72}$$

which when compared with (4.34) gives

$$M = \frac{3\pi\lambda k^2}{2G(1+\nu-\lambda)} . \tag{4.73}$$

The two angular momenta for the doubly spinning black ring are calculated in the same way as for the singly spinning ring, except now there is also angular momentum in the ϕ direction. In this instance, the $g_{t\phi}$ coefficient of the ring has to be compared with the expansion of the corresponding metric coefficients from the Myers Perry metric. The first term of the Taylor expansions for the $g_{t\psi}$ and $g_{t\phi}$ coefficients of the black ring are

$$g_{t\psi} = \frac{4k^3\lambda(1+\lambda-6\nu+\lambda\nu+\nu^2)\sqrt{2(1+\lambda+\nu)(1+\nu-\lambda)}\sin^2\theta}{(\nu^3+\nu\lambda^2-\nu-2\lambda\nu^2+2\lambda+\nu^2-\lambda^2-1)(1-\lambda)r^2} \tag{4.74}$$

$$g_{t\phi} = \frac{8\lambda k^3\sqrt{2\nu(1+\lambda+\nu)(1+\nu-\lambda)}\cos^2\theta}{(\nu^2-\lambda\nu+\lambda-1)(1-\lambda)r^2} . \tag{4.75}$$

These expressions can then be re-scaled according to (4.71) and compared with (4.38) and

$$g_{t\phi} = \frac{4GJ_\phi\cos^2\theta}{\pi r^2} , \tag{4.76}$$

to give

$$J_\psi = \frac{\pi\lambda k^3(1+\lambda-6\nu+\lambda\nu+\nu^2)\sqrt{2(1+\lambda+\nu)(1+\nu-\lambda)}}{2G(1-\nu)^2(1+\nu-\lambda)^2} \tag{4.77}$$

$$J_\phi = \frac{\pi\lambda k^3\sqrt{2\nu(1+\lambda+\nu)(1+\nu-\lambda)}}{G(1-\nu)^2(1+\nu-\lambda)} . \tag{4.78}$$

To calculate the area of the horizon, the integral

$$A = \int\sqrt{|\gamma|} = \int\sqrt{g_{xx}\left[g_{\psi\psi}g_{\phi\phi}-g_{\psi\phi}^2\right]} \tag{4.79}$$

must be evaluated at the event horizon. The integral is taken for $x=-1\rightarrow 1$ and $\psi,\phi=0\rightarrow 2\pi$ and, after evaluating the integral, is given by

$$A = \frac{8\sqrt{2}\pi^2k^3\lambda y_h(1+\lambda+\nu)}{(1-\nu)^2(1-y_h)^2} . \tag{4.80}$$

The angular velocity of the horizon is determined in a similar manner as for the singly spinning ring, except in this case there are two different angular velocities Ω_ψ and Ω_ϕ representing the angular velocities in the ψ and ϕ directions respectively. This complicates matters because the Killing vector that generates the event horizon

is now given by $\partial_t + \Omega_\psi \partial_\psi + \Omega_\phi \partial_\phi$. This Killing vector is null on the horizon, thus giving the equation

$$g_{tt} + 2g_{t\psi}\Omega_\psi + 2g_{t\phi}\Omega_\phi + 2g_{\psi\phi}\Omega_\psi\Omega_\phi + g_{\psi\psi}\Omega_\psi^2 + g_{\phi\phi}\Omega_\phi^2 = 0 \,. \tag{4.81}$$

This equation can't in principle be solved on its own because there are now two unknowns representing the angular velocities in the two different planes. Fortunately, a judicious selection of the point on the horizon at which the angular velocities are calculated allows some of the terms to be set to zero. In fact, selecting $x = \pm 1$ reduces the equation to

$$g_{tt}\Omega_\psi + g_{t\psi} = 0 \tag{4.82}$$

This can now be used to calculate Ω_ψ on the horizon as in the previous section. Substituting in $y = y_h$ gives

$$\Omega_\psi = \frac{1}{k\sqrt{2}}\sqrt{\frac{1+\nu-\lambda}{1+\nu+\lambda}} \,. \tag{4.83}$$

This then allows the angular velocity in the ϕ direction to be calculated by substituting $x = 0$ and evaluating the full expression given in (4.81). Doing this gives

$$\Omega_\phi = \frac{\lambda(1+\nu) - (1-\nu)\sqrt{\lambda^2 - 4\nu}}{2k\lambda\sqrt{2\nu}}\sqrt{\frac{1+\nu-\lambda}{1+\nu+\lambda}} \,. \tag{4.84}$$

The surface gravity of the doubly spinning ring could in principle be calculated using (4.48) but it is much quicker to use the Smarr formula, which is

$$\frac{2}{3}M = TS + J_\phi\Omega_\phi + J_\psi\Omega_\psi \tag{4.85}$$

where S is the entropy of the black hole and is defined as $S = A/4G$. Plugging in the values that have already been calculated gives the black ring temperature (and hence the surface gravity)

$$T = \frac{({y_h}^{-1} - y_h)(1-\nu)\sqrt{\lambda^2 - 4\nu}}{4\sqrt{2}\pi k\lambda(1+\nu+\lambda)} \,. \tag{4.86}$$

The curvature singularity is still located at $y = -\infty$ but the addition of angular momentum in the ϕ direction has introduced an extra event horizon which means that the singularity has to be timelike. The consequence of this is that it is now not inevitable that all timelike/null geodesics that fall through the horizon will terminate

at the curvature singularity. It is now possible to construct geodesic paths that go through both horizons to the interior of the black ring and then continue out to timelike/null infinity in a new asymptotic region.

Chapter 5

Graphical Representations of Spacetime

This chapter considers the geodesics of various different solutions to Einstein's equations and then looks at two different methods of visualising the geodesics and the spacetimes. After plotting some sample geodesics, it is then possible to distinguish the essential features of any particular spacetime by observation, without having to consider the detailed mathematical properties of the metric.

5.1 Conformal Diagrams

The best known method for visualising a particular metric is the Penrose or Conformal diagram. The idea behind this is to transform the coordinates of the metric in such a way as to highlight the causal connection between the points in the spacetime, without necessarily giving a faithful representation of how the space varies from point to point. Emphasising the causal connection between the spacetime points, rather than demanding that the variation of the space or time directions be accurately reproduced, allows for much more flexibility in the way the spacetime is portrayed and thus allows the causal features to be depicted in a way that is very simple to interpret. Another advantage of Penrose diagrams is the ability to contain all of the (potentially infinite) spacetime within a compact representation, meaning it is then possible to examine what the spacetime will look like an infinite distance

away from the origin of the coordinate system.

The causal structure of any spacetime is determined by considering the light cones at any particular point. Fortunately, conformal transformations leave light cones invariant, so they provide a perfect candidate for a diagram to illustrate the causal nature of a particular metric. To show that the light cones are invariant under conformal transformations, it is necessary to consider a null curve $x^\mu(\lambda)$ with respect to a metric with coefficients $g_{\mu\nu}$. If $x^\mu(\lambda)$ is null with respect to $g_{\mu\nu}$ then its tangent vector $\mathrm{d}x^\mu/\mathrm{d}\lambda$ satisfies

$$g_{\mu\nu}\frac{\mathrm{d}x^\mu}{\mathrm{d}\lambda}\frac{\mathrm{d}x^\nu}{\mathrm{d}\lambda} = 0\,. \tag{5.1}$$

Conformal transformations are simply transformations that provide a local change of scale i.e. they rescale distances with the scaling changing from point to point so, seeing as the metric and its associated coefficients indicate how the distance varies from point to point, a conformal transformation can be expressed as

$$\tilde{g}_{\mu\nu} = \omega^2 g_{\mu\nu}\,, \tag{5.2}$$

where ω^2 is a non-zero function of the coordinates x^μ.

Expressing (5.1) for the conformal frame and using the transformation in (5.2), gives

$$\tilde{g}_{\mu\nu}\frac{\mathrm{d}x^\mu}{\mathrm{d}\lambda}\frac{\mathrm{d}x^\nu}{\mathrm{d}\lambda} = \omega^2 g_{\mu\nu}\frac{\mathrm{d}x^\mu}{\mathrm{d}\lambda}\frac{\mathrm{d}x^\nu}{\mathrm{d}\lambda} = 0\,. \tag{5.3}$$

Seeing as ω^2 is everywhere non-zero, this condition will hold for null curves defined with respect to both $g_{\mu\nu}$ and $\tilde{g}_{\mu\nu}$.

Utilising the fact that the light cones will remain invariant under conformal transformations, it is now possible to construct new coordinates which have one timelike coordinate and one spacelike coordinate that always have radial light cones represented by a line at 45°. These conformal coordinates can then be compactified by a further suitable choice of coordinate transformation, e.g. the arctan function, to bring infinity to a finite coordinate value. Combining these coordinate transformations allows a Penrose diagram of a 2D cross-section to be drawn, where the lines at 45° represent the paths of null rays and the boundaries of the diagram represent infinity. Usually a 2D diagram is sufficient to characterise the space since

most physical solutions of Einstein's equations have some symmetry that can be exploited to negate the need to represent the extra dimensions. For example, each of the points on the Schwarzschild Penrose diagram can be thought of as representing a two-sphere, since the symmetry of the solution means that the θ and ϕ coordinates vary in the same way, no matter what values of t and r are chosen.

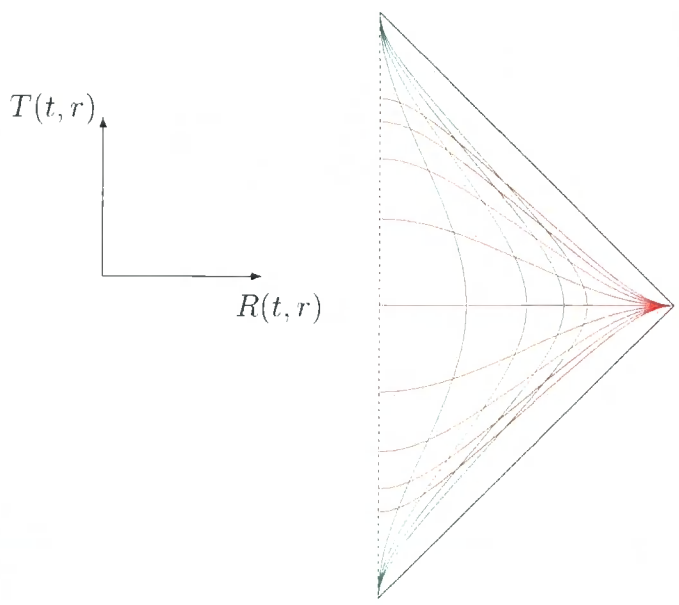

Figure 5.1: Penrose diagram of flat space with the vertical axis representing the conformal time T and the horizontal axis representing the conformal radius R.

The diagram shown in figure 5.1 shows the Penrose diagram for flat space, with the conformal time given by T and the conformal radius given by R. The vertical dotted line on the left hand side of the diagram represents $R = 0$, the origin of the space, and the lower and upper 45° lines represent past and null infinity. The bottom left corner corresponds to past timelike infinity with future timelike infinity given by the top left corner of the triangle. The third corner represents spacelike infinity because only spacelike paths starting away from infinity can reach this point. Timelike paths starting at past timelike infinity will always eventually terminate at future timelike infinity and the lines of null infinity delimit the spacetime.

The red and green lines on the Penrose diagram of figure 5.1, represent lines of constant r and t. These lines of constant r and t are no longer straight as in a standard spacetime diagram of r and t, but if a local light cone is drawn at any point

then the green lines of constant t will always be within the light cone and the red lines of constant r will always be outside the light cone. This is as expected since the lines of constant t and r represent timelike and spacelike paths respectively. The representation of flat space geodesics on the Penrose diagram is explored further in the following section.

5.2 Flat Space Geodesics

This section describes how to calculate the geodesics of 5D Minkowski space and then goes on to plot them on a Penrose diagram. Usually Penrose diagrams are only used as a means of visualising the global nature of a particular spacetime without necessarily considering any causal paths on the diagram. The intuitive nature of the Penrose diagram often means that it is quite simple to sketch various timelike or spacelike paths without much effort. The fact that, in the absence of the test particles having any angular momentum, all null rays are represented as 45° lines means that the path of timelike or spacelike particles can be predicted from point to point. However, it is not necessarily obvious which of the many possible causal routes across the Penrose diagram represents a geodesic and if the test particle has angular momentum the task is made much harder because the null lines are no longer at 45°. It is with this in mind that some example geodesics have been plotted in the following sections.

The high level of symmetry of flat space means that the essential properties of the space can be illustrated by only considering the radial coordinate r, and the time coordinate t. The other coordinates describe the familiar three-sphere so each point on the Penrose diagram can be thought of as representing a three-sphere with the θ, ψ and ϕ coordinates representing rotation in this sphere.

5.2.1 Geodesic Equations

Minkowski space has many Killing vectors which make the geodesics very simple to calculate. In five dimensions the Minkowski metric is given by

$$ds^2 = -dt^2 + dr^2 + r^2(d\theta^2 + \cos^2\theta d\psi^2 + \sin^2\theta d\phi^2) \,. \tag{5.4}$$

The geodesics of this metric can then be found directly by forming the Lagrangian

$$\mathcal{L} = \frac{1}{2}(-\dot{t}^2 + \dot{r}^2 + r^2\dot{\theta}^2 + r^2\cos^2\theta\dot{\psi}^2 + r^2\sin^2\theta\dot{\phi}^2) \,, \tag{5.5}$$

where the factor of $1/2$ is conventional as it gives more convenient expressions for the geodesic equations. The geodesic equations are calculated by plugging (5.5) into the Euler-Lagrange equation given by

$$\frac{d}{d\lambda}\left(\frac{\partial\mathcal{L}}{\partial\dot{x}^\mu}\right) - \frac{\partial\mathcal{L}}{\partial x^\mu} = 0 \,, \tag{5.6}$$

where λ is the geodesic parameter and the over-dot refers to differentiation with respect to this parameter. From here on, it will be assumed that the geodesic parameter is chosen so that it is affine.

Equation (5.4) has three obvious killing directions, which is reflected in the equations for t, ψ, and ϕ, giving three conserved quantities

$$\dot{t} = E \tag{5.7}$$

$$r^2\cos^2\theta\dot{\psi} = l \tag{5.8}$$

$$r^2\sin^2\theta\dot{\phi} = m \,. \tag{5.9}$$

The constants E, l, and m refer to the conserved quantities corresponding to the energy, angular momentum in the ψ direction, and the angular momentum in the ϕ direction respectively. In the following equations, l and m will be set to zero for the sake of brevity since they correspond to symmetries of the metric. In light of this, the θ equation reduces to

$$r^2\dot{\theta} = k \tag{5.10}$$

It is also possible to derive the r equation from the Lagrangian but it is more convenient to use the first integral of the geodesic equation given by

$$-\dot{t}^2 + \dot{r}^2 + r^2\dot{\theta}^2 = \epsilon \tag{5.11}$$

where ϵ is a constant of motion that determines the nature of the geodesic. The geodesic parameter is chosen such that ϵ determines the geodesic as

$$\epsilon = \begin{cases} -1 & \text{timelike} \\ 0 & \text{null} \\ +1 & \text{spacelike} \end{cases} \tag{5.12}$$

Substituting (5.7) into (5.11) and solving with (5.10) gives two differential equations for θ and r

$$\dot{r} = \pm\frac{\sqrt{r^2(\epsilon + E^2) - k^2}}{r} \tag{5.13}$$

$$\dot{\theta} = \frac{k}{r^2} \tag{5.14}$$

Solving these equations gives

$$r(\lambda) = \pm\sqrt{\frac{\lambda^2(E^2+\epsilon)^2 + k^2}{E^2+\epsilon}} \tag{5.15}$$

$$\theta(\lambda) = \pm\int \frac{k(E^2+\epsilon)}{\lambda^2(E^2+\epsilon)^2 + k^2}\,\mathrm{d}\lambda\,. \tag{5.16}$$

It is now possible to plot the geodesics as functions of λ but, in practice, it is more convenient to use r as the parameter rather than λ. This is achieved by combining the equations to give

$$\frac{\mathrm{d}\theta}{\mathrm{d}r} = \frac{k}{r\sqrt{r^2(\epsilon + E^2) - k^2}}\,, \tag{5.17}$$

which can easily be solved for r. A similar equation can be derived for t, giving

$$\frac{\mathrm{d}t}{\mathrm{d}r} = \frac{Er}{\sqrt{r^2(\epsilon + E^2) - k^2}}\,. \tag{5.18}$$

5.2.2 Flat Space Penrose Diagrams

The metric in the t and r coordinates already has null lines at 45° at all points in the spacetime so, technically, a conformal transformation is not required. However, to plot the geodesics on a Penrose diagram it is necessary to transform the t and r coordinates so that they cover a finite range. To do this construct two null coordinates v and u

$$u = t - r \qquad\qquad v = t + r \tag{5.19}$$

These null coordinates can now be combined to give two new compactified coordinates - one spacelike and one timelike. These are

$$R = \arctan v - \arctan u \tag{5.20}$$

$$T = \arctan v + \arctan u\,, \tag{5.21}$$

where R is a radial spacelike coordinate and T is a timelike coordinate. The ranges of these coordinates are then given by

$$0 \leq R < \pi \,, \qquad\qquad |T| + R < \pi \,. \tag{5.22}$$

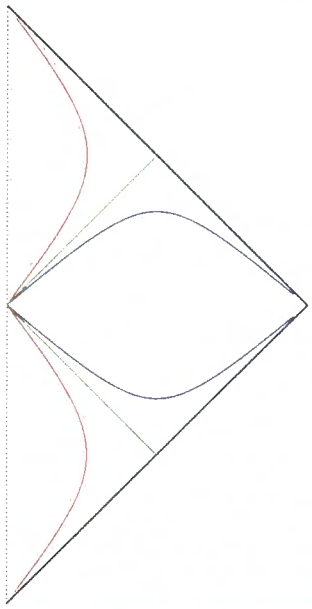

Figure 5.2: The zero angular momentum geodesics of 5D Minkowski spacetime. The timelike, null, and spacelike geodesics are plotted in red, green, and blue respectively. All the geodesics have $E = 3$.

Figure 5.2 shows the Penrose diagram for Minkowski space with three geodesics plotted on it. All of the geodesics are plotted with the angular momentum in the θ direction set to zero i.e. $k = 0$. The red line is the timelike geodesic starting at past timelike infinity, going through the origin and then progressing to future timelike infinity. The green line shows the null geodesic starting at past null infinity, going through $r = 0$ and then progressing off to future null infinity. The blue line is the analogous spacelike geodesic starting and ending at spacelike infinity and going through $r = 0$. If the initial conditions were chosen so that the geodesics always had $r > 0$ then they wouldn't all intersect on the dotted line and would instead follow paths more like those shown in figure 5.1.

If k is varied away from zero then the geodesics have some angular momentum in the θ direction, which correspondingly alters the shape of the geodesics. Figure 5.3 shows how the shape of the geodesics changes as the angular momentum is increased, with k increasing in each subsequent Penrose diagram from left to right. When the

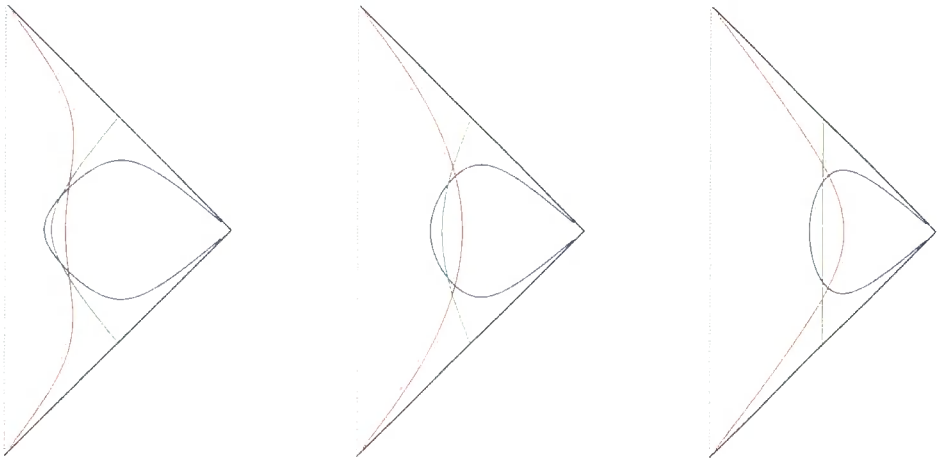

Figure 5.3: The geodesics of the 5D Minkowski metric with the angular momentum chosen so that $k = 1$, $k = 2$, and $k = 3$ from left to right respectively. For all the geodesics the energy is chosen so that $E = 3$. The colour coding is as in figure 5.2.

angular momentum is increased from zero, the geodesics no longer make it to the origin, as would be expected by considering a particle with angular momentum in Newtonian mechanics. If the particle has angular momentum about $r = 0$, then no matter what trajectory it is on, its radius will always be non-zero as long as its angular momentum remains constant. If its angular momentum is increased then it will orbit further and further away from the origin, as is shown in the various Penrose plots of figure 5.3.

The transformations applied in (5.20) and (5.21) mean that the detail in the Penrose plots is biased toward smaller values of u and v, and hence smaller values of t and r. This is why the variation between the different geodesics is most pronounced in the middle of the plot near to the dotted line at $r = 0$. When the angular momentum is increased the geodesics necessarily take larger values of r at all times, so the variation between the different Penrose diagrams becomes less pronounced as k is increased.

5.3 Schwarzschild Geodesics

The Schwarzschild metric provides a slightly more interesting space for the propagation of the geodesics. This is because it has an event horizon which acts to globally

conceal the interior of the black hole from observers outside of it. The addition of an event horizon also means that the Penrose diagram is divided into several sections where the past and future event horizons prevent null and timelike geodesics from passing from one sector to the other. The Schwarzschild metric also has a curvature singularity at $r = 0$ where null and timelike geodesics eventually terminate once they cross the event horizon.

This section will concentrate on the 5D version of the Schwarzschild metric, as it is useful in gaining an understanding of some of the properties of the black ring solutions that will be considered in the following chapters. The black ring solutions don't exist in four dimensions, so it is more informative to examine the 5D Schwarzschild solution, since this can be derived as a particular limit of the black ring metric. In any event, the properties of the four and five dimensional Schwarzschild black holes are qualitatively similar, so there is little to be gained by describing the 4D solution separately.

5.3.1 Geodesic Equations

The 5D Schwarzschild metric in spherical polar coordinates is given by

$$ds^2 = -\left(1 - \frac{M}{r^2}\right) dt^2 + \frac{dr^2}{\left(1 - \frac{M}{r^2}\right)} + r^2(d\theta^2 + \cos^2\theta d\psi^2 + \sin^2\theta d\phi^2) \qquad (5.23)$$

and the event horizon is where $g^{rr} = 0$ i.e. where the hypersurface described by $r =$ constant is everywhere null. This is a simple calculation for the Schwarzschild metric, and in this case is given by $r = M$. Unfortunately, this particular value of r also represents a singularity in the metric, since $g_{rr} = \infty$ at $r = \sqrt{M}$. This, however, turns out to be a coordinate singularity, so changing to a different coordinate system removes the singularity and allows the geodesics to be followed all the way to the true curvature singularity at $r = 0$.

As in the Minkowski case, the easiest way to calculate the geodesics is to form the Lagrangian from the metric

$$\mathcal{L} = \frac{1}{2}\left[-\left(1 - \frac{M}{r^2}\right)\dot{t}^2 + \frac{\dot{r}^2}{\left(1 - \frac{M}{r^2}\right)} + r^2\dot{\theta}^2 + r^2\cos^2\theta\dot{\psi}^2 + r^2\sin^2\theta\dot{\phi}^2\right] . \qquad (5.24)$$

It is obvious from this that ∂_ψ and ∂_ϕ are killing vectors so the angular momentum in these directions will once again be set to zero. This leaves three equations for t,

r, and θ

$$\dot{t} = -\frac{E}{\left(1-\frac{M}{r^2}\right)} \tag{5.25}$$

$$\dot{\theta} = \frac{l}{r^2} \tag{5.26}$$

$$\dot{r}^2 = \left(\epsilon - \frac{l^2}{r^2}\right)\left(1-\frac{M}{r^2}\right) + E^2 \,, \tag{5.27}$$

where l is a constant corresponding to the angular momentum in the θ direction, E is the energy, and ϵ is as previously defined. To solve these equations it is necessary to consider two cases: $l = 0$ (no angular momentum) and $l \neq 0$ (angular momentum in the θ direction only).

5.3.2 Zero Angular Momentum Geodesics

After setting l to zero, only equations (5.25) and (5.27) remain. These can then be combined to give a differential equation for $\frac{dt}{dr}$ in terms of r.

$$\frac{dt}{dr} = -\frac{Er^3}{(r^2-M)\sqrt{(E^2+\epsilon)r^2-\epsilon M}} \,. \tag{5.28}$$

This equation can then be directly integrated to give an analytic solution for t in terms of r, providing care is taken to consider the different values of ϵ. The minus sign on the right hand side has been chosen so that the solution will give ingoing geodesics. For null geodesics ($\epsilon = 0$) the solution is given by

$$t = -r + \sqrt{M}\tanh^{-1}\left(\frac{r}{\sqrt{M}}\right) \,. \tag{5.29}$$

For the timelike and spacelike geodesics, the solution is given by

$$t = -\frac{E\sqrt{r^2(E^2+\epsilon)-\epsilon M}}{E^2+\epsilon} + \sqrt{M}\tanh^{-1}\left(\frac{\sqrt{r^2(E^2+\epsilon)-\epsilon M}}{E\sqrt{M}}\right) \,. \tag{5.30}$$

5.3.3 Geodesics with Angular Momentum in the θ direction

Having obtained a solution for the geodesics with zero angular momentum it remains to find the solution for non-zero values of l. In this case the equations given by (5.25) - (5.27) are combined to give two differential equations with t and θ in terms of r

$$\frac{dt}{dr} = \frac{Er^4}{(r^2-M)\sqrt{r^4(E^2+\epsilon)-r^2(M\epsilon+l^2)+Ml^2}} \,, \tag{5.31}$$

$$\frac{d\theta}{dr} = \frac{l^2}{\sqrt{r^4(E^2+\epsilon)-r^2(M\epsilon+l^2)+Ml^2}} \,. \tag{5.32}$$

These equations can be solved analytically but the solutions give complicated functions of elliptical integrals, which don't lend themselves to any intuitive understanding of the behaviour of the geodesics. A better idea is to consider the simplified case where E is chosen such that the expression in the square root of the denominator reduces to a perfect square. As will be seen later, this corresponds to the situation where the geodesic has the same energy as the peak of the centrifugal barrier.

To achieve this it is necessary to choose different energies for the different geodesics. The critical energy for the spacelike and timelike geodesics is given by

$$E = \frac{(M - \epsilon l^2)}{2l\sqrt{M}} \tag{5.33}$$

and the critical energy for the null geodesics is given by

$$E = \frac{l}{2\sqrt{M}} \,. \tag{5.34}$$

Substituting these values for the energy into equations (5.31) and (5.32) and solving for $\epsilon = \pm 1$ gives

$$\begin{aligned} t + t_0 &= \epsilon \left(\frac{M - l^2}{l^2 + M}\right)^{\epsilon} r - \epsilon\sqrt{M}\tanh^{-1}\left(\frac{r}{\sqrt{M}}\right) \\ &\quad + \frac{l^3\epsilon}{M}\left(\frac{2M}{l^2 + \epsilon M}\right)^{3/2}\tanh^{-1}\left(\frac{r\sqrt{l^2 + \epsilon M}}{\sqrt{2Ml^2}}\right) \end{aligned} \tag{5.35}$$

$$\theta = -\frac{l^2\sqrt{2}}{\sqrt{(l^2 + \epsilon M)}}\tanh^{-1}\left(\frac{r\sqrt{l^2 + \epsilon M}}{l\sqrt{2M}}\right) \,. \tag{5.36}$$

The corresponding equations for the null geodesics are

$$t + t_0 = r + \sqrt{M}\tanh^{-1}\left(\frac{r}{\sqrt{M}}\right) - 2\sqrt{2M}\tanh^{-1}\left(\frac{r}{\sqrt{2M}}\right) \tag{5.37}$$

$$\theta = -l\sqrt{2}\tanh^{-1}\left(\frac{r}{\sqrt{2M}}\right) \,. \tag{5.38}$$

Although this set of solutions, for very specific values of energy, limits the exploration of how the geodesics change with energy, they do provide a useful basis for comparison because they represent the minimum energy limit where a "particle" on a geodesic can overcome the centrifugal barrier and progress to $r = 0$ i.e. cross the event horizon and approach the curvature singularity.

In order to get some feeling for how different energy values will alter the path of the geodesics it is helpful to calculate the pseudo-potential function for the geodesics.

This is achieved very easily for the Schwarzschild metric because of the form of equation (5.27). The equation of motion for a particle of unit mass in a Newtonian potential well $V(r)$ is given by

$$\frac{1}{2}\left(\frac{dr}{dt}\right)^2 + V(r) = \mathcal{E} \,, \tag{5.39}$$

where $\mathcal{E}$ is the total energy of the particle and r represents the particle's position in the potential. If (5.27) is re-written as

$$\frac{1}{2}\dot{r}^2 - \frac{1}{2}\left(\epsilon - \frac{l^2}{r^2}\right)\left(1 - \frac{M}{r^2}\right) = \frac{1}{2}E^2 \,, \tag{5.40}$$

then by comparison with (5.39), it can be seen that $\mathcal{E} = \frac{1}{2}E^2$ and

$$V(r) = -\frac{1}{2}\left(\epsilon - \frac{l^2}{r^2}\right)\left(1 - \frac{M}{r^2}\right) \,, \tag{5.41}$$

thus allowing the pseudo potential for the Schwarzschild metric to be drawn. Figure 5.4 shows the potential plotted for different values of l and ϵ. Substituting $l = 0$ and $\epsilon = 0$ into (5.41) shows that the zero angular momentum potential for null geodesics is given by $V(r) = 0$, so it is not plotted in figure 5.4.

The potential plots in figure 5.4 clearly show the centrifugal barrier getting bigger, for all values of ϵ, as l is increased. The only exception is for the spacelike geodesics, where the barrier becomes infinite for $l = 0$. This is a consequence of the spacelike geodesics being repelled by the spacelike singularity in the Schwarzschild spacetime but this is overcome as soon as the angular momentum is increased from zero, which is why the barrier only becomes infinitely large for $l = 0$. The energy for which a particular geodesic is able to cross the centrifugal barrier and continue to $r = 0$, is given by the value at the peak of the barrier. Using the expression given by (5.41) to calculate the energy for which the geodesic will cross the potential barrier, gives the expressions calculated in (5.33) and (5.34) as previously mentioned. It is worth pointing out, however, that the potentials shown in figure 5.4 are equivalent to E^2, so the values on the vertical axes don't directly correspond to the energy of the geodesics.

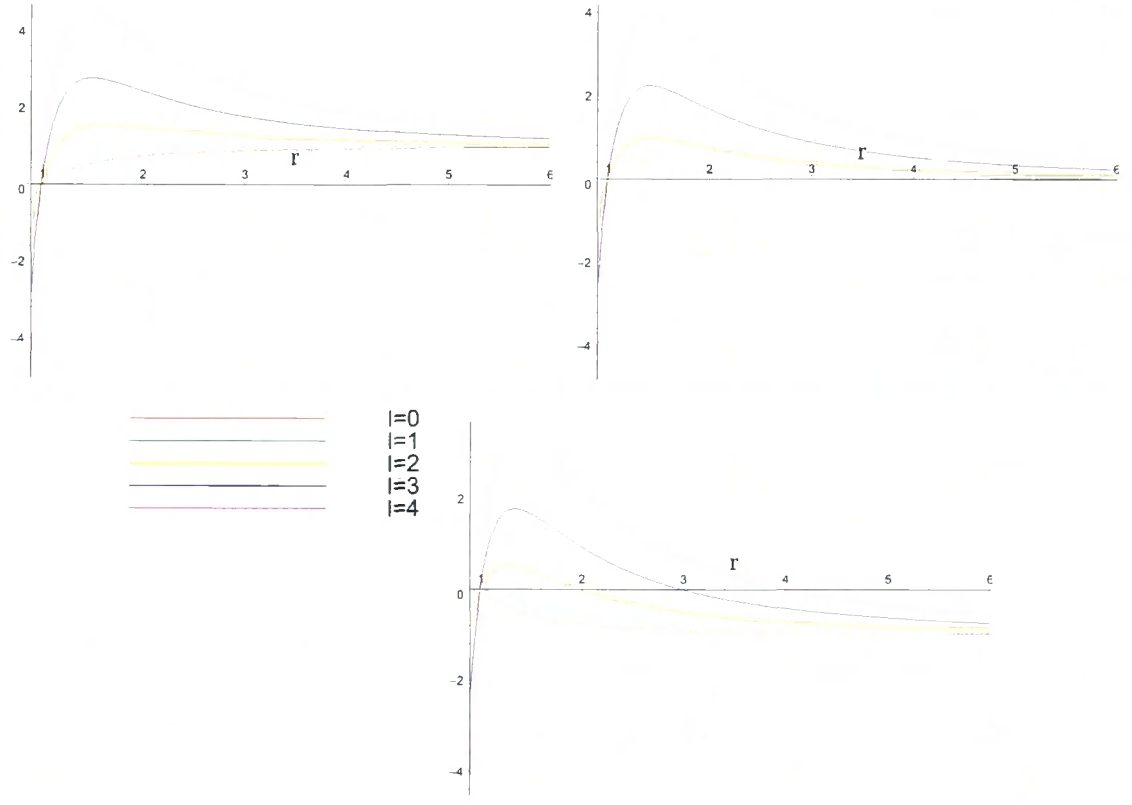

Figure 5.4: Potential plots for the timelike, null, and spacelike geodesics respectively

5.3.4 Schwarzschild Penrose Diagrams

The Penrose diagram isn't as easy to construct as for the flat space case because of the coordinate singularity at $r = \sqrt{M}$. To avoid this it is useful to transform to Kruskal coordinates. These coordinates allow the whole of the spacetime to be plotted without encountering any coordinate singularities. To derive the Kruskal coordinates it is necessary to from two null coordinates as follows

$$U = -e^{r^*-t} , \qquad V = e^{r^*+t} , \tag{5.42}$$

where r^* is the tortoise coordinate and is given by

$$r^* = \int \frac{\mathrm{d}r}{\left(1 - \frac{M}{r^2}\right)} = r - \sqrt{M}\tanh^{-1}\left(\frac{r}{\sqrt{M}}\right) . \tag{5.43}$$

This transformation ensures that r^* becomes infinite as r approaches $r = \sqrt{M}$. This effectively "stretches out" the space as the event horizon is approached, meaning that the event horizon is only encountered when $r^* = -\infty$ and thus circumvents the problem of the singularity at $r = \sqrt{M}$.

Having defined the null coordinates U and V they can now be combined into a timelike and a spacelike coordinate (with the other coordinates given by θ, ψ, and ϕ)

$$T = \frac{1}{2}(V + U) , \qquad R = \frac{1}{2}(V - U) . \tag{5.44}$$

These coordinates allow the geodesics to be integrated over the event horizon without any problems but they need to be compactified in order to plot the Penrose diagram. This is done by going back to the null coordinates given in (5.42) and bringing them to within a finite coordinate range using the arctan function

$$U' = \tan^{-1}\left(-e^{r^*-t}\right) , \qquad V' = \tan^{-1}\left(e^{r^*+t}\right) . \tag{5.45}$$

These coordinates can now be combined to give a set of one timelike coordinate and four spacelike coordinates $(T', R', \theta, \psi, \phi)$, where the coordinates of interest for the Penrose diagram are (T', R')

$$\begin{aligned} T' &= \frac{1}{2}\left[\tan^{-1}\left(e^{r^*+t}\right) + \tan^{-1}\left(-e^{r^*-t}\right)\right] , \\ R' &= \frac{1}{2}\left[\tan^{-1}\left(e^{r^*+t}\right) - \tan^{-1}\left(-e^{r^*-t}\right)\right] . \end{aligned} \tag{5.46}$$

With these coordinates it is now possible to transform the geodesics calculated in the (t, r) coordinates to a global coordinate system that doesn't breakdown in the vicinity of the event horizon. The (t, r) coordinates are well behaved so long as they are restricted to either inside the event horizon ($r < \sqrt{M}$) or outside of it ($r > \sqrt{M}$) but in order to follow geodesics through the event horizon to $r = 0$ it will be necessary to consider the coordinates inside and outside the event horizon at the same time. This can be done so long as the extra imaginary parts, that are introduced upon crossing the pole at the event horizon, are kept track of. The imaginary part from the coordinate singularity can be calculated by considering null radial geodesics. This means that (5.28) becomes

$$\frac{\mathrm{d}t}{\mathrm{d}r} = \frac{r^2}{r^2 - M} , \tag{5.47}$$

which can then be integrated over the geodesic path from r to r_0, giving

$$t = t_0 + \left[r' - \sqrt{M} \tanh^{-1}\left(\frac{r'}{\sqrt{M}}\right) \right]_{r'=r}^{r'=r_0} , \tag{5.48}$$

where (t_0, r_0) gives the initial time and position. This equation is valid for $r < \sqrt{M}$ and $r > \sqrt{M}$ separately but breaks down when considering r_0 and r on opposite sides of the event horizon. To resolve this, consider

$$t = t_0 + \left[r' - \sqrt{M} \tanh^{-1}\left(\frac{r'}{\sqrt{M}}\right) \right]_{r'=\sqrt{M}+\epsilon}^{r'=r_0} + \left[r' - \sqrt{M} \tanh^{-1}\left(\frac{r'}{\sqrt{M}}\right) \right]_{r'=r}^{r'=\sqrt{M}-\epsilon} , \tag{5.49}$$

where ϵ is a small distance, r_0 is outside the event horizon, and r is inside the event horizon. This expression will reduce to (5.48) as $\epsilon \to 0$. Evaluating this expression and considering the terms that involve ϵ gives

$$\sqrt{M}\left[\tanh^{-1}\left(\frac{\sqrt{M}+\epsilon}{\sqrt{M}}\right) - \tanh^{-1}\left(\frac{\sqrt{M}-\epsilon}{\sqrt{M}}\right) \right] = \frac{\sqrt{M}}{2} \ln\left(\frac{\epsilon + 2\sqrt{M}}{\epsilon - 2\sqrt{M}}\right) . \tag{5.50}$$

Thus, taking the limit as $\epsilon \to 0$ and writing out the expression in full gives

$$t = t_0 + r_0 - r - \sqrt{M} \tanh^{-1}\left(\frac{r_0}{\sqrt{M}}\right) + \sqrt{M} \tanh^{-1}\left(\frac{r}{\sqrt{M}}\right) + \frac{i\pi\sqrt{M}}{2} . \tag{5.51}$$

This shows that if the time coordinate is complexified and split up into a real Lorentzian part and an imaginary Euclidean part, i.e. $t = t_L + it_E$, then t_E is

incremented by $\frac{\pi\sqrt{M}}{2}$ as each event horizon is crossed. The imaginary part of the complexified time coordinate can be thought of as an extra Euclidean coordinate because when $-\mathrm{d}t^2$ is formed the sign of $\mathrm{d}{t_E}^2$ is positive, so it can be thought of as an extra spatial coordinate. Armed with this knowledge it is now possible to follow geodesics anywhere in the Schwarzschild spacetime by solving the geodesic equations in the r-t coordinates and then transforming to the Kruskal coordinates.

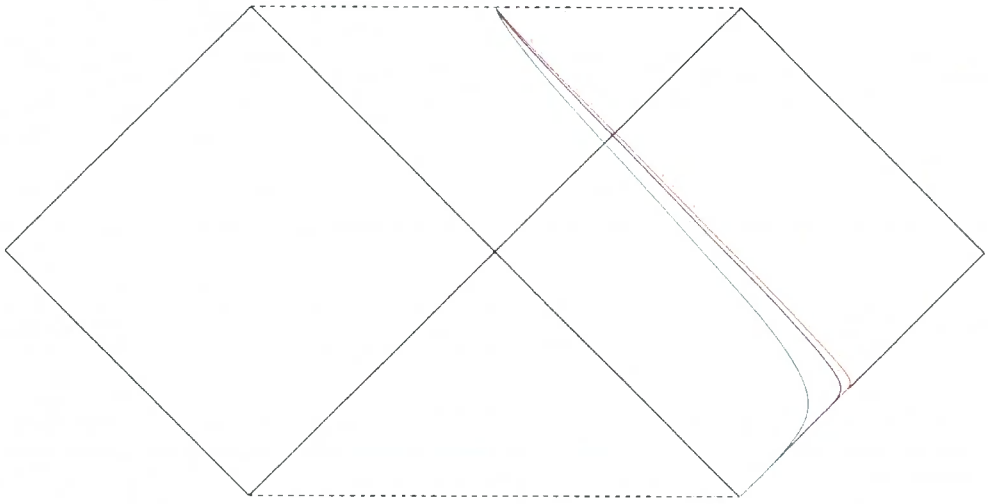

Figure 5.5: Penrose diagram of Schwarzschild spacetime showing zero angular momentum timelike geodesics with the green, blue, and red curves showing the energy increasing from $E = 1.1$ to $E = 3.1$ respectively, with the energy incremented by 1 each time.

Figure 5.5 shows the zero angular momentum timelike geodesics for the Schwarzschild metric in the Penrose diagram. The right hand diamond represents the asymptotically flat space outside the event horizon; the top triangle is the interior of the black hole, with the singularity represented by the dotted line at the top; the left hand diamond is a parallel asymptotically flat spacetime that is only accessible by spacelike geodesics; and the bottom triangle represents a white hole, which is similar to the black hole except that timelike and null geodesics can only move away from the singularity.

All of the geodesics in figure 5.5 start out at past timelike infinity and then proceed to cross the event horizon before falling into the singularity at $r = 0$. The gradient of timelike curves is restricted to be less than one, since particles on timelike geodesics are restricted to move slower than the speed of light. This is reflected in

the shape of each of the curves as they all curve in the same direction before crossing the event horizon, after which ∂_t becomes spacelike and ∂_r becomes timelike, so the gradient becomes negative and the geodesics curve in the opposite direction.

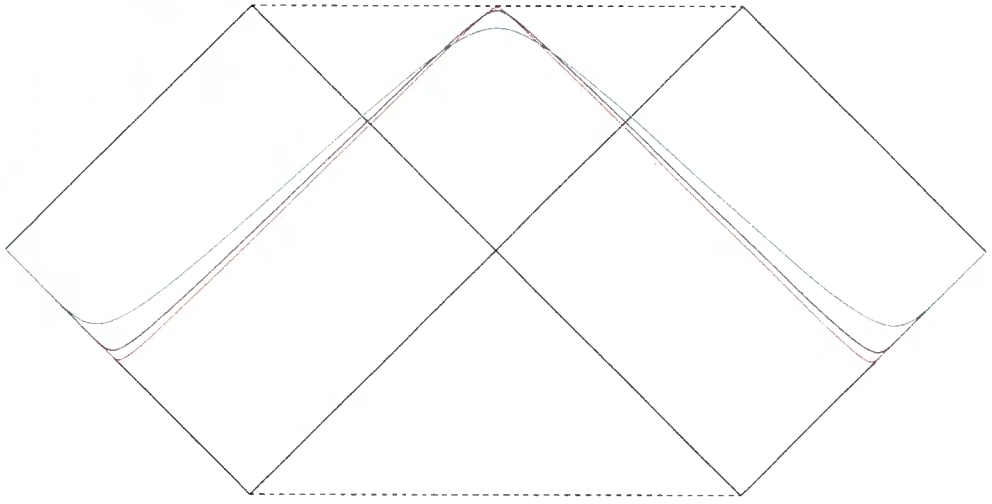

Figure 5.6: Penrose plot of Schwarzschild spacetime with zero angular momentum spacelike geodesics . The green, blue, and red curves show spacelike geodesics with energy increasing from $E = 1.1$ to $E = 3.1$ respectively, where the energy is increased in increments of 1.

Comparing the behaviour of the geodesics with different energy, it can be seen that the curves with higher energy are longer, indicating that they take a longer time to cross the event horizon. This is exactly the same behaviour as would be expected for a particle in a Newtonian potential. The timelike geodesics should also approach the path taken by null geodesics as the energy is increased. This is indicated in figure 5.5 because the timelike geodesics with higher energy get closer and closer to straight lines at 45°, which would represent the paths that null geodesics follow.

Figure 5.6 shows the spacelike geodesics with zero angular momentum. These plots demonstrate how the parallel asymptotically flat region can be reached by following spacelike geodesics. The geodesics start out at spacelike infinity on the right but as they cross the future event horizon they are repelled by the singularity at $r = 0$ and are thus free to exit across the mirror event horizon and proceed to spacelike infinity on the left hand side of the Penrose diagram.

The spacelike geodesics show many similar properties to the timelike geodesics, except that the spacelike geodesics are always moving faster than the speed of light,

so the gradient at all points on the geodesic has to be larger than one. This causes the geodesics to curve in the opposite direction to their timelike counterparts and also explains why they don't reach the singularity.

As the energy is increased the spacelike geodesics slow down and approach the straight lines indicative of the null geodesics. This causes the spacelike geodesics with higher energy to take longer to travel through the spacetime. The higher energy geodesics are also able to progress further into the black hole interior toward the singularity at $r = 0$. Indeed, the $E = 3.1$ geodesic appears to "bounce off" the singularity, but closer inspection shows that although it gets close to $r = 0$ it never reaches it. This confirms what would be expected by examining the spacelike potential in figure 5.4 - it would require an infinite energy for a zero angular momentum spacelike geodesic to reach $r = 0$.

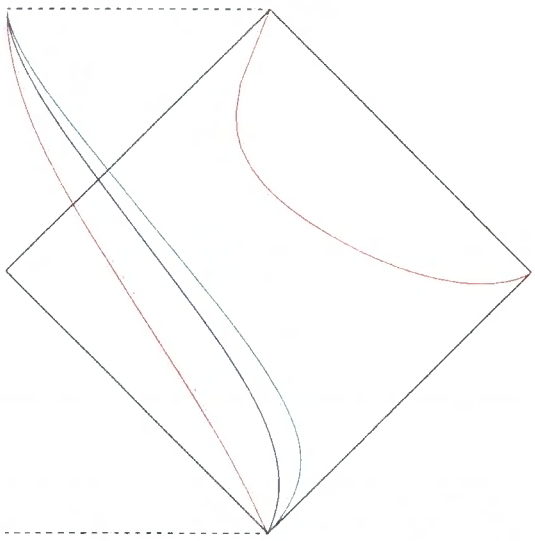

Figure 5.7: The right hand half of a Penrose diagram showing timelike, null, and spacelike geodesics with energy $E = 1.02$, $E = 0.60$ and $E = 0.18$, in green, blue, and red respectively. All geodesics have been plotted with angular momentum $l = 1.2$.

Increasing the angular momentum from zero causes a qualitative change in the shape of the geodesics. Figure 5.7 shows the Penrose diagram for the geodesics calculated in (5.36) and (5.38). The timelike geodesics are similar to those with zero angular momentum but the null and spacelike geodesics are very different. The null geodesics are no longer represented by straight lines, as they were in the zero angular momentum case, and the spacelike geodesic now reaches the singularity at $r = 0$.

The reason that the spacelike geodesic appears to be discontinuous is because the energy of the geodesic is exactly equal to the height of the centrifugal barrier. This means that it takes an infinite amount of time for the geodesic to go from spacelike infinity to the top of the centrifugal barrier; this is represented in the diagram by the

line section going from spatial infinity to timelike infinity. The red curve starting from past timelike infinity represents the case where the geodesic starts inside the centrifugal barrier, and thus is free to proceed through the event horizon toward the singularity at $r = 0$. The spacelike geodesic doesn't actually become timelike, even though it appears to on the Penrose diagram. This is because the plot suppresses the angular motion of the geodesic. The geodesic takes an infinite amount of time to reach the peak of the centrifugal barrier so it's motion becomes increasingly circular as $\frac{dr}{dt}$ approaches zero, making the curve appear to be timelike as the geodesic gets close to the centrifugal barrier. In reality the motion is channelled into the θ direction. This can be seen from (5.32), where the angular velocity $\frac{d\theta}{dt} \to \infty$ at the centrifugal barrier.

The null and timelike geodesics should also be represented as two curves but the region beyond the centrifugal barrier is asymptotically flat so the curves would just look the same as for Minkowski space. This is why only the curves representing timelike and null geodesics starting slightly inside the centrifugal barrier have been plotted on the Penrose diagram. If the geodesics started exactly at the peak of the centrifugal barrier then $\frac{dr}{dt} = 0$ and they would orbit in circles around the black hole.

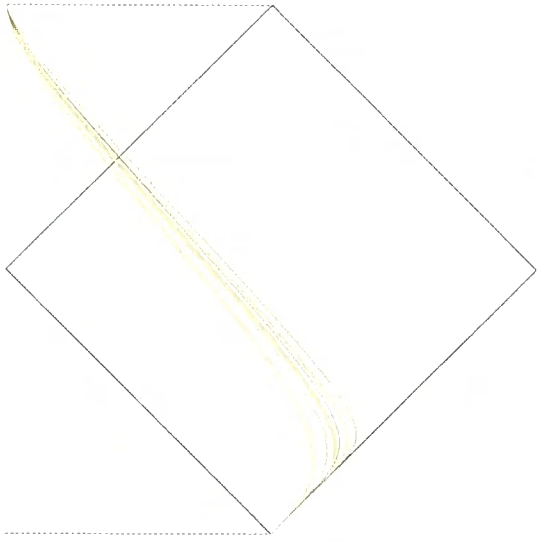

Figure 5.8: Timelike geodesics with angular momentum varying between $l = 1$ and $l = \frac{5}{3}$, and energy varying between $E = \frac{4}{3}$ and $E = \frac{5}{3}$. The redder the colour, the higher the angular momentum, and the greener the colour the higher the energy.

In order to plot the diagrams for more general values of E and l it is simplest to solve the geodesic equations numerically for different values of E and l, and then use the coordinate transformations given by (5.46) to plot the Penrose diagram. Figures 5.8, 5.9, and 5.10 show the Penrose diagrams for timelike, null, and spacelike geodesics with varying values of angular momentum and energy. None of the geodesics

in these cases manage to cross into the mirror region represented by the left hand half of the Penrose diagram so only the right hand half of the Penrose diagrams have been plotted.

Figure 5.8 shows how increasing the energy and angular momentum of the geodesics affects the shape of the geodesic. If the energy is increased, whilst keeping the angular momentum constant, the curves tend to bow out more, while increasing the angular momentum whilst keeping the energy constant causes the curves to stay closer to null infinity before curving back over more sharply. The combination of the two effects seems to arrange the curves into different "spectra" with the "ground state" defined by the energy and the "excitations" dictated by the angular momentum. Although altering E and l corresponds to changing different physical attributes of the geodesic the effect on the Penrose plot is qualitatively the same because increasing E or l serves to increase the proper time it takes for the particle to go from one point to another i.e. the geodesic between two points becomes longer, so it has to take a more circuitous path to go from one point in spacetime to another.

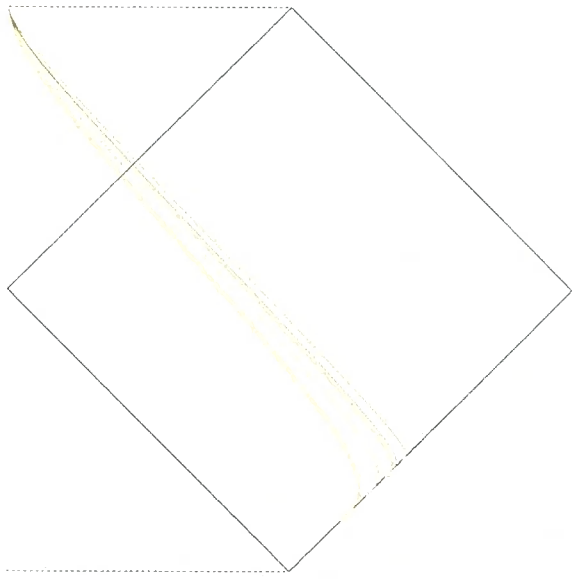

Figure 5.9: Null geodesics with angular momentum varying between $l = 1$ and $l = \frac{5}{3}$, and energy varying between $E = \frac{4}{3}$ and $E = \frac{5}{3}$. The redder the colour, the higher the angular momentum, and the greener the colour the higher the energy.

Figure 5.9 looks very similar to the Penrose diagram for the timelike geodesics. This is because the null geodesics represent the limit that the timelike geodesics approach as their energy is increased. The null geodesics are no longer straight lines because they are moving in an extra dimension described by θ, meaning that they will travel further to go the same radial distance as a similar null geodesic with zero angular momentum does. For the null geodesics the energy and angular momenta

have no independent meaning since substituting $\epsilon = 0$ in (5.41) reduces l to the role of an overall scale factor, however, the plots for varying angular momentum have been included to allow for comparison with the timelike and spacelike diagrams.

The spacelike geodesics shown in figure 5.10 show how the spacelike geodesics change with energy and angular momentum. The geodesics share the same "spectral" organisation that the timelike and null geodesics do, with the spacing between the geodesics reducing as the energy is increased. Unlike the spacelike geodesic in figure 5.7 all of these geodesics have sufficient energy to overcome the centrifugal barrier so there is a complete curve going from spacelike infinity, through the event horizon, to the singularity at $r = 0$.

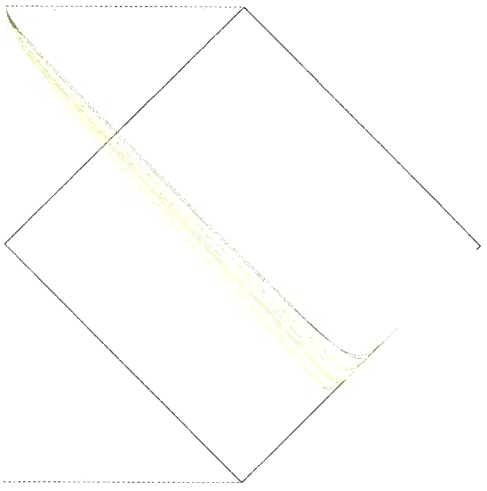

Figure 5.10: Spacelike geodesics with angular momentum varying between $l = 1$ and $l = \frac{5}{3}$, and energy varying between $E = \frac{4}{3}$ and $E = \frac{5}{3}$. The redder the colour, the higher the angular momentum, and the greener the colour the higher the energy.

5.4 Kerr Geodesics

The Kerr metric describes a black hole with S^2 topology, like the Schwarzschild metric, but this time the black hole is no longer static but spinning in the ϕ direction, with angular momentum per unit mass given by a. The addition of angular momentum in the ϕ direction means that the spacetime is no longer spherically symmetric i.e. the spacetime is foliated by oblate spheres rather than the perfect spheres of the Schwarzschild solution. This means that the spacetime varies with varying θ, so it is more difficult to visualise than the Schwarzschild black hole. Indeed, in order to faithfully represent the motion of the Kerr geodesics it would be necessary to incorporate the θ coordinate in the diagram, but 3D cross sections of the Kerr solution aren't conformally flat, so the θ coordinate can't be incorporated in the

same way as the t and r coordinates. Fortunately, most of the interesting features of this spacetime are described by the variation in t and r, so the θ dependence can usually be ignored.

5.4.1 Geodesic Equations

The metric for the Kerr spacetime, in Boyer-Lindquist coordinates, is given by [56]

$$ds^2 = \Sigma\left(\frac{\mathrm{d}r^2}{\Delta} + \mathrm{d}\theta^2\right) + (r^2 + a^2)\sin^2\theta \mathrm{d}\phi^2 - \mathrm{d}t^2 + \frac{2Mr}{\Sigma}(a\sin^2\theta\mathrm{d}\phi - \mathrm{d}t)^2 \,, \quad (5.52)$$

where M is the ADM mass and

$$\Sigma = r^2 + a^2\cos^2\theta \,, \quad (5.53)$$

$$\Delta = r^2 - 2Mr + a^2 \,. \quad (5.54)$$

This space has two event horizons where the Killing vector $\chi^\mu = K^\mu + \Omega_H R^\mu$ becomes null and $K^\mu = \partial_t$, $R^\mu = \partial_\phi$, and Ω_H is the angular velocity of the black hole. The radii where this occurs can be calculated by considering where $g^{rr} = 0$, and g^{rr} is given by

$$g^{rr} = \frac{\Delta}{\Sigma} \,. \quad (5.55)$$

Assuming that $a < M$ gives two solutions

$$r_\pm = M \pm \sqrt{M^2 - a^2} \,. \quad (5.56)$$

In this metric the curvature singularity is no longer given by a constant r hypersurface because the singularity is where $\Sigma = 0$ and Σ is a function of both r and θ. Fortunately, Σ is the sum of two non-negative terms, r^2 and $a^2\cos^2\theta$, so the curvature singularity will be where both terms go to zero. A cursory examination finds that this is when $r = 0$ and $\theta = \frac{\pi}{2}$.

The increased complexity of the Kerr metric means that it is easier to derive the geodesic equations using the Hamiltonian formulation. To derive the Hamiltonian, form the Lagrangian

$$\mathcal{L} = \frac{1}{2} g_{\mu\nu}\dot{x}^\mu\dot{x}^\nu \,. \quad (5.57)$$

Choosing $\tau = m\lambda$ normalises this equation so that the first integral of the geodesic equation is given by

$$g_{\mu\nu}\dot{x}^{\mu}\dot{x}^{\nu} = -m^2 \,, \tag{5.58}$$

where m is the mass of the test particle. Using (5.57) it is now possible to calculate the conjugate momenta using

$$p_{\mu} = g_{\mu\nu}\dot{x}^{\nu} \equiv \frac{\partial \mathcal{L}}{\partial \dot{x}^{\mu}} \tag{5.59}$$

and thus the Hamiltonian

$$H = \frac{1}{2} g^{\mu\nu} p_{\mu} p_{\nu} \,. \tag{5.60}$$

Since (5.52) has two Killing vectors ∂_t and ∂_ϕ the corresponding momenta must be constants of motion, giving

$$p_t = -E \,, \qquad\qquad p_\phi = l \,. \tag{5.61}$$

This leaves only two momenta to calculate from the Lagrangian

$$p_r = \frac{\Sigma}{\Delta}\dot{r} \,, \qquad\qquad p_\theta = \Sigma\dot{\theta} \,. \tag{5.62}$$

To obtain the equations of motion for the geodesics, use the Hamilton-Jacobi equation

$$g^{\mu\nu} p_{\mu} p_{\nu} + m^2 = 0 \,, \tag{5.63}$$

where p_μ can be calculated using

$$p_{\mu} = \frac{\partial S}{\partial x^{\mu}} \tag{5.64}$$

and S is the desired action. Calculating (5.63) for the Kerr metric gives

$$\left[a^2 \sin^2\theta - \frac{(r^2+a^2)^2}{\Delta}\right] p_t^2 + \Delta p_r^2 + p_\theta^2 + \left(\frac{1}{\sin^2\theta} - \frac{a^2}{\Delta}\right) p_\phi^2 - \frac{4Mra}{\Delta} p_t p_\phi + \Sigma m^2 = 0 \,. \tag{5.65}$$

After substituting for p_t and p_ϕ, from (5.61), this equation can be separated into terms only involving r and terms only involving θ. Doing this gives two equations as follows

$$\Delta p_r^2 + r^2 m^2 - \frac{1}{\Delta}\left[(r^2+a^2)^2 E^2 + a^2 l^2 - 4MarEl\right] = -K \,, \tag{5.66}$$

$$p_\theta^2 + \frac{l^2}{\sin^2\theta} + m^2 a^2 \cos^2\theta + E^2 a^2 \sin^2\theta = K \,, \tag{5.67}$$

where K is the separation constant.

Seeing as the Hamilton-Jacobi equation is separable it is possible to express the action as

$$S = \int p_r dr + \int p_\theta d\theta - Et + l\phi + \frac{1}{2}m^2\tau \ , \tag{5.68}$$

where the constants of motion are given by m^2, E, K, l and the equations of motion can be derived by differentiating with respect to them. Following through this procedure gives the four equations of motion

$$\frac{dt}{d\tau} = \frac{1}{\Delta\Sigma}\left[(r^2+a^2)\Sigma E + 2Mra(aE\sin^2\theta - l)\right] \ , \tag{5.69}$$

$$\frac{dr}{d\tau} = \frac{\Delta p_r}{\Sigma} \ , \tag{5.70}$$

$$\frac{d\theta}{d\tau} = \frac{p_\theta}{\Sigma} \ , \tag{5.71}$$

$$\frac{d\phi}{d\tau} = \frac{1}{\Delta\Sigma\sin^2\theta}\left[\Sigma l + 2Mr(aE\sin^2\theta - l)\right] \ . \tag{5.72}$$

These equations can all be solved in their present form but for practical purposes it is more convenient to remove the dependence on τ by dividing each of the equations by (5.70). This gives three differential equations for t, θ, and ϕ

$$\frac{dt}{dr} = \frac{1}{\Delta^2 p_r}\left[(r^2+a^2)\Sigma E + 2Mra(aE\sin^2\theta - l)\right] \ , \tag{5.73}$$

$$\frac{d\theta}{dr} = \frac{p_\theta}{\Delta p_r} \ , \tag{5.74}$$

$$\frac{d\phi}{dr} = \frac{1}{\Delta^2 p_r\sin^2\theta}\left[\Sigma l + 2Mr(aE\sin^2\theta - l)\right] \ . \tag{5.75}$$

These equations can all be solved analytically but the solutions aren't particularly concise. In practice the geodesics have to be solved numerically.

To get some idea of how the geodesics will behave it is advantageous to construct a potential function for the r and θ directions. In the r direction, this is carried out in much the same manner as for the Schwarzschild metric but there is a complication due to the non-trivial way in which the motion depends on θ. For the Schwarzschild metric a 1D potential was constructed in the form of

$$\frac{1}{2}\left(\frac{dr}{d\tau}\right)^2 + V(r) = \mathcal{E} \tag{5.76}$$

and then compared with the radial geodesic equation to ascertain the potential.

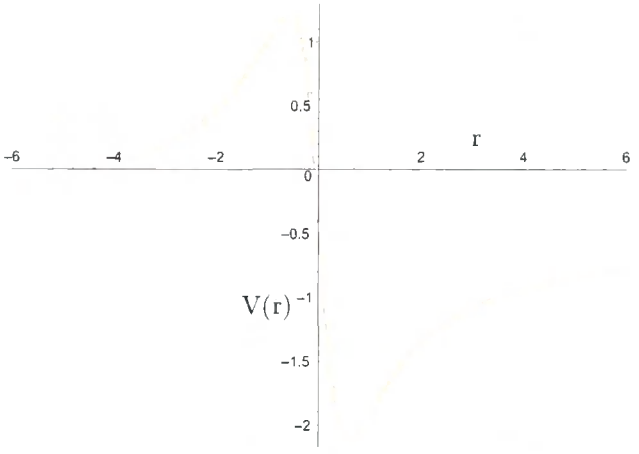

Figure 5.11: Radial potential for a timelike geodesic with $\theta = 0$, $a = 0.6$, $K{=}a^2$, $M = 1$, $l = 0$, and $E = 1.2$

Constructing the analogous expression for the Kerr metric gives

$$\frac{1}{2}\left(\frac{dr}{d\tau}\right)^2 = \frac{\Delta^2 p_r^2}{2\Sigma^2} = \frac{(r^2+a^2)^2E^2 + a^2l^2 - r^2m^2\Delta - 4MarEl - K\Delta}{2\Sigma^2} = \mathcal{E} - V(r,\theta)\,. \tag{5.77}$$

There are two problems with this expression if it is to be used to derive an effective potential. Firstly, the energy dependence E is implicit, since there are terms with E^2 as well as E. The way to avoid this dilemma is to consider the difference between the energy and the potential, $\mathcal{E} - V$, rather than just the potential. This means that the energy of the geodesic is insufficient to cross the potential barrier when (5.77) goes to zero, rather than when the potential is equal to the energy of the geodesic. Considering the difference between the energy and the potential basically means that the potential plot has been translated vertically downwards by E.

The second problem with (5.77) is that the potential no longer solely depends on r. This would consequently require a 3D plot of the potential, showing how the potential varies with r and θ. This wouldn't be very useful, however, as it usually isn't obvious what value θ will take at a particular radius - it would have to be calculated from (5.74). Not everything is lost though because where the energy of the geodesic is equal to the effective potential $\mathcal{E} - V = 0$, which is only true when the numerator of (5.77) goes to zero, so is independent of θ.

The potential given by (5.77) can be used to calculate the potentials exactly in

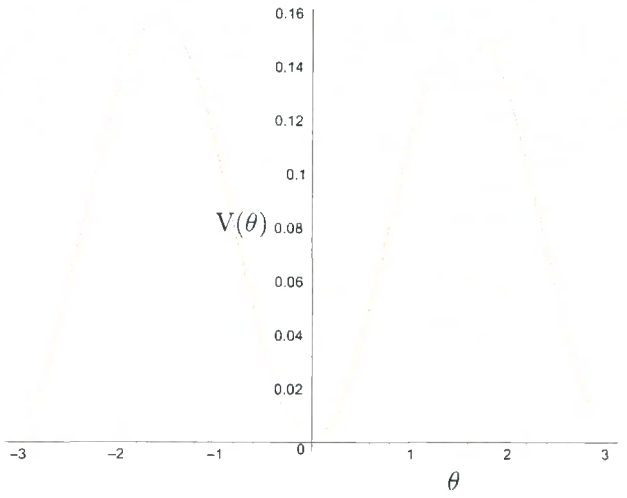

Figure 5.12: A graph of the p_θ^2 potential for a timelike geodesic with $a = 0.6$, $K{=}a^2$, $M = 1$, $l = 0$, and $E = 1.2$

the special case where $\frac{\mathrm{d}\theta}{\mathrm{d}\tau} = 0$. In this case the θ coordinate is always the same so can be substituted into (5.77) to show exactly how the potential varies. Figure 5.11 gives an example of this for a timelike geodesic. The curve crosses the r axis at -0.081, so a massive particle falling into the black hole, with its angular momentum chosen so that $\frac{\mathrm{d}\theta}{\mathrm{d}\tau} = 0$, would only have enough energy to reach $r = -0.081$ before it reversed its direction and proceeded back through the event horizon.

To analyse the motion in the θ direction it is less useful to plot the potential function for the θ coordinate because it is also dependent on r, which has an overriding effect on the shape of the potential. However, as in the radial case, it is still possible to calculate where $\frac{d\theta}{dt} = 0$ and thus where θ changes direction by calculating where the potential function goes to zero. For the θ direction the potential function is given by

$$\mathcal{E} - V = \frac{p_\theta^2}{2\Sigma^2} = \frac{1}{2\Sigma^2}\left(K - \frac{l^2}{\sin^2\theta} - m^2a^2\cos^2\theta - E^2a^2\sin^2\theta\right) . \tag{5.78}$$

The r dependence is only in the denominator, so by considering where the numerator goes to zero gives the value of θ at which θ changes direction. This potential can also be used to calculate values of θ that will produce quasi-radial curves i.e. where θ remains constant for all values of r. The two conditions that have to be satisfied for this to occur are

$$p_\theta^2(\theta_0) \;=\; 0 \,, \tag{5.79}$$

$$\frac{d}{d\theta}(p_\theta)^2\Big|_{\theta=\theta_0} = 0\,, \tag{5.80}$$

where θ_0 is the initial value of θ for which it subsequently remains constant. This physically corresponds to a particle being at either the maximum or minimum of the potential and not having any energy to displace itself. This is easily seen by examining a plot of $-p_\theta^2$ i.e. $V - \mathcal{E}$.

The p_θ^2 plot corresponding to the same geodesic as plotted in figure 5.11 is shown in figure 5.12. From this plot it is obvious that θ will remain constant if $\theta_0 = 0$. Furthermore, since p_θ^2 is linearly dependent on K, it is easily seen that the quasi-radial curves for $K = l^2 + E^2a^2$ will be when $\theta_0 = \pm\frac{\pi}{2}$.

5.4.2 Illustrating Kerr Geodesics

Once the geodesic equations for the Kerr metric have been solved it is possible to plot them so that their behaviour, as the parameters are varied, can be easily contrasted. In principle the Kerr geodesics can be plotted on a Penrose diagram, as the Schwarzschild geodesics were in the previous section, using the Hayward coordinates of section 2. These coordinates are basically a generalisation of the Kruskal coordinates to the case where the black hole is spinning in the ϕ direction, so the ϕ coordinate has to be transformed even though it doesn't explicitly appear in the construction of the null coordinates.

Writing out the new coordinates (that will be used to construct the Penrose diagram) explicitly gives

$$T = \frac{1}{2}\left(e^{\kappa(r^*+t^*)} - e^{\kappa(r^*-t^*)}\right)\,, \qquad R = \frac{1}{2}\left(e^{\kappa(r^*+t^*)} + e^{\kappa(r^*-t^*)}\right)\,, \tag{5.81}$$

where

$$t^* = t - a\sin\theta \tag{5.82}$$

and

$$r^* = \int \frac{\sqrt{r^4 + a^2r^2 + 2Ma^2r}}{r^2 - 2Mr + a^2}\mathrm{d}r\,. \tag{5.83}$$

These coordinate transformations can then be used to draw the geodesics on the Kerr Penrose diagram, after solving (5.73) inside and outside of the event horizons.

Figure 5.13 shows a sample timelike geodesic when it is plotted on the Penrose diagram for the Kerr metric. The Kerr metric has two horizons so the test particle on the timelike geodesic starts in the bottom right hand diamond, crosses the outer horizon, passes through the middle diamond representing the space between the two horizons, and then proceeds to cross the inner event horizon before coming to rest at $r = 0$. In this case the particle stops at $r = 0$, rather than hitting the singularity, because $\theta = \pi/4$ at $r = 0$.

It is immediately obvious from the left hand plot of figure 5.13 that there is a problem with the particular coordinate transformations used. Although the Hayward coordinates are perfectly good for following particle trajectories across an individual event horizon they breakdown when the particle approaches the other horizon. This means that the geodesic has to be plotted on two different patches: one covering the region outside the inner horizon and one covering the region inside the outer horizon. In each case κ has to be chosen to ensure that the coordinates don't break down on the horizon within each respective patch.

This particular problem is exemplified in figure 5.13 because the two lines, representing the same geodesic, don't match up at all in the region between the two horizons but both lines cross their respective event horizon without anything untoward happening. It is possible to make the lines in the two patches join up by judicious selection of the constant of integration in the definition of r^*, which amounts to shifting the origin of the r^* coordinate. Unfortunately, this doesn't ensure that the gradients of the two lines match up and there doesn't appear to be an obvious way to adapt the coordinate transformations so that they do. The only case when the gradients of the two lines will match up is when $\kappa_1 = \kappa_2$ i.e. when the two horizons are degenerate.

The right hand plot in figure 5.13 gives an approximation of the true geodesic to give an idea of how the geodesic would look if the two coordinate patches could be made to match up completely. The two lines have been joined up by translating the coordinate patch across the inner horizon and then splicing the two lines together at about the half way point between the two horizons, where the patches overlap. Since the gradients of the two lines are never actually equal this has introduced a

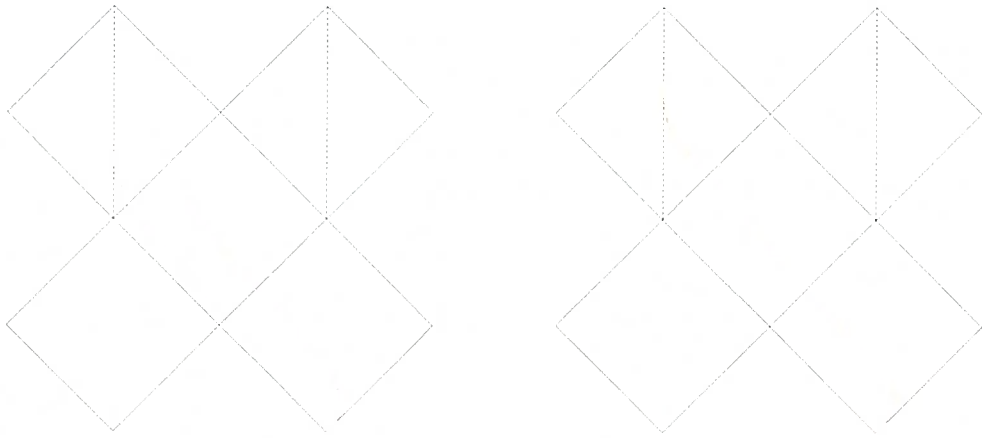

Figure 5.13: Both plots show a timelike geodesic with $M = 1$, $a = \sqrt{2}/2$, $E = 1$, $l = 0$, and $K = 1/2$. The left hand plot shows how the geodesic looks when plotted for the two different coordinate patches and the right hand plot gives an approximation of the Penrose diagram when the two patches are shifted so that they join up in the region where they overlap.

slight kink into the plot of the geodesic, which can be seen at the half way point of the middle diamond.

Although this method does give a fairly pleasing curve, and also allows the familiar Penrose diagrams to be used, it is clearly an unsatisfactory method for plotting the geodesics since the two curves have essentially been joined up using guesswork. Clearly a completely different method is required if geodesics that cross both horizons are to be plotted. A better coordinate system would be one that allows any geodesic to be drawn on the same coordinate patch without constraint. This can be at least partially realised using a method devised by Klösch and Strobl.

The basic idea of the Klösch Strobl approach is to describe any metric of the form

$$\mathrm{d}s^2 = h(r)\mathrm{d}t^2 - \frac{1}{h(r)}\mathrm{d}r^2 - r^2\mathrm{d}\Omega \tag{5.84}$$

using a single global system of coordinates. There already exists a global coordinate system for the Schwarzschild metric, but this approach allows similar coordinate charts to be found for other metrics that are of the above form. This is achieved by considering the most general possible solution to the 2D gravity action, within the restrictions of the gauge conditions, and then choosing the remaining functions so that the general solution locally reduces to the required metric (5.84).

The metric given in (5.84) is reduced to a 2D metric by concentrating on the non-killing directions, namely the t and r directions. This means that the metric can be re-written as

$$ds^2 = g - r^2 \mathrm{d}\Omega \,. \tag{5.85}$$

The 2D action is given by

$$S[g,\phi] = -1/2 \int_M \mathrm{d}^2x \sqrt{-\det g}[\phi R - V(\phi)] \,, \tag{5.86}$$

where g is a Minkowski metric on a 2-manifold, R is the Levi-Civita curvature scalar, ϕ is a scalar function on the manifold, and V is a smooth potential. The 2D action can be re-written in an Einstein-Cartan formulation as

$$S[e^a,\omega,\psi_a,\phi] = \int_M \psi_a De^a + \phi \mathrm{d}\omega - \frac{1}{2}V(\phi)e^+ \wedge e^- \,, \tag{5.87}$$

where e^a ($a \in \{+,-\}$) is the zweibein, $\epsilon^a{}_b\omega$ is the spin connection, ψ_a are the Lagrange multiplier fields, and the metric is given by $g = 2e^+e^-$.

Any local solution to (5.86) can be given by

$$g = h(r)\mathrm{d}t^2 - \frac{1}{h(r)}\mathrm{d}r^2 \,, \tag{5.88}$$

with V given by

$$V = h'(r) \,. \tag{5.89}$$

This fixes the potential in (5.87) so that it describes the required metric given by (5.84). Having fixed $V(\phi)$ there is still considerable gauge freedom, so it is possible to choose a solution to (5.87) that gives the metric in light cone gauge

$$\mathrm{d}s^2 = 2\mathrm{d}x^0\mathrm{d}x^1 + k(x^0,x^1)(\mathrm{d}x^1)^2 \,. \tag{5.90}$$

A simple choice for the zweibein that brings (5.87) into this form is

$$e^+ = \mathrm{d}x^1 \,, \qquad e^- = \mathrm{d}x^0 + \frac{1}{2}k\mathrm{d}x^1 \,. \tag{5.91}$$

The function k is determined by the equations of motion of (5.87) in terms of two other functions $F(x^1)$ and $G(x^1)$

$$k = \frac{2F'(x^1)x^0 + G'(x^1)}{F(x^1)} + \frac{h(F(x^1)x^0 + G(x^1))}{F(x^1)^2} \tag{5.92}$$

and also

$$\phi = F(x^1)x^0 + G(x^1) \; . \tag{5.93}$$

The functions $F(x^1)$ and $G(x^1)$ aren't completely unrestricted, the equations of motion give two constraint equations

$$h(G\mid_{F(x^1)=0}) = 0 \tag{5.94}$$

and

$$F'(x^1)\mid_{F(x^1)=0} = -\frac{1}{2}V(G\mid_{F(x^1)=0}) = -\frac{1}{2}h'(G\mid_{F(x^1)=0}) \; . \tag{5.95}$$

Remarkably these are the only constraints on the two functions, apart from requiring that they are smooth functions of x^1.

To show how $k(x^0, x^1)$ relates to the starting metric (5.84), manipulate the remaining gauge freedom to make

$$k(x^0, x^1) = h(x^0) \tag{5.96}$$

locally. This means that for each value of x^1 the global metric can be reduced to the local metric given by (5.84).

The metric given in (5.90) is unaffected if an x^1 dependent linear transformation is applied to the affine parameter x^0 and then compensated by a diffeomorphism in the x^1 variable i.e.

$$\begin{aligned} x^0 &= \frac{1}{f'(\tilde{x}^1)}\tilde{x}^0 + l(\tilde{x}^1) \; , \\ x^1 &= f(\tilde{x}^1) \; . \end{aligned} \tag{5.97}$$

Ultimately, it is only necessary to be concerned with how the metric looks for a constant value of x^1 since the desired metric (5.84) is only dependent upon a single variable. If the transformations given by (5.97) are substituted into (5.93) they suggest the following transformations for $F(x^1)$ and $G(x^1)$

$$F(x) \to \frac{F(f(x))}{f'(x)} \; , \qquad\qquad G(x) \to G(f(x)) + F(f(x))l(x) \; . \tag{5.98}$$

A quick examination of (5.92) reveals that the simplest way to achieve the equivalence given by (5.96) is to transform $F \to 1$ and $G \to 0$. If $f(x)$ is chosen so that it solves the differential equation $f'(x) = F(f(x))$ then (5.98) indicates that $F \to 1$.

The choice $f(x) = x$ thus fulfills this requirement. Furthermore, combining $f(x) = x$ with $l(x) = -G(x)$ gives $G(x) \to 0$. This also has the by-product of transforming $\phi \to x^0$. To recover the metric given by (5.84) a further diffeomorphism is required

$$r = x^0 , \qquad t = x^1 + \int^{x^0} \frac{\mathrm{d}z}{h(z)} . \tag{5.99}$$

The obvious limitation of the Klösch Strobl method is that it can only deal with spacetimes that can be described by a 2D metric plus some other non-interacting part. To apply this technique to the Kerr metric (5.52), it has to be reduced to a 2D metric plus some symmetric part. This can be achieved by only considering the geodesics where $\theta = 0$. As previously described, geodesics that start at $\theta = 0$ don't deviate in the θ direction, which greatly simplifies the metric to give

$$\mathrm{d}s^2 = \frac{r^2 + a^2 - 2Mr}{r^2 + a^2} \mathrm{d}t^2 - \frac{(r^2 + a^2)}{r^2 + a^2 - 2Mr} \mathrm{d}r^2 . \tag{5.100}$$

This is already of the form given in (5.88) if

$$h = \frac{r^2 + a^2 - 2Mr}{r^2 + a^2} , \tag{5.101}$$

which has two simple zeros at

$$r_\pm = M \pm \sqrt{M^2 - a^2} . \tag{5.102}$$

To determine the functions $F(x^1)$ and $G(x^1)$ that satisfy the gauge conditions given by (5.94) and (5.95), label the zeros of F by $x^1 = n\pi$ ($n \in \mathbf{Z}$) and thus choose $F(x^1)$ to be of the form

$$F(x^1) = \alpha(x^1) \sin x^1 . \tag{5.103}$$

Having chosen this form for the zeros, the constraint equation given by (5.94) demands that $G(x^1)$ be of the form

$$\begin{aligned} G(x^1) &= \frac{r_+ + r_-}{2} - \frac{r_+ - r_-}{2} \cos x^1 \\ &= M - \sqrt{M^2 - a^2} \cos x^1 . \end{aligned} \tag{5.104}$$

The other constraint equation (5.95) now demands that $\alpha(n\pi) = \frac{1}{2}h'(r_-) = \alpha_-$ for n even and $\alpha(n\pi) = \frac{1}{2}h'(r_+) = \alpha_+$ for n odd. A simple choice for α is then given by

$$\alpha(x^1) = C_1 + C_2 \cos x^1 , \tag{5.105}$$

where $C_1 = \frac{1}{2}\alpha_- + \alpha_+$ and $C_2 = \frac{1}{2}\alpha_- - \alpha_+$ i.e.

$$C_1 = \frac{\sqrt{M^2 - a^2}}{2a^2} , \qquad C_2 = \frac{M^2 - a^2}{2Ma^2} . \tag{5.106}$$

Having established the functions $F(x^1)$ and $G(x^1)$ that satisfy the equations of motion, $k(x^0, x^1)$ (and thus the metric in the global coordinate system) can be found by substituting into (5.92) and (5.90).

To make contact with the Kerr metric given in (5.100), calculate the local transformation that will convert the global coordinates (x^0, x^1) into the time and radial coordinates (t, r). For clarity it is useful to re-label the global coordinates so that $x^1 \to x$ and $x^0 \to y$.

As before, to get from the global coordinate system to the local one, transform $F(x) \to 1$ and $G(x) \to 0$. As shown previously, this automatically makes $\phi \to y$ which yields the first transformation

$$x^0 = \phi = F(x)y + G(x) . \tag{5.107}$$

The differential equation for the transformation $F(x) \to 1$ was given earlier by

$$f'(x) = F(f(x)) = (C_1 + C_2 \cos(x)) \sin(x) , \tag{5.108}$$

where the second equality is given by (5.103) and (5.105). Solving this differential equation for $f(x)$ gives

$$f(x) = \frac{C_1 \ln(\tan\frac{x}{2}) + C_2 \ln(2C_1 + 2C_2 \cos x) - C_2 \ln(\sin x)}{(C_1 + C_2)(C_1 - C_2)} . \tag{5.109}$$

The transformation $F \to 1$ is also satisfied by $f(x^1) \to x^1$ which implies

$$x^1 = \frac{C_1 \ln(\tan\frac{x}{2}) + C_2 \ln(2C_1 + 2C_2 \cos x) - C_2 \ln(\sin x)}{(C_1 + C_2)(C_1 - C_2)} . \tag{5.110}$$

Note that x^1 & x^0 are now local coordinates rather than the original global coordinates.

The transformations (5.99) are then used to recover the desired metric (5.100). These are explicitly given by

$$r = x^0 , \tag{5.111}$$

$$t = x^1 + x^0 + M \ln(x^{0^2} + a^2 - 2Mx^0) + \frac{2M^2}{\sqrt{a^2 - M^2}} \arctan\left(\frac{x^0 - M}{\sqrt{a^2 - M^2}}\right) . \tag{5.112}$$

Unfortunately, because (5.110) cannot be inverted, there is no way to transform from the local coordinates to the global coordinates. This means that the geodesics of the global metric (5.90) have to be calculated in the (x, y) coordinates. In these coordinates, the first integral is given by

$$2\dot{x}\dot{y} + \left(\frac{2\partial_x\phi}{F(x)} + \frac{h(\phi)}{F(x)^2}\right)\dot{x}^2 = \epsilon\,, \tag{5.113}$$

where $\phi = F(x)y + G(x)$ and ϵ determines the nature of the geodesics as before. The other geodesic equation, required to solve for x and y, is

$$\ddot{x} - \left(F'(x) + \frac{M(\phi^2 - a^2)}{(\phi^2 + a^2)^2}\right)\frac{\dot{x}^2}{F(x)} = 0\,. \tag{5.114}$$

In order to construct a Penrose diagram for these coordinates it is necessary to isolate the null directions in terms of the global coordinates (x, y). It is obvious that $x^1 =$ constant is one null direction, due to the form of the metric, but the other null direction isn't so simple to calculate. It is given by the solution to

$$2\dot{y} + \left(\frac{2\partial_x\phi}{F(x)} + \frac{h(\phi)}{F(x)^2}\right)\dot{x} = 0\,, \tag{5.115}$$

which cannot be separated because ϕ is a function of y as well as x. This means that the transformation into the form required to construct the Penrose diagram can't be written down explicitly. Furthermore, the geodesic equations (5.113) and (5.114) have to be solved numerically because there is no obvious way to separate them.

The radial curves in the new coordinates are easy to calculate because they are given by the lines of constant ϕ. This can be seen from the transformations given by (5.107) and (5.111). The radial curves have been drawn in figure 5.14, with the hue of the colours varying to indicate the different radii. The three dotted lines from left to right are: the outer event horizon, the inner event horizon, and the origin $r = 0$. The nature of the coordinate transformations means that there are an infinite number of repeating, causally separated coordinate patches, that stretch from $-\infty$ to $+\infty$ along the x axis. Figure 5.14 only shows the two patches that make up one cycle.

Figure 5.15 shows a sample timelike geodesic in the (x, y) coordinates. The timelike geodesic is in red, with the blue, purple, and green lines showing the radial

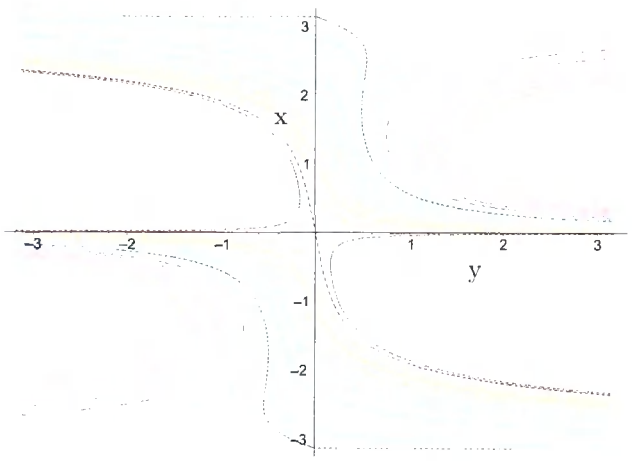

Figure 5.14: Radial curves in the Klösch Strobl coordinates. The colours get darker with increasing r and r ranges from 0.08 to 1.82 in increments of 0.25.

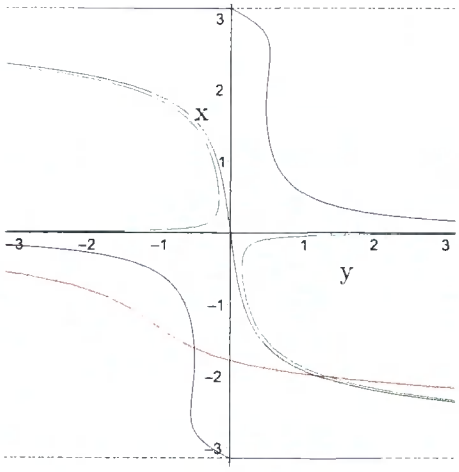

Figure 5.15: Timelike geodesic starting out at $2M$ and falling inward through both the event horizons and through the centre of the ring singularity at $r = 0$

curves corresponding to $r = r_+$, $r = r_-$, and $r = 0$ respectively. The dotted lines are the null extremals given by x = constant. The timelike geodesic starts out at $r = 2M$ and then falls through both the inner and outer event horizons before passing through $r = 0$. The radial curves help to illustrate the direction of motion of the timelike geodesic as well as indicating the causally accessible parts of the coordinate patch.

Using the Klösch Strobl technique allows the on-axis Kerr geodesics to all be plotted on a single coordinate patch, and thus avoids the problems of the Penrose diagram approach. Unfortunately, it isn't immediately obvious how this approach could be generalised to include more general classes of geodesics. This would obviously require more work to find out whether this would be possible.

Chapter 6

Black Ring Geodesics

Given all that is known about the geodesics of the Kerr black hole it seems logical to go on and investigate the corresponding situation for Black Rings to see whether any of the properties of the Kerr geodesics are shared by those of the Black Ring. The physical properties of the neutral rotating Black Ring solution have been extensively studied in papers such as [61] and [26] but very little is known about the geodesics associated with this metric. There has been some rudimentary work in some papers such as [62], [63] and [64], but the geodesic calculations are very much secondary to the other facets under consideration. The calculations in these papers were very restricted in their application, so one would expect more general classes of geodesics to be more complicated. The results given in this chapter are based on [65].

The Black Ring has horizon topology $S^2 \times S^1$, as opposed to the S^3 topology of the 5D Kerr horizon, giving greater scope for interesting classes of geodesics. This chapter explores these different situations as well as seeing whether any of the special classes of Kerr geodesics described above can be reproduced in the Black Ring metric. The toroidal nature of the Black Ring means that there won't be any spherical orbits, but the analogous situation, where the geodesic remains at a constant distance from the event horizon, will be examined.

Some work has been done on the geodesics of the doubly spinning black ring metric in [66]. In this paper, Durkee mainly concentrates on the zero energy null geodesics in the ergoregion, as it is possible to separate the Hamilton-Jacobi equation of motion in this region to get two equations of motion for the evolution of the x

and y coordinates separately. He shows that these zero energy particles will bounce back and forth inside the ergoregion with the bounds of the motion determined by the angular momentum in the ϕ direction.

Durkee also gives a brief exposition on the geodesics along the two rotational axes of the doubly spinning black ring. In this case, the geodesics along the ψ axis of rotation are analogous to the geodesics along the $y = -1$ line of the singly spinning ring, explained in this chapter. It is also concluded that the geodesics corresponding to motion along the ϕ axis of rotation do not exhibit any qualitatively different behaviour to those on the ψ axis.

This chapter, on the singly spinning ring, is divided into 5 main sections: section 6.1 derives the geodesic equations for the Black Ring metric and presents the conserved quantities associated with the symmetries of the metric. The remaining sections 6.2 through 6.5 investigate some specific classes of geodesics where the equations of motion become separable. Section 6.2 investigates the case where the geodesics are confined to the rotational axis of the ring, section 6.3 describes the geodesics that orbit at a constant radius in the equatorial plane of the ring, section 6.4 looks at the case where the geodesics are restricted to move along circles of constant radius through the ring, and the final section calculates which classes of geodesics can perform "pseudo-radial" motion. These geodesics are the analogue of radial curves in, for example, the Schwarzschild spacetime, but in the Black Ring coordinates the rotation of the ring means that these "pseudo-radial" geodesics have to rotate in the same direction as the ring.

6.1 Geodesic Equations and Conserved Quantities

To obtain the geodesic equations of motion, the following lagrangian is formed

$$\mathcal{L} = \frac{R^2 F(x)}{2(x-y)^2}\left[-\frac{G(y)}{F(y)}\dot{\psi}^2 - \frac{\dot{y}^2}{G(y)} + \frac{\dot{x}^2}{G(x)} + \frac{G(x)}{F(x)}\dot{\phi}^2\right] - \frac{F(y)}{2F(x)}\left(\dot{t} - \frac{CR(1+y)}{F(y)}\dot{\psi}\right)^2 \tag{6.1}$$

The conjugate momenta can then be calculated using

$$p_\mu = g_{\mu\nu}\dot{x}^\nu \tag{6.2}$$

It is obvious from the form of (4.1) that there are three Killing vectors given by ∂_t, ∂_ψ, and ∂_ϕ. This means that the momenta in these directions will be conserved, giving

$$p_t = -E = -\frac{F(y)}{F(x)}\dot{t} + \frac{CR(1+y)}{F(x)}\dot{\psi} \tag{6.3}$$

$$p_\phi = \ell = \frac{R^2 G(x)}{(x-y)^2}\dot{\phi} \tag{6.4}$$

$$p_\psi = \Psi = \frac{CR(1+y)}{F(x)}\dot{t} - \frac{C^2R^2(1+y)^2}{F(x)F(y)}\dot{\psi} - \frac{G(y)R^2F(x)}{F(y)(x-y)^2}\dot{\psi} \tag{6.5}$$

$$p_x = \frac{R^2F(x)\dot{x}}{G(x)(x-y)^2} \tag{6.6}$$

$$p_y = -\frac{R^2F(x)\dot{y}}{G(y)(x-y)^2} \tag{6.7}$$

where E is the energy, and ℓ and Ψ are the constants associated with the angular momenta in the ϕ and ψ directions respectively. The momenta in the x and y direction have also been included for future reference.

Unfortunately, these conserved quantities aren't sufficient to allow the equations of motion to be separated immediately. The easiest way to check whether the equations can be separated is to consider the Hamilton-Jacobi equation

$$g^{\mu\nu}p_\mu p_\nu = -m^2 \tag{6.8}$$

Calculating the inverse metric components from (4.1) and substituting into (6.8) gives

$$Y(y) + X(x) = \frac{F(x)}{(x-y)^2}\left(\frac{E^2F(x)}{F(y)} - m^2\right) \tag{6.9}$$

where $Y(y)$ and $X(x)$ are given by

$$Y(y) = -\frac{F(y)}{G(y)}\left(\frac{\Psi}{R} - \frac{EC(1+y)}{F(y)}\right)^2 - \frac{G(y)p_y^2}{R^2} \tag{6.10}$$

$$X(x) = \frac{\ell^2F(x)}{R^2G(x)} + \frac{G(x)p_x^2}{R^2} \tag{6.11}$$

The right hand side of equation (6.9) indicates that the Hamilton-Jacobi equation can't be separated for arbitrary values of the constants of motion but if $E = 0$ and

$m = 0$ then the function on the right hand side will go to zero, allowing the equation to be separated out into terms involving only x and y.

These particular values of E and m correspond to null geodesics that don't move relative to the space. In the case of the black ring, this means that the geodesics will rotate with the ring, but won't move in the x, y, or ϕ directions. Null geodesics with $E = 0$ aren't physically realisable, but this does provide a way to check whether the numerical solutions to the equations of motion are consistent.

Applying the variational principle to (6.1) gives three equations of motion for the Killing directions as per equations (6.3)-(6.5). The remaining two equations of motion are calculated by varying with respect to x and y respectively

$$H(x,y) - J(x) = \frac{\ell^2(x-y)^2 G'(x)}{2R^2 G(x)^2} \tag{6.12}$$

$$H(y,x) - J(y) = \frac{(x-y)^2\left[ECR(1+y)+\Psi F(y)\right]^2}{RF(x)^2 G(y)F(y)} \times \left[\frac{G'(y)F(y)}{2RG(y)} - \frac{EC(1-\lambda)}{ECR(1+y)+\Psi F(y)}\right] \tag{6.13}$$

where

$$H(\zeta,\eta) = \frac{R^2F(\zeta)}{(\zeta-\eta)^2}\left[\frac{\ddot{\zeta}}{G(\zeta)} - \frac{G'(\zeta)\dot{\zeta}^2}{2G(\zeta)^2} - \frac{[F(\zeta)+F(y)]\dot{\zeta}^2}{2F(\zeta)G(\zeta)(\zeta-\eta)} + \frac{[F(x)+F(\zeta)]\dot{\eta}\dot{\zeta}}{G(\zeta)F(x)(\zeta-\eta)} - \frac{[F(\zeta)+F(y)]\dot{\eta}^2}{2F(\zeta)G(\eta)(\zeta-\eta)}\right] \tag{6.14}$$

$$J(\zeta) = \frac{x-y}{R^2F(x)}\left[\frac{\left[ECR(1+y)+\Psi F(y)\right]^2\left[F(y)+F(\zeta)-\lambda(x-\zeta)\right]}{2F(x)F(y)G(y)} - \frac{\ell^2F(\zeta)}{G(x)}\right] + \frac{E^2\lambda}{2F(y)} \tag{6.15}$$

These two equations have been expressed in terms of the conserved quantities by substituting for $\dot{\phi}$, $\dot{\psi}$, and $\dot{t}$ from equations (6.3)-(6.5). In certain circumstances it is also useful to use the first integral of motion, which is given by

$$\frac{R^2F(x)}{(x-y)^2}\left(\frac{\dot{x}^2}{G(x)} - \frac{\dot{y}^2}{G(y)}\right) + \frac{\ell^2(x-y)^2}{R^2G(x)} - \frac{E^2F(x)}{F(y)} - \frac{(x-y)^2\left[RE(1+y)C+\Psi F(y)\right]^2}{F(x)F(y)R^2G(y)} = \epsilon \tag{6.16}$$

where ϵ determines the nature of the geodesics as

$$\epsilon = \begin{cases} -1 & \text{timelike} \\ 0 & \text{null} \\ +1 & \text{spacelike} \end{cases}$$

As previously mentioned, equation (6.9) isn't separable in the general case, so the following four sections consider some special cases where either x or y remain constant throughout the geodesic's motion. These specific cases give the limiting behaviour of geodesics in different parts of the space with varying angular momenta and energy. They can then be used to give a good idea of how the geodesics behave when their initial conditions are similar to any of the cases examined in sections 6.2-6.5. As the initial conditions are varied away from these limiting cases, the behaviour of the geodesics gradually breaks down until the motion is completely dissimilar.

6.2 Geodesics Along the Rotational Axis of the Ring

The geodesic equations, as they are presented in equations (6.3-6.13), are too complicated to analyse straight away. In order to reduce the complexity of the problem, it is necessary to look for certain values of the initial conditions and conserved quantities that simplify the equations. The most obvious way to do this is to look for initial values of y that solve $G(y_0) = 0$. The reasoning behind this is easiest to see by multiplying (6.16) by $G(y)$ and then choosing $y = y_0$ to be a root of $G(y)$, so that $G(y) \to 0$. The remaining terms are then given by

$$\frac{R^2 F(x)}{(x-y_0)^2}\dot{y}^2 + \frac{(x-y_0)^2\left[RE(1+y_0)C + \Psi F(y_0)\right]^2}{F(x)F(y_0)R^2} = 0 \qquad (6.17)$$

From this equation it is obvious that the velocity in the y direction, given by $\dot{y}$, will be zero if the second term is zero. $G(y)$ is already a fully factored cubic function with three real roots, so the solutions of $G(y) = 0$ are given by: $y_0 = \pm 1, -\frac{1}{\nu}$. The y coordinate is necessarily constrained such that $-\infty \leq y \leq -1$, which reduces the

possible values for y_0 to -1 or $-\frac{1}{\nu}$. Fortunately, $y_0 = -1$ will cause the second term in (6.17) to go to zero, provided $\Psi = 0$[1]. The line $y = -1$ represents the axis of rotation of the ring, so it is not surprising that the equations of motion become considerably simpler along this line.

Ensuring that the initial value of $\dot{y}$ is zero will make sure that the geodesic doesn't move away from $y = -1$ immediately but, for the geodesic to remain on the line $y = -1$, $\ddot{y}$ also has to be zero for all subsequent times. To check that $\ddot{y} = 0$, multiply (6.13) by $G(y)$ and substitute $\dot{y} = 0$. This gives

$$\frac{(x-y)\left[RE(1+y)C + \Psi F(y)\right]^2}{2R^2F(x)}\left[\frac{F(y)G'(y)(x-y)}{G(y)} + 2F(y) - \lambda(x-y)\right]$$
$$-\frac{R^2F(y)^2F(x)\ddot{y}}{(x-y)^2} - \frac{EC(x-y)^2(1-\lambda)[RE(1+y)C + \Psi F(y)]}{RF(x)} = 0 \qquad (6.18)$$

At first glance it looks like substituting $y = -1$ and $\Psi = 0$ will ensure that $\ddot{y} = 0$ but the $G(y)$ factor in the denominator of the first term causes problems because it doesn't cancel with all the terms in the numerator. More specifically, there will be a term of the form[2]

$$\frac{\left[(1+y) + \Psi F(y)\right]^2}{G(y)} \qquad (6.19)$$

which will be indeterminate when $y = -1$, due to $G(y) \to 0$. To take the limit as $y \to -1$, it is necessary to express $G(y)$ explicitly as $G(y) = (1-y)(1+y)(1+\nu y)$. Expanding the numerator as well gives

$$\frac{(1+y)^2}{(1-y)(1+y)(1+\nu y)} + \frac{2(1+y)\Psi F(y)}{(1-y)(1+y)(1+\nu y)} + \frac{\Psi^2F(y)^2}{(1-y)(1+y)(1+\nu y)} \qquad (6.20)$$

It is now obvious that the first two terms will go to zero in the limit as $y \to -1$ but the only way to ensure that the third term doesn't blow up is to define $\Psi = 0$. Since, $y = -1$ corresponds to the axis of rotation of the ring, one would expect that Ψ would have to be zero because the angular momentum of the particle is zero when it is on the axis. This can be quickly verified by substituting $y = -1$ into (6.5).

[1]It also appears that Ψ and E can be chosen to effect the same outcome for $y = -\frac{1}{\nu}$ but, as will be seen later, Ψ has to be set to zero if $G(y) = 0$.

[2]The following analysis is slightly cavalier. A more detailed analysis of the singularities caused when $y = -1$ is given in Appendix C

Equation (6.20) also explains why $y = -\frac{1}{\nu}$ can't be used as an initial condition because, from (6.17), $\dot{y}$ can't be made to go to zero while $\Psi = 0$, unless $y = -1$. Furthermore, the line $y = -\frac{1}{\nu}$ corresponds to the event horizon, so this possibility can be excluded on physical grounds.

Having ensured that $\dot{y} = 0$ for all motion along the axis of rotation, it is now much simpler to calculate how the geodesic varies in the x direction. The x evolution is calculated by substituting $\dot{y} = 0$ and $y = -1$ into (6.12) and then integrating it numerically. Before doing that, it is helpful to calculate an effective potential for the motion along the axis to get some idea of the allowed motion.

To calculate the effective potential substitute $\dot{y} = 0$ and $y = -1$ into (6.16). Rearranging and expressing in terms of p_x now gives

$$p_x^2 + \frac{\ell^2 F(x)}{G(x)^2} - \frac{\epsilon R^2 F(x)}{(x+1)^2 G(x)} - \frac{E^2 R^2 F(x)^2}{(x+1)^2 G(x)(1-\lambda)} = 0 \tag{6.21}$$

This form of the equation can be compared with the equation of motion for a classical particle, with unit mass, in a one dimensional potential i.e.

$$\frac{1}{2}p_x^2 + V(x) - \mathcal{E} = 0 \tag{6.22}$$

where $\mathcal{E}$ is the total energy of the particle. In this case the effective potential $V(x)$ can be found by solving for $\mathcal{E}$ when $p_x = 0$ i.e. when the total energy is the same as the effective potential. Equation (6.21) is not quite of this form, since the equation is quadratic in E, but it is possible to construct an effective potential in an analogous way by setting $p_x = 0$ and then solving for E to find two solutions $V_\pm(x)$. The motion of a particle in this potential is now possible only when $E \geq V_+(x)$ or $E \leq V_-(x)$.

The effective potential for (6.21) can now be calculated, giving

$$V_\pm(x) = \pm\sqrt{\frac{\ell^2(x+1)^2(1-\lambda)}{G(x)R^2F(x)} - \frac{\epsilon(1-\lambda)}{F(x)}} \tag{6.23}$$

In the following it is assumed that $E \geq 0$ so, in this case, the only relevant potential is $V(x) \equiv V_+(x)$. Some example potential plots for timelike geodesics are given in figures 6.1 and 6.6.

The position of the turning points in the potential is given by the solution to

$$\frac{dV(x)}{dx} = 0 \tag{6.24}$$

The general form of this equation when $R = 1$ and $\lambda = \lambda_c$ is

$$Sx^4 + Tx^3 + Ux^2 + Vx + W = 0 \tag{6.25}$$

where

$$S = 2\epsilon\nu^3 \tag{6.26}$$

$$T = (4\ell^2\nu^2 + 4\epsilon\nu^2 - 4\epsilon\nu^3) \tag{6.27}$$

$$U = (4\ell^2\nu^2 + 3\ell^2\nu + \ell^2\nu^3 + 2\epsilon\nu^3 + 2\epsilon\nu - 8\epsilon\nu^2) \tag{6.28}$$

$$V = (4\epsilon\nu^2 + 6\ell^2\nu + 2\ell^2\nu^3 - 4\epsilon\nu - 4\ell^2\nu^2) \tag{6.29}$$

$$W = (2\ell^2 + 2\ell^2\nu^2 - \ell^2\nu^3 - 3\ell^2\nu + 2\epsilon\nu) \tag{6.30}$$

In general this is a quartic equation so it is best to solve it for specific values of ν and ℓ. It reduces to a cubic for $\epsilon = 0$ but the general solution is still too cumbersome to manipulate algebraically. Solving (6.25) gives the value of x for which a test particle will remain stationary. To calculate the minimum energy a particle can have, the solution to equation (6.25) has to be substituted back into (6.23).

6.2.1 Timelike Geodesics on the Rotational Axis

Having calculated the effective potential and its turning points, it is now simple to deduce the shape of the geodesics on the $y = -1$ axis. Substituting values for ℓ and ν into (6.23) gives the effective potentials shown in figure 6.1. These plots show that, in general

- the geodesics with low angular momentum penetrate further toward the origin at $x = 1$.
- the potential goes from being attractive at $\ell = 0$ to wholly repulsive for large values of ℓ.
- the potential has a local minimum when ν is large.
- there is a local maximum for certain values of ν.
- when $\ell \neq 0$, the centrifugal barrier is infinite at $x = 1$.

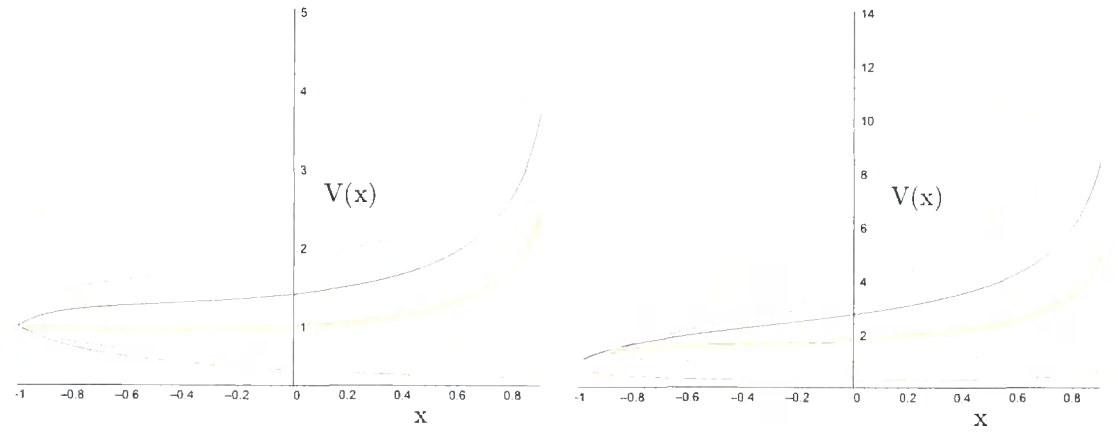

Figure 6.1: The left hand plot shows the effective potential for timelike geodesics on the rotational axis with $\ell = 0, 1, 2, 3, 4$, when $\nu = 0.5$. The lowest curve corresponds to $\ell = 0$ and ℓ increases with each consecutive curve. The right hand plot show how the same potential varies for $\nu = 0.1, 0.3, 0.5, 0.7, 0.9$, when $\ell = 4$. The lowest curve corresponds to $\nu = 0.9$ and ν decreases with each consecutive curve. $R = 1$ in both of these plots.

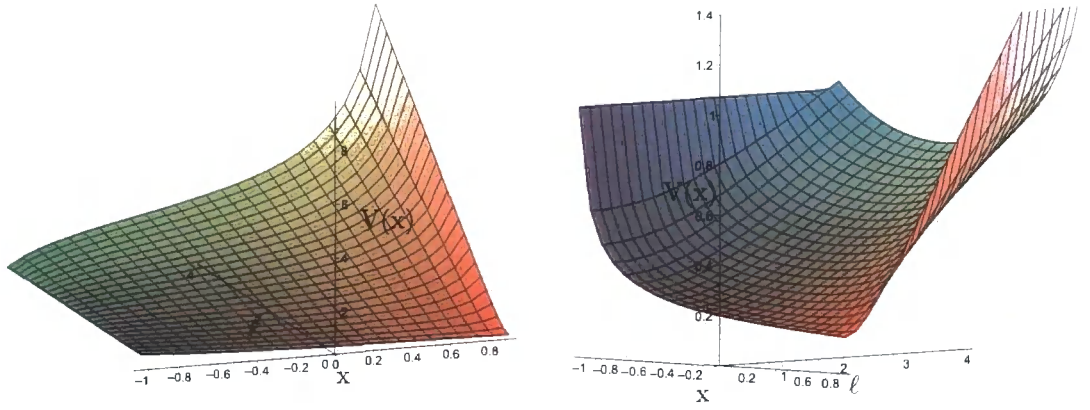

Figure 6.2: 3D plots showing the variation of the timelike effective potential with ℓ and x for $\nu = \frac{1}{4}$ and $\nu = \frac{3}{4}$ respectively. In both of these plots $R = 1$.

Figure 6.2 shows how the effective potential varies for timelike geodesics when the angular momentum is varied between 0 and 4 for two different values of ν. In the case of $\nu = \frac{1}{4}$ and $R = 1$, the potential is initially attractive for $\ell = 0$ but as ℓ is increased the centrifugal barrier at $x = 1$ becomes infinite and then widens toward $x = -1$. This also shifts the minimum toward $x = -1$ and makes the well shallower. This process continues until the centrifugal barrier cancels out the potential well completely and the potential becomes repulsive for all values of x. Although the centrifugal barrier, on the right of the plots in figure 6.1, widens with ℓ, $V(-1) = 1$ for all values of ℓ and ν. This means that the potential well can usually only trap particles with $E < 1$ but, as can be seen from the blue line in the right hand plot of figure 6.1, for some values of ν there is a local maximum near $x = -1$. This maximum is more apparent in the right hand plot of figure 6.2 where a ridge appears at $l \approx 3.5$ and $x \approx -0.9$. This maximum only exists for certain values of ν and l, which can be determined for balanced rings by analysing (6.23) when $\epsilon = -1$, and $\lambda = \lambda_c$.

The limits on ℓ are in general dependent upon ν, so the upper limit of ℓ is given by

$$\begin{aligned}\ell_+ &= R(\Upsilon^2 + \sqrt{2}\Upsilon + 2)\left[1 - \nu(\Upsilon^2 + \sqrt{2}\Upsilon + 1)\right]\left[\frac{1}{2}(\nu^2 - 32\nu + 3)\Upsilon^4 - 2\nu\Upsilon^6\right. \\ &\quad \left. -6\sqrt{2}\nu\Upsilon^5 + \sqrt{2}(\nu^2 - 12\nu + 3)\Upsilon^3 + (\nu^2 - 8\nu + 3)\Upsilon^2 - \frac{1}{\nu}(\nu - 1)^3\right]^{(-1/2)} \quad (6.31)\end{aligned}$$

where $\Upsilon^3 = \sqrt{2}(\nu - 1)\nu^{-1}$. The lower limit on ℓ is given by

$$\ell_- = \frac{2R\sqrt{\nu}}{\sqrt{1-\nu}} \quad (6.32)$$

Both of these equations assume that ℓ is positive but it is always possible for ℓ to be negative, in which case the lower and upper limits swap over and both acquire an overall minus sign.

Having found the limits on ℓ it is necessary to consider the possible values of ν that produce a local maximum in the potential. Considering the roots of (6.25) shows that the minimum value that ν can take, for which there can be a local maximum in the potential, is given by $\nu = \frac{1}{3}$. Below this value it is impossible to have a local maximum near $x = -1$ and the potential will increase continuously

with increasing x. Plugging $\nu = \frac{1}{3}$ into (6.31) and (6.32) shows that there is only one possible value of ℓ at this point given by $\ell_+ = \ell_- = \sqrt{2}$.

One other interesting feature of equation (6.31) is that the denominator becomes imaginary for $\nu > 0.654$. This indicates that the potential will always have a local maximum for all values of ℓ, so all rings with $\nu > 0.654$ will be able to capture particles along the axis of rotation with $V_{max} > E > 1$, no matter how large their angular momentum. For rings with $\nu < 0.654$, increasing ℓ will eventually smooth out the potential well and cause the potential to be continuously increasing with increasing x.

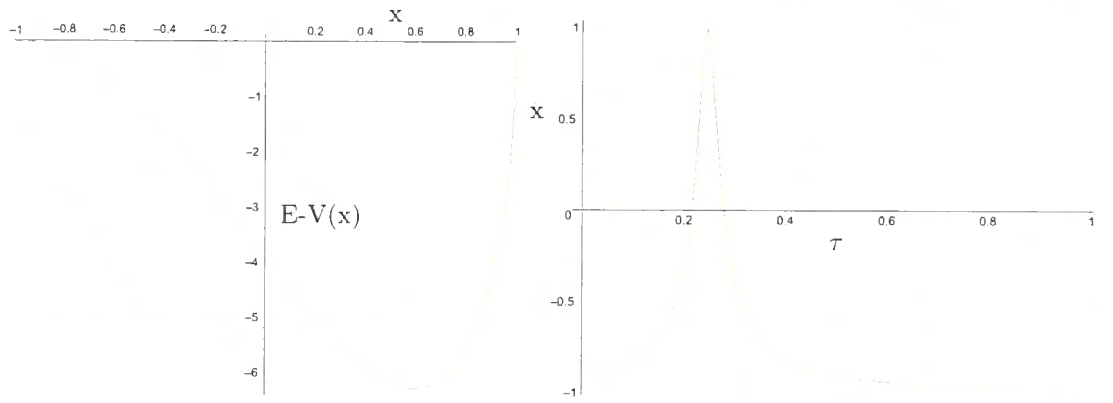

Figure 6.3: The plot on the left shows $E - V(x)$ for a timelike geodesic with $\ell = 0$, $\nu = 0.9$ and $R = 1$. The right hand plot shows the evolution of x with τ when the particles are started at $x_0 = -0.900$ with $E = 2$. The initial velocity is chosen so that $\dot{x} = 0.508$.

Figure 6.3 shows plots of $E - V(x)$ vs x and also x vs τ, where τ is the affine parameter, for a timelike geodesic with $\ell = 0$. The left hand plot is now dependent on the energy and gives a better indication of how the velocity of the test particle changes as it moves along the path, particularly at $x = +1$. The allowed region of motion is now given by the area under the x axis, so the plot indicates that the test particle will approach $x = 1$, pass through the origin, and then continue out to infinity at $x = -1$. This behaviour is confirmed by the numerical simulation shown in the right hand plot.

The numerical simulation has a discontinuity at $x = 1$ i.e. at the origin. This is a consequence of the coordinate system, since there is a singularity in the equations of motion at $x = 1$ and $y = -1$. Naively substituting $x = +1$ into (6.12) causes

some problems because the terms which have $G(x)^2$ in the denominator will blow up but, so long as $\ell = 0$, it can be shown that these terms are zero when transformed into polar coordinates. The fact that ℓ has to be zero for the particle to go through the origin is obvious when one considers that ℓ measures the angular momentum around the axis perpendicular to $y = -1$, so any point on this axis (including the origin) will automatically have zero angular momentum.

Unfortunately, at the origin, the transformations to polar coordinates become undefined, meaning that the previous analysis isn't valid and a further coordinate transformation is required. To analyse the behaviour of the geodesics at the origin it is necessary to transform to Cartesian coordinates, for which the transformations are given in Appendix C. These transformations show that for Cartesian coordinates, given by (z_0, z_1), $\dot{z}_0 \not\to 0$ when $\dot{x} \to 0$ at the origin. This means that the test particle is still moving, even though $\dot{x}$ appears to be zero, so the particle will pass through the origin and out into the other side of the ring. On the other side of the ring, the potential is exactly the same but the particle is moving in the opposite direction in the potential, so $\dot{x}$ becomes negative.

Rearranging (6.12) to give $\ddot{x}$ in terms of the other quantities and substituting $x = 1$, $y = -1$, $\ell = 0$, and $\dot{y} = 0$ leaves[3]

$$\ddot{x} = -\frac{(\nu+1)\dot{x}^2}{G(1)} + \frac{[(1+\lambda)+(1-\lambda)]\dot{x}^2}{4(1+\lambda)} \tag{6.33}$$

Transforming $\frac{\dot{x}^2}{G(x)}$ to Cartesian coordinates and taking the appropriate limit, gives

$$\frac{\dot{x}^2}{G(1)} = \lim_{z_0 \to 0}\left[\lim_{z_1 \to 0}\frac{\dot{x}^2}{G(x)}\right] = \frac{4\dot{z}_0^2}{R^2(1+\nu)} \tag{6.34}$$

The line $z_1 = 0$ corresponds to the rotational axis $y = -1$, where z_0 parameterises points along this line and $z_0 = z_1 = 0$ gives the origin. Transforming $\dot{x}$ into these coordinates and taking the limit as $z_1 \to 0$ gives

$$\lim_{z_1 \to 0}\dot{x} = -\frac{4R^2 z_0 \dot{z}_0}{(R^2 + {z_0}^2)^2} \tag{6.35}$$

[3]Although $\dot{y}$ is technically zero at the origin, the term in question is $\frac{\dot{y}^2}{G(y)}$, so slightly more care has to be taken. It is shown in Appendix C that choosing $\frac{\dot{y}^2}{G(y)} = 0$ is equivalent to ensuring that the particle remains on the rotational axis.

It is obvious from this expression that $\dot{x} \to 0$ as $z_0 \to 0$ but there is no requirement that $\dot{z}_0 \to 0$. This shows that even though $\dot{x} \to 0$, it doesn't necessarily mean that the test particle is at rest. The fact that $\dot{x} = 0$ when $x = 1$ is purely an artefact of the Black Ring's toroidal coordinate system.

Using (6.34) and (6.35) to express (6.33) in Cartesian coordinates gives

$$\ddot{x} = -\frac{4\dot{z}_0^2}{R^2} \tag{6.36}$$

where the second term in (6.33) goes to zero because $z_0 = 0$ at the origin. This shows explicitly that the point at the origin is just a coordinate singularity and that the test particle passes through it without anything out of the ordinary happening.

The centrifugal barrier exhibited in the potential plots of figure 6.1 shows that it is possible to have low energy geodesics that oscillate back and forth along the rotational axis. When the angular momentum ℓ is non-zero, the geodesics never reach the origin at $x = 1$, meaning that the particles will orbit in the x-ϕ plane, with the minimum and maximum distances away from the origin determined by the potential barriers on the right and left of the potential respectively. The ability of the geodesics to move in the ϕ direction means that the geodesics still pass through the centre of the ring but don't reach the origin. This is because the rotational axis $y = -1$ is actually a plane when the particles are allowed to move in the ϕ direction, thus allowing the particles to pass through the ring without going through the origin where $x = 1$.

Figure 6.4 gives an example of this motion when low energy particles are placed within the potential well. The minimum of the potential is at $x_{min} = -0.096$ and has value $E = 0.642$. The lower plot clearly exhibits periodic motion, but the period is dependent upon the amplitude. As the amplitude is increased the period is also increased. This is most easily seen by comparing the period of the green curve (with the largest amplitude) with that of the red one (with the smallest amplitude.) The top left hand plot indicates why this happens. The unsymmetrical shape of the potential is more marked further away from the minimum, so only the curves with the larger amplitude will show this effect.

The potential is steeper on the right hand side of the minimum potential line than it is on the left. This causes the maximum displacement to be greater to the left

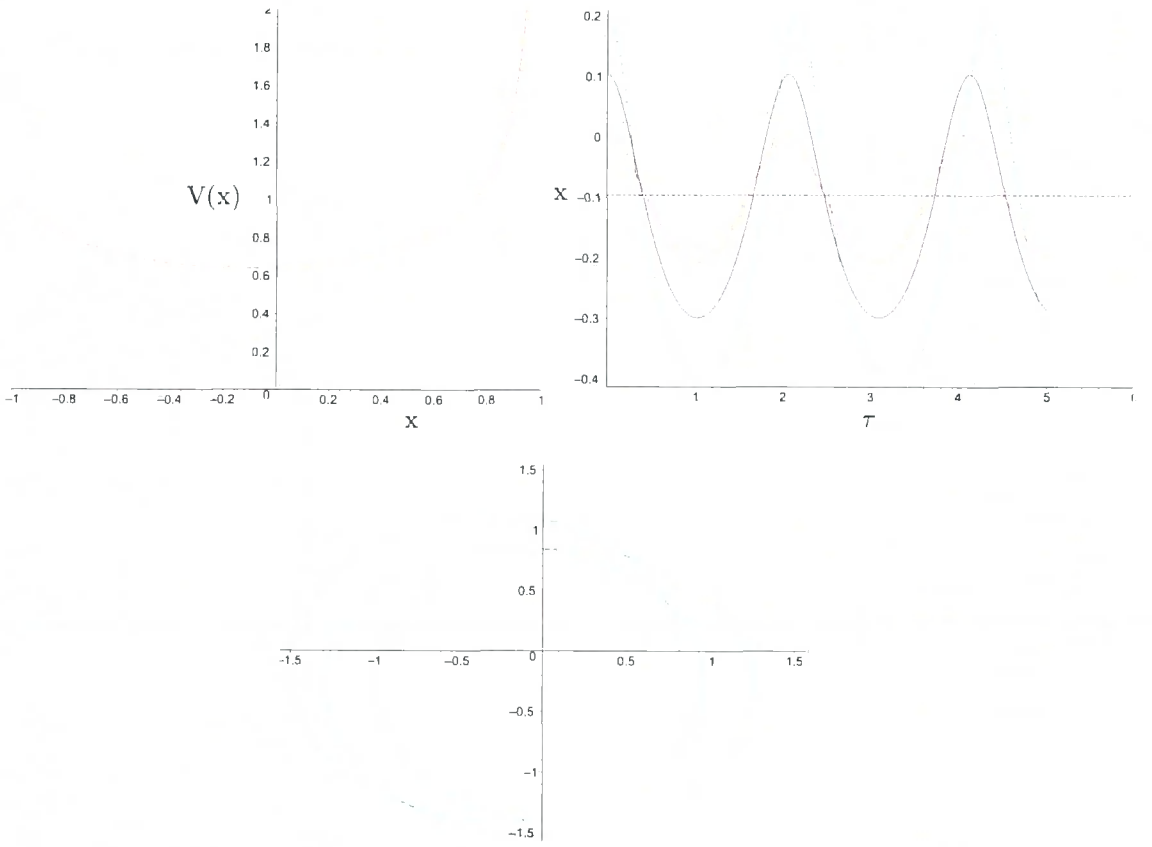

Figure 6.4: These plots show the motion of a massive particle when it is started at different distances away from the minimum. The initial conditions were set up so that $\nu = 0.8$, $\ell = 4$, and $R = 1$. The top left hand plot shows the potential for the timelike geodesics. The top right plot shows the motion of massive particles when started at 0.1, 0.2, and 0.3 away from the minimum of the potential in red, blue, and green respectively, with the dotted black line indicating the position of the minimum. The lower graph gives a specimen polar plot showing how the distance from the origin varies with ϕ. The initial conditions are the same as for the green curve in the middle plot and τ ranges from 0 to 5. In all cases $\dot{x} = 0$ and $\phi = 0$ initially.

than it is to the right, meaning that the particle spends longer on the left hand side of the minimum potential. This gives the x displacement plot a slightly "bottom-heavy" appearance, with the maximum displacement being greater for negative x. The effect is most apparent for small displacements from the minimum, with the maximum displacement becoming more equal as the initial displacement is increased.

When this is interpreted in terms of the physical motion of a test particle, it means that the particle orbits slowly when it is in the exterior of the ring and accelerates as it moves through the centre of the ring, before decelerating again on the other side. The acceleration is most marked when the geodesic passes close to the origin, so the particles with the highest energies will move very rapidly through the centre of the ring on a flat trajectory and those with lower energy will move through the ring on more of a curved orbit.

The polar plot on the top right hand side of figure 6.4 shows how the particle, corresponding to the green plot, moves in the x-ϕ plane, with the angle from the horizontal axis given by ϕ and the distance from the origin calculated using (4.12). This gives a clearer picture of the unsymmetric nature of the potential as each orbit is oblate with the trace precessing anti-clockwise after every revolution. If the trace is plotted over a longer time period then it does eventually return to its starting point. The polar plots corresponding to the red and blue curves (with smaller amplitudes) in the middle graph of figure 6.4 show qualitatively similar behaviour, but the precession of the orbits isn't as large, due to the potential becoming more asymmetric further away from the minimum point.

Figure 6.5 gives a sample of the behaviour of a timelike geodesic when the angular momentum is large. In this case the potential is repulsive for all values of x, so a particle initially at rest will head off to infinity. If the initial velocity is increased then the particle can pass through the ring, with the minimum approach to the origin dependent on the energy of the particle. The particle will then go off to infinity on the other side of the ring.

The second plot in figure 6.5 shows how x varies with ϕ i.e. the path of the test particle in the x-ϕ plane. In this case $\frac{\mathrm{d}\phi}{\mathrm{d}\tau}$ is given by

$$\frac{\mathrm{d}\phi}{\mathrm{d}\tau} = \frac{\ell(1+x)}{R^2(1-x)(1+\nu x)} \tag{6.37}$$

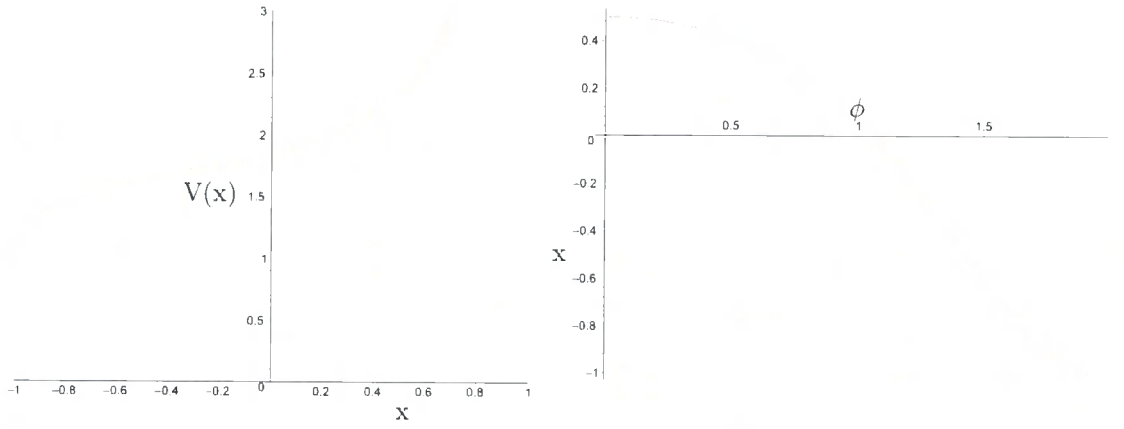

Figure 6.5: The left hand plot shows the potential for $\ell = 4$, $\nu = \frac{1}{2}$, and $R = 1$. The right hand plot shows the motion of the timelike particle when it is started from rest at $x = 0.5$ and $\phi = 0$.

This shows that ϕ initially varies rapidly, when the particle is close to the origin, and then asymptotically approaches a constant as $x \to -1$. This is reflected in the right hand plot of figure 6.5, where the curve levels off at $\phi \approx 2$. Physically $\frac{\mathrm{d}\phi}{\mathrm{d}\tau} \to 0$ because the particle is approaching infinity and thus travels further and further for each interval in ϕ.

6.2.2 Null Geodesics on the Rotational Axis

The potential for null geodesics is shown in figure 6.6, with the variation of the potential for different values of ν plotted for permissible values of x. These graphs show most of the properties of the null geodesics, principally:

- geodesics of low angular momentum have a closer minimum approach to the origin.
- there is an infinite centrifugal barrier at $x = 1$.
- only geodesics with $\ell = 0$ are able to pass through the origin.
- the potential for geodesics with large ℓ is repulsive for all x.
- the potential can have a local maximum near $x = -1$ for large values of ν.

The variation of the potential with ν and x is shown in figure 6.7 for null geodesics. In this case the angular momentum (and indeed R) is purely a scale factor,

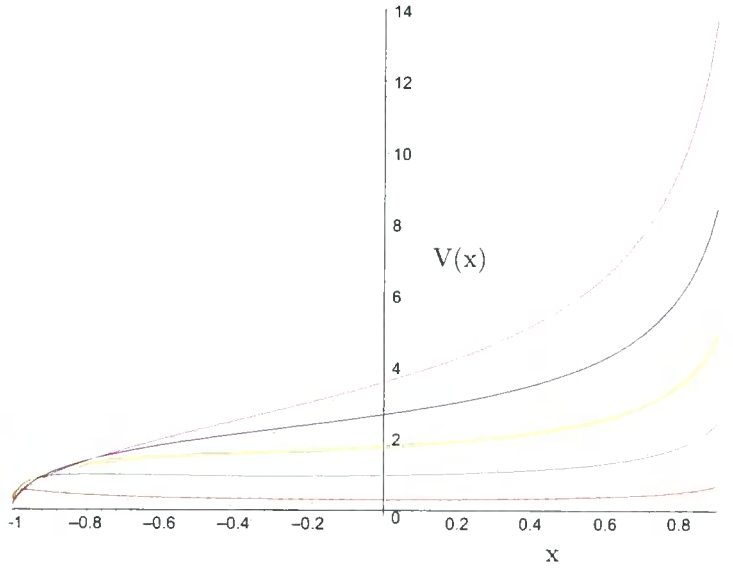

Figure 6.6: This plot shows how the effective potential for null geodesics varies for $\nu = 0.1, 0.3, 0.5, 0.7, 0.9$, when $\ell = 4$. The lowest curve corresponds to $\nu = 0.9$ and ν decreases with each consecutive curve. $R = 1$ in both plots.

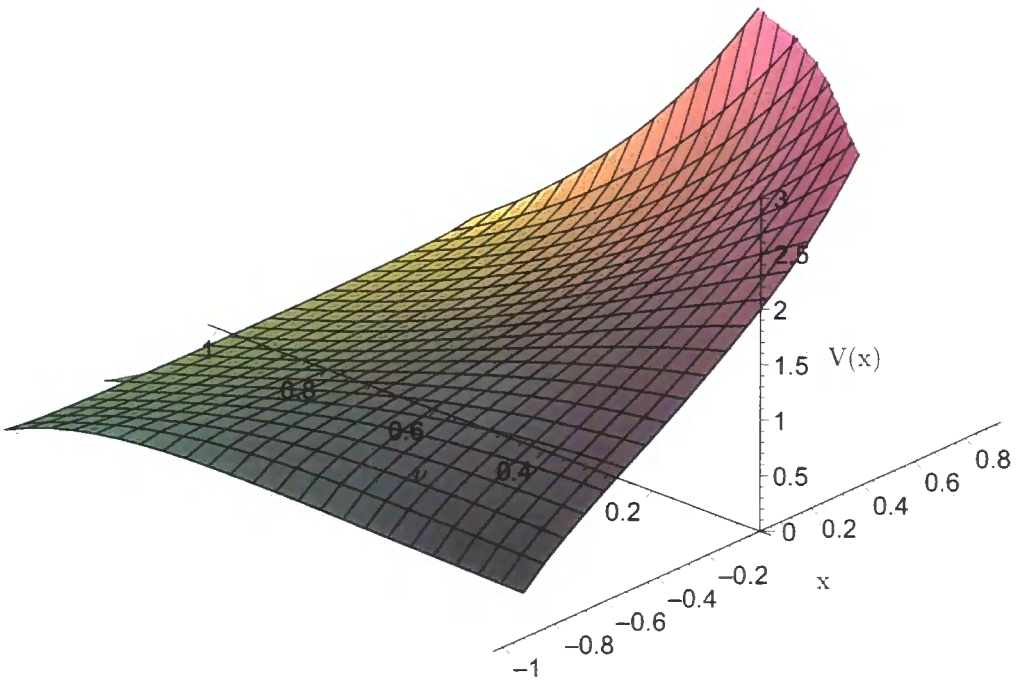

Figure 6.7: 3D plot showing how the effective potential for a null geodesic varies with ν and x. In this plot $\ell = 4$ and $R = 1$.

as can be seen by substituting $\epsilon = 0$ into (6.23), so the plot shown in figure 6.7 gives the variation of the potential with ν rather than ℓ. This potential shares many of the same traits as that of the timelike geodesics, even exhibiting a local maximum near $x = -1$, as can be seen in figure 6.7 when ν is large. The surface near $x = -1$ and $\nu \approx 1$ is where the difference between the local maximum and minimum is most pronounced, but the width of the peak is the smallest, so it isn't very visible in figure 6.7. The maximum height of the peak is when $\nu = 0.653$, which explains why it appears more marked at this point on the 3D plot.

For the null geodesics, ℓ and E have no independent meaning, since the test particles on null geodesics are massless, so it is only the ratio $\frac{\ell}{E}$ that is important. This is the reason why only one potential plot is given in figure 6.6. When $\ell = 0$ the potential for the null geodesics is identically zero, so the null particles move as if in flat space when they go directly through the centre of the ring.

For the null geodesics, ℓ has no bearing on whether the maximum exists (unless of course $\ell = 0$), so the lower limit on ν for a potential barrier to exist, is given by the solution to

$$\nu_-^4 - 26\nu_-^3 + 36\nu_-^2 - 54\nu_- + 27 = 0 \tag{6.38}$$

This has four solutions but $0 \leq \nu \leq 1$ for the equilibrium ring, so the only pertinent solution is given by $\nu_- = 0.653$. Values of ν less than ν_- will give potentials with no potential barrier, like the upper curves in the right hand plot of figure 6.6. For values of ν greater than ν_- there will always be a local maximum, with the position of the peak given by the solution to (6.24).

If $\ell = 0$ then the null geodesics pass through the origin of the ring with the motion being almost identical to that of the timelike geodesic shown in figure 6.3. The major difference between the null and timelike geodesics, in this case, is that the null geodesics can't oscillate back and forth through the ring as the low energy timelike geodesics do. These null geodesics, in the toroidal coordinates, have the same problem at the origin as the timelike geodesics but the coordinate singularity is resolved in a similar manner.

Physically, null geodesics with large E relative to ℓ behave in a similar manner to the timelike geodesics with large E. When the timelike geodesics have large energy

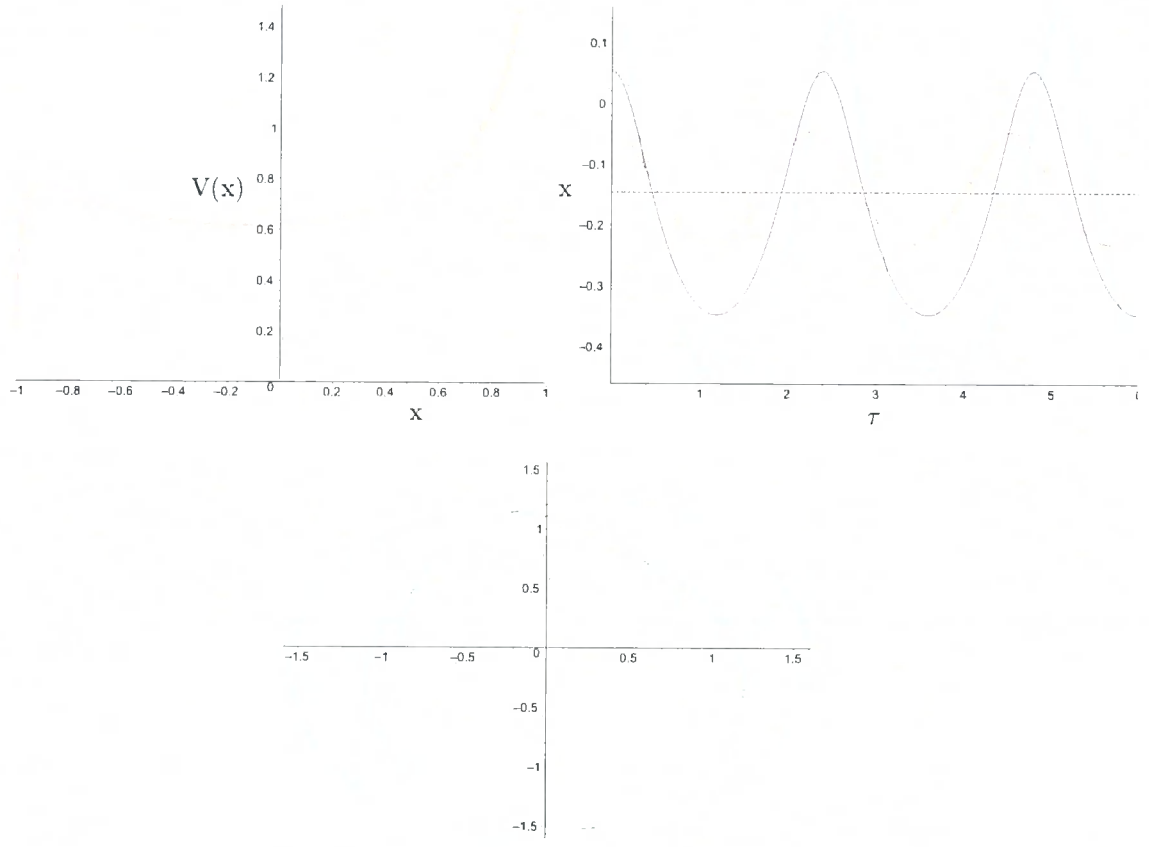

Figure 6.8: These plots show the motion of a null particle when it is started at different distances away from the minimum. The initial conditions were set up so that $\nu = 0.8$, $\ell = 4$, and $R = 1$. The left hand plot shows the potential for the null geodesics. The middle plot shows the motion of null particles when started at 0.1, 0.2, and 0.3 away from the minimum of the potential in red, blue, and green respectively, with the dotted black line indicating the position of the minimum. The right hand graph gives a specimen polar plot showing how the distance from the origin varies with ϕ. The initial conditions are the same as for the green curve in the middle plot and τ ranges from 0 to 6. In all cases $\dot{x} = 0$ and $\phi = 0$ initially.

the difference between the null and timelike potentials is largely irrelevant, so high energy massive particles and the corresponding massless particles aren't affected by the black ring at large distances. As these particles approach the centre of the ring at $x = 1$, the centrifugal barrier comes into play, meaning that the distance of closest approach increases with ℓ, as per spherical black holes.

If the null geodesics have small E relative to ℓ and $\nu > 0.653$, then the curvature of the space allows for the null geodesics to be captured. In this case there are two orbits at a constant distance from the ring. These are found by solving (6.24), the largest solution giving the position of the stable orbit and the next largest giving the position of the unstable orbit i.e. at the local maximum of the potential.

The local minimum in the potential for $\nu > 0.653$ means that it is also possible to have null geodesics that oscillate through the ring. The plots of the potential and some examples of test particle motion are given in figure 6.8. The motion in this case is similar to the timelike case but the potential is less symmetrical, so the differences in the period of the motion are more pronounced. The period of the oscillations is also longer for the null geodesics than for their timelike counterparts.

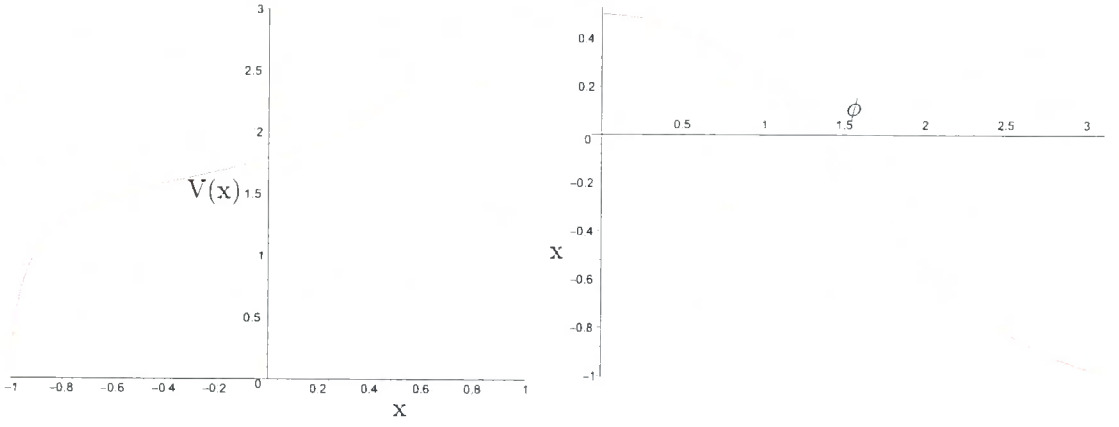

Figure 6.9: The left hand plot shows the potential for $\ell = 4$, $\nu = \frac{1}{2}$, and $R = 1$. The right hand plot shows the motion of the null particle when it is started at $x = 0.5$ and $\phi = 0$, with $\dot{x} = 0$ initially.

As ℓ is increased the potential well is gradually smoothed out until the potential is always repulsive and takes the form given in figure 6.9. The plot shown in this figure shows the path of the null geodesic when it is moving away from the centre of the ring. The null particles in this potential behave in a similar way to the massive

particles shown in figure 6.5 but the null particles approach $x = -1$ in a much shorter time. The null geodesics can pass through the centre of the ring but, as in the $\ell = 0$ case they will then continue off to infinity.

6.3 Planar Circular Geodesics

To find circular orbits in the Black Ring metric it is necessary to solve the equations of motion so that x and y are constant for all of the motion and thus form an orbit by rotating in the ψ and ϕ directions. In practice, this means solving (6.12) and (6.13) so that $\ddot{x} = \ddot{y} = 0$. In general (6.12) and (6.13) are dependent on $\dot{x}$, $\dot{y}$, x, and y, so finding initial values for these variables that solve $\ddot{y} = 0$ from (6.13) won't guarantee that $\ddot{x} = 0$ when they are substituted in (6.12). If $\ddot{x} \neq 0$ then this will cause $\dot{x}$ to vary, which will in turn cause $\ddot{y}$ to vary. This means that both equations have to be solved simultaneously to find values of x and y that will give $\ddot{y} = \ddot{x} = 0$ when $\dot{x} = \dot{y} = 0$ but attempting to do this in general leads to intractable expressions that are of very high order.

The simplest way to avoid this problem is to look for values of x which give $\ddot{x} = 0$ when $\dot{y} = \dot{x} = 0$ for all values of y, thus negating the need to consider both of the geodesic equations simultaneously, and allowing the circular orbits to be found by solving (6.13) when $\ddot{y} = \dot{y} = 0$. It turns out that the only way to achieve this is to set $x = \pm 1$, therefore ensuring that $\ddot{x} = \dot{x} = 0$, no matter what happens to y. This choice of $x = \pm 1$ confines the geodesics to the plane perpendicular to the axis of rotation and also forces ℓ to be zero, since the geodesics can't simultaneously remain on this plane and have angular momentum with respect to it. This equatorial plane is split into two sections with $x = -1$ being the region "outside" of the ring and $x = +1$ being the region "inside" the ring.

The constraints discussed above are equivalent to demanding that the test particle be at a stationary point on the effective potential, with $\ddot{x} = 0$. The effective potentials for particles on the inner and outer equatorial planes are given in figure 6.10, with the derivation of the effective potentials given in Appendix D. The potentials plotted in figure 6.10 are in terms of a transformed coordinate z, which can

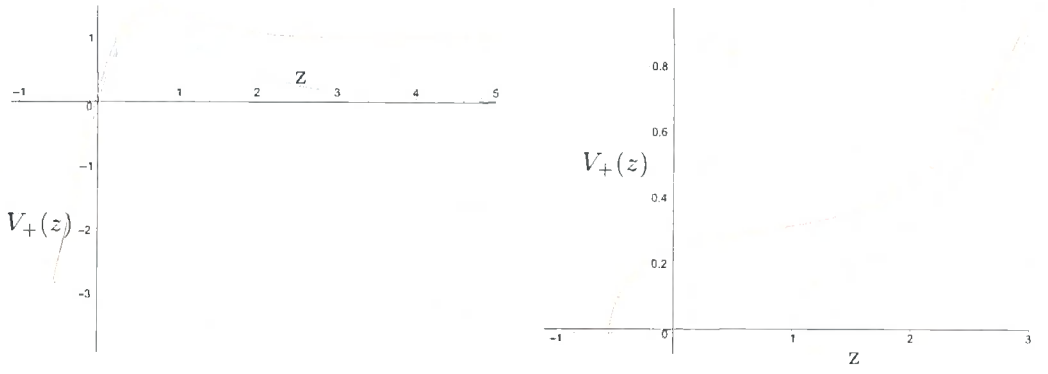

Figure 6.10: These plots show some sample effective potentials $V_+(z)$ for red timelike and green null geodesics that are constrained to the equatorial plane. The left hand plot is the potential for the outer equatorial plane given by $x = -1$, when $\Psi = 7$. The right hand plot is for the inner plane given by $x = +1$, when $\Psi = 0.1$. Both plots are for $\nu = \frac{1}{2}$, and $R = 1$.

be expressed in terms of y using

$$z = -\tanh^{-1}\left(\frac{1+\lambda y}{y+\lambda}\right) \tag{6.39}$$

This coordinate transformation is used to avoid the singularity caused when $y \to -\frac{1}{\lambda}$ i.e. the ergosurface, due to the $F(y)$ terms in the denominator of (6.16). In terms of z, the ergosurface is at $z = 0$, with $z = \infty$ corresponding to asymptotic infinity when $x = -1$ or the rotational axis when $x = 1$. The event horizon is at $z = \tanh^{-1}\frac{\lambda-\nu}{\lambda\nu-1}$ and the curvature singularity is then reached at $z = -\tanh^{-1}\lambda$. Thus the range of z is given by

$$-\tanh^{-1}\lambda \leq z \leq \infty \tag{6.40}$$

The example effective potentials shown in figure 6.10 plot $V_+(z)$ for the inner and outer equatorial planes, and are roughly indicative of all of the effective potentials. Varying the angular momentum for the $x = -1$ potential increases or decreases the height of the centrifugal barrier, as one would expect. In this case, the only circular orbits will be at the peak of the potential, and thus will be unstable. If the angular momentum, given by Ψ, is decreased to zero then the centrifugal barrier disappears and the timelike potential is strictly decreasing as $z \to -\tanh^{-1}\lambda$, whilst the null potential is identically zero for all values of z. This indicates that circular orbits can only exist when $\Psi \neq 0$.

The sample plot for the $x = +1$ potential allows one to immediately deduce that the black ring won't support circular orbits in the inner equatorial plane. When $\Psi \neq 0$ both the null and timelike potentials increase with increasing z and have a centrifugal barrier at $z = \infty$ i.e. as they approach the axis of rotation $y = -1$. When $\Psi = 0$ the centrifugal barrier disappears, allowing both null and timelike geodesics to reach $z = \infty$ and thus go through the origin. In this case the null potential is everywhere zero and the timelike potential levels off at $V_+(z) = \frac{1}{3}$. As the angular momentum is increased the centrifugal barrier dominates both the timelike and null potentials, with the two potential curves converging rapidly as z increases. This has the effect of making the null and timelike potentials look identical for large Ψ.

When Ψ is negative, both the potentials for the inner and outer equatorial planes are qualitatively similar to those given in figure 6.10. The major difference is for the potential of the outer equatorial plane, where the centrifugal barrier moves from being outside the ergosurface to being between the ergosurface and the event horizon. This is due to the frame dragging effect, whereby an incoming particle can make a closer approach to the event horizon if it is moving in the opposite direction to the rotation of the black hole.

Having chosen the values of x and $\dot{x}$ such that the geodesics are confined to the plane, it is necessary to choose values of y that ensure that $\dot{y} = 0$ and $\ddot{y} = 0$ i.e. the particle has to be on the peak of the centrifugal barrier. This ensures that the orbits will close up after each rotation. To find the values of y that solve $\dot{y} = 0$ it is sufficient to consider the first integral equation given by (6.16). Substituting $\ell = 0$, $x = \pm 1$ and $\dot{x} = 0$ into this equation simplifies it substantially. After rearranging to isolate $\dot{y}$ and solving for $\dot{y} = 0$, the equation becomes

$$\frac{E^2(1 \pm \lambda)G(y_0)}{F(y_0)} + \frac{(\pm 1 - y_0)^2 \left[RE(1 + y_0)C + \Psi F(y_0)\right]^2}{(1 \pm \lambda)F(y_0)R^2} + \epsilon G(y_0) = 0 \qquad (6.41)$$

Solving this equation for y_0 gives values of y_0 that are on the effective potential line when $x = \pm 1$. Equation (6.41) is a cubic in y_0 due to the $G(y_0)$ coefficients, but for $x = \pm 1$ a factor of $(y \mp 1)$ can be removed. This reduces the equation to a quadratic making it much easier to analyse. Unfortunately, the coefficients of y are very complicated, so it is easiest to choose particular values for the conserved quantities and then solve the equation.

To find the values of y for which the particle is at a turning point in the potential, it is necessary to simultaneously solve (6.13) for $\ddot{y} = \dot{y} = \dot{x} = \ell = 0$. Substituting in $x = \pm 1$ leaves

$$\frac{(\pm 1 - y_0)^2 \left[RE(1+y_0)C + \Psi F(y_0)\right]^2}{2R^2(1 \pm \lambda)G(y_0)} \left[\frac{\lambda(\pm 1 - y_0) - 2F(y_0)}{(\pm 1 - y_0)} - \frac{F(y_0)G'(y_0)}{G(y_0)}\right]$$
$$\frac{E(\pm 1 - y_0)^2 C(1-\lambda)\left[RE(1+y_0)C + \Psi F(y_0)\right]}{R(1 \pm \lambda)G(y_0)} - \frac{E^2\lambda(1 \pm \lambda)}{2} = 0 \qquad (6.42)$$

This is a quartic equation in y but, once again, it is possible to factor out $F(y_0)^2$, leaving a quadratic in y. Expanding the functions in (6.42) and re-writing in fully factored form gives

$$\frac{(1+\lambda y_0)^2(1-\nu)(\alpha_\pm y_0^2 + \beta_\pm y_0 + \gamma_\pm)}{2R^2(1+\nu^2)^2(\lambda - 1)(1+\nu y_0)^2(1 \pm y_0)^2(\pm 1 + \lambda)} = 0 \qquad (6.43)$$

where

$$\begin{aligned}
\alpha_+ &= 2\nu(1+\nu)^3R^2E^2 - 2\nu(1+\nu)^2\sqrt{2(1-\nu^2)}R\Psi E \\
&\quad +\nu\Psi^2(\nu-1)(\nu^2 - 4\nu - 1) && (6.44)\\
\alpha_- &= 2\nu(7\nu^3 + \nu^2 + \nu - 1)R^2E^2 - 2\nu(1+\nu)(3\nu-1)\sqrt{2(1-\nu^2)}R\Psi E - \\
&\quad \nu\Psi^2(\nu-1)(\nu^2 + 4\nu - 1) && (6.45)\\
\beta_+ &= 4\nu(1+\nu)^3R^2E^2 - 4\nu(1+\nu)^2\sqrt{2(1-\nu^2)}R\Psi E \\
&\quad -2\nu\Psi^2(\nu-1)(\nu^2+3) && (6.46)\\
\beta_- &= 4\nu(\nu^3 + 7\nu^2 - \nu + 1)R^2E^2 - 4\nu(1+\nu)^2\sqrt{2(1-\nu^2)}R\Psi E \\
&\quad -2\nu\Psi^2(\nu-1)(\nu^2+3) && (6.47)\\
\gamma_+ &= 2\nu(1+\nu)^3R^2E^2 - 2\nu(1+\nu)^2\sqrt{2(1-\nu^2)}R\Psi E \\
&\quad -\Psi^2(\nu-1)(\nu^3 + 2\nu^2 - \nu + 2) && (6.48)\\
\gamma_- &= 2\nu(-\nu^3 + \nu^2 + 9\nu - 1)R^2E^2 - 2\nu(1+\nu)(3-\nu)\sqrt{2(1-\nu^2)}R\Psi E + \\
&\quad \Psi^2(\nu-1)(\nu^3 - 2\nu^2 - \nu - 2) && (6.49)
\end{aligned}$$

It is obvious from (6.43) that $y_0 = -\frac{1}{\lambda}$ is always going to be a solution to this equation, so the roots of the quadratic part will give the non-trivial solutions to (6.42). The roots are given by

$$y_0 = \frac{-\beta_\pm \pm \sqrt{{\beta_\pm}^2 - 4\alpha_\pm\gamma_\pm}}{2\alpha_\pm} \qquad (6.50)$$

At this point it is worth checking that these roots can become real for $x = 1$ and $x = -1$ because the imaginary results are unphysical. The condition for the roots to be real is given by

$$\beta_{\pm}{}^2 - 4\alpha_{\pm}\gamma_{\pm} \geq 0 \tag{6.51}$$

For $R = 1$ and $x = +1$ this becomes

$$-8\Psi^2\nu(1+\nu)^2(\nu-1)^4\left[2(1+\nu)E^2 - 2\Psi\sqrt{2(1-\nu^2)}E + \Psi^2(1-\nu)\right] \geq 0 \tag{6.52}$$

The factor in front of the square brackets is always negative so, apart from the trivial solutions at $\nu = \pm 1$ and $\Psi = 0$, there can only be real solutions when the term in the square brackets is negative. The coefficient of the E^2 term is always positive, so the term will become negative for values of E between the two roots. Solving for E gives a repeated root at

$$E_{\pm} = \frac{\Psi\sqrt{2(1-\nu^2)}}{2(1+\nu)} \tag{6.53}$$

This means that the term in the square brackets will never become negative and thus there will only ever be a single real solution to (6.43) for y. Substituting $E_{\pm}$ into the quadratic part of (6.43) gives

$$2(\nu-1)^2(1+\nu y)^2\Psi^2 = 0 \tag{6.54}$$

which has only one solution at $y = -\frac{1}{\nu}$ i.e. on the event horizon. Equation (6.41) can only be satisfied for null geodesics at this point, so it is a trivial solution. The solution where $\Psi = 0$ is equally trivial because (6.43) then reduces to

$$2E^2\nu(1+\nu)^3(1+y)^3 = 0 \tag{6.55}$$

This only has a solution at $y = -1$, which corresponds to asymptotic infinity. Therefore there are no non-trivial solutions for geodesics inside the ring at $x = +1$. This is in agreement with the conclusions drawn from the potential plot given in figure 6.10.

When $x = -1$, (6.51) is quartic in E and thus has real solutions for various values of E, Ψ, and ν. These solutions are explored for timelike and null geodesics in the following two sub-sections.

6.3.1 Circular Orbits for Timelike Geodesics

For timelike geodesics, one of the non-trivial solutions to (6.42) has to be discounted because it is always less than $y = -\frac{1}{\nu}$, meaning that this solution is always inside the event horizon for all values of ν, E, and Ψ. Geodesics starting at this point can't form circular orbits because they are compelled to move toward the curvature singularity by virtue of the ∂_t Killing vector being spacelike. This leaves two possible solutions to (6.42) and (6.41) respectively.

After discounting the invalid solution curves, the circular orbits are given by the points where the solution curve for (6.41) intersects with that of (6.42). This is equivalent to finding a point where both $\dot{y}$ and $\ddot{y}$ are zero. Figure 6.11 shows how these solution curves vary with ν for some specific values of E and Ψ.

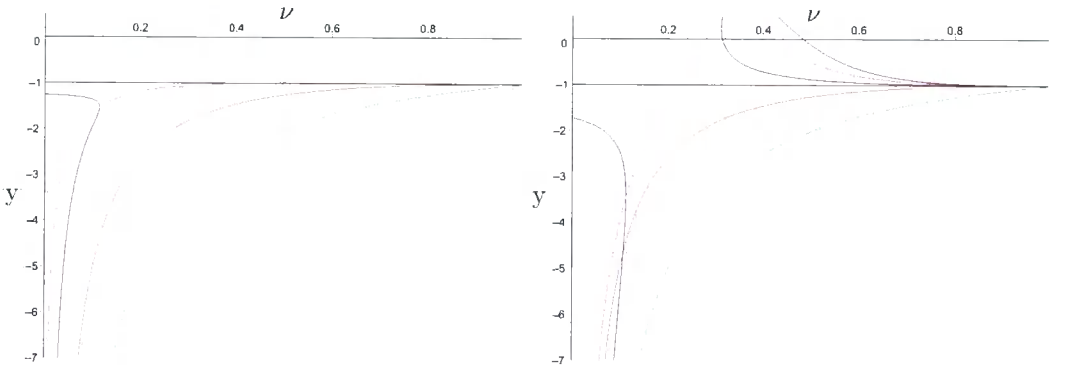

Figure 6.11: These plots show the solution curves for the outer equatorial plane when $\ddot{y} = 0$ in purple and red and those when $\dot{y} = 0$ in blue. In this instance the red line also indicates the ergosurface, since this is also a solution to (6.42). The green line gives the position of the event horizon at $-\frac{1}{\nu}$ and the black line shows asymptotic infinity at $y = -1$. The left hand plot is for $\Psi = 2.00$ and the right hand plot is for $\Psi = -1.29$. Both these plots use $E = 1.20$.

The plots shown in figure 6.11 show that the blue curve, where $\dot{y} = 0$, intersects the purple curve, where $\ddot{y} = 0$, at $\nu = 0.11385$. The values of Ψ were chosen specifically so that the value of ν where the curves intersect is the same for both of the plots. The purple curve corresponds to the non-trivial solution to (6.42), so the particular set of values used for this plot will form a circular orbit at $y = -1.52508$. The left hand plot indicates that there will only be one circular orbit when $\Psi > 0$ but when Ψ is negative, i.e. when the particle is moving in the opposite direction to the

rotation of the ring, there can be two solutions, as indicated in the right hand plot. These solution are represented by the points where the blue curve intersects the purple and red curves. The blue and red curves can only intersect when the particle is rotating counter to the ring because the red curve represents the ergosurface, and at this point a circular orbit can only be formed if the particle is moving against the rotation of the ring, otherwise the frame dragging effect causes the particle to rotate too quickly.

In general, the point where the blue curve intersects the purple curve will always be at the turning point in the blue line. This point is where both of the roots of (6.41) converge. This can be understood by considering the plot shown in figure 6.12. In this plot the points where the curves cross the horizontal axis is where $\dot{y} = 0$ and the turning points of the curves are where $\ddot{y} = 0$. In order for $\ddot{y} = \dot{y} = 0$ for the same value of y, the turning point has to be where the curve intersects the horizontal axis i.e. the curve must have a repeated root. The plot in figure 6.12 gives some example curves for different values of ν either side of the critical value. It verifies that there is a curve with a double root between 0.1125 and 0.1250, since the blue curve has it's turning point just above the axis and the yellow curve doesn't quite reach the axis. This agrees with the value of ν indicated by the intersection of the two curves shown in figure 6.11.

Armed with this knowledge, the point where the curves intersect can be calculated by solely considering equation (6.41). Once the trivial solution at $y = -1$ is factored out the remaining equation is a quadratic, so the double root will be where

$$\begin{aligned}&(\nu-1)^2\Psi^4 + 2R^2(\nu-1)[(E^2+\epsilon)(3\nu^2+4\nu+1)+4\nu E^2]\Psi^2 \\ &+16R^3E\nu\sqrt{2(1-\nu^2)}(E^2+\epsilon)(1+\nu)\Psi + R^4\left[E^4(\nu^4-24\nu^3-18\nu^2-8\nu+1)\right. \\ &\left.+2\epsilon(1+\nu)(\nu^3-13\nu^2-5\nu+1)E^2+\epsilon^2(1-\nu^2)^2\right] = 0 \end{aligned} \tag{6.56}$$

This is a quartic in Ψ so will technically have four solutions, but only the largest and smallest roots are pertinent since the intermediate solutions are always for positive values of y. Solving this for Ψ in terms of E and ν, when $\epsilon = -1$ gives

$$\Psi = \pm\frac{R}{\sqrt{1-\nu}}\left(2E\sqrt{\nu} + \sqrt{(E^2-1)\left(3\nu+1\pm 2\sqrt{2}\sqrt{\nu(1+\nu)}\right)(1+\nu)}\right) \tag{6.57}$$

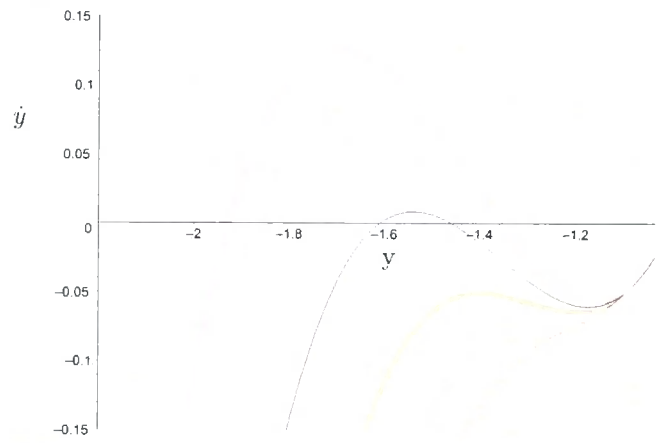

Figure 6.12: This graph plots $\dot{y}$ against y for values of ν from 0.1, for the uppermost curve, to 0.15 for the lowest curve, in 0.0125 increments. All the curves are plotted for $E = 1.2$ and $\Psi = 2$, so that they correspond to the left hand plot of figure 6.11. It indicates how the point where the curves cross in figure 6.11 is where (6.41) has a double root. A similar plot is formed if the corresponding negative value of Ψ is used.

This equation shows how the angular momentum has to be varied for different ring geometries (different values of ν) and different particle energies (given by E). The two solutions for Ψ represent the circular orbits when the particle is rotating with and against the motion of the ring respectively. The positive Ψ solution will always be outside the ergosurface but for larger ν the negative Ψ solution can give a circular orbit within the ergosurface.

In figure 6.11, the red curve represents the ergosurface, given by $y_0 = -\frac{1}{\lambda} = -\frac{(1+\nu^2)}{2\nu}$. When the blue line intersects this line the circular orbit is on the ergosurface. This circular orbit will always exist for all values of E and ν, unlike the solution given by (6.57), which is complex for $E < 1$.

To find the value of Ψ for which the circular orbit exists, substitute $y = -\frac{1}{\lambda}$ into (6.41) for $\epsilon = -1$ and $x = -1$. This allows Ψ to be expressed in terms of E and ν as

$$\Psi = \frac{R\left[\nu^2(1-E^2) + 2\nu(1-4E^2) + 1 - 3E^2\right]}{2E\sqrt{2(1-\nu^2)}} \tag{6.58}$$

Figure 6.13 gives some examples of the permissible values of Ψ, the angular momentum about the rotational axis of the ring, as ν varies for a range of different energies. In general $|\Psi|$ increases with the energy and also with ν. The sign of Ψ

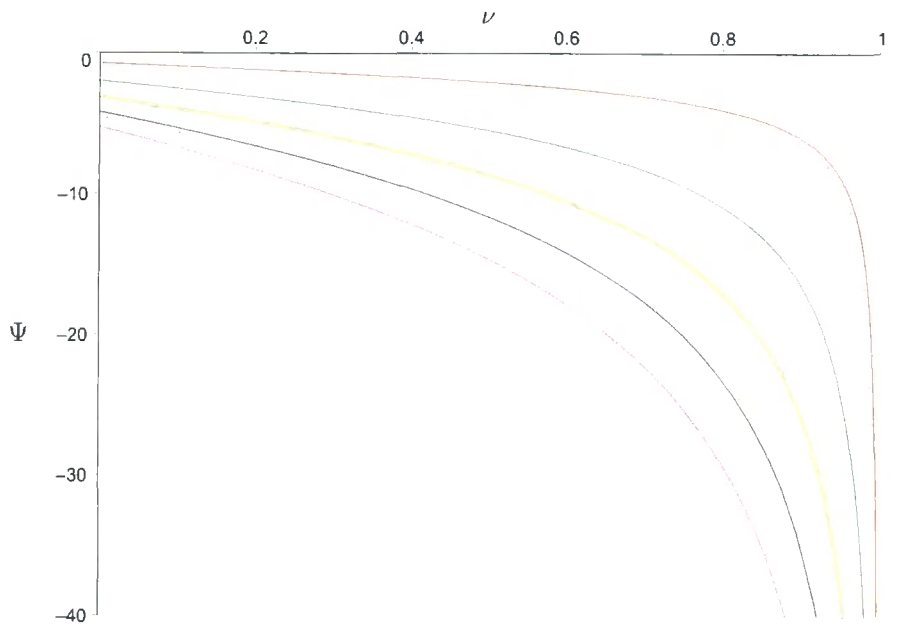

Figure 6.13: This graph shows how Ψ varies with ν to produce circular orbits on the ergosurface. The value of Ψ has been plotted for 5 different energies ranging from $E = 1$ to $E = 5$. The graph shows that the circular orbits of fatter rings, given by larger values of ν, have to have higher angular momentum in order to produce a circular orbit.

remains constant as ν is varied, so the trace shown in figure 6.13 will never cross the axis. This confirms that the particle's angular momentum has to always be in the opposite direction to the rotation of the ring for circular orbits on the ergosurface.

6.3.2 Circular Orbits for Null Geodesics

The analysis of null geodesics is similar to the timelike case. The solutions to (6.41) and (6.42) still give four valid solution curves, two from each equation respectively, with one of the non-trivial solutions to (6.42) giving unphysical positive y solutions. Figure 6.14 shows the equivalent plots to figure 6.11 for the null geodesics.

In this figure it is immediately obvious where the curves intersect and thus the points where $\ddot{y} = \dot{y} = 0$ for the null geodesics. The values of E and Ψ for these plots have been chosen so that the circular orbits exist for the black rings with $\nu = 0.11385$, as in figure 6.11. This makes it easy to compare the position of the circular orbits for the null geodesics with the timelike ones. The main difference between the two figures is encapsulated by the blue curves in the various plots. The

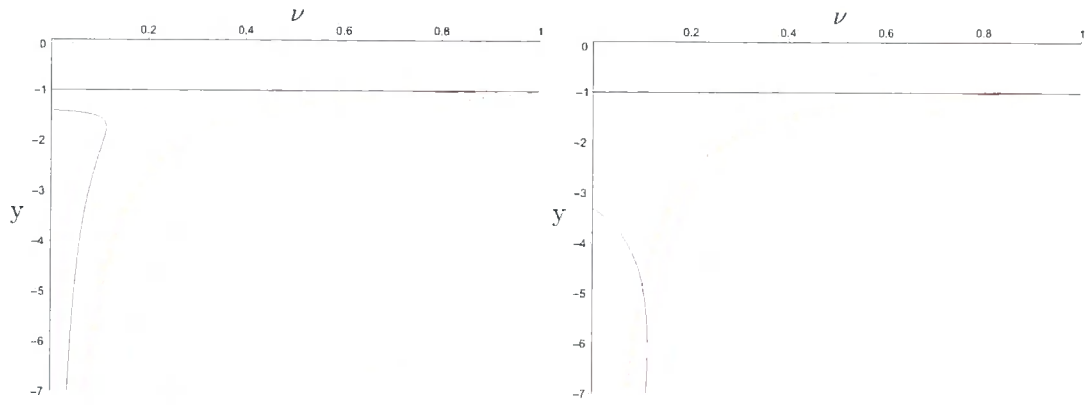

Figure 6.14: In both the left and right hand graphs, the red and purple lines represent the solution curves for $\ddot{y} = 0$ and the blue lines represent the solution curves for $\dot{y} = 0$. The points where circular orbits exist are given by the points of intersection of these lines. The green line gives the position of the event horizon and the black line shows asymptotic infinity at $y = -1$. The left hand plot has $\Psi = 2.92$ and the right hand plot has $\Psi = -1.64$. The constants in both plots have been set to $R = 1$ and $E = 1.20$.

red and purple curves are identical in general for null and timelike geodesics because they represent the second order geodesic equations. The reason that the red and purple lines are slightly different between figures 6.11 and 6.14 is because the two figures use different values for Ψ, which does affect the second order equations and thus their solution curves.

Figure 6.14 shows that the null circular orbits, that are off the ergosurface, are closer to the curvature singularity (at $y = -\infty$) than the respective timelike orbits, as one might expect. The difference is particularly pronounced for the negative angular momentum plots, shown on the right of figures 6.11 and 6.14, where the circular orbit is outside the ergosurface for the timelike geodesics but inside for the null case. For any particular shape of black ring, given by fixing the value of ν, the null circular orbits will always be closer to the curvature singularity of the ring than the respective timelike orbits.

The derivation for the relationship between the various conserved quantities is similar to that given for the timelike geodesics. For the null circular orbits, the critical value of Ψ that allows the geodesics to form a circular orbit, is found by substituting $\epsilon = 0$ into (6.56) and solving for Ψ. To calculate the position of the circular orbit it is then necessary to substitute this value of Ψ into either (6.41) or

(6.42) and then solve for y. Solving (6.56) for null geodesics gives

$$\Psi = \pm\frac{RE}{\sqrt{1-\nu}}\left(2\sqrt{\nu}+\sqrt{\left(3\nu+1\pm 2\sqrt{2}\sqrt{\nu(1+\nu)}\right)(1+\nu)}\right) \tag{6.59}$$

As in the analysis of the timelike case, the intermediate roots have been discarded as they are non-physical. The two remaining solutions represent the circular orbits when the null geodesic is orbiting with and against the direction of rotation of the ring respectively. The positive Ψ solution is always outside the ergosurface because of the frame dragging effect caused by the rotation of the ring. The negative solution can be either inside or outside the ergosurface, depending on the magnitude of Ψ.

The other null circular orbit is found where the blue curve in figure 6.14 intersects the red $y = -\frac{1}{\lambda}$ curve. This is easily calculated by substituting $y = -\frac{1}{\nu}$ into (6.41) and then solving for Ψ in terms of E and ν. Doing this gives

$$\Psi = -\frac{ER(\nu^2+8\nu+3)}{2\sqrt{2(1-\nu^2)}} \tag{6.60}$$

thus allowing the position of the second circular orbit to be calculated as above.

As for the timelike geodesics, there will always be a null circular orbit on the ergosurface but unlike the timelike circular orbits, there will always be a second solution with angular momentum given by (6.59). This means that for null geodesics on circular orbits there will always be two possible circular orbits for particular values of E and ν. For the timelike case there will sometimes only be one solution for particular values of E and ν, specifically when $E < 1$.

There is one specific instance where the null geodesics can only form one circular orbit for given values of E and ν. This is when the values of (6.60) and (6.59) are the same. For the null geodesics E and R are only scaling constants, so the angular momenta will only be degenerate for a particular value of ν. Equating (6.60) and (6.59) shows that a thin ring with $\nu = 0.04042$ will have both of the null circular orbits on the ergosurface.

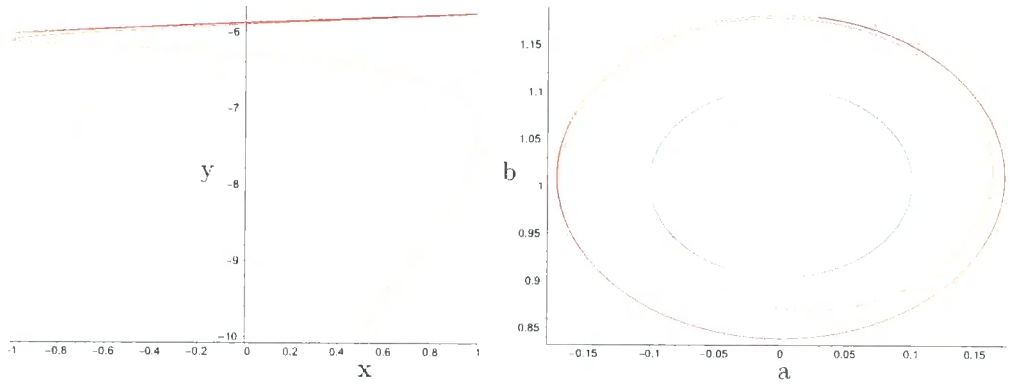

Figure 6.15: These plots show the numerical integration of the equations of motion for a timelike geodesic started at x, $\dot{x}$, y, $\dot{y}$=-0.99000, 3.03072, -6.01041, 0 respectively, with $E = 2$ and $\ell = \Psi = 0$. The Black Ring has radius $R = 1$ and $\nu = 0.1$. The left hand plot shows the orbit of the particle in the toroidal coordinates, with the right hand plot showing the orbit in polar coordinates. The green lines indicate the position of the event horizon.

6.4 Geodesics Orbiting through the Ring

For geodesics that orbit through the ring at constant y, equation (6.13) becomes

$$\frac{R^2F(y)^2F(x)\ddot{y}}{G(y)(x-y)^2} - \frac{(x-y)^2\left[ECR(1+y)+\Psi F(y)\right]^2}{2R^2F(x)G(y)}\left[\frac{F(y)G'(y)}{G(y)}+\lambda\right] + \frac{\epsilon F(y)^2}{x-y}$$
$$-\frac{E^2F(x)\left[\lambda(x-y)-2F(y)\right]}{2(x-y)} + \frac{E(x-y)^2C(1-\lambda)\left[RCE(1+y)+\Psi F(y)\right]}{RF(x)G(y)} = 0 \tag{6.61}$$

where $\dot{y} \to 0$ and $\dot{x}$ has been eliminated using (6.16). To find possible solutions to this equation it is necessary to look for specific values of the constants $\nu, \Psi, \epsilon, y, E$ that cause all of the terms not involving $\ddot{y}$ to go to zero. In practice this means expanding all of the terms to give a polynomial in x, since x is free to vary while y is constrained to be a constant throughout all the motion.

In order to get a feel for the equations without having to look for general solutions it is helpful to look at the special case where $\left[ECR(1+y)+\Psi F(y)\right] = 0$. This is possible in this case because y is being treated as a constant and all of the other terms are constants. This means that Ψ can be chosen so that

$$\Psi = -\frac{ECR(1+y)}{F(y)} \tag{6.62}$$

Applying this to (6.61) reduces the equation to

$$\frac{R^2F(y)^2F(x)\ddot{y}}{G(y)(x-y)^2} = -\frac{\epsilon F(y)^2}{x-y} + \frac{E^2F(x)\left[\lambda(x-y)-2F(y)\right]}{2(x-y)} \tag{6.63}$$

It can be seen straight away that the only way that the terms on the right hand side can be set to zero is by choosing $E = \epsilon = 0$, which is the same constraint as was imposed in order to separate the equations of motion in section 6.1.

If the constants aren't constrained in any way (other than the physical constraints) then (6.61) becomes an eighth order polynomial in x. This unfortunately doesn't have any solutions for physically applicable values for $\nu, \Psi, \epsilon, y, E$.

Figure 6.15 gives an example of a timelike geodesic in the exterior of the black ring, in a reference frame which is rotating in the ψ direction with the particle. The particle's initial angular momentum is carefully chosen so that it doesn't fall straight into the black hole, but it does eventually spiral into the ring when the integration is continued. It is possible to keep fine tuning the initial velocity, so that the particle stays out of the black ring longer but in the end, the particle will either spiral into the event horizon, or escape to asymptotic infinity at $y = -1$.

The right hand plot in figure 6.15 converts the orbit into polar coordinates, given in (4.12) and (4.13), and then plots it using

$$a = r\cos\theta \tag{6.64}$$

$$b = r\sin\theta \tag{6.65}$$

This plot gives a more intuitive picture of what is happening to the particle. As one might expect, the particle initially appears to be in a stable orbit but, after approximately two revolutions, the orbit starts to decay and then rapidly falls through the event horizon. If the initial angular momentum is fine-tuned further, then it is possible to have the particle orbit the ring for a significantly longer period with the radius varying as it orbits. Unfortunately, the orbit always seems to decay eventually.

The orbit shown in the right hand plot of figure 6.15 appears to be circular but closer inspection shows that it is slightly elliptical. The eccentricity of the orbit increases as the energy is reduced until $E \sim 0.8$ where it is no longer possible to find a bound orbit. It would appear from the numerical simulations that bound orbits can be found for all values of E greater than 0.8 though.

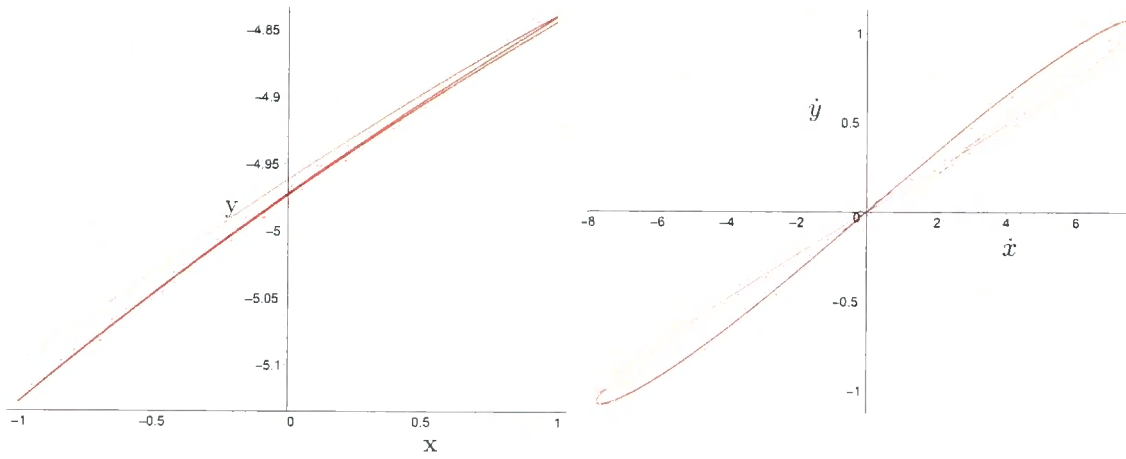

Figure 6.16: These plots show the numerical integration of the equations of motion for a timelike geodesic in the toroidal coordinates. The initial conditions are set to $(x, y, \dot{y}) = (-0.9900000, -5.0948494, 0)$, with $\ell = \Psi = 0$, for $R = 1$ and $\nu = 0.1$. The other initial conditions are $(E, \dot{x}) = (1, 0.9085145)$.

If the starting value of y is fine tuned further, then the orbit of the particle looks something like that given in figure 6.16. The two plots in this figure show how y varies with x and how $\dot{y}$ varies with $\dot{x}$. The left hand plot gives a more detailed view of the periodic motion as the particle orbits in a relatively stable ellipse. Apart from the first revolution, before the particle falls into the stable orbit, it would appear that the particle is moving back and forth along a line with y depending linearly on x, although this isn't quite true, since the trace is slightly curved.

The right hand plot gives the phase curve for the motion of the particle. The particle slows down at $x = \pm 1$, with both $\dot{y}$ and $\dot{x}$ going to zero at these two points. The plot also shows how the motion is fairly consistent with the curves being well grouped, apart from at the beginning and near the end of the plotted motion, where the curve starts to diverge from the bow-tie shape. It is tempting to conclude from this shape that the motion in the x and y directions is given by some trigonometric function but this unfortunately doesn't appear to be so. The only solvable case (given by substituting $E = 0$ and $\epsilon = 0$ into equation (6.16)) has solutions in terms of elliptic functions, so it seems reasonable to assume that the solutions for the more complicated motion would also be in terms of these elliptic functions.

6.5 Pseudo Radial Geodesics

It was mentioned at the beginning of the chapter that the Kerr metric has some "pseudo" radial geodesics, where the azimuthal angle remains constant throughout the motion, so that the geodesic only moves in the (r, ϕ) plane. The analogue of this for the Black Ring metric would be to find geodesics that move along lines of constant x, as shown in figure 4.1.

As in the Kerr metric, it is impossible to have purely radial geodesics for the Black Ring because there is an analogous frame dragging effect in the Black Ring metric. Combining (6.5) and (6.3) gives an expression for $\dot{\psi}$ in terms of the constants of motion

$$\dot{\psi} = \frac{(x-y)^2[ECR(1+y) - \Psi F(y)]}{R^2 F(x) G(y)} \tag{6.66}$$

In order for $\dot{\psi}$ to be zero for all values of y

$$ECR(1+y) - \Psi F(y) = 0 \tag{6.67}$$

Expanding this, and collecting in terms of y, gives

$$ECR - \Psi + (ECR - \Psi\lambda)y = 0 \tag{6.68}$$

In order for this to hold for all values of y, it would require

$$ECR = \Psi \tag{6.69}$$

$$ECR = \Psi\lambda \tag{6.70}$$

These two equations can only simultaneously be true if $\lambda = 1$, in which case the event horizon reduces to a three-sphere, which is a rather trivial solution. This indicates that there are no radial geodesics for the Black Ring metric, where $\dot{\psi} = 0$.

If ψ is allowed to vary throughout the motion, then the situation becomes the opposite of that investigated in the "Geodesics Orbiting through the Ring" section. In this case only x is held constant, which means that the equation of motion (6.12) reduces to

$$\frac{\ell^2(x-y)^3}{2R^2}\left[\frac{G'(x)}{G(x)} - \frac{\lambda}{F(x)}\right] - E^2 G(x) - \frac{\epsilon G(x)\,[F(x)+F(y)]}{2F(x)G(y)} = 0 \tag{6.71}$$

where (6.16) has been used to eliminate the $\dot{y}$ dependence.

Examining the solutions to equation (6.71) indicates that there are only physically consistent solutions for $x = \pm 1$. This class of solutions has already been examined in some detail in the Planar Circular Geodesics section.

Chapter 7

Generating Solutions with String Charges

Of all the solutions to general relativity that have thus far been discovered, asymptotically flat black hole solutions are possibly of the most interest since they are thought to be the most likely candidates to exist in the physical world - this naturally means that more research has been carried out on solutions of this type. Of particular relevance to this chapter is the development of a microscopic interpretation of the entropy of asymptotically flat black holes solutions. Strominger and Vafa were the first to investigate this in [70], where they examined a class of supersymmetric spherical 5D black holes with non-zero charge and showed that it was possible to derive their entropy by counting the degeneracy of BPS states. Further work building on this has been done for black holes with both S^3 and $S^2 \times S^1$ topology in papers such as [44,61,71–74]. These papers examine a mixture of charged and neutral black hole solutions with the charged solutions calculated for each specific metric. The procedure described in this chapter gives a five parameter metric which can be used to analyse the microscopic origin of the entropy for a much broader range of black hole solutions, since the only constraint on the uncharged starting metric is that it has three Killing vectors.

Although the method presented in this chapter [76] has already been used to find charged versions of the Myers-Perry and the singly spinning black ring, it hasn't yet been used to generate charged solutions for the doubly spinning black ring and other

recently discovered multi-black hole solutions. Given that the procedure for adding string charges to a neutral metric is virtually identical for all asymptotically flat metrics it seems useful to give the solution in as general a form as possible. The first part of this chapter gives the necessary theory for adding charges to a generic metric with three Killing vectors before going on to apply the results to the specific case of the doubly spinning ring.

Although a two charge solution hasn't previously been calculated for the doubly spinning ring, using the method presented here, a three charge solution to minimal supergravity has been calculated in [77]. Their method produces a three charge version of the doubly spinning black ring with all of the charges being equal. This differs from the results presented in this chapter, as the method presented here allows the two charges to be set independently of one another. It is possible in principle to add a third charge through a further series of dualisations and boosts but the unavoidable by-product of adding the extra charge is the introduction of Dirac-Meisner string singularities (as is seen in [77]), so the three charge metric is not considered in this chapter.

The first two sections of this chapter are concerned with developing the procedure whereby string and momentum charges are added to a generic five dimensional metric. The basic idea is to lift the neutral metric to ten dimensions by adding five extra flat dimensions, and then applying a series of boosts and T-duality transformations to the metric. The ten dimensional metric is then Kaluza-Klein reduced back down to five dimensions with the boosts in the extra spatial dimensions appearing as fundamental string and momentum charges. The resulting charged metric is then presented, along with a derivation of the physical properties of this generic charged solution.

The final section of this chapter looks at the physical properties of the two charge generic metric derived in section 7.2, using the dual rotating black ring as a specific example. The charged solution has two extra parameters relating to the two string charges, so the physical properties of the charged metric are compared with those of the neutral starting metric for different values of these charges. The differences between the generic charged metric and the neutral metric are independent of the

form of the original metric coefficients so the analysis can be applied to any metric that is charged up in the manner described in section 7.1.

7.1 Theory of Generating Charges

Having obtained a solution to Einstein's field equations, it is possible to generate a new solution that has different charges corresponding to the different string sectors. The method presented here, which adds charges to a generic uncharged metric, is essentially the same as that presented in [78, 79] and more pertinently applied to the singly spinning ring in [61]. The main idea is to lift the five dimensional metric to ten dimensions through the inclusion of five flat dimensions, which will be labelled as {w,6,7,8,9}. The w dimension is singled out as this plays an important part in constructing the charges. The remaining four dimensions are compactified on a T^4 and play a passive role in the generation of the various charges. Having constructed a ten dimensional metric, the application of a series of boosts and duality transformations will then produce a new solution to the string equations of motion. Once this is done, the ten dimensional solution can then be Kaluza-Klein compactified to reduce it back down to the desired five dimensional metric with various string charges.

Any solution to Einstein's equations will automatically satisfy the equations of motion for low energy superstrings when lifted to ten dimensions, as long as the gauge fields are turned off. This can easily be seen by examining the action for the low energy NS-NS superstring, when compactified on T^4 [61]

$$S_6 = \frac{1}{2\kappa_6^2}\int \mathrm{d}^6x\sqrt{-g^{(6)}}e^{-2\Phi}\left(R^{(6)} + 4(\nabla\Phi)^2 - \frac{1}{12}H^{(6)^2}\right) \tag{7.1}$$

where Φ is the scalar dilaton, κ_6 is related to the six dimensional Planck length, and $H^{(6)}$ is a 3-form flux given by $H^{(6)} = \mathrm{d}B^{(6)}$, where $B^{(6)}$ and $F^{(6)}$ are 2-form fields that couple electrically to the dual rotating ring. The four extra flat dimensions have been suppressed here as they don't enter into any of the subsequent calculations. If Φ and B are set to zero then the action given by (7.1) reduces to the Einstein-Hilbert action for a six dimensional metric.

The charges are produced by Lorentz boosting the six dimensional metric in the w direction to produce a black-string or black-tube, depending on the topology of the starting solution. This is achieved via a coordinate transformation where α_1 is the boost parameter. This gives the solution linear momentum in the w direction but in order to create a non-trivial charge a subsequent T-dualisation must be performed. The application of the T-duality transformation converts the type IIA solution[1] with linear momentum, to a type IIB solution with a fundamental string charge. The T-duality transformations are given by [80]

$$\begin{aligned} g_{ww} &\to \tfrac{1}{g_{ww}} & g_{w\alpha} &\to \tfrac{B_{w\alpha}}{g_{ww}} \\ g_{\alpha\beta} &\to g_{\alpha\beta} - \left(\tfrac{g_{w\alpha}g_{w\beta} - B_{w\alpha}B_{w\beta}}{g_{ww}}\right) & B_{w\alpha} &\to \tfrac{g_{w\alpha}}{g_{ww}} \\ B_{\alpha\beta} &\to B_{\alpha\beta} - 2\tfrac{g_{w[\alpha}B_{\beta]w}}{g_{ww}} & \Phi &\to \Phi - \tfrac{1}{2}\log g_{ww} \end{aligned} \tag{7.2}$$

Having T-dualised the metric, a second charge can be added by boosting again in the w direction, with parameter α_2. This gives a black tube with linear momentum in the w direction and a fundamental charge $F(w)$. To obtain the five dimensional solution with two charges it is then simply a case of KK reducing this 10d metric along the w direction.

In order to carry out the KK compactification, assume that the w direction forms a circle of radius R_w. The Kaluza-Klein ansatz is then given by

$$g^{(6)}_{MN}\mathrm{d}x^M\mathrm{d}x^N = g_{\mu\nu}\mathrm{d}x^\mu\mathrm{d}x^\nu + e^{2\sigma}(\mathrm{d}z + A^{(1)}_\mu \mathrm{d}x^\mu)^2 \tag{7.3}$$

where the Greek indices cover $\{t,\rho,z,\psi,\phi\}$ and the Latin indices cover $\{x^\mu,w\}$. Here, $e^{2\sigma} = g_{ww}$ and $A^{(1)}$ is a 1-form field, induced by the compactification of the six dimensional metric, which sources the $P(w)$ charge.

Applying (7.3) to the 6d action (7.1), gives

$$\begin{aligned} S_5 = \frac{1}{2\kappa_5^2}\int \mathrm{d}^5x\sqrt{-g}e^{-2\Phi+\sigma}\Big(&R^{(5)} + 4(\nabla\Phi)^2 - 4\nabla\Phi\nabla\sigma - \frac{1}{12}H^2 \\ &-\frac{1}{4}e^{2\sigma}(F^{(1)})^2 - \frac{1}{4}e^{-2\sigma}(F^{(2)})^2\Big) \end{aligned} \tag{7.4}$$

[1]This is not a unique choice since the starting solution can equally be thought of as a type IIB solution. In which case, the T-duality transformation would produce a type IIA solution with fundamental charge.

where $\kappa_5^2 = \kappa_6^2/(2\pi R_w)$ and the $^{(6)}$ superscript has been dropped where it is obvious that the fields are now five dimensional.

The reduction of the string action to five dimensions has created two new fields $F^{(1)}$ and $F^{(2)}$ where $F^{(1)}_{\mu\nu} = \partial_\mu A^{(1)}_\nu - \partial_\nu A^{(1)}_\mu$ and $F^{(2)}_{\mu\nu} = \partial_\mu A^{(2)}_\nu - \partial_\nu A^{(2)}_\mu$, with $A^{(2)}_\mu = B^{(6)}_{\mu w}$. The three form H has now picked up a Chern-Simons term, so is now given by $H = \mathrm{d}B - A^{(1)} \wedge F^{(2)}$.

It is possible to transform the string action into something more like the Einstein action by defining an effective dilaton $\Phi_{eff} = \Phi - \sigma/2$, thus allowing the string metric to be transformed into the Einstein frame via $g^E_{\mu\nu} = e^{-\frac{4}{3}\Phi_{eff}} g_{\mu\nu}$. This means that the action in the Einstein frame becomes

$$S_5 = \frac{1}{2\kappa_5^2}\int \mathrm{d}^5x\sqrt{-g}\left(R^{(5)} + 4(\nabla\Phi)^2 - 4\nabla\Phi\nabla\sigma - \frac{1}{12}H^2 - \frac{1}{4}e^{2\sigma}(F^{(1)})^2 - \frac{1}{4}e^{-2\sigma}(F^{(2)})^2\right) \tag{7.5}$$

Note that all of the fields inside of the brackets have also changed with the change of frame.

7.2 Charging Up A Three Killing Field Metric

7.2.1 The [F(w),P] Charged Metric

Having established the formalism required to charge up a metric which solves Einstein's field equations, it is now possible to apply it to a general metric with three Killing vectors. Any metric with three Killing vectors given by ∂_t, ∂_ψ, and ∂_ϕ can be written in the form

$$ds^2 = g_{tt}\mathrm{d}t^2 + 2g_{t\phi}\mathrm{d}t\mathrm{d}\phi + g_{\phi\phi}\mathrm{d}\phi^2 + 2g_{t\psi}\mathrm{d}t\mathrm{d}\psi + g_{\psi\psi}\mathrm{d}\psi^2 + 2g_{\psi\phi}\mathrm{d}\psi\mathrm{d}\phi + g_{\rho\rho}\mathrm{d}\rho^2 + g_{zz}\mathrm{d}z^2 \tag{7.6}$$

where all of the metric functions $g_{\mu\nu}$ are solely functions of ρ and z. The non-Killing directions ρ and z are inspired by the canonical coordinates used in the inverse scattering technique (although the form given in (7.6) differs in that $g_{\rho\rho}$ and g_{zz} are not necessarily equal), allowing any three Killing vector solution to be used.

It is now possible to charge up this general metric, using the technique of boosting and T-dualising described in the previous section, to give a solution to type IIB string theory with fundamental and momentum charges in the w direction. Having done this, the new 6D charged metric is given by

$$\begin{aligned} ds^2 &= \left[g_{ww}\cosh^2\alpha_1 + g_{tt}\sinh^2\alpha_1\right]^{-1}\left[(g_{ww}g_{tt}\cosh^2\alpha_2 + \sinh^2\alpha_2)\mathrm{d}\tilde{t}^2\right. \\ &+2g_{t\psi}g_{ww}\cosh\alpha_1\cosh\alpha_2\mathrm{d}\tilde{t}\mathrm{d}\tilde{\psi} + 2g_{t\phi}g_{ww}\cosh\alpha_1\cosh\alpha_2\mathrm{d}\tilde{t}\mathrm{d}\tilde{\phi} \\ &+(g_{ww}g_{\psi\psi}\cosh^2\alpha_1 + (g_{tt}g_{\psi\psi} - g_{t\psi}^2)\sinh^2\alpha_1)\mathrm{d}\tilde{\psi}^2 \\ &+2(g_{tt}g_{ww}+1)\cosh\alpha_2\sinh\alpha_2\mathrm{d}\tilde{t}\mathrm{d}\tilde{w} + 2g_{t\psi}g_{ww}\cosh\alpha_1\sinh\alpha_2\mathrm{d}\tilde{\psi}\mathrm{d}\tilde{w} \\ &+2(g_{ww}g_{\psi\phi}\cosh^2\alpha_1 + (g_{tt}g_{\psi\phi} - g_{t\psi}g_{t\phi})\sinh^2\alpha_1)\mathrm{d}\tilde{\psi}\mathrm{d}\tilde{\phi} \\ &+(g_{ww}g_{\phi\phi}\cosh^2\alpha_1 + (g_{tt}g_{\phi\phi} - g_{t\phi}^2)\sinh^2\alpha_1)\mathrm{d}\tilde{\phi}^2 \\ &\left.+2g_{t\phi}g_{ww}\cosh\alpha_1\sinh\alpha_2\mathrm{d}\tilde{\phi}\mathrm{d}\tilde{w} + (\cosh^2\alpha_2 + g_{ww}g_{tt}\sinh^2\alpha_2)\mathrm{d}\tilde{w}^2\right] \\ &+g_{\rho\rho}\mathrm{d}\tilde{\rho}^2 + g_{zz}\mathrm{d}\tilde{z}^2 \end{aligned} \tag{7.7}$$

with the auxiliary two form field given by

$$B_{\tilde{t}\tilde{\psi}} = \frac{g_{t\psi}\sinh\alpha_1\sinh\alpha_2}{g_{ww}\cosh^2\alpha_1 + g_{tt}\sinh^2\alpha_1} \tag{7.8}$$

$$B_{\tilde{t}\tilde{\phi}} = \frac{g_{t\phi}\sinh\alpha_1\sinh\alpha_2}{g_{ww}\cosh^2\alpha_1 + g_{tt}\sinh^2\alpha_1} \tag{7.9}$$

$$B_{\tilde{w}\tilde{t}} = \frac{(g_{ww}+g_{tt})\sinh\alpha_1\cosh\alpha_1}{g_{ww}\cosh^2\alpha_1 + g_{tt}\sinh^2\alpha_1} \tag{7.10}$$

$$B_{\tilde{w}\tilde{\psi}} = \frac{g_{t\psi}\sinh\alpha_1\cosh\alpha_2}{g_{ww}\cosh^2\alpha_1 + g_{tt}\sinh^2\alpha_1} \tag{7.11}$$

$$B_{\tilde{w}\tilde{\phi}} = \frac{g_{t\phi}\sinh\alpha_1\cosh\alpha_2}{g_{ww}\cosh^2\alpha_1 + g_{tt}\sinh^2\alpha_1} \tag{7.12}$$

and the scalar dilaton given by

$$e^{-2\tilde{\Phi}} = g_{ww}\cosh^2\alpha_1 + g_{tt}\sinh^2\alpha_1 \tag{7.13}$$

The metric given in (7.7) only has a fundamental charge in the w direction, so to create the P(w) charge the metric has to be Kaluza-Klein reduced back down to five dimensions. In practice, the supplementary w dimension is always added to the metric by setting $g_{ww} = 1$ so, for the sake of simplicity, this constraint has been applied in all of the following equations. Bearing this in mind, the compactified

[F(w),P(w)] charged metric in the string frame is given by

$$\begin{aligned} ds_5^2 &= \frac{1}{h_1 h_2}\Big\{h_2(g_{tt}\cosh^2\alpha_2+\sinh^2\alpha_2)\mathrm{d}\tilde{t}^2+2h_2\cosh\alpha_1\cosh\alpha_2(g_{t\psi}\mathrm{d}\tilde{t}\mathrm{d}\tilde{\psi} \\ &\quad +g_{t\phi}\mathrm{d}\tilde{t}\mathrm{d}\tilde{\phi})-\sinh^2\alpha_2[(g_{tt}+1)\cosh\alpha_2\mathrm{d}\tilde{t}+g_{t\psi}\cosh\alpha_1\mathrm{d}\tilde{\psi}+g_{t\phi}\cosh\alpha_1\mathrm{d}\tilde{\phi}]^2 \\ &\quad +E_{\psi\psi}\mathrm{d}\tilde{\psi}^2+2E_{\psi\phi}\mathrm{d}\tilde{\psi}\mathrm{d}\tilde{\phi}+E_{\phi\phi}\mathrm{d}\tilde{\phi}^2\Big\}+g_{\rho\rho}\mathrm{d}\rho^2+g_{zz}\mathrm{d}z^2 \end{aligned} \tag{7.14}$$

where

$$h_n = \cosh^2\alpha_n + g_{tt}\sinh^2\alpha_n \tag{7.15}$$

$$E_{\mu\nu} = h_2\left[g_{\mu\nu}\cosh^2\alpha_1+(g_{tt}g_{\mu\nu}-g_{t\mu}g_{t\nu})\sinh^2\alpha_1\right] \tag{7.16}$$

and $\mu \in \{\psi, \phi\}$.

The compactification of the six dimensional metric has introduced two new 1-form fields $A^{(1)}$ and $A^{(2)}$, as well as the 2-form field B, and the scalar field Φ. These 1-form fields are given by

$$A^{(1)} = \frac{\sinh\alpha_1}{h_1}\Big[(1+g_{tt})\cosh\alpha_1\mathrm{d}t+g_{t\psi}\cosh\alpha_2\mathrm{d}\psi+g_{t\phi}\cosh\alpha_2\mathrm{d}\phi\Big] \tag{7.17}$$

$$A^{(2)} = \frac{\sinh\alpha_2}{h_2}\Big[(1+g_{tt})\cosh\alpha_2\mathrm{d}t+g_{t\psi}\cosh\alpha_1\mathrm{d}\psi+g_{t\phi}\cosh\alpha_1\mathrm{d}\phi\Big] \tag{7.18}$$

with the two form B being reduced to

$$B_{\tilde{t}\tilde{\mu}} = \frac{g_{t\mu}\sinh\alpha_1\sinh\alpha_2}{h_1} \tag{7.19}$$

The dilaton is unchanged by the compactification process so with $g_{ww} = 1$, it is now given by

$$e^{-2\tilde{\Phi}} = \cosh^2\alpha_1 + g_{tt}\sinh^2\alpha_1 = h_1 \tag{7.20}$$

and the other scalar field, introduced by the compactification, is given by

$$e^{2\sigma} = \frac{\cosh^2\alpha_2+g_{tt}\sinh^2\alpha_2}{\cosh^2\alpha_1+g_{tt}\sinh^2\alpha_1} = \frac{h_2}{h_1} \tag{7.21}$$

7.2.2 Physical Properties of The Charged Metric

The process of charging up the metric only affects the metric coefficients involving t, ψ, and ϕ, so any of the properties of the metric that depend upon the coefficients involving ρ and z are unchanged. In most cases this means that the position of the

event horizon is unchanged, since the coordinates of the neutral metric are usually chosen so that the event horizon is described by a hypersurface where one of the non-Killing directions is held constant. This is exemplified by the dual rotating ring, described in the next section. Having said this, the addition of string charges to the neutral metric does alter the thermodynamic properties of the metric.

If the mass, angular momenta, and area of the neutral metric are given by M, J_ψ, J_ϕ, and A respectively, then it is possible to calculate how these will change with the addition of extra charges. It is assumed in the following that the metric given in (7.6) is asymptotically flat, which in turn implies that the charged metric (7.7) is also asymptotically flat.

For an asymptotically flat metric, the ADM mass can be derived by examining the g_{tt} coefficient near asymptotic infinity. This function will then fall off as

$$g_{tt} = -1 + \frac{8GM}{3\pi r^2} + \mathcal{O}\left(\frac{1}{r^4}\right) \tag{7.22}$$

at infinity, so the Taylor expansion of the metric function can then be compared to this and the mass M extracted. Since the charged metric is also asymptotically flat, its mass can be calculated in a similar manner. Expressing the $g_{\tilde{t}\tilde{t}}$ coefficient of the charged metric in terms of the original metric gives

$$g_{\tilde{t}\tilde{t}} = \frac{g_{tt}}{h_1 h_2} \tag{7.23}$$

If it is assumed that g_{tt} takes the form given by (7.22), then the above equation becomes

$$g_{\tilde{t}\tilde{t}} = -1 + \frac{4GM(\cosh 2\alpha_1 + \cosh 2\alpha_2)}{3\pi r^2} + \ldots \tag{7.24}$$

Comparing this with (7.22), the charged metric mass $\tilde{M}$ can be defined as

$$\tilde{M} = \frac{M}{2}(\cosh 2\alpha_1 + \cosh 2\alpha_2) \tag{7.25}$$

The angular momenta in the ψ and ϕ directions can be calculated using a similar process, but this time comparing the different coefficients for $g_{t\psi}$ and $g_{t\phi}$ respectively. The necessary expressions for the charged metric coefficients are given by

$$g_{\tilde{t}\tilde{\phi}} = \frac{g_{t\phi}\cosh\alpha_1\cosh\alpha_2}{h_1 h_2} \tag{7.26}$$

$$g_{\tilde{t}\tilde{\psi}} = \frac{g_{t\psi}\cosh\alpha_1\cosh\alpha_2}{h_1 h_2} \tag{7.27}$$

In this case, the form of the $g_{t\psi}$ and $g_{t\phi}$ coefficients at infinity is

$$g_{t\mu} \sim \frac{J_\mu}{r^2} + \mathcal{O}\left(\frac{1}{r^4}\right) \tag{7.28}$$

where $\mu \in \{\psi, \phi\}$. Bearing this in mind, the charged metric coefficients after substituting for g_{tt} from (7.22) become

$$g_{\tilde{t}\tilde{\phi}} = \frac{J_\phi}{r^2}\cosh\alpha_1\cosh\alpha_2 + \ldots \tag{7.29}$$

$$g_{\tilde{t}\tilde{\psi}} = \frac{J_\psi}{r^2}\cosh\alpha_1\cosh\alpha_2 + \ldots \tag{7.30}$$

These equations can then be compared with (7.28) to construct expressions for the charged metric angular momenta

$$\tilde{J}_\phi = J_\phi\cosh\alpha_1\cosh\alpha_2 \tag{7.31}$$

$$\tilde{J}_\psi = J_\psi\cosh\alpha_1\cosh\alpha_2 \tag{7.32}$$

Unfortunately, the above method cannot be used to calculate how the area varies when string charges are added to the neutral metric, since the area is given by

$$A = \int\sqrt{|\gamma|} = \int\sqrt{g_{zz}\left[g_{\psi\psi}g_{\phi\phi} - g_{\psi\phi}\right]} \tag{7.33}$$

where γ is the induced metric on the horizon, the integral is taken over the event horizon and it is assumed that the horizon is a hypersurface of constant ρ. This integral is problematic because of the terms in the square root, which make it difficult to compare with any corresponding expression derived by substituting in the charged metric coefficients. A more useful form for the induced metric is derived in Appendix E.

Re-writing the integral in terms of this new expression for the induced metric and transforming to the Einstein frame gives

$$A^E = \int\sqrt{|\gamma^E|} = \int\frac{\sqrt{-g_{zz}h_1h_2}}{g_{tt}}\left(g_{t\psi}\sqrt{g_{t\phi}^2 - g_{\phi\phi}g_{tt}} + g_{t\phi}\sqrt{g_{t\psi}^2 - g_{\psi\psi}g_{tt}}\right) \tag{7.34}$$

Having re-expressed the area integrand in a more manageable form it is now possible to substitute for the charged metric coefficients obtained by comparing (7.6) and (7.14). After substituting for the various metric factors, the area of the charged metric becomes

$$\tilde{A}^E = \int\sqrt{|\gamma^E|}\cosh\alpha_1\cosh\alpha_2 = A^E\cosh\alpha_1\cosh\alpha_2 \tag{7.35}$$

It was shown in [81] that the horizon entropy is invariant under duality transformations and thus invariant for all varieties of string charge. This implies that the expression for the horizon area is definitive for all two charge metrics.

Having charged up the metric, it is necessary to calculate the conserved charges associated with the two 1-form fields $A^{(1)}$ and $A^{(2)}$. In general the gauge charges in five dimensions are given by

$$Q_i = \frac{1}{4\pi^2}\int_{S^3} e^{-2\Phi_i} \star F^{(i)} \tag{7.36}$$

where $F = \mathrm{d}A^{(i)}$ and the $e^{-2\Phi_i}$ factors, obtained by inspection of the Kaluza Klein reduced action given in (7.4), are

$$\Phi_1 = \Phi + \frac{\sigma}{2} \qquad\qquad \Phi_2 = \Phi - \frac{3\sigma}{2} \tag{7.37}$$

The integral given in (7.36) has to be taken over a three sphere at infinity, so to simplify the algebra, it is convenient to work in spherical polar coordinates where $(\rho, z) \rightarrow (r, \theta)$ with t, ψ, and ϕ remaining unchanged. This means that the only pertinent component is $\star F^{(i)}_{\theta\psi\phi}$, since the integral has to be taken for a constant t and r cross-section. Furthermore, the components of $\star F^{(i)}$ only need to be known at asymptotic infinity, so only the first order terms of the Taylor expansion at infinity need to be considered. The $\star F^{(i)}_{\theta\psi\phi}$ component can immediately be reduced to the sum of three terms, by virtue of the metric having three Killing vectors and $g_{\theta t} = 0$ since there is assumed to be no rotation in the θ direction. This gives

$$\star F^{(i)}_{\theta\psi\phi} = \frac{1}{\sqrt{|g|}}\left[g_{\theta\theta}g_{\psi\psi}g_{\phi\phi}\tilde{\epsilon}^{rt\theta\psi\phi}F_{rt} + g_{\theta\theta}g_{\psi t}g_{\phi\phi}\tilde{\epsilon}^{r\psi\theta t\phi}F_{r\psi} + g_{\theta r}g_{\psi\psi}g_{\phi\phi}\tilde{\epsilon}^{\theta tr\psi\phi}F_{\theta t}\right] \tag{7.38}$$

where $\tilde{\epsilon}^{\mu\nu\rho\sigma\tau}$ is the Levi-Civita tensor density and $\tilde{\epsilon}^{tr\theta\psi\phi} = 1$.

The leading order terms for the metric functions can be determined by considering the asymptotic expansion at infinity of the general spherical five dimensional metric given in [25]. This series expansion indicates that the metric coefficients at infinity are unchanged by the process of adding charges to (7.6), which allows (7.38) to be simplified further because it is now evident that the $g_{\psi t}$ and $g_{\theta r}$ coefficients are zero at infinity. Substituting the leading order terms for $g_{\psi\psi}$, $g_{\phi\phi}$, $g_{\theta\theta}$, and g into (7.38) gives

$$\star F^{(i)}_{\theta\psi\phi} = -r^3 \sin\theta\cos\theta F^{(i)}_{rt} \tag{7.39}$$

To obtain an expression for $F_{rt} \equiv \partial_r A_t - \partial_t A_r$ at infinity, it is necessary to substitute for g_{tt} from (7.22) to give

$$A_t^{(i)} = \frac{8GM}{3\pi r^2 + 8GM \sinh^2 \alpha_i} \sinh \alpha_i \cosh \alpha_i \stackrel{r=\infty}{\rightarrow} \frac{8GM}{3\pi r^2} \sinh \alpha_i \cosh \alpha_i \tag{7.40}$$

This then allows F_{rt} to be calculated

$$F_{rt}^{(i)} = -\frac{8GM}{3\pi r^3} \sinh 2\alpha_i \tag{7.41}$$

Putting this together with (7.39) gives

$$\star F_{\theta\psi\phi}^{(i)} = \frac{4GM \sin 2\theta}{3\pi} \sinh 2\alpha_i \tag{7.42}$$

The $e^{-2\Phi_i}$ factors will both go to one by virtue of them being functions of h_i, which go to one at infinity, as is easily verified by substituting for g_{tt} from (7.22) and taking the limit as $r \rightarrow \infty$. This now allows the integral given in (7.36) to be evaluated, and the conserved charges to be calculated, as

$$Q_i = \frac{4GM}{3\pi} \sinh 2\alpha_i \tag{7.43}$$

7.3 The Two Charge Dual Rotating Ring Metric

The full 10D type IIB string solution for the dual rotating metric, after substituting in (7.7), is given by

$$\begin{aligned} ds_6^2 = & -\frac{m_2(y,x)}{m_1(x,y)} \mathrm{d}t^2 - \frac{H(y,x)\left(\cosh\alpha_2 \mathrm{d}t + \sinh\alpha_2 \mathrm{d}w\right)^2}{m_1(x,y)} \\ & + \frac{H(y,x)\left(\cosh\alpha_2 \mathrm{d}t + \sinh\alpha_2 \mathrm{d}w + \Omega \cosh\alpha_1\right)^2}{m_1(x,y)} - \frac{F(x,y)}{H(y,x)} \mathrm{d}\psi^2 \\ & - 2\frac{J(x,y)}{H(y,x)} \mathrm{d}\phi \mathrm{d}\psi + \frac{F(y,x)}{H(y,x)} \mathrm{d}\phi^2 + \frac{k^2 H(x,y)}{(x-y)^2(1-\nu)^2} \left(\frac{\mathrm{d}x^2}{G(x)} - \frac{\mathrm{d}y^2}{G(y)} \right) \\ & + \frac{m_2(x,y)}{m_1(x,y)} \mathrm{d}w^2 + \frac{2\cosh\alpha_2 \sinh\alpha_2 \left[H(y,x) - H(x,y)\right]}{m_1(x,y)} \mathrm{d}t \mathrm{d}w \end{aligned} \tag{7.44}$$

where

$$m_n(x,y) = H(y,x) \sinh^2 \alpha_n - H(x,y) \cosh^2 \alpha_n \tag{7.45}$$

The four additional dimensions have been suppressed for brevity, but they are given by $g_{\mu\nu} = \delta_{\mu\nu}$ where $\mu, \nu = 6, 7, 8, 9$. The additional fields, introduced through the

duality process are given by

$$B^{(6)}_{t\phi} = \frac{\sqrt{2}k\lambda y\sqrt{\nu}\sinh\alpha_1\sinh\alpha_2\sqrt{1+\lambda+\nu}\sqrt{1-\lambda+\nu}(x^2-1)}{m_1(x,y)} \tag{7.46}$$

$$B^{(6)}_{t\psi} = \frac{\sqrt{2}k\lambda\sqrt{1+\lambda+\nu}(1+y)\left[(\lambda+\nu-1)(yx^2\nu-1)+2\nu(1-x+xy)-2\right]}{m_1(x,y)\sqrt{1-\lambda+\nu}}\times \sinh\alpha_1\sinh\alpha_2 \tag{7.47}$$

$$B^{(6)}_{tw} = -\frac{\sinh\alpha_1\cosh\alpha_1\left[H(y,x)-H(x,y)\right]}{m_1(x,y)} \tag{7.48}$$

$$B^{(6)}_{\phi w} = -\frac{\sqrt{2}k\lambda y\sqrt{\nu}\sinh\alpha_1\cosh\alpha_2\sqrt{1+\lambda+\nu}\sqrt{1-\lambda+\nu}(x^2-1)}{m_1(x,y)} \tag{7.49}$$

$$B^{(6)}_{\psi w} = \frac{\sqrt{2}k\lambda(1+y)\sqrt{1+\lambda+\nu}\left[2-(\lambda+\nu-1)(yx^2\nu-1)-2\nu(1-x+xy\right]}{m_1(x,y)\sqrt{1-\lambda+\nu}}\times \cosh\alpha_2\sinh\alpha_1 \tag{7.50}$$

and

$$e^{-2\Phi} = -\frac{m_1(x,y)}{H(x,y)} \tag{7.51}$$

In this metric, the canonical coordinates have been replaced with the toroidal $(x,\ y)$ coordinates[2] which may be concerning, since the derivation of the previous section was in terms of the $(\rho,\ z)$ coordinates. Fortunately, all of the transformations used to charge up the generic metric were independent of these coordinates, so they can be transformed with impunity.

In order to calculate the various physical properties of the charged ring it is necessary to now reduce the metric back down to five dimensions. This has already been done in (7.14), so substituting for the various metric coefficients and transforming to the Einstein frame gives[3]

$$\begin{aligned} ds^2_5 = & -\frac{\left[(H(y,x)-H(x,y))\cosh\alpha_2\sinh\alpha_2\mathrm{d}t+H(y,x)\sinh\alpha_2\cosh\alpha_1\Omega\right]^2}{(m_1(x,y)m_2(x,y))^{2/3}H(x,y)^{1/3}} \\ & -\left(\frac{m_2(x,y)}{m_1(x,y)^2H(x,y)}\right)^{1/3}\left(m_2(y,x)\mathrm{d}t^2+H(y,x)\Omega^2\cosh^2\alpha_1\right. \\ & \left.+2H(y,x)\cosh\alpha_1\cosh\alpha_2\Omega\mathrm{d}t\right)-\left(\frac{m_1(x,y)m_2(x,y)}{H(x,y)}\right)^{1/3}\left[\frac{F(x,y)}{H(y,x)}\mathrm{d}\psi^2-\right. \\ & \left.2\frac{J(x,y)}{H(y,x)}\mathrm{d}\phi\mathrm{d}\psi+\frac{F(y,x)}{H(y,x)}\mathrm{d}\phi^2+\frac{k^2H(x,y)}{(x-y)^2(1-\nu)^2}\left(\frac{\mathrm{d}x^2}{G(x)}-\frac{\mathrm{d}y^2}{G(y)}\right)\right] \end{aligned} \tag{7.52}$$

[2]The transformations used can be found in [27]

[3]Inspection of the Ω function shows that this metric is free from Dirac-Misner singularities.

The 1-form gauge fields are now given by

$$A_t^{(1)} = \frac{[H(y,x)-H(x,y)]\cosh\alpha_2\sinh\alpha_2}{m_2(x,y)} \tag{7.53}$$

$$A_\psi^{(1)} = -\frac{k\lambda\sqrt{2(1+\nu)^2-2\lambda^2}(1+y)\left[1+\lambda-\nu+x^2y\nu(1-\lambda-\nu)+2\nu x(1-y)\right]}{(1-\lambda+\nu)m_2(x,y)} \times \sinh\alpha_2\cosh\alpha_1 \tag{7.54}$$

$$A_\phi^{(1)} = -\frac{k\lambda\sqrt{2(1+\nu)^2-2\lambda^2}(1-x^2)y\sqrt{\nu}\sinh\alpha_2\cosh\alpha_1}{m_2(x,y)} \tag{7.55}$$

$$A_t^{(2)} = -\frac{[H(y,x)-H(x,y)]\cosh\alpha_1\sinh\alpha_1}{m_1(x,y)} \tag{7.56}$$

$$A_\psi^{(2)} = -\frac{\sqrt{2}k\lambda(1+y)\sqrt{1+\lambda+\nu}\left[(\lambda+\nu-1)(yx^2\nu-1)+2\nu(1-x+xy)-2\right]}{m_1(x,y)\sqrt{1-\lambda+\nu}} \times \cosh\alpha_2\sinh\alpha_1 \tag{7.57}$$

$$A_\phi^{(2)} = -\frac{\sqrt{2}k\lambda y\sqrt{\nu}\sinh\alpha_1\cosh\alpha_2\sqrt{1+\lambda+\nu}\sqrt{1-\lambda+\nu}(x^2-1)}{m_1(x,y)} \tag{7.58}$$

The 2-form field is given by

$$B_{t\phi} = \frac{\sqrt{2}k\lambda y\sqrt{\nu}\sinh\alpha_1\sinh\alpha_2\sqrt{1+\lambda+\nu}\sqrt{1-\lambda+\nu}(x^2-1)}{m_1(x,y)} \tag{7.59}$$

$$B_{t\psi} = \frac{\sqrt{2}k\lambda\sqrt{1+\lambda+\nu}(1+y)\left[(\lambda+\nu-1)(yx^2\nu-1)+2\nu(1-x+xy)-2\right]}{m_1(x,y)\sqrt{1-\lambda+\nu}} \times \sinh\alpha_1\sinh\alpha_2 \tag{7.60}$$

and the scalar functions are given by

$$e^{-2\Phi} = -\frac{m_1(x,y)}{H(x,y)} \qquad e^{2\sigma} = \frac{m_2(x,y)}{m_1(x,y)} \tag{7.61}$$

7.4 Physical Properties of the Generic Charged Metric

Having obtained the metric for the [F(w),P] charged black ring (7.52) and the more general two charge metric (7.14), it is now possible to work out some of the physical properties of these solutions. In fact, most of the distinguishing features of the charged solutions are the same as for the neutral solution: the x, y (or ρ, z for the general solution), ψ, and ϕ coordinates vary over the same ranges, any physical constraints on the original neutral metric will be unchanged e.g. the limits on λ and

ν are exactly the same for the two charge black ring, and the horizons will still be given by $g^{\rho\rho} = 0$ or in the case of the charged ring (4.61). The reason that these properties are unchanged for the charged solution is because they all depend, to some extent, upon the $g_{\rho\rho}$ and g_{zz} coefficients of the metric, which are unaffected by the boost and T-duality transformations. The addition of the charges does have some effect on the ADM mass, angular momenta, and the area but these have all been calculated in (7.25), (7.32), and (7.35) respectively. The conserved gauge charges for the charged metric have also been calculated in (7.43) and are explicitly given by

$$Q_1 = \frac{4G}{3\pi} M_0 \sinh 2\alpha_1 \qquad\qquad Q_2 = \frac{4G}{3\pi} M_0 \sinh 2\alpha_2 \tag{7.62}$$

It is worth noting that the charges are directly related to their respective boosts, which verifies the physical picture of the linear momentum being exchanged for winding charges when the metric is T-dualised.

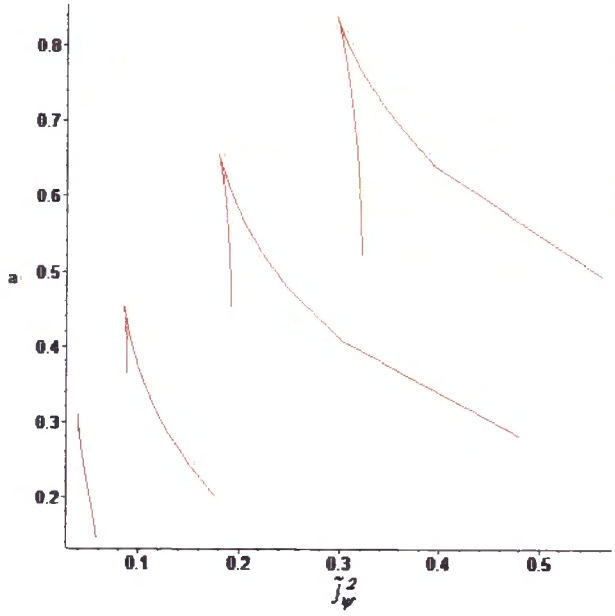

Figure 7.1: This gives an example of how the a vs ${j_\psi}^2$ plots change for the dual spinning black ring as the charge is increased, with $\alpha_1 = \alpha_2 = 1, \frac{3}{4}, \frac{1}{2}, \frac{3}{10}$ from the top right to the bottom left respectively.

To get an idea of how the behaviour of the charged solution differs from that of the neutral ring, it is a good idea to plot some phase diagrams showing how the physical properties, like the angular momentum and horizon area, vary with the charge. To this end, the charged dual rotating ring solution given in (7.52)

will be considered. The phase space of the dual rotating black ring has been fairly extensively studied in [44] and [69], so the following discussion will concentrate on where the behaviour of the charged dual rotating ring (and hence the more general solution given by (7.14)) departs from that of the neutral ring.

Before plotting the various physical properties, it is beneficial to re-define them so they are scale independent. The obvious candidate for fixing the scale is the ADM mass, so expressing the angular momentum and horizon area in terms of this, along with the conventional normalisation, gives the following relations

$$j^2 = \frac{27\pi J^2}{32GM^3} \qquad a_H = \frac{3}{16}\sqrt{\frac{3}{\pi}}\frac{A}{(GM)^{3/2}} \tag{7.63}$$

The square of the angular momentum is given above because it is more convenient to plot in terms of j^2, since it is always positive. For the neutral ring, j_ψ and j_ϕ are constrained such that

$$j_\phi \leq \frac{1}{4} \qquad j_\psi \geq \frac{3}{4} \tag{7.64}$$

This means that the angular momenta can never be equal and $j_\phi/j_\psi \leq 1/3$ for all permissible values of ν and λ. The constraints on j_ψ and j_ϕ are dependent on the form of the metric coefficients, with the constraints on the angular momenta for the dual rotating ring being a consequence of the restrictions on λ and ν. In general these restrictions will always have to be calculated for each given metric.

As can be seen by examining (7.32) and (7.35), the only difference between the angular momenta and area of the neutral metric and the charged metric is a factor of $\cosh\alpha_1 \cosh\alpha_2$, which is the same for J_ψ, J_ϕ, and A. When these are combined with the ADM mass to give the dimensionless quantities of (7.63), the relationship between the neutral metric physical properties and the charged metric physical properties is

$$\{\tilde{j}, \tilde{a}\} = \frac{2\sqrt{2}\cosh\alpha_1 \cosh\alpha_2}{(\cosh 2\alpha_1 + \cosh 2\alpha_2)^{(3/2)}}\{j, a\} \tag{7.65}$$

where the tilde denotes the charged angular momentum and area. Unfortunately, because the factors are all equal for the various quantities they all tend to cancel out, meaning that the physics of the charged metric is very similar to that of the neutral metric. This is exemplified by the fact that the maximum and minimum of

$\tilde{j}$ is exactly the same as for the neutral metric, no matter how large the charges are. This is because the multiplying factor varies between 0 and 1.

The multiplying factor in (7.65) encodes all of the differences between the properties of the charged metric and the neutral metric. The denominator of the multiplying factor in (7.65) is larger than the terms in the numerator for all $|\alpha_i| > 0$ so this factor has a maximum of 1 for $\alpha_1 = \alpha_2 = 0$ and then exponentially decays toward 0 as the charges are increased. This means that the charged metric angular momenta and horizon area will always be smaller than the corresponding neutral metric if only the charges are varied. In the case of the dual rotating black ring, this agrees with the intuitive interpretation of the ring being balanced by the charge as well as the angular momentum. The charge helps to balance the tension trying to collapse the ring and thus allows a ring that would otherwise be unstable, if only balanced by the centrifugal force, to remain in equilibrium.

The form of the expressions for the angular momentum shows that for any given ring, as the charge is increased the angular momentum in the ϕ and the ψ plane will have to decrease for the ring to remain in equilibrium, with the speed of the rotation decreasing as the charge increases. Unfortunately, since the multiplying factor in (7.65) only asymptotically approaches zero, there is no way that the ring can only be balanced by rotation in the ϕ direction, or by the charge alone. In order for the angular momentum in either direction to reach zero, the charge would have to be infinite.

Figure 7.1 shows how the ring area a varies with $\tilde{j}_\psi^2$ for various different values of α_1 and α_2. The curves are constrained so that $\tilde{j}_\phi^2 = 1/500$. The effect of increasing or decreasing α_1 or α_2 is to move the phase curve closer or further away from the origin respectively. It doesn't matter whether α_1 or α_2 is varied, since the factor in (7.65) is symmetrical under interchange of α_1 and α_2. The basic effect of varying the charge is to replicate the phase curve of a neutral ring with larger j_ψ^2 other than that, the phase curves are identical in shape to those of the neutral ring. This behaviour can be generalised to any other metric given by (7.14) but, obviously, the physical interpretation would depend upon the physics of the neutral metric (7.6).

To find the point where the black ring angular momentum in the ψ direction is

minimized and the area maximized it is necessary to deploy a Lagrange multiplier to fix $\tilde{j}_\phi$ whilst $\tilde{j}_\psi$ is minimized. Doing this gives the value of λ in terms of ν where $\tilde{j}_\psi$ and hence a are maximized. Unsurprisingly, this gives exactly the same expression as for the neutral ring, where

$$\lambda = \frac{1}{4}\left(-1-\nu+\sqrt{(9+\nu)(1+9\nu)}\right) \tag{7.66}$$

This is because the form of $\tilde{j}_\psi$ and $\tilde{j}_\phi$ is exactly the same, so any factors that are introduced by $\alpha_i \neq 0$ cancel out completely.

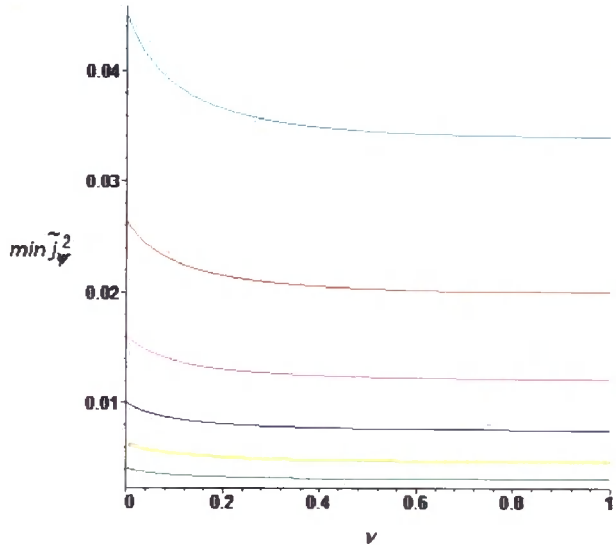

Figure 7.2: This plot shows how the minimum angular momentum along the S^1 reduces as the charge is increased from $\alpha_1 = \alpha_2 = 1$ through to $\alpha_1 = \alpha_2 = 2$ in increments of 0.2. The highest curve represents the smallest total charge and the lowest curve represents the largest total charge.

Figure 7.2 gives some examples of how the ring angular momentum $\tilde{j}_\psi^2$ decreases as $\nu \to 1$ i.e. as the rings get fatter, and decreases for all ν as the charge is increased. Although the minimum angular momentum curves for larger values of α_1 and α_2 seem to be approaching $\tilde{j}_\psi = 0$ rapidly, they will only ever asymptotically approach it. This means that even though the addition of a small charge will significantly decrease the angular momentum needed for the ring to remain balanced, it will never sustain a balanced ring without angular momentum in at least the ψ direction. The variation of the angular momentum with the charge is similar for a generic metric but the form of the plots will obviously vary.

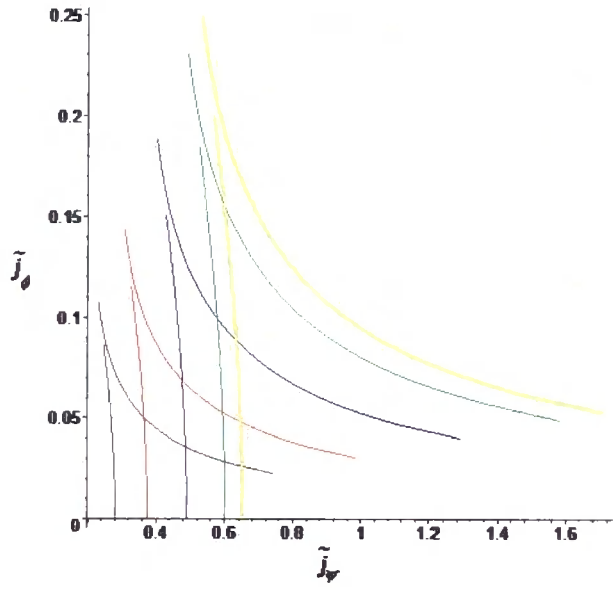

Figure 7.3: This plot gives the lines delimiting the phase space of the charged ring when the charges are equal for $\alpha_1 = \alpha_2 = 0, 0.2, 0.4, 0.6, 0.8$ from top to bottom respectively.

Figure 7.3 shows the phase space of the charged black ring for $\tilde{j}_\phi$ against $\tilde{j}_\psi$ for various values of α_1 and α_2 ranging from 0 to 0.8. For any given charge, the permissible values of $\tilde{j}_\psi$ and $\tilde{j}_\phi$ are those that are enclosed by the curve and the $\tilde{j}_\psi$ axis. Values of $\tilde{j}_\psi$ and $\tilde{j}_\phi$ outside of this enclosed region are not physically permissible. As with all the other plots, the increased charge has the effect of decreasing the angular momentum, so the larger the charge the smaller the range of the permissible angular momenta in the ψ and ϕ directions.

To analyse the extremal doubly spinning ring, it is necessary to substitute $\lambda = 2\sqrt{\nu}$. For this case, the analysis of the charged version proceeds in a similar manner to that of the non-extremal doubly spinning ring. The mass, angular momentum and horizon area are still given by the expressions in (7.25), (7.32), and (7.35) which differ from the uncharged versions by functions only involving $\cosh\alpha_1$ and $\cosh\alpha_2$. Thus all of the physical properties, that depend upon the charge, will vary in the same way as previously described.

Chapter 8

Conclusion

The main body of this work was concerned with investigating the geometrical and physical properties of black hole solutions in higher dimensions. The main tool that was used to examine the geometry of various 5D solutions was the plotting of geodesics on representative Penrose diagrams, as in chapter 5. By plotting the actual geodesics on the Penrose diagram it gave a much better idea of what was happening to the test particle since Penrose diagrams have inherent features which allow the reader to identify various regions of interest in the spacetime, such as the event horizon and any curvature singularities.

Once the geodesics were plotted on the diagram it was possible to see at a glance what was happening to different test particles when the constants of motion were changed. In general, for all of the plots, increasing the energy or angular momentum of the test particle would increase the curvature of the geodesic and thus increase the proper time that the test particle experienced. Thus it is possible to get an intuitive feel for how a test particle will react under different conditions in the various spacetimes.

Another advantage of plotting the geodesics on the Penrose diagram was in the case where the test particle was given some angular momentum (or gained it by virtue of the black hole spinning). In this instance it is no longer obvious where the future and past light cones are at any particular point in space, but by plotting the null geodesics it was possible to interpret how the light cones deformed as the angular momentum of the test particles was increased. Ideally the Penrose diagram

should be extended to include the additional dimension when the test particle is given angular momentum in one of the compact directions but in practice it is very difficult to interpret a two dimensional image of a three dimensional phenomenon. Also, in a lot of the more interesting cases it isn't even possible to extend the Penrose diagram to three dimensions because this would require at least a three dimensional cross section of the space time to be conformally flat, which isn't the case for either the Kerr or black ring solutions.

At the end of chapter 5 a different method of plotting the geodesics was examined to try and circumvent this problem. Unfortunately, the Klösch Strobl mapping also has some severe limitations - mainly due to the increased complexity of the coordinate transformations used. The major advantage of the method is that the coordinate transformations allow the whole of the spacetime to be covered with only one coordinate patch and thus avoid the problems caused when several patches have to be considered, such as in the case of the Kerr geodesics. However, the fact that the coordinate transformations are so unrestricted makes it very difficult to derive any transformations that are practically useful. In the Kerr case, the geodesics had to be restricted to the axis of rotation in order to make the problem tractable. It may be possible to adapt the method presented here so that it is applicable to all of the Kerr geodesics but it is far from obvious how this could be done.

In chapter 6, the equations of motion for the geodesics of the neutral rotating Black Ring metric were set up and numerically integrated for some special classes of solutions. The solutions can be broadly separated into those that are confined to the axis of rotation and those that gave circular orbits in the plane of the ring. It was also shown that there are no circular geodesics that orbit through the ring or any "pseudo-radial" geodesics. Although it was shown that there aren't any circular orbits through the ring, some numerical evidence was presented that bound orbits of this form may exist.

The effective potential for the on-axis solutions is very similar to that for a static black hole, with the potential being attractive for the geodesics with zero angular momentum. In this case both the null and timelike particles can pass through the origin of the ring and out to infinity, or in the case of the timelike geodesics, oscillate

back and forth. This agrees with the analogous Newtonian case of a massive ring when a small test particle is placed on the axis of symmetry and then displaced slightly.

Increasing the angular momentum of the geodesics causes a centrifugal barrier to appear which stops the geodesics from approaching the origin of the ring, as in the case of the Schwarzschild black hole. Even though timelike and null particles can't reach the origin it is still possible for them to pass through the centre of the ring by virtue of the black ring being five dimensional, so the axis of rotation is actually a plane meaning that the particles can go from one side of the ring to the other without passing through $y = -1$ and $x = +1$. The particle motion in the x-ϕ plane is similar to a small asteroid moving in the Sun's gravitational field. The particle can either be captured and orbit indefinitely, or it can escape to infinity.

The timelike potential has a local minimum, which allows for a rich array of geodesic motion because it is possible to have a geodesic that is in a stable orbit in the x-ϕ plane near to the centre of the ring. The shape of the potential well is unsymmetric so the orbit is always elliptical with the period of the orbit depending on the initial radius: the larger the radius, the longer the period of oscillation.

The effective potential for the null geodesics is very similar to that for the timelike ones when the angular momentum is zero, but once the angular momentum is increased the potential becomes totally repulsive for small ν. If ν is large enough then it is possible to create a small local minimum for values of $\nu > 0.653$. This potential is interesting, since it means that it is possible for the Black Ring to have light rays in stable orbits circling through it. If ν is decreased, then the null geodesic will always go off to infinity, no matter what the angular momenta of the geodesic is.

In the case of the planar circular orbits, the angular momentum in the ϕ direction has to be zero in order for them to remain on the plane through the centre of the ring. This means that the geodesics are confined to move in only one spatial dimension. For timelike geodesics it is only possible to have a constant circular orbit on the ergosurface at $y = -\frac{1}{\lambda}$. This requires the energy and angular momentum in the ψ direction to be carefully chosen though. Also, this orbit only exists in the outer

equatorial plane. It is impossible to have any circular orbits in the interior of the ring.

For null geodesics there is always at least one solution for ψ that will give a circular orbit for all values of ν. If the angular momentum in the ψ direction is chosen to go against the rotation of the ring, it is also possible to have two static orbits for the same value of ν. These circular orbits do require a certain amount of tuning because for small values of Ψ it is impossible to have any circular orbits, no matter what the shape and size of the ring.

The possibility of the Black Ring metric having geodesics that orbit through the ring at constant y and radial geodesics of constant x was also examined but it was shown that these cannot occur, at least not for these particular toroidal coordinates, where orbits of constant y describe circles. The numerical evidence suggests that there may be elliptical orbits through the ring for at least one value of y, but the lack of separability of the equations of motion means that it is impossible to interpret these orbits quantitatively. It would be interesting to investigate these orbits more thoroughly, to see if the motion of the geodesics reveals any underlying properties of the Black Ring metric that have been thus far overlooked. A more systematic way of doing this might be to look for regions of the space where the geodesics are bounded, by numerically integrating the fully specified equations of motion for varying initial positions. The regions of space close to the $x = \pm 1$ planes and the $y = -1$ axis have properties similar to the results presented here, so this may provide a way of estimating values for the conserved momenta that could give bounded geodesics at some points.

The final chapter was principally concerned with constructing a two charge supersymmetric string solution, in the low energy limit, given an initial solution to Einstein's field equations. It then used the dual rotating black ring found by Pomeransky and Sen'kov in [27] as an example of how the general method can be applied to obtain specific solutions. The generic charged metric and its physical properties were derived in section 7.2 and thus allowed the various physical properties of the charged metric to be examined using the dual spinning black ring as an example.

The main aim of this chapter was to present a technique that would charge up

a generic three-Killing field metric. It basically involved lifting the metric to ten dimensions, boosting the metric, T-dualising it to obtain a fundamental charge, and then boosting again to produce a second charge. The resulting solution was then Kaluza-Klein compactified back down to five dimensions, so that the physical properties of the solution could be explored. The first part of section 7.2 defined a generic starting metric and then applied the above techniques to generate a new solution with fundamental and momentum string charges.

Having obtained a general expression for a charged metric, the physical properties of it in terms of those of the neutral metric were derived. The analysis showed that the ADM mass, angular momentum, and the horizon area of the charged metric were directly proportional to the respective quantities for the neutral metric with the multiplying factor being a function of the boost parameters used to generate the charged solution. The derivation of the conserved charges showed that the gauge charges were related to the boost parameters by a factor of $\sinh 2\alpha$, where α is the boost parameter. This was elaborated on more at the end of the chapter.

The addition of the string charges varied the physical properties of the generic black hole solution, and the dual rotating black ring in particular. It was found that the addition of the charges had little effect overall with the angular momenta and area being the only properties that were affected. In general the area and angular momenta were reduced as the charges were increased but the angular momentum could never be decreased to zero for finite charge. This is because the area and angular momenta of the charged solution only differed from those of the neutral solution by a multiplying factor which was a function of the boost parameters. This multiplying factor decayed exponentially from 1 when the charges were set to zero and asymptotically approached 0 for large values of the boost parameters. This resulted in the behaviour of the charged black ring being virtually identical to that of the neutral ring, with the charge playing a similar role to that of the angular momentum in the neutral case. This was as expected but it was shown that the charged ring must have non-zero angular momentum in the ψ and ϕ direction to remain balanced. As the charge is increased, the angular momentum required to keep the ring in equilibrium decreases exponentially but only ever asymptotically

approaches zero.

Although the method here looked at adding fundamental string and momentum charges it is theoretically possible to generate a $[D1, D5]$ charged solution by carrying out some further duality transformations. It would be interesting to see whether it would be possible to extend the methods used in this paper to charge up the generic metric, given at the beginning of section 7.2, so that a generic $[D1, D5]$ solution could be produced. It is possible to do this when the specific form of the metric coefficients are known (such as in [61]) but this requires some of the 2-forms, generated from the original metric coefficients, to be differentiated and integrated. Given this requirement, it is not immediately obvious whether this method could be applied to a generic metric solution. The $[D1, D5]$ solution would have exactly the same physical properties [81] as the solution presented here, but it would provide a broader basis for the investigation of the microscopic entropy of the black hole solutions.

Bibliography

[1] J. Michell, "On the Means of Discovering the Distance, Magnitude, & c. of the Fixed Stars, in Consequence of the Diminution of the Velocity of Their Light, in Case Such a Diminution Should be Found to Take Place in any of Them, and Such Other Data Should be Procured from Observations, as Would be Farther Necessary for That Purpose," Phil. Trans. R. Soc. (London) **74** (1784) 35-57.

[2] K. Schwarzschild, "On The Gravitational Field Of A Mass Point According To Einstein's Theory," Sitzungsber. Preuss. Akad. Wiss. Berlin (Math. Phys.) **1916** (1916) 189 [arXiv:physics/9905030].

[3] B. Carter, "Complete Analytic Extension of the Symmetry Axis of Kerr's Solution of Einstein's Equations," Phys. Rev. **141** (1966) 1242.

[4] J. L. Synge, "The Gravitational Field Of A Particle," Proc. Roy. Irish Acad. (Sect. A) **53** (1950) 83.

[5] D. Finkelstein, "Past-Future Asymmetry of the Gravitational Field of a Point Particle," Phys. Rev. **110** (1958) 965.

[6] J. Ehlers, "Konstruktionen und Charakterisierung von Losungen der Einsteinschen Gravitationsfeldgleichungen,"

[7] C. Fronsdal, "Completion and Embedding of the Schwarzschild Solution," Phys. Rev. **116** (1959) 778.

[8] M. D. Kruskal, "Maximal extension of Schwarzschild metric," Phys. Rev. **119** (1960) 1743.

[9] R. P. Kerr, "Gravitational field of a spinning mass as an example of algebraically special metrics," Phys. Rev. Lett. **11** (1963) 237.

[10] R. P. Kerr and A. Schild, *Am. Math. Soc. Symposium, New York, 1964*

[11] R. H. Boyer and T. G. Price "An interpretation of the Kerr metric in general relativity," Math. Proc. Camb. Phil. Soc. **61** (1965) 531.

[12] J. M. Cohen, "Note on the Kerr Metric and Rotating Masses," J. Math. Phys. **8** (1967) 1477

[13] B. Carter, "Global structure of the Kerr family of gravitational fields," Phys. Rev. **174** (1968) 1559.

[14] R. H. Boyer and R. W. Lindquist, "Maximal analytic extension of the Kerr metric," J. Math. Phys. **8** (1967) 265.

[15] B. Carter, "Hamilton-Jacobi and Schrodinger separable solutions of Einstein's equations," Commun. Math. Phys. **10** (1968) 280.

[16] F. de Felice and G. Preti, "On The Meaning Of The Separation Constant In The Kerr Metric," Class. Quant. Grav. **16** (1999) 2929.

[17] W. Israel, "Event Horizons In Static Vacuum Space-Times," Phys. Rev. **164** (1967) 1776.

[18] B. Carter, "Axisymmetric Black Hole Has Only Two Degrees of Freedom," Phys. Rev. Lett. **26** (1971) 331.

[19] D. C. Robinson, "Uniqueness of the Kerr black hole," Phys. Rev. Lett. **34** (1975) 905.

[20] J. P. Gauntlett, "M-theory: Strings, duality and branes," Contemp. Phys. **39** (1998) 317.

[21] C. Kokorelis, "Exact standard model structures from intersecting D5-branes," Nucl. Phys. B **677** (2004) 115 [arXiv:hep-th/0207234].

[22] I. Antoniadis, N. Arkani-Hamed, S. Dimopoulos and G. R. Dvali, "New dimensions at a millimeter to a Fermi and superstrings at a TeV," Phys. Lett. B **436** (1998) 257 [arXiv:hep-ph/9804398].

[23] O. Aharony, S. S. Gubser, J. M. Maldacena, H. Ooguri and Y. Oz, "Large N field theories, string theory and gravity," Phys. Rept. **323** (2000) 183 [arXiv:hep-th/9905111].

[24] P. Kanti, "Black holes in theories with large extra dimensions: A review," Int. J. Mod. Phys. A **19** (2004) 4899 [arXiv:hep-ph/0402168].

[25] R. C. Myers and M. J. Perry, "Black Holes In Higher Dimensional Space-Times," Annals Phys. **172** (1986) 304.

[26] R. Emparan and H. S. Reall, "A rotating black ring in five dimensions," Phys. Rev. Lett. **88**, 101101 (2002) [arXiv:hep-th/0110260].

[27] A. A. Pomeransky and R. A. Sen'kov, "Black ring with two angular momenta," arXiv:hep-th/0612005.

[28] G. C. Debney, R. P. Kerr and A. Schild, "Solutions of the Einstein and Einstein-Maxwell Equations," J. Math. Phys. **10** (1969) 1842.

[29] S. A. Hayward, "Kerr black holes in horizon-generating form," Phys. Rev. Lett. **92** (2004) 191101 [arXiv:gr-qc/0401111].

[30] T. Regge, "Stability Of A Schwarzschild Singularity," Phys. Rev. **108** (1957) 1063.

[31] S. M. Carroll, "Spacetime and geometry: An introduction to general relativity," *San Francisco, USA: Addison-Wesley (2004) 513 p*

[32] F. R. Tangherlini, "Schwarzschild field in n dimensions and the dimensionality of space problem," Nuovo Cim. **27** (1963) 636.

[33] H. Weyl, "The Theory Of Gravitation," Annalen Phys. **54** (1917) 117.

[34] R. Emparan and H. S. Reall, "Generalized Weyl solutions," Phys. Rev. D **65** (2002) 084025 [arXiv:hep-th/0110258].

[35] T. Harmark, "Stationary and axisymmetric solutions of higher-dimensional general relativity," Phys. Rev. D **70** (2004) 124002 [arXiv:hep-th/0408141].

[36] H. F. Dowker and S. N. Thambyahpillai, "Many accelerating black holes," Class. Quant. Grav. **20** (2003) 127 [arXiv:gr-qc/0105044].

[37] R. M. Wald, "General Relativity," *Chicago, Usa: Univ. Pr. (1984) 491p*

[38] C. S. Gardner, J. M. Greene, M. D. Kruskal and R. M. Miura, "Method For Solving The Korteweg-Devries Equation," Phys. Rev. Lett. **19** (1967) 1095.

[39] V. Belinski and E. Verdaguer, "Gravitational solitons," *Cambridge, UK: Univ. Pr. (2001) 258 p*

[40] V.A. Belinski and V.E. Zakharov Sov. Phys. JETP. **48** (1978) 985.

[41] V.A. Belinski and V.E. Zakharov Sov. Phys. JETP. **50** (1979) 1.

[42] D. Maison Phys. Rev. Lett. **41** (1978) 521.

[43] H. Elvang and P. Figueras, "Black Saturn," JHEP **0705** (2007) 050 [arXiv:hep-th/0701035].

[44] H. Elvang and M. J. Rodriguez, "Bicycling Black Rings," JHEP **0804**, 045 (2008) [arXiv:0712.2425 [hep-th]].

[45] Y. Morisawa, S. Tomizawa and Y. Yasui, "Boundary Value Problem for Black Rings," Phys. Rev. D **77**, 064019 (2008) [arXiv:0710.4600 [hep-th]].

[46] R. Emparan and H. S. Reall, "Black rings," Class. Quant. Grav. **23**, R169 (2006) [arXiv:hep-th/0608012].

[47] A. Chamblin and R. Emparan, "Bubbles in Kaluza-Klein theories with space- or time-like internal dimensions," Phys. Rev. D **55** (1997) 754 [arXiv:hep-th/9607236].

[48] J. Evslin and C. Krishnan, "The Black Di-Ring: An Inverse Scattering Construction," arXiv:0706.1231 [hep-th].

[49] S. Novikov, S. V. Manakov, L. P. Pitaevsky and V. E. Zakharov, "Theory Of Solitons. The Inverse Scattering Method," *New York, Usa: Consultants Bureau (1984) 276 P. (Contemporary Soviet Mathematics)*

[50] V. E. Zakharov and A. B. Shabat "Exact Theory Of 2-Dimensional Self-Focusing And One-Dimensional Self-Modulation Of Waves In Nonlinear Media," Sov. Phys. JETP **34** (1972) 62

[51] A. A. Pomeransky, "Complete integrability of higher-dimensional Einstein equations with additional symmetry, and rotating black holes," Phys. Rev. D **73** (2006) 044004 [arXiv:hep-th/0507250].

[52] S. Tomizawa, Y. Morisawa and Y. Yasui, "Vacuum solutions of five dimensional Einstein equations generated by inverse scattering method," Phys. Rev. D **73** (2006) 064009 [arXiv:hep-th/0512252].

[53] T. Azuma and T. Koikawa, "Infinite number of stationary soliton solutions to five-dimensional vacuum Einstein equation," Prog. Theor. Phys. **116** (2006) 319 [arXiv:hep-th/0512350].

[54] S. Tomizawa and M. Nozawa, "Vaccum solutions of five-dimensional Einstein equations generated by inverse scattering method. II: Production of black ring solution," Phys. Rev. D **73** (2006) 124034 [arXiv:hep-th/0604067].

[55] H. Iguchi and T. Mishima, "Solitonic generation of five-dimensional black ring solution," Phys. Rev. D **73** (2006) 121501 [arXiv:hep-th/0604050].

[56] S. Chandrasekhar, "The mathematical theory of black holes," *Oxford, UK: Clarendon (1992) 646 p.*

[57] R. Bousso, "The holographic principle," [arXiv:hep-th/0203101] *Prepared for NATO Advanced Study Institute and EC Summer School on Progress in String, Field and Particle Theory, Cargese, Corsica, France, 25 Jun - 11 Jul 2002*

[58] V. P. Frolov and D. Stojković, "Particle and light motion in a space-time of a five-dimensional rotating black hole," Phys. Rev. D **68** (2003) 064011 [arXiv:gr-qc/0301016].

[59] M. Vasudevan, K. A. Stevens and D. N. Page, "Particle motion and scalar field propagation in Myers-Perry black hole spacetimes in all dimensions," Class. Quant. Grav. **22** (2005) 1469 [arXiv:gr-qc/0407030].

[60] E. Teo "Spherical photon orbits around a Kerr black hole," General Relativity and Gravitation **35** (2003) pp. 1909-1926

[61] H. Elvang and R. Emparan, "Black rings, supertubes, and a stringy resolution of black hole non-uniqueness," JHEP **0311** (2003) 035 [arXiv:hep-th/0310008].

[62] M. Nozawa and K. i. Maeda, "Energy extraction from higher dimensional black holes and black rings," Phys. Rev. D **71** (2005) 084028 [arXiv:hep-th/0502166].

[63] A. Sahay and G. Sengupta, "Brane World Black Rings," JHEP **0706** (2007) 006 [arXiv:0704.0996 [hep-th]].

[64] H. Elvang, R. Emparan and A. Virmani, "Dynamics and stability of black rings," JHEP **0612** (2006) 074 [arXiv:hep-th/0608076].

[65] J. Hoskisson, "Particle motion in the rotating black ring metric," Phys. Rev. D **78** (2008) 064039 [arXiv:0705.0117 [hep-th]].

[66] M. Durkee, "Geodesics and Symmetries of Doubly-Spinning Black Rings," arXiv:0812.0235 [gr-qc].

[67] H. Iguchi and T. Mishima, "Black di-ring and infinite nonuniqueness," Phys. Rev. D **75**, 064018 (2007) [arXiv:hep-th/0701043].

[68] K. Izumi, "Orthogonal black di-ring solution," Prog. Theor. Phys. **119**, 757 (2008) [arXiv:0712.0902 [hep-th]].

[69] R. Emparan and H. S. Reall, "Black Holes in Higher Dimensions," arXiv:0801.3471 [hep-th].

[70] A. Strominger and C. Vafa, "Microscopic Origin of the Bekenstein-Hawking Entropy," Phys. Lett. B **379**, 99 (1996) [arXiv:hep-th/9601029].

[71] D. Mateos and P. K. Townsend, "Supertubes," Phys. Rev. Lett. **87** (2001) 011602 [arXiv:hep-th/0103030]

[72] G. T. Horowitz and M. M. Roberts, "Counting the Microstates of a Kerr Black Hole," Phys. Rev. Lett. **99** (2007) 221601 [arXiv:0708.1346 [hep-th]].

[73] F. Larsen, "Entropy of thermally excited black rings," JHEP **0510** (2005) 100 [arXiv:hep-th/0505152].

[74] H. S. Reall, "Counting the microstates of a vacuum black ring," JHEP **0805** (2008) 013 [arXiv:0712.3226 [hep-th]].

[75] P. Figueras, "A black ring with a rotating 2-sphere," JHEP **0507**, 039 (2005) [arXiv:hep-th/0505244].

[76] J. Hoskisson, "A Charged Doubly Spinning Black Ring," arXiv:0808.3000 [hep-th].

[77] A. Bouchareb, G. Clement, C. M. Chen, D. V. Gal'tsov, N. G. Scherbluk and T. Wolf, "G_2 generating technique for minimal D=5 supergravity and black rings," Phys. Rev. D **76** (2007) 104032 [arXiv:0708.2361 [hep-th]].

[78] J. C. Breckenridge, D. A. Lowe, R. C. Myers, A. W. Peet, A. Strominger and C. Vafa, "Macroscopic and Microscopic Entropy of Near-Extremal Spinning Black Holes," Phys. Lett. B **381**, 423 (1996) [arXiv:hep-th/9603078].

[79] M. Cvetic and D. Youm, "General Rotating Five Dimensional Black Holes of Toroidally Compactified Heterotic String," Nucl. Phys. B **476**, 118 (1996) [arXiv:hep-th/9603100].

[80] G. T. Horowitz, "The Dark Side Of String Theory: Black Holes And Black Strings," arXiv:hep-th/9210119.

[81] G. T. Horowitz and D. L. Welch, "Duality invariance of the Hawking temperature and entropy," Phys. Rev. D **49** (1994) 590 [arXiv:hep-th/9308077].

Appendix A

Orthonormal Bases

It is sometimes convenient to use a basis that isn't defined by the coordinates on the manifold. This section presents the notation used to describe the various non-coordinate constructs that are required for more general orthonormal bases. The notation used will follow [31], so that the general basis vectors will be given by $\hat{e}_{(a)}$, where the Latin index is used to differentiate it from the vectors that describe the coordinate basis. The basis vectors are defined to be orthonormal, so

$$g(\hat{e}_{(a)}, \hat{e}_{(b)}) = \eta_{ab} \ , \tag{A.0.1}$$

where $g(\ ,\ )$ denotes taking the inner product with respect to a particular metric $g_{\mu\nu}$.

The relationship between the general basis and the coordinate basis is given by

$$\hat{e}_{(\mu)} = e_{\mu}{}^{a}\hat{e}_{(a)} \tag{A.0.2}$$

where the vielbein $e_{\mu}{}^{a}$ is an $n \times n$ invertible matrix which describes the transformation between the coordinate and the general basis. The inverse of this matrix is denoted $e^{\mu}{}_{a}$ so that

$$e^{\mu}{}_{a}e_{\nu}{}^{a} = \delta^{\mu}_{\nu} \ , \qquad\qquad e_{\mu}{}^{a}e^{\mu}{}_{b} = \delta^{a}_{b} \tag{A.0.3}$$

In terms of these vielbiens, (A.0.1) becomes

$$g_{\mu\nu}e^{\mu}{}_{a}e^{\nu}{}_{b} = \eta_{ab} \ . \tag{A.0.4}$$

This expression implies that the components of the metric, referring to the general orthonormal basis, are just those of the Minkowski metric $\eta_{\mu\nu}$. This means that the Latin indices can be raised and lowered as normal using $\eta_{\mu\nu}$ and $\eta^{\mu\nu}$ e.g.

$$e^{\mu}{}_{a} = \eta_{ab} e^{\mu b} \tag{A.0.5}$$

It is possible to construct expressions for one-forms $\hat{e}^{(a)}$ in a similar way as above, so that

$$\hat{e}^{(\mu)} = e^{\mu}{}_{a} \hat{e}^{(a)} , \qquad \hat{e}^{(a)} = e_{\mu}{}^{a} \hat{e}^{(\mu)} . \tag{A.0.6}$$

Note that this construction implies that the expressions for the one-forms are compatible with those of the vectors, such that

$$\hat{e}^{(a)} \hat{e}_{(b)} = \delta^{a}_{b} . \tag{A.0.7}$$

These expressions for vectors and one-forms can now be combined to express a general tensor $V^{\mu}{}_{\nu}$, in the coordinate basis, in terms of a general orthonormal basis

$$V^{a}{}_{b} = e_{\mu}{}^{a} e^{\nu}{}_{b} V^{\mu}{}_{\nu} \tag{A.0.8}$$

To define covariant differentiation for the general orthonormal basis, it is necessary to introduce the spin connection $\omega_{\mu}{}^{a}{}_{b}$, to give the coordinate derivative as

$$\nabla_{\mu} X^{a}{}_{b} = \partial_{\mu} X^{a}{}_{b} + \omega_{\mu}{}^{a}{}_{c} X^{c}{}_{b} - \omega_{\mu}{}^{c}{}_{b} X^{a}{}_{c} , \tag{A.0.9}$$

where $X^{a}{}_{b}$ is a general tensor. Demanding that this tensor expression is invariant upon switching between the two coordinate systems gives a relationship between the spin connection and the ordinary connection $\Gamma^{\lambda}_{\mu\nu}$

$$\omega_{\mu}{}^{a}{}_{b} = e_{\nu}{}^{a} e^{\lambda}{}_{b} \Gamma^{\nu}_{\mu\nu} - e^{\lambda}{}_{b} \partial_{\mu} e_{\lambda}{}^{a} . \tag{A.0.10}$$

This can be re-expressed in terms of the vanishing of the covariant derivative of the vielbein by forming

$$\nabla_{\mu} e_{\nu}{}^{a} = \partial_{\mu} e_{\nu}{}^{a} - \Gamma^{\lambda}_{\mu\nu} e_{\lambda}{}^{a} + \omega_{\mu}{}^{a}{}_{b} e_{\nu}{}^{b} . \tag{A.0.11}$$

Now, demanding that this be zero gives

$$\omega_{\mu}{}^{a}{}_{b} e_{\nu}{}^{b} = \Gamma^{\lambda}_{\mu\nu} e_{\lambda}{}^{a} - \partial_{\mu} e_{\nu}{}^{a} \tag{A.0.12}$$

which can be re-arranged to give the expression in (A.0.10).

So far, the only constraint on the choice for a general basis is that it should be orthonormal i.e. it should satisfy equation (A.0.1). Under this constraint it is still possible to perform a local Lorentz transformation on the basis vectors without violating (A.0.1), this means that in general a transformation law is needed for the Latin indices:

$$T^{a'}{}_{b'} = \Lambda^{a'}{}_{a}\Lambda^{b}{}_{b'}T^{a}{}_{b} \,, \tag{A.0.13}$$

where $\Lambda^{a'}{}_{a}$ is an $n \times n$ matrix encoding the Lorentz transformations. This transformation law can now be used to see how the spin connection transforms under local Lorentz transformations, giving

$$\omega_{\mu}{}^{a'}{}_{b'} = \Lambda^{a'}{}_{a}\Lambda^{b}{}_{b'}\omega_{\mu}{}^{a}{}_{b} - \Lambda^{c}{}_{b'}\partial_{\mu}\Lambda^{a'}{}_{c} \,. \tag{A.0.14}$$

Having defined the transformation law for the spin connection, it is now possible to define exterior derivatives that are invariant under local Lorentz transformations, as well as general coordinate transformations. The usual expression for the exterior derivative of a one form X_{μ} is given by

$$(\mathrm{d}X)_{\mu\nu}{}^{a} = \partial_{\mu}X_{\nu}{}^{a} - \partial_{\nu}X_{\mu}{}^{a} \,, \tag{A.0.15}$$

which is a tensor under general coordinate transformations but not under local Lorentz transformations. This can be rectified by introducing a spin connection term as follows

$$(\mathrm{d}X)_{\mu\nu}{}^{a} + (\omega \wedge X)_{\mu\nu}{}^{a} = \partial_{\mu}X_{\nu}{}^{a} - \partial_{\nu}X_{\mu}{}^{a} + \omega_{\mu}{}^{a}{}_{b}X_{\nu}{}^{b} - \omega_{\nu}{}^{a}{}_{b}X_{\mu}{}^{b} \,. \tag{A.0.16}$$

This expression will now transform as a tensor under both general coordinate transformations and local Lorentz transformations.

It is now possible to express the tensors for the torsion T^{a} and the curvature $R^{a}{}_{b}$ in terms of the spin connection. These are

$$T^{a} = \mathrm{d}e^{a} + \omega^{a}{}_{b} \wedge e^{b} \,, \qquad R^{a}{}_{b} = \mathrm{d}\omega^{a}{}_{b} + \omega^{a}{}_{c} \wedge \omega^{c}{}_{b} \,, \tag{A.0.17}$$

where the Greek indices on the basis and spin-connection one-forms have been suppressed so that

$$e^{a} = e_{\mu}{}^{a}\mathrm{d}x^{\mu} \,, \qquad \omega^{a}{}_{b} = \omega_{\mu}{}^{a}{}_{b}\mathrm{d}x^{\mu} \,. \tag{A.0.18}$$

The usual convention is to use torsion-free connections, which means that the first expression in (A.0.17) will be zero.

The assumption of metric compatibility ($\nabla_\mu g_{\mu\nu} = 0$) can be used to generate an important identity for $\omega_{\mu ab}$. In the general orthonormal basis, the metric is given by η_{ab}, so the condition for metric compatibility can be written

$$\begin{aligned} \nabla_\mu \eta_{ab} &= \partial_\mu \eta_{ab} - \omega_\mu{}^c{}_a \eta_{cb} - \omega_\mu{}^c{}_b \eta_{ac} \\ &\quad -\omega_{\mu ab} - \omega_{\mu ba} = 0 \, . \end{aligned} \tag{A.0.19}$$

This therefore implies

$$\omega_{\mu ab} = -\omega_{\mu ba} \, , \tag{A.0.20}$$

which can similarly be shown to hold for $\omega^{\mu ab}$. The anti-symmetry condition of (A.0.20) can now be used with the torsion free condition to find the spin connection in terms of the vielbeins.

Appendix B

Ricci Tensor for the Canonical Form of the Metric

In this appendix, part of the Ricci Tensor for the form of the metric given in (3.64) is calculated to show that

$$\sum_{i,j=1}^{D-2} G^{ij} R_{ij} = -\frac{\partial_\rho \Lambda}{2e^{2\nu}\Lambda\rho}. \tag{B.0.1}$$

Calculating the non-zero Christoffel symbols for the metric given in (3.64) gives

$$\begin{gathered}
\Gamma^{\rho}_{ij} = -\frac{1}{2}e^{-2\nu}\partial_\rho G_{ij}, \qquad \Gamma^{z}_{ij} = -\frac{1}{2}e^{-2\nu}\Lambda^{-1}\partial_z G_{ij} \\
\Gamma^{i}_{\rho j} = \frac{1}{2}\sum_{k=1}^{D-2} G^{ik}\partial_\rho G_{jk}, \qquad \Gamma^{i}_{zj} = \frac{1}{2}\sum_{k=1}^{D-2} G^{ik}\partial_z G jk \\
\Gamma^{\rho}_{\rho\rho} = \partial_\rho \nu, \qquad \Gamma^{z}_{zz} = \partial_z \nu + \frac{1}{2\Lambda}\partial_z \Lambda, \qquad \Gamma^{\rho}_{\rho z} = \partial_z \nu, \qquad \Gamma^{z}_{z\rho} = \partial_\rho \nu + \frac{1}{2\Lambda}\partial_\rho \Lambda \\
\Gamma^{\rho}_{zz} = -\Lambda\partial_\rho \nu - \frac{1}{2C}\partial_\rho \Lambda, \qquad \Gamma^{z}_{\rho\rho} = -\frac{1}{\Lambda}\partial_z \nu\,.
\end{gathered} \tag{B.0.2}$$

Using the fact that $\rho = \sqrt{|\det G_{ij}|}$, the following relations for G_{ij} can be calculated

$$\sum_{i,j=1}^{D-2} G^{ij}\partial_\rho G_{ij} = \frac{2}{\rho}\,, \qquad \sum_{i,j=1}^{D-2} G^{ij}\partial_z G_{ij} = 0\,. \tag{B.0.3}$$

These expression can then be used with the expressions for the Christoffel symbols that have already been calculated to give

$$\sum_{i,j=1}^{D-2} G^{ij}\Gamma^{\rho}_{ij} = -\frac{1}{\rho}e^{-2\nu}, \qquad \sum_{i,j=1}^{D-2} G^{ij}\Gamma^{z}_{ij} = 0, \qquad \sum_{i=1}^{D-2} \Gamma^{i}_{\rho i} = \frac{1}{\rho}, \qquad \sum_{i=1}^{D-2} \Gamma^{i}_{zi} = 0\,. \tag{B.0.4}$$

All these expressions can now be combined to calculate an expression for the Ricci tensor

$$\begin{aligned} 2e^{2\nu}R_{ij} &= -\partial_\rho^2 G_{ij} - \frac{1}{\rho}\partial_\rho G_{ij} - \frac{\partial_\rho \Lambda}{2\Lambda}\partial_\rho G_{ij} - \frac{1}{\Lambda}\partial_z^2 G_{ij} + \frac{\partial_z \Lambda}{2\Lambda^2}\partial_z G_{ij} \\ &\quad + \sum_{k,l=1}^{D-2} G^{kl}\partial_\rho G_{ki}\partial_\rho G_{lj} + \frac{1}{\Lambda}\sum_{k,l=1}^{D-2} G^{kl}\partial_z G_{ki}\partial_z G_{lj} \,. \end{aligned} \tag{B.0.5}$$

This expression can be simplified further by noting that

$$\begin{aligned} -\sum_{i,j=1}^{D-2} G^{ij}\partial_\rho^2 G_{ij} + \sum_{i,j,k,l=1}^{D-2} G^{ij}G^{kl}\partial_\rho G_{ki}\partial_\rho G_{lj} &= \frac{2}{\rho^2} \,, \\ -\sum_{i,j=1}^{D-2} G^{ij}\partial_z^2 G_{ij} + \sum_{i,j,k,l=1}^{D-2} G^{ij}G^{kl}\partial_z G_{ki}\partial_z G_{lj} &= 0 \,, \end{aligned} \tag{B.0.6}$$

along with the expressions in (B.0.3), can be substituted into (B.0.5) to give

$$\sum_{i,j=1}^{D-2} G^{ij}R_{ij} = -\frac{\partial_\rho \Lambda}{2e^{2\nu}\Lambda\rho} \,. \tag{B.0.7}$$

Appendix C

Singular Terms in the Black Ring Geodesic Equations

In certain situations the equations of motion given by (6.3) - (6.5) and (6.12) - (6.13) break down, such as when $y = -1$ is substituted into (6.13). In cases such as this, certain terms become indeterminate in the x, y coordinates. Once these terms are isolated, they can be analysed by transforming to spherical polar coordinates, as given in (4.12) and (4.13). In the case of (6.13) the singularities occur in

$$\frac{\Psi^2}{G(y)} \qquad \text{and} \qquad \frac{\dot{y}^2}{G(y)} \tag{C.0.1}$$

In section 6.2 it was stated that so long as $\Psi = 0$ the $G(y)$ term would not blow up. This is more evident if $G(y)$ is converted into spherical polar coordinates. Doing this gives

$$G(y) = -\frac{4R^2r^2\sin^2\theta[P - \nu(R^2 + r^2)]}{P^3} \tag{C.0.2}$$

where $P = \sqrt{r^4 + 2R^2r^2\cos 2\theta + R^4}$.

The rotational axis, given by $y = -1$ is equivalent to $\theta = 0$, so it is obvious that $G(y)^{-1} \to \infty$ as $\theta \to 0$ because of the $\sin^2\theta$ term. Fortunately, the Ψ^2 term will cancel out the $\sin^2\theta$ term if it is initially chosen to be zero.

Transforming the other problematic term into spherical polar coordinates gives

$$\frac{\dot{y}^2}{G(y)} = -\frac{4R^2[(r^2 - R^2)\dot{r}\sin\theta - (r^2 + R^2)r\dot{\theta}\cos\theta]^2}{P^3[P - \nu(R^2 + r^2)]} \tag{C.0.3}$$

Taking the limit as $\theta \to 0$ gives

$$\lim_{\theta \to 0} \frac{\dot{y}^2}{G(y)} = -\frac{4R^2 r^2 \dot{\theta}^2}{(R^2 + r^2)^2(1 - \nu)} \tag{C.0.4}$$

In this form it is obvious that this term is not singular, as R^2 is always positive and $\nu < 1$.

There are similar problems with equation (6.12) when the geodesics on the equatorial plane are to be considered. The terms in question are

$$\frac{\dot{x}^2}{G(x)} \qquad \text{and} \qquad \frac{\ell^2}{G(x)} \tag{C.0.5}$$

Using the same process as above the terms can be transformed as follows

$$\frac{\dot{x}^2}{G(x)} = \frac{4R^2[r\dot{\theta}\sin\theta(R^2 - r^2) - \dot{r}\cos\theta(R^2 + r^2)]^2}{P^3[P + \nu(R^2 - r^2)]} \tag{C.0.6}$$

The equatorial plane corresponds to $\theta = \frac{\pi}{2}$, so taking the limit gives

$$\lim_{\theta \to \frac{\pi}{2}} \frac{\dot{x}^2}{G(x)} = \frac{4R^2 r^2 \dot{\theta}^2}{(R^2 - r^2)^2(1 + \nu)} \tag{C.0.7}$$

This term is very similar to (C.0.4). In this case the denominator is always positive because the $(R^2 - r^2)^2$ term is always positive.

Transforming the other term in (C.0.5) gives

$$\frac{\ell^2}{G(x)} = \frac{S^3 \ell^2}{4R^2 r^2 \cos^2\theta[P + \nu(R^2 - r^2)]} \tag{C.0.8}$$

This will obviously blow up for $\theta = \frac{\pi}{2}$ unless $\ell = 0$. In a similar manner to the geodesics on the rotational axis, ℓ has to be zero for geodesics on the equatorial plane, since the ϕ coordinate is measured with respect to the $x = \pm 1$ axis.

Equation (C.0.6) also causes a problem when calculating geodesics that pass through the origin. In the toroidal coordinates, the origin corresponds to $x = 1$ and $y = -1$, unfortunately the transformation given in (4.13) becomes undefined. This means that a different coordinate system will have to be used to remove the singularity at this point. A good candidate is Cartesian coordinates.

The transformations between the Cartesian coordinates and the toroidal coordinates are given by

$$z_0 = \pm\frac{R\sqrt{1 - x^2}}{y - x} \tag{C.0.9}$$

$$z_1 = \pm\frac{R\sqrt{y^2 - 1}}{y - x} \tag{C.0.10}$$

where z_0 and z_1 are the Cartesian coordinates on the (x, y) plane. In these coordinates

$$\dot{x} = -\frac{4R^2 z_0[R^2\dot{z}_0 + 2z_0 z_1\dot{z}_1 + {z_0}^2\dot{z}_0 - {z_1}^2\dot{z}_0]}{Q^3} \tag{C.0.11}$$

$$\dot{y} = -\frac{4R^2 z_1[R^2\dot{z}_1 - 2z_0 z_1\dot{z}_0 - {z_1}^2\dot{z}_1 + {z_0}^2\dot{z}_1]}{Q^3} \tag{C.0.12}$$

$$G(x) = \frac{4R^2 {z_0}^2(\nu R^2 - \nu {z_0}^2 - \nu {z_1}^2 + Q)}{Q^3} \tag{C.0.13}$$

$$G(y) = \frac{4R^2 {z_1}^2(\nu R^2 + \nu {z_0}^2 + \nu {z_1}^2 - Q)}{Q^3} \tag{C.0.14}$$

where $Q = \sqrt{[(z_1 - R)^2 + z_0^2][(z_1 + R)^2 + z_0^2]}$. Expressing the terms that become singular at $x = 1$ and $y = -1$ in Cartesian coordinates gives

$$\frac{\dot{x}^2}{G(x)} = \frac{4R^2[R^2\dot{z}_0 + 2z_0 z_1\dot{z}_1 + {z_0}^2\dot{z}_0 - {z_1}^2\dot{z}_0]^2}{(\nu R^2 - \nu {z_0}^2 - \nu {z_1}^2 + Q)\,Q^3} \tag{C.0.15}$$

$$\frac{\dot{y}^2}{G(y)} = \frac{4R^2[R^2\dot{z}_1 - 2z_0 z_1\dot{z}_0 - {z_1}^2\dot{z}_1 + {z_0}^2\dot{z}_1]^2}{(\nu R^2 + \nu {z_0}^2 + \nu {z_1}^2 - Q)\,Q^3} \tag{C.0.16}$$

In Cartesian coordinates the origin is at $z_0 = z_1 = 0$, so substituting these values into the above equations gives

$$\lim_{z_0 \to 0}\left[\lim_{z_1 \to 0}\frac{\dot{x}^2}{G(x)}\right] = \frac{4\dot{z}_0^2}{R^2(\nu + 1)} \tag{C.0.17}$$

$$\lim_{z_0 \to 0}\left[\lim_{z_1 \to 0}\frac{\dot{y}^2}{G(y)}\right] = \frac{4\dot{z}_1^2}{R^2(\nu - 1)} \tag{C.0.18}$$

It is now manifest that these terms are non-singular at the origin and are dependent on $\dot{z}_0$ and $\dot{z}_1$ respectively.

Appendix D

Effective Potential on the Black Ring Equatorial Plane

For geodesics confined to the equatorial planes, given by $x = \pm 1$, $\dot{y}^2$ can be calculated from the first integral equation. Substituting $\dot{x} = 0$ and $\ell = 0$ in (6.16) gives

$$-\frac{R^2 F(x)\dot{y}^2}{G(y)(x-y)^2} - \frac{E^2 F(x)}{F(y)} - \frac{(x-y)^2\left[RE(1+y)C + \Psi F(y)\right]^2}{F(x)F(y)R^2 G(y)} = \epsilon \tag{D.0.1}$$

In principle, the effective potential can now be calculated but there is a problem caused by the $F(y)$ terms in the denominator. These terms become singular when $y = -\frac{1}{\lambda}$ so a coordinate transformation is required to make sure that the effective potential is continuous across the ergosurface. The transformation

$$z = -\tanh^{-1}\left(\frac{1+\lambda y}{y+\lambda}\right) \tag{D.0.2}$$

is continuous when $y \to -\frac{1}{\lambda}$ and approaches infinity as $y \to -1$.

Expressing (D.0.1) in terms of z gives

$$\dot{z}^2 = KE^2 + LE + M \tag{D.0.3}$$

where

$$\begin{aligned} K &= -\frac{(-\lambda - \tanh z + \nu + \nu\lambda \tanh z)(x\lambda + x\tanh z + 1 + \lambda \tanh z)^2}{R^2 \tanh z(1-\lambda^2)^2(1-\tanh^2 z)} \\ &\quad -\frac{(x\lambda + x\tanh z + 1 + \lambda\tanh z)^4 C^2(\lambda-1)^2}{R^2 \tanh z F(x)^2(1-\lambda^2)^3(1+\tanh z)^2(\lambda+\tanh z)} \end{aligned} \tag{D.0.4}$$

$$L = -\frac{2(x\lambda + x\tanh z + 1 + \lambda\tanh z)^4\Psi C(\lambda-1)(1-\tanh(z))}{R^3F(x)^2(1-\lambda^2)^2(1-\tanh^2 z)^2(\lambda+\tanh z)} \tag{D.0.5}$$

$$\begin{aligned} M = & -\frac{(-\lambda-\tanh z+\nu+\nu\lambda\tanh z)(x\lambda+x\tanh z+1+\lambda\tanh z)^2\epsilon}{(1-\lambda^2)(1-\tanh^2 z)(\lambda+\tanh z)R^2F(x)} \\ & -\frac{(x\lambda+x\tanh z+1+\lambda\tanh z)^4\tanh z\Psi^2}{R^4F(x)^2(1-\lambda^2)(1-\tanh^2 z)^2(\lambda+\tanh z)} \end{aligned} \tag{D.0.6}$$

The effective potentials for these planar geodesics can be calculated in a similar way to those at the beginning of section 6.2, so solving (D.0.3) for E when $\dot{z}=0$ gives

$$V_\pm = \frac{-L \pm \sqrt{L^2-4KM}}{2K} \tag{D.0.7}$$

Technically both effective potentials need to be considered, since the L term is not equal to zero, as was the case for the on axis geodesics considered in section 4, but in practice it is usually possible to consider only V_+, since V_- is usually negative for all values of z. However, if $\Psi<0$, V_- is positive for some values of z, in which case V_+ and the portion of V_- that is positive will be considered as the effective potential function.

Appendix E

The Induced Metric on the Event Horizon

This appendix examines the form of the induced metric, on the event horizon, in terms of generic metric coefficients and derives some identities that prove useful when manipulating unspecified metric coefficients. The relationship between the area of a metric when string charges have been added and that of the neutral metric appears to be simple but substitution of the charged metric coefficients in terms of the neutral coefficients doesn't immediately give the desired relationship between the two horizon areas. Instead, consider the determinant of the neutral metric (7.6)

$$\begin{vmatrix} g_{tt} & g_{t\psi} & g_{t\phi} & 0 & 0 \\ g_{t\psi} & g_{\psi\psi} & g_{\psi\phi} & 0 & 0 \\ g_{t\phi} & g_{\psi\phi} & g_{\phi\phi} & 0 & 0 \\ 0 & 0 & 0 & g_{\rho\rho} & 0 \\ 0 & 0 & 0 & 0 & g_{zz} \end{vmatrix} = \Lambda(\rho, z) \tag{E.0.1}$$

where $\Lambda(\rho, z)$ is an arbitrary function depending on the metric coefficients. It is only a function of the variables ρ and z, since the other coordinates can't appear in the metric coefficients by virtue of their being Killing vectors.

A little manipulation shows that the $g_{\rho\rho}$ and g_{zz} coefficients can be factored out

to give

$$g_{\rho\rho}g_{zz}\begin{vmatrix} g_{tt} & g_{t\psi} & g_{t\phi} \\ g_{t\psi} & g_{\psi\psi} & g_{\psi\phi} \\ g_{t\phi} & g_{\psi\phi} & g_{\phi\phi} \end{vmatrix} = \Lambda(\rho, z) \tag{E.0.2}$$

This can then be rearranged to give

$$\begin{vmatrix} g_{tt} & g_{t\psi} & g_{t\phi} \\ g_{t\psi} & g_{\psi\psi} & g_{\psi\phi} \\ g_{t\phi} & g_{\psi\phi} & g_{\phi\phi} \end{vmatrix} = \frac{\Lambda(\rho, z)}{g_{\rho\rho}g_{zz}} = \frac{g^{\rho\rho}\Lambda(\rho, z)}{g_{zz}} \tag{E.0.3}$$

where it is assumed that the event horizon is a hypersurface of constant ρ. In this case $g^{\rho\rho} = 0$ so, after expanding the determinant, the above equation gives an identity relating some of the coefficients in the neutral metric.

$$g_{tt}(g_{\psi\psi}g_{\phi\phi} - g_{\psi\phi}^2) - g_{t\psi}^2 g_{\phi\phi} + 2g_{t\psi}g_{t\phi}g_{\psi\phi} - g_{t\phi}^2 g_{\psi\psi} = 0 \tag{E.0.4}$$

The main difficulty in calculating the area in terms of the metric functions is due to the square root in the integral. The only non-trivial way to eliminate this is to express the determinant of the induced metric in a manifestly squared form. To do this complete the square on the metric given in (7.6)

$$\begin{aligned} ds^2 &= g_{tt}\left(dt + \frac{g_{t\psi}\mathrm{d}\psi + g_{t\phi}\mathrm{d}\phi}{g_{tt}}\right)^2 - \frac{(g_{t\psi}\mathrm{d}\psi + g_{t\phi}\mathrm{d}\phi)^2}{g_{tt}} + 2g_{\psi\phi}\mathrm{d}\psi\mathrm{d}\phi + g_{\psi\psi}\mathrm{d}\psi^2 \\ &\quad + g_{\phi\phi}\mathrm{d}\phi^2 + g_{\rho\rho}\mathrm{d}\rho^2 + g_{zz}\mathrm{d}z^2 \end{aligned} \tag{E.0.5}$$

Armed with this expression and the identity given in (E.0.4), it is now possible to express the determinant of the induced metric in a manifestly squared form

$$\begin{aligned} \gamma &= g_{zz}\left(g_{\psi\psi}g_{\phi\phi} - g_{\psi\phi}^2\right) \\ &\equiv g_{zz}\left[\frac{g_{t\psi}^2 g_{t\phi}^2}{g_{tt}^2} - \frac{g_{t\psi}^2}{g_{tt}}\left(\frac{g_{t\phi}^2}{g_{tt}} - g_{\phi\phi}\right) - \frac{g_{t\psi}^2 g_{t\phi}^2}{g_{tt}^2} + \left(\frac{g_{t\phi}^2}{g_{tt}} - g_{\phi\phi}\right)\left(\frac{g_{t\psi}^2}{g_{tt}} - g_{\psi\psi}\right)\right. \\ &\quad \left. - \frac{g_{t\phi}^2}{g_{tt}}\left(\frac{g_{t\psi}^2}{g_{tt}} - g_{\psi\psi}\right) + 2\frac{g_{t\psi}g_{t\phi}}{g_{tt}}\left(\frac{g_{t\psi}g_{t\phi}}{g_{tt}} - g_{\psi\phi}\right) - \left(\frac{g_{t\psi}g_{t\phi}}{g_{tt}} - g_{\psi\phi}\right)^2\right] \end{aligned} \tag{E.0.6}$$

Now consider

$$\begin{aligned} &\left(\frac{g_{t\phi}^2}{g_{tt}} - g_{\phi\phi}\right)\left(\frac{g_{t\psi}^2}{g_{tt}} - g_{\psi\psi}\right) - \left(\frac{g_{t\psi}g_{t\phi}}{g_{tt}} - g_{\psi\phi}\right)^2 = \\ &\qquad (g_{\psi\psi}g_{\phi\phi} - g_{\psi\phi}^2) - \frac{g_{t\psi}^2 g_{\phi\phi} - 2g_{t\psi}g_{t\phi}g_{\psi\phi} + g_{t\phi}^2 g_{\psi\psi}}{g_{tt}} \end{aligned} \tag{E.0.7}$$

which goes to zero by virtue of (E.0.4). It is also implicitly assumed that the particular metric under consideration represents a rotating black hole, so that $g^{tt} \not\to 0$ and hence $g_{tt} \not\to \infty$.

Simplifying and expanding the remaining terms for γ gives

$$\gamma = -\frac{g_{zz}}{g_{tt}^2}\left(g_{t\psi}\sqrt{g_{t\phi}^2 - g_{\phi\phi}g_{tt}} + g_{t\phi}\sqrt{g_{t\psi}^2 - g_{\psi\psi}g_{tt}}\right)^2 \tag{E.0.8}$$

where (E.0.4) has been used again to give

$$-g_{\psi\psi}g_{t\phi}^2 g_{tt} - g_{\phi\phi}g_{t\psi}^2 g_{tt} + g_{\phi\phi}g_{\psi\psi}g_{tt}^2 = g_{\psi\phi}^2 g_{tt}^2 - 2g_{\psi\phi}g_{t\psi}g_{t\phi}g_{tt} \tag{E.0.9}$$

This then implies

$$\sqrt{|\gamma|} = \frac{\sqrt{-g_{zz}}}{g_{tt}}\left(g_{t\psi}\sqrt{g_{t\phi}^2 - g_{\phi\phi}g_{tt}} + g_{t\phi}\sqrt{g_{t\psi}^2 - g_{\psi\psi}g_{tt}}\right) \tag{E.0.10}$$

which is a much more useful form for comparing the neutral metric area with the charged metric area.